

**INVESTIGATING THE ENZYMATIC MECHANISM  
OF PLATINUM NANOPARTICLE SYNTHESIS IN  
SULFATE-REDUCING BACTERIA**

A thesis submitted in fulfilment of the requirements for the degree of

MASTER OF SCIENCE

Of

RHODES UNIVERSITY

in the

Department of Biochemistry, Microbiology and Biotechnology

Faculty of Science

By

**Tamsyn Louise Riddin**

November 2008

---

---

## ABSTRACT

---

---

Efforts to discover an efficient yet environmentally friendly mode of metal nanoparticle (NP) synthesis are increasing rapidly. A 'green' route that avoids the high costs, toxic wastes and complicated protocols associated with chemical synthesis methods is therefore highly sought after. A biologically based protocol will provide the possibility of gaining control over the mechanism merely by manipulating the experimental conditions of the system. Given that the properties of nanoparticles are highly dependant on the morphology of the particles themselves, this mechanistic control will provide significant industrial advantages with regards to tailoring specific properties of the nanoparticles produced. The key objectives of this study were to: a) determine whether a consortium of sulfate-reducing bacteria was capable of platinum nanoparticle synthesis, b) elucidate the bioreductive, enzymatic mechanism responsible, and c) attempt to control the morphologies of the particles produced.

A consortium of sulfate-reducing bacteria (SRB), isolated from sewage sludge, was used in these investigations due to the advantages a consortium provides in comparison to pure cultures. The syntrophic relationships established within the constituent species not only prevent the growth of contaminant microbes, but increases the oxygen-tolerance of the system as a whole. The sulfate-reducing consortium was shown to possess an aerobic mechanism for Pt(IV) reduction which, though different from the anaerobic bioreductive mechanism previously identified in literature, did not require an exogenous electron donor. It was demonstrated that the Pt(IV) ion becomes reduced to Pt(0) via a two-cycle mechanism involving Pt(II) as the intermediate. Further investigation elucidated the reduction of Pt(IV) to Pt(II) to be dependant on a novel Pt(IV) reductase which becomes upregulated in the presence of Cu(II), while the reduction of Pt(II) to Pt(0) occurred by means of a periplasmic hydrogenase. To our knowledge, this is the first time a coupled mechanism for Pt(IV) reduction by micro-organisms has been proposed.

A cell-free, crude protein solution from the consortium produced both geometric and irregular platinum nanoparticles. The wavelength of 334 nm was chosen as a non-quantitative indicator of Pt(0) nanoparticle formation over time. The optimum conditions for nanoparticle synthesis were pH 9.0, 65 °C and 0.75 mM Pt(IV) as H<sub>2</sub>PtCl<sub>6</sub> salt. In the absence of a buffer a Pt(IV) concentration > 1 mM resulted in the precipitation of protein-nanoparticle bioconjugates, due to unfavourable acidic conditions. This demonstrated that the nanoparticles were binding to and becoming stabilised by general protein in the cell-free solution. Upon addition of a sodium-bicarbonate buffer, a general increase in Pt(IV) reduction to Pt(II) was observed. The addition of the buffer also resulted in an unexplained change in particle morphology and for this reason was not used in subsequent investigations.

Polyvinylpyrrolidone (PVP) was shown to compromise the reduction rate of the Pt(IV) ion by SRB cells. The presence of extracellular NP's was suggested by the colour of the supernatant turning brown and the A<sub>334</sub> increasing over time. Attempts to visualise the particles by transmission electron microscopy (TEM) resulted in an unexpected phenomenon where nanoparticles could be observed to form dynamically upon irradiation by the electron beam. Extended irradiation by the electron beam also resulted in structural changes of the particles occurring during observation. An increase in temperature was shown to increase the reduction rate which in turn resulted in particles decreasing in size. The starting pH was shown to have a significant effect on the reduction rate and particle morphology although specific trends could not be identified.

In conclusion, the cell-soluble extract from the sulfate-reducing consortium investigated, is capable of Pt(0) nanoparticle synthesis. Precise control over the particle morphology was not attained although the mechanism was further clarified and optimal conditions for nanoparticle synthesis were determined.

Keywords: *Bioreduction, Hydrogenase, Nanoparticle, Platinum, Pt(IV) Reductase, Sulfate-reducing bacteria*

---

---

## TABLE OF CONTENTS

---

---

<b>TITLE PAGE.....</b>	<b>i</b>
<b>ABSTRACT.....</b>	<b>ii</b>
<b>TABLE OF CONTENTS.....</b>	<b>iv</b>
<b>LIST OF FIGURES.....</b>	<b>xii</b>
<b>LIST OF TABLES.....</b>	<b>xxi</b>
<b>LIST OF ABBREVIATIONS.....</b>	<b>xxii</b>
<b>ACKNOWLEDGEMENTS.....</b>	<b>xxv</b>
<b>CHAPTER ONE – Literature Review.....</b>	<b>1</b>
<b>1.1. Introduction: Nanoparticles and nanobiotechnology.....</b>	<b>1</b>
<b>1.2. Applications of nanoparticles.....</b>	<b>2</b>
<b>1.3. Metal nanoparticles.....</b>	<b>3</b>
1.3.1. Properties of metal nanoparticles.....	3
1.3.2. Synthesis methods for metal nanoparticles.....	4
1.3.2.1. Chemical synthesis.....	4
1.3.2.2. Biological synthesis.....	5
1.3.3. The “Active” versus “Passive” mechanism debate.....	6
<b>1.4. Safety aspects of nanoparticles.....</b>	<b>9</b>
<b>1.5. Metal-ions and bacteria.....</b>	<b>10</b>
1.5.1. Heavy metals - Definition and classification.....	10
1.5.2. Microbial interactions with toxic metals.....	11
1.5.3. Transport of metal-ions into micro-organisms.....	11
1.5.4. Heavy metal resistance of microbes.....	12
<b>1.6. Metal immobilisation by microbes.....</b>	<b>14</b>

1.6.1. Biosorption.....	14
1.6.2. Enzymatic metal reduction.....	15
1.6.3. Hydrogenase enzymes and characterisation.....	15
1.6.3.1. Catalytic action.....	16
1.6.3.2. Metal-ion reduction by the hydrogenase.....	17
<b>1.7. Platinum.....</b>	<b>18</b>
1.7.1. Economic impact.....	19
1.7.2. Toxicity.....	19
<b>1.8. Sulfate-reducing bacteria (SRB).....</b>	<b>19</b>
1.8.1. Classification of sulfate-reducing bacteria.....	20
1.8.1.1. Group I sulfate-reducers (non-acetate oxidizers).....	20
1.8.1.2. Group II sulfate-reducers (acetate oxidizers).....	20
1.8.2. Physiology, growth and economic importance.....	21
1.8.2.1. Bioenergetics of sulfate reduction.....	21
1.8.2.2. Ecology.....	25
1.8.2.3. Environmental and economic importance.....	25
<b>1.9. Present research.....</b>	<b>26</b>
1.9.1. Hypothesis.....	26
1.9.2. Aims.....	26
1.9.3. Objectives.....	26
<b>CHAPTER TWO - Elucidating the bioreductive mechanism of Pt(IV)</b>	
<b>by an unknown consortium of sulfate-reducing bacteria.....</b>	<b>28</b>
<b>2.1. Introduction.....</b>	<b>28</b>
<b>2.2. Materials &amp; Methods.....</b>	<b>30</b>
2.2.1. Materials.....	30
2.2.2. Methods.....	30
2.2.2.1. Preparation of stock solutions.....	30
2.2.2.2. Analysis of platinum ions in solution.....	30
2.2.3. Growth of sulfate-reducing bacteria.....	30
2.2.3.1. Source of micro-organism and culturing conditions.....	30

2.2.3.2. Cell harvesting and preparation of SRB cells for reduction experiments.....	31
2.2.4. Metal salt reduction experiments.....	31
2.2.4.1. Hydrogen as a suitable electron donor with Pt(IV) reduction by cells.....	31
2.2.4.2. Effect of low, hydrogen concentration on Pt(IV) reduction.....	32
2.2.4.3. Effect of oxic conditions with no exogenous electron donor.....	32
2.2.5. Scanning Electron Microscopy – Energy Dispersive Analysis of X-Rays (SEM-EDAX) for Pt(0) determination.....	33
2.2.6. Transmission electron microscopy (TEM) analysis.....	33
2.2.6.1. Embedding and fixing of cells for TEM analysis.....	33
2.2.6.2. Digital image capture.....	34
<b>2.3. Results &amp; Discussion.....</b>	<b>35</b>
2.3.1. Growth of an uncharacterised mixed SRB consortium.....	35
2.3.2. Metal salt reduction experiments.....	38
2.3.2.1. Hydrogen as a suitable electron donor with Pt(IV) reduction by cells.....	38
2.3.2.2. Effect of low hydrogen concentration on Pt(IV) reduction.....	40
2.3.2.3. Effect of oxic conditions with no exogenous electron donor.....	48
2.3.3. Elucidating the mechanism.....	50
2.3.4. TEM & SEM-EDAX analysis.....	53
2.3.4.1. Control SRB experiment in the absence of Pt(IV).....	53
2.3.4.2. Cell-free Pt(IV) control in the presence of high levels of hydrogen.....	54
2.3.4.3. SRB sample challenged with Pt(IV) in the presence of high levels of hydrogen.....	55
2.3.4.4. SRB cells challenged with Pt(IV) in the absence of hydrogen.....	56
2.3.4.5. Heat-killed SRB cells challenged with Pt(IV) with low levels of hydrogen.....	58
<b>2.4. Summary &amp; Conclusions.....</b>	<b>58</b>

<b>CHAPTER THREE - Periplasmic hydrogenase: Role in the bioreductive mechanism of Pt(IV) to Pt(0).....</b>	<b>60</b>
<b>3.1. Introduction.....</b>	<b>60</b>
<b>3.2. Materials &amp; Methods.....</b>	<b>64</b>
3.2.1. Materials.....	64
3.2.2. Methods.....	64
3.2.2.1. Growth and culture of SRB consortium.....	64
3.2.2.2. Preparation of cells for Cu(II) inhibition studies.....	64
3.2.2.3. Metal salt reduction experiments.....	64
3.2.2.4. Hydrogenase assay of whole cells.....	65
3.2.2.5. TEM analysis.....	65
3.2.2.6. SEM-EDAX analysis.....	65
<b>3.3 Results &amp; Discussion.....</b>	<b>66</b>
3.3.1. Pt(IV) bioreduction.....	66
3.3.2. Pt(II) bioreduction.....	69
3.3.3 Hydrogenase assay of whole cells.....	72
3.3.4. TEM and SEM-EDAX analysis.....	73
3.3.4.1. Control experiments.....	73
3.3.4.1.1. SRB cells in the absence of Pt(IV)/Pt(II).....	73
3.3.4.1.2. Pt(IV) bioreduction with native SRB cells.....	73
3.3.4.1.3. Pt(II) bioreduction with native SRB cells.....	75
3.3.4.2. Metal reduction by SRB cells after pre-treatment with an inhibitor.....	76
3.3.4.2.1. Bioreduction of platinum ions with cells incubated in 0.5 m Cu(II).....	76
3.3.4.2.2. Bioreduction of platinum ions with cells incubated in 5 mM Cu(II).....	77
<b>3.4. Summary &amp; Conclusions.....</b>	<b>78</b>
 <b>CHAPTER FOUR - Screening an SRB cell-free crude extract for Pt(IV) reductase activity and metal nanoparticle synthesis.....</b>	 <b>79</b>





4.3.4. Investigating the effect of the bioreductive mechanism on Pt(II) reduction.....	111
4.3.4.1. TEM analysis.....	112
<b>4.4. Summary &amp; Conclusions.....</b>	<b>113</b>
<b>CHAPTER FIVE: Effects of experimental factors on biogenic nanoparticle morphology.....</b>	<b>114</b>
<b>5.1. Introduction.....</b>	<b>114</b>
<b>5.2. Materials &amp; Methods.....</b>	<b>117</b>
5.2.1. Materials.....	117
5.2.2. Methods.....	117
5.2.2.1. Cell harvesting and preparation of SRB cells for experiments...	117
5.2.2.2. Analysis of platinum ions.....	117
5.2.2.3. Morphology control.....	117
<b>Part A: SRB whole cell investigation.....</b>	<b>117</b>
5.2.2.3.1. Effect of PVP on Pt(IV) reduction by SRB cells.....	117
<b>Part B: Cell-soluble extract (CSE) investigations.....</b>	<b>118</b>
5.2.2.3.2. Effect of PVP on Pt(IV) reduction by the CSE.....	118
5.2.2.3.3. Effect of CSE protein as a biological capping agent.....	118
5.2.2.3.4. Effect of temperature.....	118
5.2.2.3.5. Effect of pH.....	119
5.2.2.4. Investigating the hydrogenase activity of the CSE.....	119
5.2.2.5. TEM analysis.....	119
5.2.2.6. SEM-EDAX analysis.....	119
<b>5.3. Results &amp; Discussion.....</b>	<b>120</b>
5.3.1. Morphology control.....	120
<b>Part A: SRB whole cell investigation.....</b>	<b>120</b>
5.3.1.1. Effect of PVP on Pt(IV) reduction by SRB cells.....	120
5.3.1.2. TEM and SEM-EDAX analysis of SRB cells.....	122
5.3.1.2.1. Control experiment: PVP-free.....	122

5.3.1.2.2. SRB cells with 20 mg.ml <sup>-1</sup> PVP.....	122
5.3.1.2.3. SRB cells with 100 mg.ml <sup>-1</sup> PVP.....	123
5.3.1.3. TEM analysis of SRB cell supernatants in the presence of PVP.....	125
5.3.1.3.1. Supernatant of 20 mg.ml <sup>-1</sup> PVP.....	125
5.3.1.3.2. Supernatant of 100 mg.ml <sup>-1</sup> PVP.....	128
<b>Part B: Cell-soluble extract (CSE) investigations.....</b>	<b>128</b>
5.3.1.4. Effect of PVP on the Pt(IV) bioreductive mechanism of CSE...	128
5.3.1.5. Effect of crude CSE protein as a biological capping agent.....	130
5.3.1.5.1. TEM analysis of CSE as a biological capping agent.....	134
5.3.1.6. Bioreductive mechanism and nanoparticle morphology.....	135
5.3.1.6.1. Effect of temperature.....	135
5.3.1.6.2. TEM analysis of temperature samples.....	138
5.3.1.6.3. Effect of pH.....	139
5.3.1.6.4. TEM analysis of pH samples.....	142
5.3.1.7. Investigating the hydrogenase activity of CSE.....	144
<b>5.4. Summary &amp; Conclusions.....</b>	<b>146</b>
<b>CHAPTER SIX: General discussion and conclusions.....</b>	<b>147</b>
<b>6.1. Introduction.....</b>	<b>147</b>
<b>6.2. Elucidating the bioreductive mechanism of Pt(IV) by an unknown consortium of sulfate-reducing bacteria.....</b>	<b>148</b>
<b>6.3. Periplasmic hydrogenase: Role in the bioreductive mechanism of Pt(IV) to Pt(0).....</b>	<b>149</b>
<b>6.4. Screening an SRB cell-free crude extract for Pt(IV) reductase activity and metal nanoparticle synthesis.....</b>	<b>151</b>
<b>6.5. Effects of experimental factors on biogenic nanoparticle morphology.....</b>	<b>153</b>
<b>6.6. Future work.....</b>	<b>155</b>

**REFERENCES.....156**

**APPENDICES.....177**

Appendix A: Modified Postgate Medium - C.....177

Appendix B: Buffer recipes.....178

Appendix C: Bradford standard curves.....179

Appendix D: Platinum salt standard curves.....181

Appendix E: Spectrum scan of platinum salts.....185

Appendix F: Native-PAGE Recipes for the Bio-Rad Mini-Protean II apparatus.....186

\*\*\*\*\*

**Publications from research:**

1) Govender Y, Riddin TL, Gericke M and Whiteley CG (2008), “Bioreduction of platinum salts into nanoparticles: a mechanistic perspective”, *Biotechnol. Lett.*, DOI 10.1007/s10529-008-9825-z.

2) Riddin TL, Gericke M & Whiteley CG (2006), “Analysis of the inter- and extracellular formation of platinum nanoparticles by *Fusarium oxysporum* f. sp. *lycopersici* using response surface methodology”, *Nanotechnology*, **17**:3482-3489.

---

---

## LIST OF FIGURES

---

---

<b>Figure 1.1:</b> Typical conformations of NP's acting as a scaffold upon which other biomolecules, such as fluorescent signalling probes and peptides, can be attached (Adapted from Salata, 2004).....	2
<b>Figure 1.2:</b> The Bohr radius of a Hydrogen atom as described by Niels Bohr (Adapted from Mills, 2000).....	4
<b>Figure 1.3:</b> Hypothesised mechanism adapted from Durán <i>et al.</i> , 2005, for the extracellular formation of silver and gold NP's by three <i>Fusarium oxysporum</i> fungi.....	7
<b>Figure 1.4:</b> Passive Process. The metal cations are expected to interact with anionic sulfhydryl groups on cysteine residues and/or imidazole rings of histidine residues of metallothioneins. It is hypothesised that the position of these residues on metal binding peptides may be responsible for the template-like formation of geometric NP's in biological systems such as fungi .....	8
<b>Figure 1.5:</b> The Active process. The positively charged metal-ion acts as an electron acceptor becoming reduced to a neutral species (Riddin, <i>et al.</i> , 2006).....	9
<b>Figure 1.6:</b> Diagrammatic representation of hydrogen activation by hydrogenase (Adapted from De Lacy <i>et al.</i> , 2000).....	17
<b>Figure 1.7:</b> <b>A)</b> ATP synthesis and electron shuttling in sulfate-reducing bacteria (Adapted from Madigan <i>et al.</i> , 2000), <b>B)</b> Dissimilatory sulfate reduction in sulfate-reducing bacteria (Adapted from Gibson, 1990).....	23

**Figure 2.1:** Bioreactor set-up (Adapted from Oyekola & Pletschke, 2006). [A) Clamp, B) Sampling pipe, C) Magnetic stirrer, D) 10/5L Bioreactor, E) Magnetic stirrer bar, F<sub>1</sub>) & F<sub>2</sub>) Rubber stopper, G) Gas inlet pipe, H) H<sub>2</sub>S outlet pipe, I) Zinc Acetate trap.].....35

**Figure 2.2:** Metabolic growth of a consortium of sulfate-reducing bacteria. [I) OD<sub>600</sub> and pH readings of BR1 over time. A typical bacterial growth curve was observed over the 9 day period consisting of a relatively insignificant lag phase (A), an exponential growth phase (B) and a stationary phase (C) (Zwietering *et al.*, 1990). II) Sulfate reduction and formation of sulfide during metabolism of sulfate reducing bacteria.].....36

**Figure 2.3:** Reduction of Pt(IV) in the presence of viable SRB cells and hydrogen. [Test: SRB cells + H<sub>2</sub>(g) + Pt(IV), Control: Cell-free + H<sub>2</sub>(g) + Pt(IV).].....38

**Figure 2.4:** Bioreduction of Pt(IV) by SRB cells [I) Pt(IV) reduced by SRB consortium over time. II) Normalised data illustrating the amount of Pt(IV) reduced by an SRB consortium over time.].....41

**Figure 2.5:** Comparison of the reduction rates of Pt(IV). [Section 2.3.2.1: Test) Cells + Pt(IV) + H<sub>2</sub>(g) bubbled through, Control) Cell-free + Pt(IV) + H<sub>2</sub>(g) bubbled through. Section 2.3.2.2: A) Cells + Pt(IV) + H<sub>2</sub>(g), B) Cells + Pt(IV) + N<sub>2</sub>(g),, C) Heat-killed cells + Pt(IV) + H<sub>2</sub>(g).].....45

**Figure 2.6:** Bioreduction of Pt(II) by SRB cells. [I) Formation and subsequent reduction of Pt(II) by SRB consortium over time. II) Normalised data for the formation and subsequent reduction of Pt(II) by SRB consortium over time.].....46

**Figure 2.7:** The reduction of Pt(IV) over time by the current consortium of SRB under an aerobic atmosphere with no exogenous electron donor .....49

**Figure 2.8:** These figure shows the conversion of Pt(IV) -> Pt(II) -> Pt(0) over time for the sample with **A)** hydrogen as the exogenous electron donor and **B)** no exogenous electron donor.....51

**Figure 2.9:** Control cells not challenged with Pt(IV). [**A<sub>1</sub>**] + **A<sub>2</sub>**): TEM images of control cell sample. Scale bars = 500 nm and 1000 nm respectively. **B)** SEM-EDAX spectrum of control sample.....54

**Figure 2.10:** Cell-free control from section 2.3.2.1., incubated with Pt(IV) under high hydrogen concentration. [**A<sub>1</sub>**] A TEM image illustrates the presence Pt(0) particles formed by the abiotic reduction of Pt(IV) by hydrogen. Scale bar = 500 nm. **A<sub>2</sub>**) enlarged version of **A<sub>1</sub>**. **B)** The EDAX spectrum obtained from a sample of the cell-free control.].....55

**Figure 2.11:** Cells incubated in Pt(IV) with hydrogen bubbled through as electron donor. [**A<sub>1</sub>**] TEM image of cells with platinum deposits in the periplasm. Scale bar = 500 nm. **A<sub>2</sub>**) Image showing selective Pt(0) uptake. Scale bar = 1000 nm. **B)** EDAX graph of this sample indicating presence of platinum.].....56

**Figure 2.12:** **A<sub>1</sub>**) TEM image of SRB consortium with no exogenous hydrogen. Scale bar = 1000 nm. **A<sub>2</sub>**) SRB cell showing electron dense deposits in the periplasm. Scale bar = 500 nm. **B)** EDAX spectrum of sample with no exogenous hydrogen.....57

**Figure 2.13:** TEM image of heat-killed SRB cell with surface-localised platinum deposits. [Scale bar = 500 nm.].....58

**Figure 3.1:** Bioreduction of Pt(IV) by whole cells pretreated with CuCl<sub>2</sub>.6H<sub>2</sub>O. [**Inset** - Image of samples post bioreduction.].....66

**Figure 3.2:** Formation and subsequent reduction of Pt(II) from Pt(IV).....68

<b>Figure 3.3:</b> Bioreduction of Pt(II) salt $\text{Na}_2\text{PtCl}_4$ by whole cells pre-treated with Cu(II) [Inset: Samples post bioreduction.].....	70
<b>Figure 3.4:</b> Bioreduction of Pt(II). <b>I)</b> Abiotic reduction of Pt(II) salt $\text{Na}_2\text{PtCl}_4$ , <b>II)</b> Graph showing small percentage of re-oxidation of Pt(II) back to Pt(IV).].....	71
<b>Figure 3.5:</b> Reduction of the methyl-viologen ion by whole cells pre-treated with Cu(II). .....	72
<b>Figure 3.6:</b> Screening for Pt(IV) reduction by native SRB cells. [ <b>A</b> <sub>1+2</sub> ) TEM images of cells with electron dense metal deposits within the periplasmic regions. Scale bars = 500 nm respectively. <b>B)</b> EDAX graph of sample clearly showing the presence of Pt(0).].....	74
<b>Figure 3.7:</b> Screening for Pt(II) reduction by native SRB cells. [ <b>A</b> <sub>1+2</sub> ) TEM images of cells with electron dense metal deposits within the periplasmic regions. Scale bars = 1000 nm and 500 nm respectively. <b>B)</b> EDAX graph of sample clearly showing the presence of Pt(0).].....	75
<b>Figure 3.8:</b> Screening for platinum ion reduction by SRB cells pre-treated with 0.5 mM Cu(II). [ <b>A</b> <sub>1+2</sub> ) TEM images of cells with low concentrations of electron dense metal deposits within the periplasmic regions, as well as on the cell surface. Scale bars = 500 nm respectively. <b>B)</b> EDAX graph of above sample showing low levels of Pt(0).].....	76
<b>Figure 3.9:</b> Screening for platinum ion reduction by SRB cells pre-treated with 5 mM Cu(II). [ <b>A</b> <sub>1+2</sub> ) TEM images of cells with particularly low concentrations of electron dense metal deposits within the periplasmic regions. Majority of the metal is located on the cell surface. Scale bars = 500 nm respectively].....	77

<b>Figure 4.1:</b> Cell-free control samples [A ) Pt(IV) at various concentrations, B) pH over time for control samples, C <sub>1+2</sub> ) Images of control sample post bioreduction.].....	85
<b>Figure 4.2:</b> Bioreduction of Pt(IV) < 1 mM by CSE. [A) Pt(IV) reduction curve, B) Spectrum scan of a 0.5 mM sample over 8 h.].....	87
<b>Figure 4.3:</b> Pt(0) formation over time at 334 nm.[Inset: Image of samples post bioreduction.].....	88
<b>Figure 4.4:</b> pH of the bioreductive samples over time.....	89
<b>Figure 4.5:</b> Effect of Pt(IV) concentration >= 1 mM. [A ) Pt(IV) reduction curve, B) Linearised reduction curve of samples >= 1 mM.].....	90
<b>Figure 4.6:</b> A <sub>334</sub> readings for samples >= 1 mM Pt(IV) [Inset: Image of samples post bioreduction].....	91
<b>Figure 4.7:</b> Change in pH of samples over time.....	92
<b>Figure 4.8:</b> Change in protein concentration of samples over time.....	92
<b>Figure 4.9:</b> Continuous native-PAGE gel (7.5 %) of crude CSE solution 1) pre and 2) post bioreduction of 0.75 mM Pt(IV). [The arrows A-J indicate the major protein bands from the CSE solution prior bioreduction, while the arrows L and K indicate the only protein bands visible post bioreduction.].....	94
<b>Figure 4.10:</b> EDAX spectrum of CSE sample post bioreduction of Pt(IV).....	95
<b>Figure 4.11:</b> Control samples in sodium-bicarbonate buffer (200 mM, pH 9). [A) Pt(IV) concentration over time; B) pH over time for control samples, C <sub>1+2</sub> ) Images of controls post bioreduction.].....	97



<b>Figure 4.12:</b> Investigating the effect of a sodium-bicarbonate (200 mM, pH 9) buffer on the bioreduction mechanism.....	98
<b>Figure 4.13:</b> Comparison of Pt(IV) concentration in test (T) versus control (C) experiments.....	98
<b>Figure 4.14:</b> Pt(0) formation over time [Inset: Image of samples post bioreduction.].....	99
<b>Figure 4.15:</b> pH of samples over time.....	100
<b>Figure 4.16:</b> Bioreduction of Pt(IV). [A] Pt(IV) concentration over time, B) Pt(IV) reduction rate.].....	102
<b>Figure 4.17:</b> Formation of Pt(0) over time. [Inset: Image of samples post bioreduction.].....	103
<b>Figure 4.18:</b> pH of samples over time.....	104
<b>Figure 4.19:</b> Comparing the reduction of the Pt(IV) ion. I) < 1 mM Pt(IV) and II) >= 1 mM in B) sodium-bicarbonate buffer (200 mM, pH 9) and W) in ddH <sub>2</sub> O.].....	105
<b>Figure 4.20:</b> TEM images comparing the particles (<1 mM) post bioreduction in water versus SBC. [A) 0.35 mM in ddH <sub>2</sub> O. Scale bar = 1000 nm, B) 0.35 mM in SBC. Scale bar = 5000 nm, C) 0.5 mM in ddH <sub>2</sub> O. Scale bar = 500 nm, D) 0.5 mM in SBC. Scale bar = 2000 nm, E) 0.75 mM in ddH <sub>2</sub> O. Scale bar = 2000 nm, F) 0.75 mM in SBC. Scale bar = 2000 nm.] .....	106
<b>Figure 4.21:</b> TEM images comparing the particles (>=1 mM) post bioreduction in water vs SBC [A) 1 mM in ddH <sub>2</sub> O. Scale bar = 2000 nm, B) 1 mM in SBC. Scale bar = 2000 nm, C) 2 mM in ddH <sub>2</sub> O. Scale bar = 2000 nm, D) 2 mM in SBC. Scale bar = 1000 nm,	

**E)** 3 mM in ddH<sub>2</sub>O. Scale bar = 1000 nm, **F)** 3 mM in SBC. Scale bar = 500 nm.].....108

**Figure 4.22:** The bioreduction of the Pt(II) ion by CSE over time. [**A)** Spectrum scan showing interference from NP spectrum, **B)** Formation of Pt(0) at 334 nm; **Inset** – Image of the test sample (T) and control (C) post bioreduction.].....111

**Figure 4.23:** Examples of particles from the bioreduction of Pt(II) [**A)** Particles bound to protein matrix, **B)** Irregular particles free in solution. Scale bar = 500 nm in both cases.].....113

**Figure 5.1:** Effect of PVP on the reduction rate by SRB cells.....120

**Figure 5.2:** Formation of Pt(0) NP's in the extracellular solution, in the presence of SRB cells, challenged with Pt(IV) in the presence of PVP [**Inset:** Supernatant of samples post bioreduction **A)** PVP-free, **B)** 20 mg.ml<sup>-1</sup> PVP, **C)** 100 mg.ml<sup>-1</sup> PVP.].....121

**Figure 5.3:** SRB cells challenged with Pt(IV) in the presence of 20 mg.ml<sup>-1</sup> PVP [**A<sub>1+2</sub>**) TEM images of cells with plate-like platinum deposits in the periplasmic space. Scale bars = 500 nm in both cases. **B)** Small platinum peaks on the EDAX graph suggest low amounts of Pt(0) present.].....123

**Figure 5.4:** SRB cells challenged with Pt(IV) in the presence of 100 mg.ml<sup>-1</sup> PVP [**A<sub>1</sub>**) TEM images of samples with extracellular platinum deposits, and **A<sub>2</sub>**) Cells with a low concentration of platinum deposits in the periplasmic space. Scale bars = 500 nm in both cases. **B)** Small platinum peaks on the EDAX graph suggest low amounts of Pt(0) present.].....124

**Figure 5.5:** TEM images of the 20 mg.ml<sup>-1</sup> PVP supernatant solution after 24 h. [**A)** Image depicting various conformations of NP's formed by irradiation with the electron

beam. Scale bar = 100 nm. **B)** Image illustrating the formation of NP's within grooves of the carbon coated TEM grid. Scale bar = 200 nm.].....125

**Figure 5.6:** Sequence of TEM images illustrating the dissipation and collapse of a rectangular NP after 60 sec irradiation under the TEM electron beam. [**A)** 0 sec, **B)** 20 sec, **C)** 40 sec **D)** 60 sec. Scale bar = 200 nm in all cases.].....127

**Figure 5.7:** Interference of Pt(0) NP's in the determination of the Pt(IV) ion. [**Inset:** Spectrum scan showing formation of NP spectrum interfering with determination of Pt(IV) ion at 261 nm. **Blue line)** 0 h, **Pink line)** 0.5 h, **Orange line)** 8 h.].....129

**Figure 5.8:** Bioreduction of Pt(IV) and NP formation by CSE in the presence of PVP. [**Inset:** Image of 20 mg.ml<sup>-1</sup> PVP sample and 100 mg.ml<sup>-1</sup> PVP sample post bioreduction.].....129

**Figure 5.9:** Initial spectrums at 0 h, for various CSE concentrations.....130

**Figure 5.10:** Bioreduction of Pt(IV) in the presence of varying CSE protein concentration. [**A)** Pt(IV) reduction and interference by Pt(0) NP's. **B)** Formation of Pt(0) NP's over time. **Inset:** 50 µg.ml<sup>-1</sup>, 250 µg.ml<sup>-1</sup>, 500 µg.ml<sup>-1</sup> post bioreduction.].....132

**Figure 5.11:** Change in pH over time.....133

**Figure 5.12:** TEM images of CSE samples. [**A<sub>1+2</sub>)** 50 µg/ml CSE, **B<sub>1+2</sub>)** 250 µg/ml CSE, **C<sub>1+2</sub>)** 500 µg/ml CSE. Scale bar = 1000 nm in all cases.].....134

**Figure 5.13:** Effect of temperature on the bioreductive mechanism. [**A)** Pt(IV) reduction and interference by NP's. **B)** Formation of Pt(0) NP's over time. **Inset:** Images of samples post bioreduction.].....136

**Figure 5.14:** Change in A<sub>334</sub> of control samples.....137

**Figure 5.15:** TEM images of samples exposed to various temperatures. [**A**<sub>1+2</sub>) 25 °C. Scale bar = 2000 nm & 500 nm, **B**<sub>1+2</sub>) 45 °C. Scale bar = 2000 nm & 200 nm. **C**<sub>1+2</sub>) 65 °C. Scale bar = 2000 nm & 2000 nm.].....138

**Figure 5.16:** Effect of pH on the bioreductive mechanism. [**A**) Pt(IV) reduction and interference by NP's. **B**) Formation of Pt(0) NP's over time. **Inset:** Images of samples post bioreduction.].....140

**Figure 5.17:** Change in absorbance at A<sub>334</sub> for the control samples.....142

**Figure 5.18:** TEM images of samples. [**A**<sub>1+2</sub>) pH 7.6. Scale bar = 1000 nm & 200 nm, **B**<sub>1+2</sub>) pH 9. Scale bar = 2000 nm & 2000 nm. **C**<sub>1+2</sub>) pH 11. Scale bar = 2000 nm & 1000 nm.].....143

**Figure 5.19:** Hydrogenase activity of CSE samples [**A**) Change in A<sub>604</sub> over time, **B**) Activity of CSE samples (nmoles.min<sup>-1</sup>.ml<sup>-1</sup>). **CSE + N2**) CSE prior bioreduction not pre-activated, kept under N<sub>2</sub>, **CSE + H2**) CSE prior bioreduction preactivated under H<sub>2</sub>, **CSE/Pt + N2**) CSE post bioreduction of Pt(IV) not pre-activated, kept under N<sub>2</sub>]......144

**Figure 6.1:** Newly proposed mechanism of Pt(IV) reduction by micro-organisms.....150

---

---

## LIST OF TABLES

---

---

<b>Table 1.1:</b> Optical properties of metal NP's of varying size and shape.....	3
<b>Table 1.2:</b> Organisms confirmed in the bioreduction of metal-ions.....	5
<b>Table 1.3:</b> Example of hard and soft acids as classified by Pearson's HSAB theory.....	11
<b>Table 1.4:</b> Properties of platinum.....	18
<b>Table 1.5:</b> Characteristics of the sulfate-reducers (Adapted from Madigan <i>et al.</i> 2000).....	21
<b>Table 1.6:</b> Examples of metabolic reactions of the sulfate-reducing bacteria (Adapted from Gibson, 1990).....	24
<b>Table 4.1:</b> Comparison of the size distributions for various samples.....	110

---

---

## LIST OF ABBREVIATIONS

---

---

### **A**

A<sub>334</sub> - Absorbance at 334 nm wavelength

Ag - Silver

APSRase - Adenophosphosulpho  
reductase

ATP - Adenosine triphosphate

Au - Gold

### **B**

BR - Bioreactor

BSA - Bovine Serum Albumin

### **C**

CA - Capping agent

Cd - Cadmium

Cl - Chlorine

CO<sub>2</sub> - Carbon dioxide

CPA - Chloroplatinic acid

Cr - Chromium

CSE - Cell-soluble extract

Cu - Copper

Cyt c<sub>3</sub> - Cytochrome c<sub>3</sub>

### **D**

DNA - Deoxyribonucleic acid

### **E**

EBRU - Environmental

Biotechnological Research Unit

EDAX - Energy dispersive analysis of  
X-rays

### **F**

FADH – Flavin adenine dinucleotide

Fe - Iron

### **H**

h - Hour

H<sub>2</sub> - Hydrogen

H<sub>2</sub>O - Water

H<sub>2</sub>S - Hydrogen sulfide

H<sub>ase</sub> - Hydrogenase

HC MAb - Heavy-chain monoclonal  
antibody

Hmc - High molecular weight  
cytochrome

HSAB - Hard-Soft-Acid-Base

### **I**

Ir – Iridium

## **K**

K - Kelvin

kDa - Kilodaltons

kV - Kilovolts

## **M**

min - Minutes

mM - Millimolar

MV - Methyl viologen

MW - Molecular weight

MWCO - Molecular Weight Cut-Off

## **N**

N - Nitrogen

NADP - Nicotinamide adenine  
dinucleotide phosphate

NADPH - Nicotinamide adenine  
dinucleotide phosphate (reduced form)

Ni - Nickel

nm – Nanometer

nM - Nanomolar

NP - Nanoparticle

## **O**

O - Oxygen

OD - Optical density

Os - Osmium

## **P**

P - Phosphate

PAGE - Polyacrylamide gel  
electrophoresis

Pd - Palladium

PGC - Postgate medium C

PGM - Platinum Group Metals

PP<sub>i</sub> - Pyrophosphate

Pt - Platinum

PTFE - polytetrafluoroethylene

PVP - Polyvinylpyrrolidone

## **Q**

QD - Quantum dot

## **R**

RNA - Ribonucleic acid

RT - Room temperature

## **S**

S - Sulfur

SBC - Sodium bicarbonate

Se - Selenium

SEM - Scanning electron microscopy

SET - Single-electron transistor

SOD - Superoxide dismutase

SOR - Superoxide reductase

SRase - Sulfite reductase

SRB - Sulfate-reducing bacteria

S<sup>2-</sup> - Sulfide

SO<sub>3</sub><sup>-</sup> - Sulfite

SO<sub>4</sub><sup>2-</sup> - Sulfate

**T**

TEM - Transmission electron  
microscopy

Tc - Technetium

**U**

U - Uranium

UV-Vis - Ultraviolet-Visible

**W**

W - Watt

**Z**

Zn – Zinc



---

---

## ACKNOWLEDGEMENTS

---

---

- Mintek, South Africa for their financial assistance and guidance throughout this project.
- The financial assistance from the Andrew Mellon Mentors Scholarship towards this research is hereby acknowledged. Opinions expressed and conclusions arrived at, are those of the author and are not necessarily to be attributed to Rhodes University or the donor.
- My supervisor, Professor CG Whiteley.
- Rhodes EM Unit staff, Mrs S. Pinchuck and Mr M. Randall.
- Professor J. Neethling, Professor M. Lee and Dr N. Hashe from the Nelson Mandela Metropolitan University (NMMU).
- My family; Winston and Marinda, Nicole and Bob. Thank you for putting up with me and for your endless support.
- Lab 309 members.

## **CHAPTER ONE: Literature Review**

---

---

### **1.1. Introduction: Nanoparticles and nanobiotechnology**

Nanoparticles (NP's), in the range of one to a few hundred nanometers, are found to have novel magnetic, electronic and optical properties dependent on their shape, size and composition (Mukherjee *et al.*, 2002). "Nanobiotechnology" is a multi-disciplinary field derived from the experimental use of these NP's in biological systems (Penn *et al.*, 2003, Salata, 2004), including the sciences of biology, biochemistry, engineering, chemistry, physics and metallurgy. The field of nanobiotechnology encompasses the use of various NP's and nanowires of various compositions, in conjunction with biomolecules, to demystify many biological processes and provide diagnostic and treatment options for previously untreatable diseases or ailments. There is much excitement around emerging nanotechniques which are far surpassing current biochemical, medical and diagnostic methods. NP's are set to revolutionise many areas of science, with a number of NP's already in use today in various areas such as cosmetics, due to their light reflective properties, and computer chip technology in the miniaturisation of components (Panyam & Labhasetwar, 2003).

NP's exist in a variety of forms, from nanowires to magnetic, noble and transition metals and non-metal water-soluble nanocrystals or quantum dots (QD's), all of which are exceptionally versatile and highly stable. Their small size allows them to interact with proteins and pass through most of the cellular machinery unnoticed by the immune system as the larger protein acts as a shield from any immune response. NP's have the desirable ability to act as a "scaffold", as they allow for the attachment of biomolecules through a number of methods including covalent and hydrogen bonding. The attachment of biomolecules such as antibodies, peptides, proteins and even DNA onto NP's, extend their already exceptional versatility (Vinogradov *et al.*, 2002) (Fig 1.1). These

interactions are surprisingly robust due to the increase in reactivity provided by the large surface-area-to-mass ratio of NP's (Aitken *et al.*, 2004).

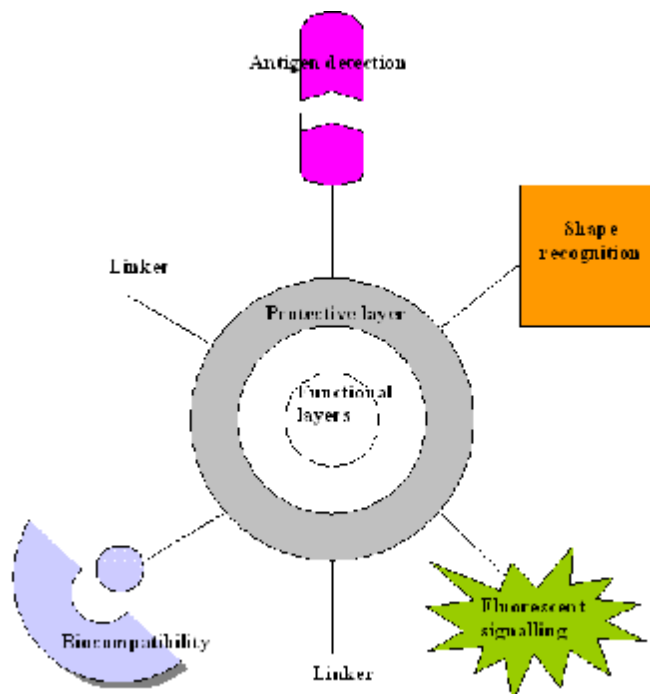


**Figure 1.1:** Typical conformations of NP's acting as a scaffold upon which other biomolecules, such as fluorescent signalling probes and peptides, can be attached (Adapted from Salata, 2004).

## 1.2. Applications of nanoparticles

A multitude of possible applications of metallic NP's exist, including single-electron transistors (SET's) (Bolotin *et al.*, 2004), fuel cells (Wazsozuk *et al.*, 2001), fluorescent labelling of biological components (Ravnic *et al.*, 2007), DNA/RNA detection via binding of DNA/RNA specific probes (Thaxton *et al.*, 2005), as well as potential uses in biomedical diagnostic devices (Jain, 2005), biosensors (Guo *et al.*, 2007), nanocomputers (Mandal *et al.*, 2005) and drug and gene transport systems (Panyam & Labhasetwar, 2003). The exotic properties of these NP's play an essential role in the potential advancement of these applications, as new avenues of research are being investigated due to the new possibilities that NP's have provided. Platinum group metals and NP's are highly significant in the industrial production of fuel cells while gold NP's have currently come under investigation in catalysis research. Currently, research is being done on the

combined effects of gold and platinum NP's, and results are suggesting that the combination of these two metals are providing far more advantages in the areas of pollution control and fuel cell production, than either of these two metals have previously been capable of alone (Thompson, 2005). A process through which the properties of these NP's can be controlled and manipulated may therefore prove to be revolutionary to many sciences (Sastry *et al.*, 2003).







### 1.3. Metal nanoparticles

The unique properties of metal NP's are determined by their size and shape which are, however, drastically hindered by current chemical production processes such as chlorine leaching and ion exchange resins which generally result in spherical NP's. A wide variety of geometric metal NP's have been found to be produced by both prokaryotic and eukaryotic organisms including bacteria, fungi, actinomycetes and yeasts (Ahmad *et al.*, 2003; Mukherjee *et al.*, 2003; Sastry *et al.*, 2003). This bioreduction of metal particles is expected to occur via an active or passive process, a combination of the two, or through the active interaction of unique nitrate-dependant reductase enzymes with certain quinones and their derivatives. In both cases, the process is hypothesised to be part of an organism's enzymatic survival mechanism, as a build up of metal-ions within a biological system could prove to be toxic (Durán *et al.*, 2005; Ibrahim *et al.*, 2001).

#### 1.3.1. Properties of metal nanoparticles

The optical properties of NP's are determined by their size and shape (see Table 1.1) (Ahmad *et al.*, 2003).

**Table 1.1:** Optical properties of metal NP's of varying size and shape:

<b>Metal</b>	Silver (Ag)	Gold (Au)	Gold (Au)	Gold (Au)	Silver (Ag)	Silver (Ag)
<b>Size</b>	100 nm	100 nm	100 nm	50 nm	90 nm	40 nm
<b>Shape</b>						
<b>Colour</b>	Red	Yellow	Orange	Green	White	Blue

The properties of NP's become most pronounced when the particles are physically smaller than the "exciton Bohr radius" of the compound which they are composed of (Beard *et al.*, 2002). The "Bohr radius", as explained by Niels Bohr, is the smallest and lowest energy level orbital for the single electron within a hydrogen atom. An "exciton" is an electron/hole pair in a hydrogen atom-like state with an electron (negative charge) and the hole (positive charge), which undergoes a Coulombic interaction and results in a bound entity. The "spatial distance" between the electron/hole pair is defined as the "exciton Bohr radius" of a particular compound (usually 1-5 nm). This nanoscale size results in "the quantum confinement effect", where the exciton of the particle is confined to an area which is physically smaller than the exciton Bohr radius resulting in the unique properties possessed by these particles (Sun *et al.*, 2001; Beard *et al.*, 2002) (Fig 1.2).

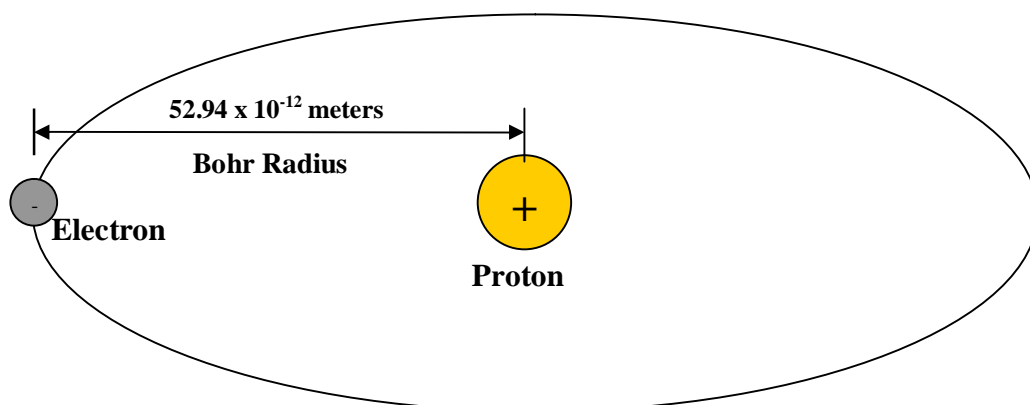


**Figure 1.2:** The Bohr radius of a Hydrogen atom as described by Niels Bohr (Adapted from Mills, 2000).

### 1.3.2. Synthesis methods for metal nanoparticles

#### 1.3.2.1. Chemical synthesis

Outdated industrial chemical techniques, including ion exchange resins, are currently employed in the production of metal NP's (Gamez *et al.*, 2003). Ion exchange resins have been used to produce nickel NP's varying in size from 3-5 nm. The nickel ions are initially adsorbed onto a polyimide surface and become reduced to nickel NP's via hydrogen reduction (Akamatsu *et al.*, 2003). These chemical methods are complicated, costly, inefficient and produce hazardous wastes which pose a sizeable risk to the environment and human health (Gamez *et al.*, 2003). A further disadvantage of these

methods is due to the fact that the shape of the NP's produced are generally limited to spheres, which in turn greatly limits their potential properties <sup>1</sup>.

The production of particles in the micrometer range ( $10^{-6}$  m) occurs by a “top-down” approach, meaning that particles of this size are formed by the whittling down of larger molecules by various chemical processes, including reduction reactions. The initial hurdle in NP synthesis, however, lay in the fact that this top-down approach could not be used due to the laws of physics, which become limiting on a nanoscale due to the effects of quantum confinement on the particle's electrons, as described earlier. Hence, a new “bottom-up” developmental approach was sought, in which the NP's are “built up”, atom by atom by self-organisation or self-assembly (Seeman & Belcher, 2002; La Van *et al.*, 2003).

#### 1.3.2.2. Biological synthesis

Both prokaryotic and eukaryotic organisms (see Table 1.2) synthesise biogenic geometric metal particles, in the nanometer range via a bioreductive process, with no added steric stabiliser, when exposed to metal chloride solutions (Ahmad *et al.*, 2003; Mukherjee *et al.*, 2003; Sastry *et al.*, 2003).

**Table 1.2:** Organisms confirmed in the bioreduction of metal-ions.

<b>Yeast</b>	<i>Schizosaccharomyces</i>			
<b>Bacteria</b>	<i>Pseudomonas</i>	<i>Bacillus</i>	<i>Desulfovibrio</i>	<i>Lactobacillus</i>
<b>Fungi</b>	<i>Fusarium</i>	<i>Verticillium</i>		
<b>Actinomycete</b>	<i>Rhodococcus</i>			

Metal NP's have novel magnetic, electronic and optical properties which vary on the basis of their shape, size and composition (Mukherjee *et al.*, 2002). The optical properties of NP's are highly desirable due to the fact that they have “tunable” emission spectra, and can therefore be made to order for a number of applications such as fluorescent

<sup>1</sup> Private communication from Mintek, (Pty) Ltd., South Africa

labelling, which requires labels with narrow absorption wavelengths for multi-labelling experiments (Wu *et al.*, 2005).

### 1.3.3. The “Active” versus “Passive” mechanism debate

A number of possible options exist which may explain the process of metal reduction in these organisms. An article by Durán and colleagues (2005), described a hypothesis with supporting experimental data of the mechanistic action of extracellular silver and gold NP formation by the fungus *Fusarium oxysporum*. They suggested that a nitrate-dependant reductase, in conjunction with an extracellular electron shuttle process involving quinones is responsible for the extracellular formation of noble metal NP's. Duran and co-workers followed protocols by Mukherjee *et al.* (2002) by performing screening experiments on three *Fusarium oxysporum* fungi and a single *Fusarium moniliforme* strain for both gold and silver NP formation. They found that, all *Fusarium oxysporum* strains screened, resulted in the formation of Ag and Au NP's at an extracellular level, while the *Fusarium moniliforme* strain did not result in any NP formation either intracellularly or extracellularly as documented earlier by Mukherjee *et al.*(2002). Duran and co-workers went on to explain that both *Fusarium* fungi contained similar reductase enzymes, thought to be significant in ferric iron ( $\text{Fe}^{3+}$ ) reduction. One specific reductase, unique to *Fusarium oxysporum*, was involved in the reduction of Ag(I) and/or Au(I) to Ag(0) and/or Au(0) respectively. Furthermore, they stated that naphthaquinones, anthraquinones and their derivatives were acting as potential electron shuttle systems since naphthaquinones were present in both *Fusarium* fungi, while anthraquinones were only found in *Fusarium oxysporum* strains. From this they hypothesised that noble metal-ion reduction occurs by the joint action of anthraquinones and the reductase enzyme found to be unique to *Fusarium oxysporum* strains (Fig 1.3).

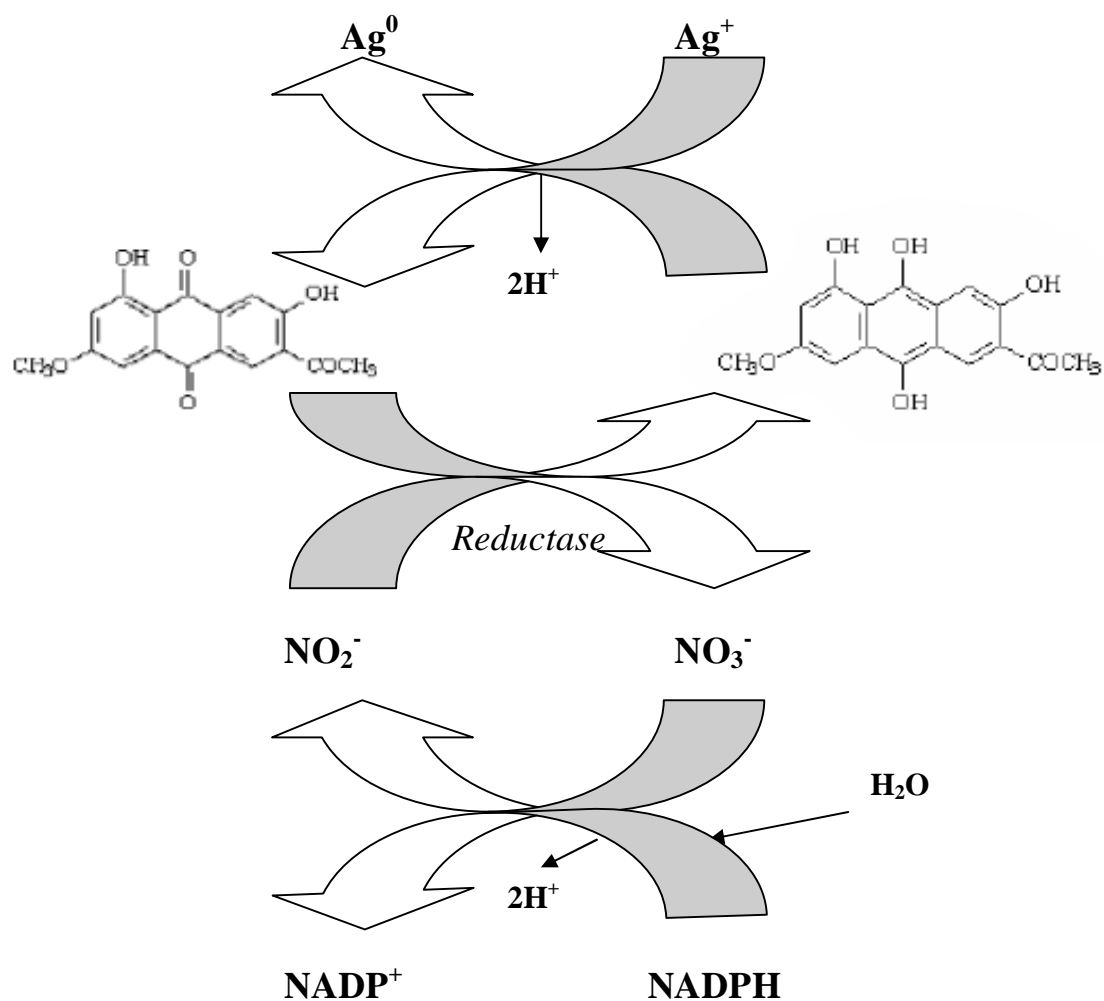


**Figure 1.3:** Hypothesised mechanism adapted from Durán *et al.*,(2005), for the extracellular formation of silver and gold NP's by three *Fusarium oxysporum* fungi.

A slightly different approach includes the hypothesis that this bioreduction of metal-ions occurs through a passive process. This involves the interaction of the positively charged metal-ions with the negative sulfhydryl groups on the cysteine residues or imidazole rings on histidine residues of metallothioneins (metal binding peptides) (Fig 1.4). The location of the cysteine/histidine residues may potentially be involved in a template-like aggregation of the metal particles resulting in the geometric shapes observed (i.e. Table 1.1)<sup>1</sup>.

<sup>1</sup> Private communication from Mintek, (Pty) Ltd., South Africa



The active process involves a reductase/hydrogenase enzyme, possibly in conjunction with an electron shuttling compound such as quinones or cytochrome  $c_3$ , where the metal-ions function as electron acceptors thereby becoming reduced to neutral metal species by the mechanism illustrated in Fig 1.5. The neutral particles then precipitate out of solution and accumulate by nucleation/bioaccumulation either on the cell wall/membrane or extracellularly (Carpentier *et al.*, 2003;<sup>1</sup>). From these results it is anticipated that the bio-reduction of platinum ions into metal NP's may occur in a similar fashion with enzymes from other micro-organisms.

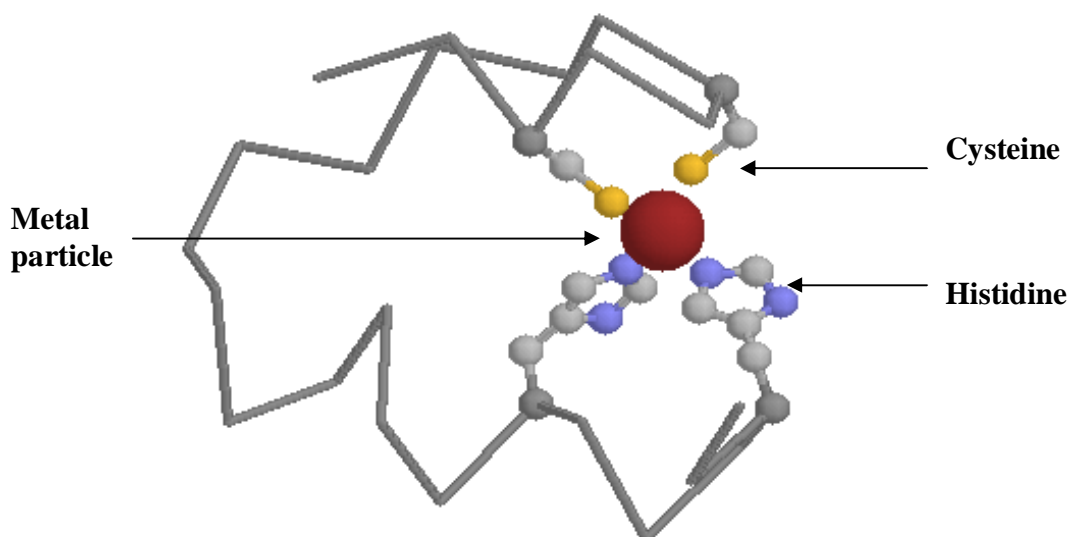


**Figure 1.4:** Passive Process. The metal cations are expected to interact with anionic sulfhydryl groups on cysteine residues and/or imidazole rings of histidine residues of metallothioneins. It is hypothesised that the position of these residues on metal binding peptides may be responsible for the template-like formation of geometric NP's in biological systems such as fungi <sup>1</sup>.

Such a biological route involving micro-organisms, provides great advantages over traditional methods, as it has the potential to be a cost efficient, simple, environmentally friendly and efficient form of metal NP synthesis, which could produce NP's that are not

---

<sup>1</sup> Private communication from Mintek, (Pty) Ltd., South Africa

only superior in quality, but far simpler to produce. The primary advantage of a biological route is the ability to manipulate the properties of the NP's by gaining control over the mechanism that determines their size and shape (Mukherjee *et al.*, 2002; Ahmad *et al.*, 2003). A potential obstacle, however, could lie in the toxicity level caused by metal accumulation within these organisms (Valix & Loon, 2003).

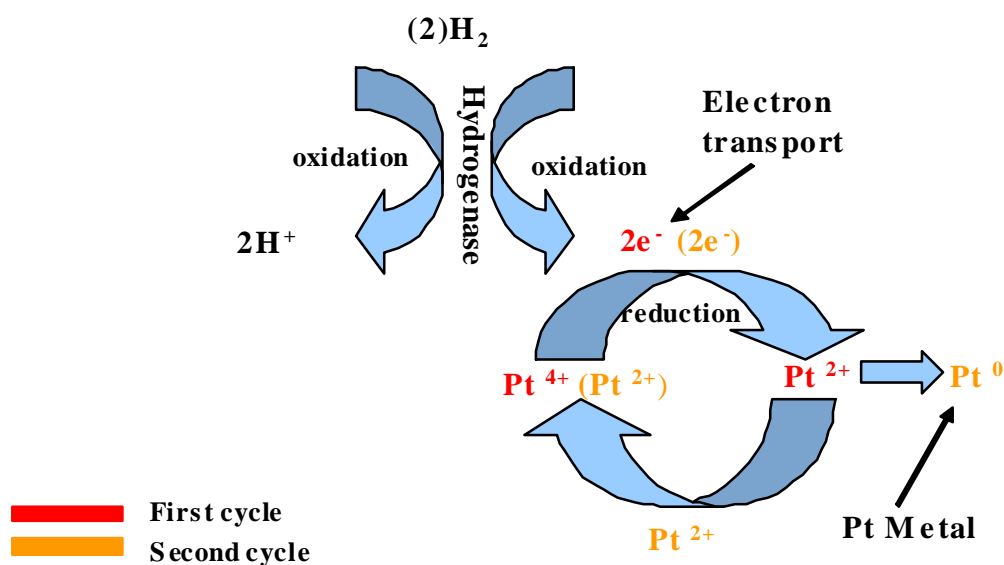


**Figure 1.5:** The Active process. The positively charged metal-ion acts as an electron acceptor becoming reduced to a neutral species (Riddin *et al.*, 2006).

#### 1.4. Safety aspects of nanoparticles

The advantages of NP's in medicine, biochemistry and nanotechnology are widely discussed and documented (Bruchez *et al.*, 1998; Akerman *et al.*, 2002; Cao *et al.*, 2002; Georganopoulou *et al.*, 2005) due to the advances that NP's have afforded many technologies. It is common knowledge that the properties of many common materials are significantly increased when reduced to a nanoscale size, as the overall increase in the particle surface area results in increased reactivity with their environment. The small size of NP's endows them with the ability to overcome the mammalian immune system and easily enter any biological system via inhalation and digestion and pass through the blood-brain barrier. Despite these unique properties, it is unsettling to note that very little research is being done on the possible implications that NP's may have on the

environment and human health (Gwinn & Vallyathan, 2006). Gunter Oberdörster, a toxicologist, has studied the effects of NP exposure on a rat model. Oberdörster and colleagues found that exposure of the rodents to polytetrafluoroethylene (PTFE) NP's [ $\sim 50 \mu\text{g}\cdot\text{cm}^3$ ] of 20 nm resulted in the death of all the animals tested within 4 h yet on exposure to the same concentration of NP's greater than 100 nm, no side-effects were observed indicating that ultrafine particles pose a greater potential risk (Oberdörster *et al.*, 2000). As the current knowledge surrounding NP toxicity is highly limited, a wise course of action would be to minimise the exposure of biological systems to NP's until concrete data supporting their safety is determined (Oberdörster *et al.*, 2000, Kubik *et al.*, 2005).

### 1.5. Metal-ions and bacteria

The type of interaction a metal will have with a micro-organism can be determined by the metal's classification as either a hard or soft acid. For example, metal-ions required by micro-organisms for cellular structure or function such as  $\text{Mg}^{2+}$  or  $\text{Ca}^{2+}$  are classified as hard acids, while soft acids generally have a negative impact on the overall cellular functioning due to the nature of their toxicity. Mercury, for example, forms methylated derivatives which strongly bind to sulfhydryl groups of proteins as well as the nucleotide bases of DNA and RNA – all with deleterious effects. Some soft acids have also been found to readily pass through biological phospholipid membranes and accumulate in cells due to their ability to form organometallic cations which are stable in water yet highly soluble in lipids (Beveridge & Doyle, 1989).

#### 1.5.1. Heavy metals - Definition and classification

A "heavy metal" is defined as a metal which usually has a specific gravity greater than  $5 \text{ g}\cdot\text{cm}^3$  (Nies, 1999), though there are exceptions as in the case of the lanthanides. The "Hard-Soft-Acid-Base" (HSAB) Principle was used by Pearson (Pearson, 1963; Pearson, 1968) to classify heavy metals as either "hard" or "soft" acids. Soft acids are characterised as having a high polarisability and low electronegativity due to their large atoms, filled outer orbitals, and weak cationic nature (see Table 1.3). Soft acids form stable chloro-complexes in basic solutions as do transition metal cations. Therefore

platinum is classified in this way as being a soft acid. The characteristics of hard acids are in direct opposition of soft acids (Gadd & Griffiths, 1978; Beveridge & Doyle, 1989).

**Table 1.3:** Example of hard and soft acids as classified by Pearson's HSAB theory:

Hard Acids	Soft Acids
$\text{Cr}^{3+}, \text{Cr}^{6+}$	$\text{Ag}^+$
$\text{H}^+$	$\text{Au}^+$
$\text{Ti}^{4+}$	$\text{Pd}^{2+}$
Alkaline metals $\text{Li}^+, \text{Na}^+, \text{K}^+$	$\text{Pt}^{2+}, \text{Pt}^{4+}$
$\text{Mg}^{2+}$	$\text{CH}_3\text{Hg}^+, \text{Hg}^{2+}, \text{Hg}^+$
$\text{Ca}^{2+}$	Metal atoms $\text{M}^0$

(Beveridge & Doyle, 1989; Mack *et al.*, 2007).

### 1.5.2. Microbial interactions with toxic metals

Micro-organisms play a significant role in the biogeochemical cycling of metals on earth, as well as a number of other essential nutrients such as sulfur, nitrogen and phosphorus (Gadd, 1999). The biotechnological implications of micro-organisms capable of the transport or transformation of various toxic metals and radionuclides to less toxic compounds, have recently received a large amount of interest in the last two decades.

Gram-positive bacteria contain potent metal chelators such as teichoic acid and carboxyl groups of peptidoglycan in their cell walls. Gram-negative bacteria, on the other hand, have structurally and chemically more complex cell walls than their gram-positive counterparts with a thinner peptidoglycan layer lacking teichoic acid and an additional outer membrane resulting in more complex interactions with metals - decreasing the chelating capabilities (Beveridge & Doyle, 1989).

### 1.5.3. Transport of metal-ions into micro-organisms

Five main mechanisms of metal transport into micro-organisms have been identified, namely;

1. Transport of essential ions such as  $Mg^{2+}$  or  $Ca^{2+}$  via carriers.
2. Specific transport: Complexing of metals with low molecular weight ligands specifically produced from the cell i.e. siderophores/ferrichromes. This route, induced in times of need by the cell, is often slow, energy consuming (via the hydrolysis of ATP) and with a high substrate specificity.
3. Non-specific transport: Metal-ions complexed to substrates acting as carrier molecules through a transport chain specific for the substrate. This route is generally very fast and driven by the chemiostatic gradient across the bacterial cell into the cytoplasm and is used by a number of substrates (Nies & Silver, 1995).
4. Passive immobilisation in the cell by binding to the cell wall via charged groups i.e. sulfhydryl groups.
5. Immobilisation in capsule/slime-layers by adsorption (Beveridge & Doyle, 1989).

#### 1.5.4. Heavy metal resistance of microbes

Due to their filled outer d-orbitals, that allow them to form complex compounds which can be redox-active (Nies, 1999), certain soft acid heavy-metals, such as  $Hg^{2+}$  and  $Cd^{2+}$ , in low concentrations (~1 nM) play important roles as trace-elements in some of the more complex biochemical reactions in microbes. At higher concentrations [ $>0.01$  mM and 0.5 mM for  $Hg^{2+}$  and  $Cd^{2+}$ , respectively] however, this same property results in toxicity of the organism due to the formation of unspecific, toxic, complex compounds. It should be noted that even the metal-ions required for natural, healthy functioning of the cell such as  $Ca^{2+}$  and  $Mg^{2+}$  can be toxic in higher doses. For any heavy-metal to have an effect on the microbe, either positive or negative, the ions are first required to enter the cell (Gadd, 1993; Nies, 1999).

The nonspecific transport system acts as an “open gate” to heavy-metals in high concentration, as it unwittingly allows heavy-metal-ions to enter the cell in unlimited amounts. Once within the cell, heavy-metal cations in high concentration either bind to sulfhydryl groups of various proteins and/or enzymes often resulting in inhibited activity and/or may interact with cations such as  $Mg^{2+}$ ,  $Ca^{2+}$  or  $Zn^{2+}$  and prevent their

physiological action (Gadd 1993; Nies, 1999). Due to the negative effects of heavy-metals on the functioning of cells, the organisms have developed systems for heavy-metal resistance as well as methods for controlling metal-ion homeostasis. Five main methods for heavy-metal resistance have been identified for bacterial systems:

- 1) **Efflux:** the active transport of the heavy-metal-ions out of the cell by efflux-systems before bioaccumulation within the cell has a chance to occur.
- 2) **Reduction:** the reduction of the heavy-metal cation to an oxidation state with lower toxicity by enzymatic redox systems.
- 3) **Extra-cellular sequestration:** the excretion of molecules, with metal-binding affinity such as glutathione, oxalate or sulfides, by the micro-organisms, into the extracellular environment in order to bind to, or precipitate, the metal and prevent it from entering the cell.
- 4) **Exclusion by permeability membrane:** three main options exist: First, the production of an exo-polysaccharide layer which prevents the uptake of metal-ions by forming a barrier as well as acting as a point for biosorption. Second, the bacteria may alter the conformation of the microbial membrane thereby decreasing the permeability of the cell wall to metal-ions. Third, the metal-ions may bind non-specifically to the outer-microbial membrane.
- 5) **Complexation:** the isolation of heavy-metal cations which bind strongly to S<sup>-</sup> groups by complexation with thiol-containing molecules such as metal-binding peptides or metallothioneins.

(Gadd, 1993; Nies & Silver, 1995; Nies, 1999; Bruins *et al.*, 2000)

Often, one or a combination of these options may be more energetically and/or physiologically favourable for the organism. In the case of reduction of the heavy-metal-ion, the product may be insoluble or even more toxic than the original ion, therefore the efflux system would need to be in place to transport the new product out of the cell. There are cases where reduction cannot be employed, then the choice exists between efflux, exclusion, extracellular sequestration and/or complexation. Efflux consumes only

1 ATP molecule for the removal of 1 heavy-metal cation, while complexation consumes 16 ATP molecules in the formation of 1 sulfide which can complex with 1 heavy-metal cation and so is the most energetically unfavourable process. Consequently, complexation is often only used when the cells are in the presence of low heavy-metal concentrations where efflux, exclusion or extracellular sequestration are ineffectual (Nies, 1999).

## 1.6. Metal immobilisation by microbes

### 1.6.1. Biosorption

Biosorption is a metabolic or physico-chemical mechanism where metal species are removed from aqueous solutions by becoming complexed or sorbed onto the biomass of various micro-organisms, whether living or dead (Eccles, 1995; Gadd, 2000). The complexation of metal-ions to microbes occurs due to the presence of a plethora of binding sites available on the biomass, originating from its biological make-up, and includes moieties such as sulfhydryl, carboxyl, amide and hydroxyl groups (Bedell & Darnall, 1990; Mack *et al.*, 2007).

Biosorption mechanisms, classified as either “metabolism dependant” or “non-metabolism dependant” can be further sub-divided by the location where biosorption occurs:

- a) **Intracellular accumulation:** only occurs in viable cells and is often induced by the microbe in times of cell stress such as in the presence of a high level of heavy-metal-ions. The transport of the metal-ion, however, into the cell is not necessarily metabolism dependant.
- b) **Extracellular accumulation/precipitation:** may or may not be a metabolism dependant process. In the metabolism dependant case, the organism may produce compounds into solution which result in heavy-metal precipitation, while in non-viable cells precipitation may occur solely because of the passive interaction between the metal-ion and functional groups on the cell surface.
- c) **Cell-surface sorption/precipitation:** is a rapid and often reversible, non-metabolic process which occurs due to physico-chemical interactions such as ion-exchange, physical adsorption or chemical sorption of the heavy-metal-ions with

the functional groups of the various biopolymers of the cell walls (Kuyucak & Volesky, 1988; Ahalya *et al.*, 2003).

### 1.6.2. Enzymatic metal reduction

As previously mentioned, the enzymatic conversion of toxic metal-ions to less toxic metal species via redox reactions is expected to be part of a microbial survival mechanism. Certain fungi are capable of transforming Cu(II) to Cu(I) due to the presence of copper-reductase in their cell walls, a redox enzyme which requires the oxidation of NADH/NADPH (Gadd, 1993). Examples of hydrogenase ( $H_{ase}$ ) metal reduction include a number of chemotrophic bacteria, which are capable of reducing a variety of heavy-metal-ions such as U(VI) (Payne *et al.*, 2002), Cr(VI) (Michel *et al.*, 2001), Fe(III) (Lojou *et al.*, 1998) and Tc(VII) (Lloyd & Macaskie, 1996) while some phototrophic bacteria have been shown to be able to reduce Ni(II), Pt(IV) and Pd(II) (Zadvorny *et al.*, 2005), all via  $H_{ase}$  action with an electron donor. In addition to bacteria a number of other micro-organisms are also capable of metal reduction, often via  $H_{ase}$  action. Riddin and colleagues (2006), demonstrated that an extracellular protein solution from a *Fusarium oxysporum* fungal strain was effective in producing biogenic Pt(0) NP's from the bioreduction of Pt(IV). They proposed that a  $H_{ase}$  enzyme was responsible and that the reduction mechanism occurred via a two-cycle process involving Pt(II) as the intermediate (section 1.3.3, Fig 1.5). Later work by Govender and colleagues (2008) confirmed the presence of a periplasmic  $H_{ase}$  enzyme in this *F. oxysporum* strain that possessed Pt(IV) reductase activity and our current work is involved in elucidating the reductive mechanism.  $H_{ase}$ 's have also been used in the recovery of precious metals from waste-water with hydrogen utilised as the electron donor (Macaskie, *et al.*, 2005).

### 1.6.3. Hydrogenase enzymes and characterisation

Hydrogenases ( $H_{ase}$ 's), belonging to a small class of oxygen-sensitive redox enzymes (Riklis & Ritenberg, 1961) are classified into three groups according to their metal-containing prosthetic groups:



- 1) **[NiFeSe]-H<sub>ase</sub>**: involved in hydrogen uptake mechanisms, sometimes contains selenium as part of the active site;
  - 2) **[Fe]-H<sub>ase</sub>**: usually involved in hydrogen production although has been known to have bidirectional functionality;
  - 3) **[metal free]-H<sub>ase</sub>**: only found in methanogenic bacteria
- (Evans & Pickett, 2003; Zadvorny *et al.*, 2005).

### 1.6.3.1. Catalytic action

The metal containing H<sub>ase</sub>'s catalyse the following reversible redox reaction involving hydrogen (Equation 1):



(Evans & Pickett, 2003).

The active-site of these enzymes are deeply buried within the protein and molecular dynamics and X-ray crystallographic studies have shown that the transport of H<sub>2</sub>/H<sup>+</sup> to/from the active site of the H<sub>ase</sub> occurs via hydrophobic channels. These stretch between the active-site and surface of the enzyme to further allow for electron-transfer to the redox partners, such as cytochrome c<sub>3</sub> (Cyt c<sub>3</sub>) (De Lacy *et al.*, 2000; Evans & Pickett, 2003).

The redox reaction mentioned above may, at first glance, appear relatively simple, but in fact requires multiple steps for catalysis to proceed (Fig 1.6):

- a) Initially, H<sub>2</sub> activation (or H<sub>2</sub> production) takes place at the H<sub>ase</sub> active site,
- b) Next, 2e<sup>-</sup> are transferred from the active site to the redox partner (i.e. Cyt c<sub>3</sub>) of the H<sub>ase</sub> via the hydrophobic-channels after which,
- c) 2H<sup>+</sup> are transferred from the active site via the same hydrophobic-channels to the medium solvent resulting in a complete catalysis reaction (De Lacy *et al.*, 2000).

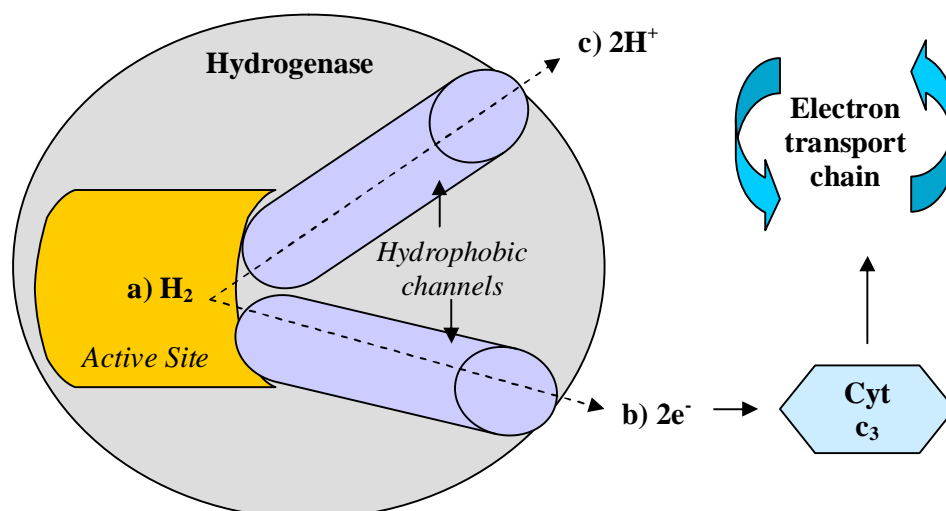


**Figure 1.6:** Diagrammatic representation of hydrogen activation by hydrogenase (Adapted from De Lacy *et al.*, 2000).

In bacterial cells, H<sub>ase</sub>'s are present in a number of cellular locations: membrane-bound, cytoplasmic, or within the periplasm (Chatelus *et al.*, 1987), and are known to play a pivotal role in the hydrogen metabolism of various micro-organisms including fungi, chemotrophic and phototrophic bacteria (Evans and Pickett, 2003; Ren *et al.*, 2005; Zadvorny *et al.*, 2005).

In sulfate reducing bacteria, H<sub>ase</sub> enzymes also play a significant role in sulfate reduction either via growth on H<sub>2</sub> itself or via the reduction of lactate to acetate, via pyruvate as an intermediate, with the subsequent evolution of H<sub>2</sub>. An example of the latter case results in the formation of a proton-gradient as the H<sub>2</sub> becomes available to the periplasmic H<sub>ase</sub>. Here, it becomes oxidised and transferred onto the rest of the dissimilatory sulfate pathway and eventually results in the formation of ATP - with approximately 1 ATP molecule being produced from the reduction of 1 sulfate molecule to H<sub>2</sub>S (Madigan *et al.*, 2000) This is discussed in further detail in section 1.8.2.

### 1.6.3.2. Metal-ion reduction by the hydrogenase

The role of the hydrogenase (H<sub>ase</sub>) enzyme, in the presence and absence of its redox partner, cytochrome c<sub>3</sub> (Cyt c<sub>3</sub>), in metal-ion reduction by a number of micro-organisms

including sulfate-reducing bacteria, has been extensively researched (Lloyd *et al.*, 2001; Payne *et al.*, 2002; Rashamuse & Whiteley, 2007; Govender *et al.*, 2008). The metal reductase activity of  $H_{ase}$  enzymes and cytochrome  $c_3$  is thought to be due to their low redox potentials (Chardin *et al.*, 2003; Michel *et al.*, 2003), although the complete enzymatic mechanism behind metal reduction by SRB has not yet been fully elucidated.  $H_{ase}$ 's have been shown to be either directly or indirectly responsible (involved in electron transport to Cyt  $c_3$ ) for the reduction of a number of metals by SRB (Lloyd *et al.*, 2001; Michel *et al.*, 2003; Whiteley & Lee, 2006). In an example of the latter case, the periplasmic  $H_{ase}$  enzyme of *D. vulgaris* was shown to act as the electron donor, via  $H_2$  oxidation, to its redox partner, Cyt  $c_3$ , which has been shown to actively reduce heavy metals such as U(VI) (Payne *et al.*, 2002) and Cr(VI) (Michel *et al.*, 2003).

### 1.7. Platinum

Platinum (Pt) belongs to a group of elements called the “Platinum Group Metals” (PGM's) which also include Osmium (Os), Iridium (Ir) and Palladium (Pd) (Earl & Wilford, 1991). Table 1.4 summarises the general properties of this metal:

**Table 1.4:** Properties of platinum.

<b>Physical properties</b>	Silvery-white, malleable, ductile metal
<b>Resistant to:</b>	Corrosion, high temperatures
<b>Oxidation states</b>	+2, +4, +6 <sup>^</sup>
<b>Period</b>	6
<b>Atomic number</b>	78
<b>Specific Gravity (g.cm<sup>-3</sup>)</b>	21.45 – hence classified as a heavy-metal
<b>Melting Point (K)</b>	2045
<b>Boiling Point (K)</b>	4100

(World Health Organisation, 2000; Earl and Wilford, 1991).

<sup>^</sup> +2 and +4 are the most stable oxidation states.

### 1.7.1. Economic impact

Platinum is present in the general lithosphere in low concentrations of 0.001–0.005 mg.kg<sup>-1</sup>. The highest concentrations [up to 500 mg.kg<sup>-1</sup>] of this metal have been found in Siberia and South Africa. The extraction and isolation of platinum world-wide is increasing rapidly, most likely due to the use of this element in the catalytic converters of exhausts in automobiles. The varied properties of platinum have afforded its use in a large number of industries including chemical, electrical, petroleum, jewellery, dentistry and in cancer therapies (World Health Organisation, 2000).

The need for a more sustainable and efficient fossil-fuel [i.e coal, crude oil] replacement has grown rapidly due to the finite stores of such fossil-fuels reaching an end. Further disadvantages of fossil-fuels are only becoming apparent recently, such as the advent of global warming, caused by the release of massive amounts of CO<sub>2</sub> gas from burning fossil-fuels (Cox *et al.*, 2000). Platinum is being utilised in the production of new-age fuel-cells, which converts oxygen and hydrogen to energy with the only by-product being H<sub>2</sub>O (Snyder, 2007). These fuel cells will hopefully be the new driving force of engines in the near future.

### 1.7.2. Toxicity

Soluble platinum salts such as ammonium chloroplatinate and platinum tetrachloride have a “permissible exposure limit” of 0.002 mg.m<sup>3</sup> of air over a period of eight hours due to a number of both short and long term side-effects. The former manifest in the form of irritation of the mucosal membranes of the eyes, nose and throat, while the latter longer term side effects result in respiratory and skin allergies that become worse with extended contact. It should be noted that elemental platinum is biologically inert (U.S. Department of Health and Human Services Occupational Health Guidelines, 1978).

## 1.8. Sulfate-reducing bacteria (SRB)

SRB are classified as a group of obligate anaerobic prokaryotes, capable of utilising oxidised sulfur compounds as electron acceptors in the dissimilation of organic material

or hydrogen for energy and are characterised both nutritionally and morphologically due to their diversity (Postgate, 1982; Gibson, 1990; Madigan *et al.*, 2000).

#### 1.8.1. Classification of sulfate-reducing bacteria

Sulfate-reducing bacteria (SRB) can be classified into 2 groups, mainly according to their ability to oxidise acetate, among a number of other characteristics (Table 1.5):

##### 1.8.1.1. Group I sulfate-reducers (non-acetate oxidisers)

Examples of the genera included in Group I are the *Desulfovibrio*, *Desulfobacula* and *Desulfomonas*. They transform sulfate to H<sub>2</sub>S via dissimilatory sulfate reduction utilising various organic compounds such as lactate, pyruvate and some fatty acids and alcohols as electron donors. They are capable of the partial oxidation of substrates to the metabolic product, acetate, which is excreted into the surrounding extracellular environment. Some *Desulfovibrio* species possess the unique ability, within Group I, to utilise hydrogen as an electron donor to reduce sulfate with CO<sub>2</sub> as the only carbon source and to thereby grow autotrophically and chemolithotrophically (Postgate, 1982; Gibson, 1990; Madigan *et al.*, 2000).

##### 1.8.1.2. Group II sulfate-reducers (acetate oxidisers)

Group II consists of *Desulfobacter*, *Desulfococcus* and *Desulfobacterium* which reduce sulfate to H<sub>2</sub>S by a specialised adaptation to utilise fatty acids such as acetate, lactate and pyruvate as electron donors resulting in the complete oxidation of the organic substrates to CO<sub>2</sub>. Unlike Group I, with the exception of the species *Desulfovibrio*, many of the genera within Group II such as *Desulfococcus* and *Desulfobacterium* are able to grow autotrophically and chemolithotrophically (Postgate, 1982; Gibson, 1990; Madigan *et al.*, 2000).

The metabolic actions of SRB on organic substrates and the ability of SRB to either completely oxidise the substrate to CO<sub>2</sub> or incompletely to acetate, make these organisms difficult to isolate from environmental sources. Furthermore they have the ability to co-exist with a number of other sulfate-reducers owing to the metabolic end product of one

group becoming the carbon source for another which allows them to create a number of syntrophic relationships resulting in large consortiums (Gibson, 1990).

**Table 1.5:** Characteristics of the sulfate-reducers (Adapted from Madigan *et al.*, 2000).

Genus	Characteristics					
	Desulfovirdin present	Gram + ve	Gram - ve	Shape	Spore-forming	GC% content
<b>Group I (Non-acetate Oxidisers)</b>						
<i>Desulfovibrio</i>	Y*		Y	Curved rods	N	46-61
<i>Desulfomicrobium</i>	N*		Y	Motile rods	N	52-57
<i>Desulfomaculum</i>	N		Y	Straight/curved rods	Y-endospores	37-46
<i>Desulfobotulus</i>	N		Y	Vibrios	-*	53
<i>Desulfobulbus</i>	N		Y	Ovoid	N	59-60
<b>Group II (Acetate Oxidisers)</b>						
<i>Desulfobacter</i>	N		Y	Rod	N	45-46
<i>Desulfococcus</i>	Y		Y	Spherical	N	57
<i>Desulfonema</i>	Y	Y		Large, filamentous	N	34-42
<i>Desulfoarculus</i>	N		Y	Vibrios	-	66
<i>Desulfosarcina</i>	N		Y	Cells in packets	N	51

### 1.8.2. Physiology, growth and economic importance

#### 1.8.2.1. Bioenergetics of sulfate reduction

Sulfur is an integral component of all biological organisms as it is required for the synthesis of amino acids and proteins. The aerobic/anaerobic biotransformation of sulfur in various ecosystems is known as a 'nutrient cycling process'. Assimilatory sulfate reduction is a biosynthetic process whereby micro-organisms reduce sulfate ( $\text{SO}_4^{2-}$ ) to sulfide ( $\text{S}^{2-}$ ) which subsequently becomes incorporated into amino acids (Peck & Lissolo, 1988). The anaerobic, sulfate reducing bacteria make use of "dissimilatory sulfate reduction" for the oxidation/degradation of organic substances for energy by utilising any

\* "Y" = Yes, "N" = No, "-" = No information

sulfur compound with an oxidation state above that of sulfide (2-) to function as an electron acceptor. A stoichiometric amount of sulfide is produced per sulfate molecule reduced (Equation 2) (Gibson, 1990):



Fig 1.7 A illustrates the synthesis of ATP within SRB as driven by the transfer of electrons within the dissimilative sulfate pathway. Cytochrome  $c_3$  [Cyt  $c_3$ ], is an electron carrier which is localised within the periplasmic space of the bacterial cell. A periplasmic hydrogenase [ $\text{H}_{ase}$ ] transfers electrons to Cyt  $c_3$ , its redox partner, which subsequently transfers the electrons to the high molecular weight cytochrome  $c$  (Hmc), which is membrane-bound. These electrons are then made available to the cytoplasmic enzymes of the dissimilatory sulfate reduction pathway, such as adenophosphosulfo reductase [APSRase] and sulfite reductase [SRase], via Hmc, which transports the electrons across the cytoplasmic membrane (Gibson, 1990; Madigan *et al.*, 2000).

The process of sulfate ion dissimilation begins with the uptake of sulfate from the extracellular environment by the cell (Fig 1.7 B). Once  $\text{SO}_4^{2-}$  enters the cell, the enzyme ATP sulfurylase produces pyrophosphate ( $\text{PP}_i$ ) - which subsequently forms inorganic phosphate after cleavage - and the high energy molecule adenosine phosphosulfate (APS) by combining ATP with  $\text{SO}_4^{2-}$ . It is only after the formation of APS that sulfur may act as a terminal electron acceptor (Hamilton, 1998). Next, the cytoplasmic enzyme, APS reductase converts the APS to  $\text{SO}_3^-$  which is then further reduced via a number of possible intermediates to  $\text{S}^{2-}$  by one of many sulfite reductases. The most common two are desulfovirdin and desulforubidin which are both bisulfite reductases (Postgate, 1965; Peck & Lissolo, 1988; Gibson, 1990; Gavel *et al.*, 1998).

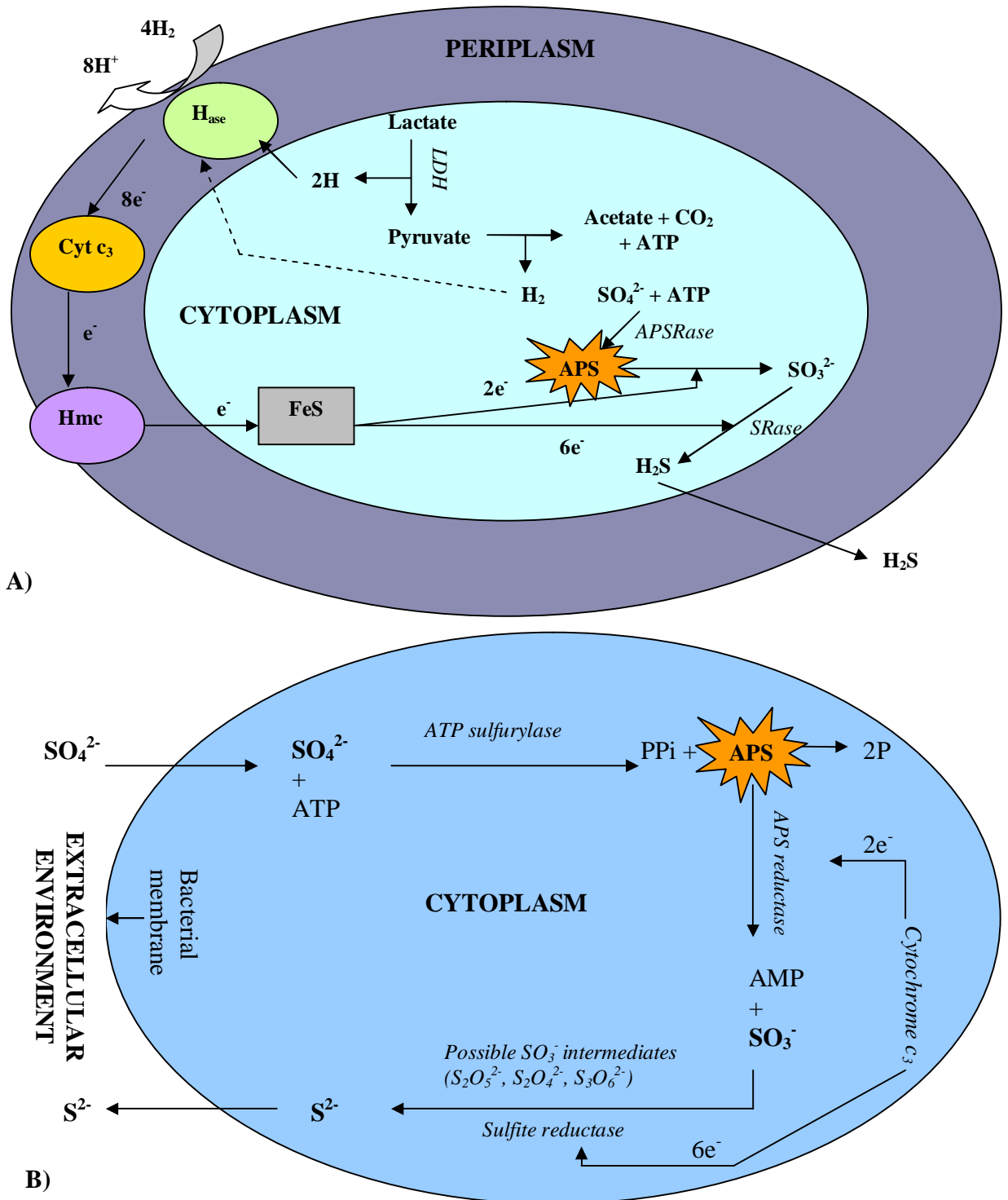


**Figure 1.7:** A) ATP synthesis and electron shuttling in sulfate-reducing bacteria (Adapted from Madigan *et al.*, 2000), B) Dissimilatory sulfate reduction in sulfate-reducing bacteria (Adapted from Gibson, 1990).



SRB have been used in various bioremediation processes of metals due to the complexation of the sulfides produced via sulfate respiration, to metal cations, resulting in the formation of insoluble metal-sulfides which precipitate out of solution allowing for collection and further down-stream processing (Lloyd *et al.*, 2001; Liamleam & Annachhatre, 2007).

A number of SRB have been found to be able to utilise sulfonates, sulfur (S<sup>0</sup>) and nitrates (NO<sub>3</sub><sup>-</sup>) as electron donors in dissimilatory growth resulting in the formation of H<sub>2</sub>S in all cases. Even in the total absence of electron donors, some species are able to use the fermentative pathway in the generation of energy (see Table 1.6) (Gibson, 1990; Madigan *et al.*, 2000).

**Table 1.6:** Examples of metabolic reactions of the sulfate-reducing bacteria (Adapted from Gibson, 1990).

<b>Oxidation reactions</b>
$4\text{H}_2 + \text{SO}_4^{2-} \rightarrow \text{HS}^- + \text{OH}^- + 3\text{H}_2\text{O}$
$\text{Acetate} + \text{SO}_4^{2-} \rightarrow \text{HS}^- + 2\text{HCO}_3^-$
$2\text{Lactate} + \text{SO}_4^{2-} + \text{H}^+ \rightarrow 2\text{Acetate} + 2\text{CO}_2 + 2\text{H}_2\text{O} + \text{HS}^-$
$2\text{Ethanol} + \text{SO}_4^{2-} \rightarrow 2\text{Acetate} + \text{HS}^- + \text{H}^+ + 2\text{H}_2\text{O}$
<b>Fermentation reactions</b>
$3\text{Lactate} \rightarrow \text{Acetate} + 2\text{Propionate} + \text{HCO}_3^- + \text{H}^+$
$\text{Pyruvate} + 2\text{H}_2\text{O} \rightarrow \text{Acetate} + \text{HCO}_3^- + \text{H}_2 + \text{H}^+$
$\text{Ethanol} + \text{HCO}_3^- + \text{H}_2 \rightarrow \text{Propionate}$
$\text{Acetate} + \text{HCO}_3^- + \text{H}^+ + 3\text{H}_2 \rightarrow \text{Propionate} + 3\text{H}_2\text{O}$

As the reduction potentials of sulfate (-0.22) are much lower than those of oxygen (+0.8) or nitrate (+0.4), it serves to predict that an organism that makes use of sulfate reduction as a form of energy production will suffer from lower biomass yields than those undergoing aerobic respiration. SRB do, however, provide themselves with sufficient energy when an electron donor, which produces NADH/FADH, is utilised (Madigan *et al.*, 2000).

### 1.8.2.2. Ecology

Anoxic environments rich in sulfate are most favourable for sulfate-reducing bacteria, therefore they are often found in the anaerobic levels of oceans, estuary sediments and brackish waters (Trüper *et al.*, 1969). Sulfate-reducing bacteria have also been isolated from non-saline sources. Although generally classified as strict anaerobes, some oxygen-tolerant sulfate-reducers such as *Desulfovibrio* have been isolated from aerobic habitats - in the presence of oxygen-producing cyanobacteria - and have been found to be able to use oxygen via aerobic respiration as an electron acceptor. This is not expected to be useful from a growth perspective but more as a survival mechanism to lower oxygen concentrations in the surrounding milieu (Battersby *et al.*, 1985; Dilling & Cypionka, 1990; Teske *et al.*, 1996; Madigan *et al.*, 2000).

SRB are classified as being ubiquitous micro-organisms since they are able to inhabit both marine and terrestrial environments encompassing a wide range of temperatures and pHs (Pfennig *et al.*, 1982; Madigan *et al.*, 2000) as well as a number of more unusual environments such as spoiled food tins (Lin & Lin, 1969), soured oil (Atlas, 1978) and sewage plants (Ueki *et al.*, 1988).

### 1.8.2.3. Environmental and economic importance

SRB are known to be of both environmental and economic significance due to their dissimilatory behaviour and ubiquitous nature. The by-product of their metabolism, H<sub>2</sub>S or “rotten-egg gas”, is highly noxious with potent reducing properties which not only plays a pivotal role in the natural ecology by functioning as an electron donor for SRB growth, but also results in growth inhibition of various aerobic organisms (Gibson, 1990). In terms of economic impact, SRB originally gained a poor reputation due to their involvement in water, sand (Alexander, 1973; Postgate & Abdollahi, 1982) and oil pollution (Atlas, 1978) as well as food spoilage (Lin & Lin, 1969) but especially noted was the rapid corrosion of metal equipment and contamination of products by the metabolic production of H<sub>2</sub>S gas and the deleterious effect on both biotic and abiotic organisms due to the subsequent formation of sulfuric acid by the dissolution of this gas in water (Alexander, 1973; Raloff, 1985; Gibson, 1990).

In the last few decades, SRB have proven to have a more positive influence on the economic and ecological arenas. Due to their ability to adapt and thrive in anoxic, environmental micro-niches rich in sulfate, they have been utilised successfully in the treatment of acid mine drainage, sewage sludge, sulfate waste from the paper industry (Clarke *et al.*, 1980; Tuttle *et al.*, 1989), oil spills (Atlas, 1978) and more recently in lowering the cost of metal remediation, via bioremediation strategies involving pure cultures or consortiums of SRB (Cohen, 2006). A number of heavy-metals such as Cr(VI) (Fude *et al.*, 1994), U(VI) (Spear *et al.*, 2000), Pd(II) (Lloyd *et al.*, 1998) , Pt(IV) (Rashamuse & Whiteley, 2007) and even Au(I) (Lengke & Southam, 2006), have been successfully recovered via bioremediation with SRB.

## 1.9. Present research

### 1.9.1. Hypothesis

The reduction of Pt(IV) by the whole cells and cell-soluble extract prepared from an SRB consortium occurs via a two-cycle mechanism from Pt(IV)  $\rightarrow$  Pt(II)  $\rightarrow$  Pt(0), involving a periplasmic  $H_{ase}$ . Variation of the experimental factors [pH, temperature, protein concentration] and addition of a capping agent (PVP) result in Pt(0) NP's of different morphologies.

### 1.9.2. Aims

To elucidate the mechanism of metal NP synthesis by the SRB consortium and subsequently propose an environmentally friendly or “green” method of platinum NP synthesis.

### 1.9.3. Objectives

- i) To screen the consortium of SRB for Pt(IV) metal reducing activity and to elucidate the mechanism.
- ii) To investigate the potential of a cell-soluble crude extract prepared from the present SRB consortium to actively and/or passively reduce Pt(IV) ions to elemental platinum [Pt(0)] NP's.

- iii) To characterise the NP's via various techniques such as transmission electron microscopy (TEM), scanning electron microscopy coupled with energy dispersive analysis of X-rays (SEM-EDAX) and UV-Vis spectroscopy.
- iv) To investigate, by inhibition studies, the role of the periplasmic H<sub>ase</sub>'s in this bioreductive mechanism
- v) To investigate the effect of the capping material polyvinylpyrrolidone (PVP) and other experimental factors [temperature, pH, protein concentration] on the bioreductive mechanism and particle morphology.

## CHAPTER TWO:

### Elucidating the bioreductive mechanism of Pt(IV) by an unknown consortium of sulfate-reducing bacteria

---

---

#### 2.1. Introduction

Sulfate-reducing bacteria (SRB) are classified according to a number of characteristics such as morphology, nutrition and the presence or absence of the sulfite reductase, desulfoviridin. Most SRB can be separated into two groups based on their dissimilatory sulfate reduction behaviours; those that are capable of fully oxidising acetate to CO<sub>2</sub> in the presence of sulfate, and those that are not (Madigan *et al.*, 2000).

SRB have been cited in literature as excellent modes of metal bioremediation. Metals are removed from solution either by precipitation, where the metal-ion becomes complexed with the sulfides - produced from sulfate metabolism in the dissimilatory sulfate reduction pathway - forming an insoluble metal-sulfide which precipitates out of solution (Lengke & Southam, 2006; Liamleam & Annachhatre, 2007), and/or via metal-reductase activity, where the metal-ion becomes reduced to a lower, often less toxic oxidation state, due to the catalytic action of the redox, H<sub>ase</sub> enzymes (Lloyd *et al.*, 1998; Rashamuse & Whiteley, 2007). Yong *et al.* (2002) demonstrated that a pure culture of *Desulfovibrio desulfuricans* was able to produce catalytically active nanocrystals of Pd(0) with hydrogen utilised as the electron donor of choice. They also demonstrated that platinum and rhodium were also recoverable in this way. Therefore it serves to suggest that platinum nanocrystals may also be formed under similar conditions with a consortium of SRB.

Although SRB were previously classified as strict anaerobes, extensive research has shown that a number of species, particularly that of *Desulfovibrio*, are highly tolerant to oxygen and in some cases even possess higher oxygen respiration rates than those of their more aerobic counterparts (Dolla *et al.*, 2006). Oxygen activated sludge has been shown to be rich in sulfate-reducing bacteria populations. As activated sludge

undergoes intermittent cycling between anoxic and oxic conditions, the SRB populations are observed to be oxygen tolerant to various degrees, due to constitutively expressed mechanisms which assist them in coping with oxidative stress (Mogenson *et al.*, 2005). These mechanisms have been shown to occur both during growth conditions, as in the example of *Desulfovibrio gigas*, where oxygen was reduced in the presence of electron donors resulting in the formation of energy (ATP) and during non-growth conditions, as in the case of *Desulfovibrio aerotolerans sp. nov.* (Lemos *et al.*, 2001), where high-energy carbohydrates, such as polyglucose accumulated during normal growth, are utilised as electron donors in oxygen reduction (Minz *et al.*, 1999; Mogenson *et al.*, 2005). Pure cultures have generally shown greater difficulty in maintaining cell viability in the presence of oxygen while mixed cultures appear more oxygen-tolerant (Bade *et al.*, 2000), possibly due to syntrophic relationships between the various populations. A mixed consortium isolated from raw, sewage sludge, was previously shown to be capable of reducing Pt(IV) to Pt(0) under anaerobic conditions with hydrogen acting as the electron donor. Amorphous platinum was observed to be present within the periplasm of the cells and a  $H_{ase}$  was reported to be responsible (Rashamuse & Whiteley, 2007). It was not determined, however whether a) the  $H_{ase}$  was solely responsible for the reduction of Pt(IV), b) whether platinum metal nanoparticles were produced from this process, or c) whether Pt(IV) reduction could occur under aerobic conditions. Elucidating the bioreduction of Pt(IV) by whole-cells will be essential in further unravelling the mechanism of metal nanoparticle formation by microbes. Once fully understood, the ability to manipulate and gain control over the mechanism, which determines nanoparticle shape and size, will allow for the nanoparticles and their properties to be mass produced to specific guidelines (Mukherjee *et al.*, 2002; Ahmad *et al.*, 2003).

The objectives of Chapter 2 are to:

- i) Screen the SRB consortium for Pt(IV) reduction in the presence of  $H_2(g)$ .
- ii) Investigate the suitability of  $H_2(g)$  as an electron donor for the bioreduction of Pt(IV) by the consortium.
- iii) Investigate the effects of oxygen on the reductive mechanism.
- iv) To elucidate the bioreductive mechanism of Pt(IV) reduction to Pt(0) by this consortium.

## **2.2. Materials & Methods**

### **2.2.1. Materials**

All chemicals, which were of analytical grade, were obtained from Sigma-Aldrich (South Africa) or Merck (South Africa) unless otherwise stated. All gases were purchased from Afrox (South Africa).

### **2.2.2. Methods**

#### *2.2.2.1. Preparation of stock solutions*

The 8 %  $\text{H}_2\text{PtCl}_6$  solution [Pt(IV)] was used as a stock solution for all experiments, and diluted appropriately.

A 10 mM stock solution of the water soluble  $\text{Na}_2\text{PtCl}_4$  salt [Pt(II)] was prepared fresh for each experiment in ddH<sub>2</sub>O and diluted appropriately for subsequent investigations.

All of the above solutions were kept in the dark.

#### *2.2.2.2. Analysis of platinum ions in solution*

A solution of each metal salt underwent spectrum analysis from 200-550 nm (2 nm intervals) on a Powerwave X (Bio-Tek, Instrumental Inc., USA) to determine the absorbance maxima's, which would allow for analysis of the platinum-ions in subsequent investigations (Appendix E). From the absorbance maxima obtained, standard curves of the platinum salts utilized in the following experiments were prepared with a correlation co-efficient of 0.989 or greater (Appendix D). Aliquots from all experiments were analysed by observing the absorbance at 230 nm and 261 nm for Pt(II) and Pt(IV) respectively. These absorbance values correlated well to values found in literature for Pt(II) (225 nm) (Henglein *et al.*, 1995) and Pt(IV) (261 nm) (Liu *et al.*, 2004). Any pH variations were observed by analysis with a hand-held pH meter with a 6 mM epoxy electrode iQ pH meter (model 3510) (pHoenix sales, South Africa).

#### *2.2.3. Growth of sulfate-reducing bacteria*

##### *2.2.3.1. Source of micro-organism and culturing conditions*

An uncharacterised mixed-consortium of sulfate-reducing bacteria (SRB) was isolated from sewage sludge obtained from the Environmental Biotechnological Research Unit

(EBRU) Bio-sure® process (Grahamstown, South Africa). The culture was enriched in a 10 L stock bio-reactor (BR1), covered by aluminium-foil to minimise exposure to light, containing modified Postgate medium C (PGC) (Postgate, 1984; Rashamuse & Whiteley, 2007) (Appendix A) (Fig 2.1). Anaerobic conditions were maintained at room temperature, in the dark, by purging the system with N<sub>2</sub> (99.9 %) for 15 min followed by 5 min with H<sub>2</sub> (99 %). Samples of this culture were harvested after the cells had reached stationary phase (7 days), and used to seed a smaller 5 L bioreactor (BR2) containing modified PGC which was maintained under anaerobic conditions as described above. This seed culture (BR2) was constantly maintained by sub-culturing BR1 every 3-4 weeks to provide fresh cells for use during subsequent experiments (BR3, etc). SRB growth was monitored using pH, sulfide and sulfate concentrations. When sulfate levels of BR1 became limiting, the bioreactor was re-fed with new modified PGC. The OD<sub>600</sub> was measured using an Aquamate spectrophotometer (Aquamate, England), while sulfate and sulfide concentrations were determined using the Spectroquant® Nova 60 and respective kits (Merck, South Africa).

#### *2.2.3.2. Cell harvesting and preparation of SRB cells for reduction experiments*

The SRB cells were harvested during stationary phase (7 days) under N<sub>2</sub> (99.9 %) into JA-14 centrifuge tubes. The cells were centrifuged (8000g, 15 min, 4 °C) to obtain a cell pellet. The supernatant was discarded while the cell pellet was washed twice in ddH<sub>2</sub>O to remove any remaining sulfide or sulfate which would result in precipitation of the platinum salt (H<sub>2</sub>PtCl<sub>6</sub>) in solution. The cell pellet was resuspended in minimal Tris-HCl buffer (20 mM, pH 7.6) (Appendix B). Though strict anaerobic conditions were difficult to maintain throughout the experiments, oxygen exposure was kept to a minimum.

#### *2.2.4. Metal salt reduction experiments*

##### *2.2.4.1. Hydrogen as a suitable electron donor with Pt(IV) reduction by cells*

In glass test-tubes covered with tin-foil to minimise exposure to light, a final volume of 10 ml consisted of SRB cells (19.2 g.L<sup>-1</sup> wet weight) challenged with 1 mM H<sub>2</sub>PtCl<sub>6</sub> in a Tris-HCl buffer (200 mM, pH 7.6) (Appendix B) at room temperature (RT). The experiment was initiated by the addition of the platinum salt and by bubbling H<sub>2</sub>(g) into the solution through a needle continuously throughout the



investigation. In order to investigate any abiotic effect of hydrogen on the metal-ions in solution, a control was set-up with no cells, the cell volume being replaced with Tris-HCl buffer (200 mM, pH 7.6). Anaerobic conditions were maintained and triplicate samples (300  $\mu$ l) were collected in 1.5 ml micro-centrifuge tubes at regular intervals. The samples were centrifuged (13000g, 2 min, RT) in a MiniSpin table-top centrifuge (Eppendorf), and the supernatant analysed by UV-Vis spectroscopy for the presence of Pt(IV).

#### *2.2.4.2. Effect of low hydrogen concentration on Pt(IV) reduction*

The experimental set-up consisted of 30 ml Frasco Rescado screw cap bottles placed at room temperature, in the dark. SRB cells (19.2 g.L<sup>-1</sup> wet weight) were added to Tris-HCl buffer (200 mM, pH 7.6), under N<sub>2</sub> (99.9 %) to minimise exposure to oxygen. Controls containing heat-killed cells, no cells and no 'added' electron donor were included as well as cells incubated at 4 °C. Heat-killed cells were placed at 148 °C for 20-25 min. In the cell-free controls, cell volumes were replaced with Tris-HCl buffer (200 mM, pH 7.6). The reaction was initiated by addition of the platinum salt (H<sub>2</sub>PtCl<sub>6</sub>) to give a final concentration of 1 mM in 10 ml, followed by purging the headspace with H<sub>2</sub> (99.9 %) or N<sub>2</sub> (99.9 %) where appropriate and then sealed. Aliquots (300  $\mu$ l) were taken at regular intervals, centrifuged (13 000g, 2 min, RT) and the supernatants kept in the dark at 4 °C until further analysis by UV-Vis spectroscopy. During sampling, the headspace was purged with N<sub>2</sub> (99.9 %) or H<sub>2</sub> (99.9 %) where appropriate and then sealed. All experiments were performed in triplicate and simultaneously. Though strict anaerobic conditions were difficult to maintain throughout the experiments, oxygen exposure was kept to a minimum.

#### *2.2.4.3. Effect of oxic conditions with no exogenous electron donor*

The experimental set-up remained the same as for section 2.2.4.2 except that the experimental sample remained open to the natural atmosphere for the duration of the experiment; furthermore no electron donor was added. Prior to addition of the cells, the sample solution was shaken to increase the oxygen content. At all sampling times, the solution was mixed by stirring to incorporate the oxygen atmosphere and resuspend any cells that had settled. This investigation was performed in triplicate with sampling and analysis occurring as previously described in section 2.2.4.2.

### 2.2.5. Scanning Electron Microscopy – Energy Dispersive Analysis of X-Rays (SEM-EDAX) for Pt(0) determination

Elemental analysis of the samples was performed using a TESCAN VEGA (LMU) SEM with INCAPentaFETX3 (Oxford Instruments) EDAX attachment operating at 20 kV. Samples were collected in 1.5 ml micro-centrifuge tubes and pelleted by centrifugation (13 000g, 2 min, RT). The supernatant was discarded and the cell pellet removed and spread thinly onto a carbon strip attached to a brass SEM support and air-dried in a Heraeus laboratory oven at 60 °C overnight. The SEM-EDAX was calibrated by quant-optimisation with a copper (Cu) standard under standard operating conditions.

### 2.2.6. Transmission electron microscopy (TEM) analysis

#### 2.2.6.1. Embedding and fixing of cells for TEM analysis

The fractions collected throughout the experiments were centrifuged (13 000g, 2 min, RT) and the supernatant removed for later analysis. The pellet was fixed overnight in a 2.5 % glutaraldehyde solution in sodium phosphate buffer (0.1 M, pH 7.0). The glutaraldehyde solution was decanted and the pellet washed (2 X 10 min) with cold sodium phosphate buffer (0.1 M, pH 7.0). The secondary staining step with 1 % OsO<sub>4</sub> was not included due to possible interference by this heavy metal. There were no anticipated issues with not including this step as OsO<sub>4</sub> stains cell walls, and since the expected location of the platinum deposits would be either on the cell wall or within the periplasm, this in turn, would allow for clear visualisation of the cells. The SRB cells were then dehydrated by a series of successive ethanol concentrations (30 %, 50 %, 70 %, 80 %, 90 %) with two changes of absolute ethanol (100 %) for 15 min per ethanol concentration. Infiltration of the cells was performed by washing twice in propylene oxide for 15 min. The cells were then subjected to a series of increasing resin (Araldite):propylene oxide concentrations (25 %:75 %, 50 %:50 % and 75 %:25 %; 60 min per step). The final infiltration step occurred in pure resin (100 %) and was left overnight. After infiltration in pure resin, the pellet samples were transferred to capsule mats containing pure resin in individual moulds for each sample. The capsule mat was allowed to polymerise (36 h, 60 °C) in an oven.

Sections (100 nm) were cut using an ultramicrotome and placed on a carbon-coated copper grid and analysed with a JEOL JEM-1210 electron microscope at an operating electron voltage of between 80-90 kV.

*2.2.6.2. Digital image capture*

Digital pictures of the samples were collected using the MegaView (Soft Imaging System) with analySIS Image Processing Software.

### 2.3. Results & Discussion

An environmental, mixed-consortium of sulfate-reducing bacteria was chosen, for metal-reduction investigations, over pure cultures due to a number of advantages provided by a consortium. Gadd and White (1996) described a mixed-consortium of SRB as having the ability to adapt and survive in a wider range of conditions than pure cultures. This adaptation arises due to the SRB populations that constitute the consortium, having different optimal growth conditions, which allow for syntrophic growth. An additional advantage provided by a consortium over a pure culture is their ability to create a “hostile environment” for possible contaminant organisms, due to their metabolic products, which prevent contaminant growth, while simultaneously ensuring the ideal environment for growth of other SRB’s (Gadd & White, 1996; Rashamuse & Whiteley, 2007).

#### 2.3.1. Growth of an uncharacterised mixed SRB consortium

In order to observe the metabolic activity of the sulfate-reducing consortium - grown on lactate-sulfate media - changes in sulfate, sulfide, OD<sub>600</sub> and pH were followed over a 9 day period. Growth was observed via OD<sub>600</sub> absorbance readings that are a representative guide for cell density (Nakayama *et al.*, 2006). For increased accuracy, the OD<sub>600</sub> samples were diluted until an absorbance value below 1.0 was obtained, after which the true absorbance was determined by multiplying by the dilution factor.

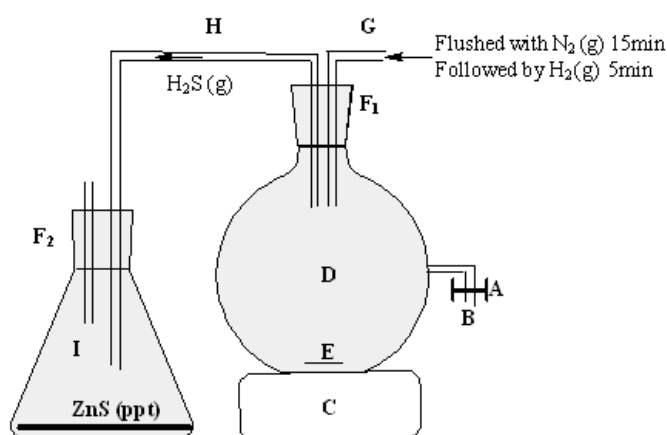


**Figure 2.1:** Bioreactor set-up (Adapted from Oyekola & Pletschke, 2006). [A] Clamp, B) Sampling pipe, C) Magnetic stirrer, D) 10/5L Bioreactor, E) Magnetic stirrer bar, F<sub>1</sub>) & F<sub>2</sub>) Rubber stopper, G) Gas inlet pipe, H) H<sub>2</sub>S outlet pipe, I) Zinc acetate trap.]

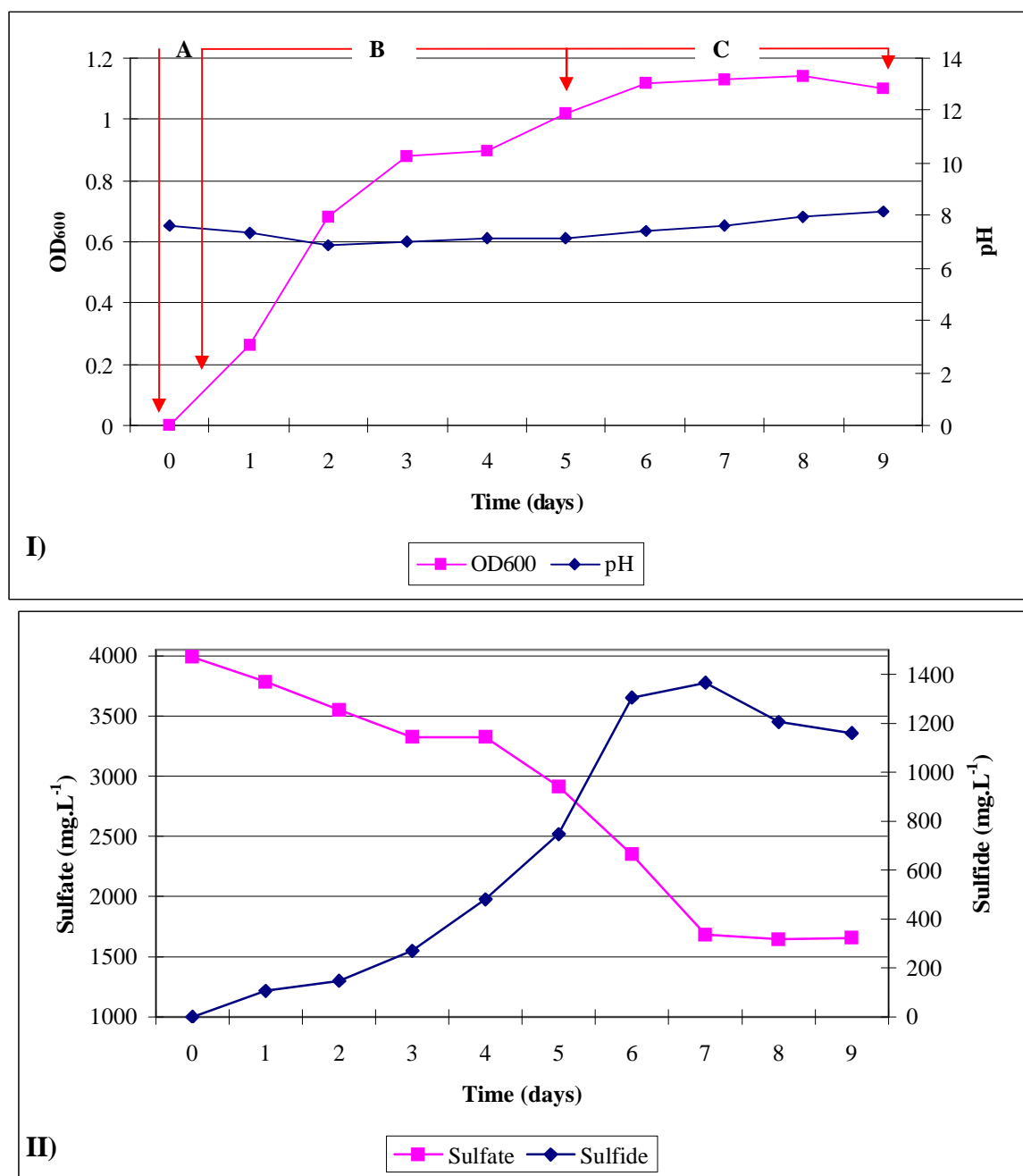


**Figure 2.2:** Growth of a consortium of sulfate-reducing bacteria. **I)** OD<sub>600</sub> and pH readings of BR1 over time. A typical bacterial growth curve was observed over the 9 day period consisting of a relatively insignificant lag phase (A), an exponential growth phase (B) and a stationary phase (C) (Zwietering *et al.*, 1990). **II)** Sulfate reduction and formation of sulfide during metabolism of sulfate reducing bacteria.]\*

In Fig 2.2 I, a rapid growth rate of the cells was observed between day 0 and day 3, which correlates to the logarithmic or exponential phase of growth (B). The stationary phase (A) in SRB may be anywhere from 0 -70 h depending on growth

\* All values shown have a standard deviation < 10 %

conditions (Postgate, 1965). Growth begins to slow and eventually level off around day 7 indicating the cells have entered stationary phase (C) (Zwietering *et al.*, 1990). Decelerated growth by bacterial cells occurs during stationary phase when the substrate or carbon source (i.e. lactate in this case) becomes limiting. The cells then enter a mode of stasis where cell viability is maintained by a lower metabolic rate which is not coupled to growth. Energy is most likely produced via the oxidation of organic acids and or hydrogen in the absence of sulfate as described in section 1.8.2.1.

The pH within the bioreactor remained relatively constant throughout growth phases beginning at pH 7.6 and varying from its lowest point of pH 6.9 on day 2 to its highest point of pH 8.2 on day 9. Since the general majority of sulfate-reducing bacteria are neutrophiles, the optimal pH for growth is between pH 6 - 8 (Eccles, 1999), however a number of species have been known to be acidophilic, thriving in conditions below pH 4 (Kolmert & Johnson, 2001). Therefore a mixed consortium would be expected to have a greater range of optimal pH due to the syntrophic relationships of SRB in mixed cultures.

The gram amount of ingredients for modified PGC was calculated to give an initial sulfate concentration of 2000 mg.L<sup>-1</sup> (Rashamuse & Whiteley, 2007). Fig 2.2 II clearly shows that the starting sulfate concentration (4050 mg.L<sup>-1</sup>) was approximately double the expected starting concentration. It was expected that due to the sludge origin of the SRB inoculum for BR1, a number of contaminants were likely to be present which interfered with the sulfate test resulting in a higher sulfate value than was truly present. The highest rate of sulfate reduction was observed between day 4 and day 7 where the concentration decreased from 3325 mg.L<sup>-1</sup> to 1683 mg.L<sup>-1</sup>, after this time the sulfate concentration levelled off to an apparent concentration of 1650 mg.L<sup>-1</sup> which correlates to the OD<sub>600</sub> readings indicating stationary phase after day 7. A cessation in sulfate reduction usually only occurs when the substrate itself becomes limiting (i.e. sulfate), therefore this supports the theory of contaminant interference with regards to the sulfate test.

The highest rate of sulfide generation, was observed between day 3 and day 6 where the sulfide concentration increased from 270 mg.L<sup>-1</sup> to 1305 mg.L<sup>-1</sup> after which the levels became stable indicating that the cells had entered stationary phase.

SRB cells were harvested for use in metal-reduction experiments during stationary phase since metabolic products such as sulfides produced during active growth would interfere with reduction investigations by precipitating the metal-ions via complexation and formation of insoluble metal sulfides (Rashamuse & Whiteley, 2007).

### 2.3.2. Metal salt reduction experiments

#### 2.3.2.1. Hydrogen as a suitable electron donor with Pt(IV) reduction by cells

Rashamuse and Whiteley (2007) demonstrated that hydrogen was the optimal electron donor for Pt(IV) uptake experiments with SRB under anaerobic conditions. The following experiment was conducted first, to confirm that the present SRB consortium had Pt(IV) reductase activity, second that hydrogen was in fact a suitable electron donor for the reduction of Pt(IV) by a viable consortium of SRB and third, to ensure that the electron donor had no abiotic effect on the Pt(IV) ion in solution.

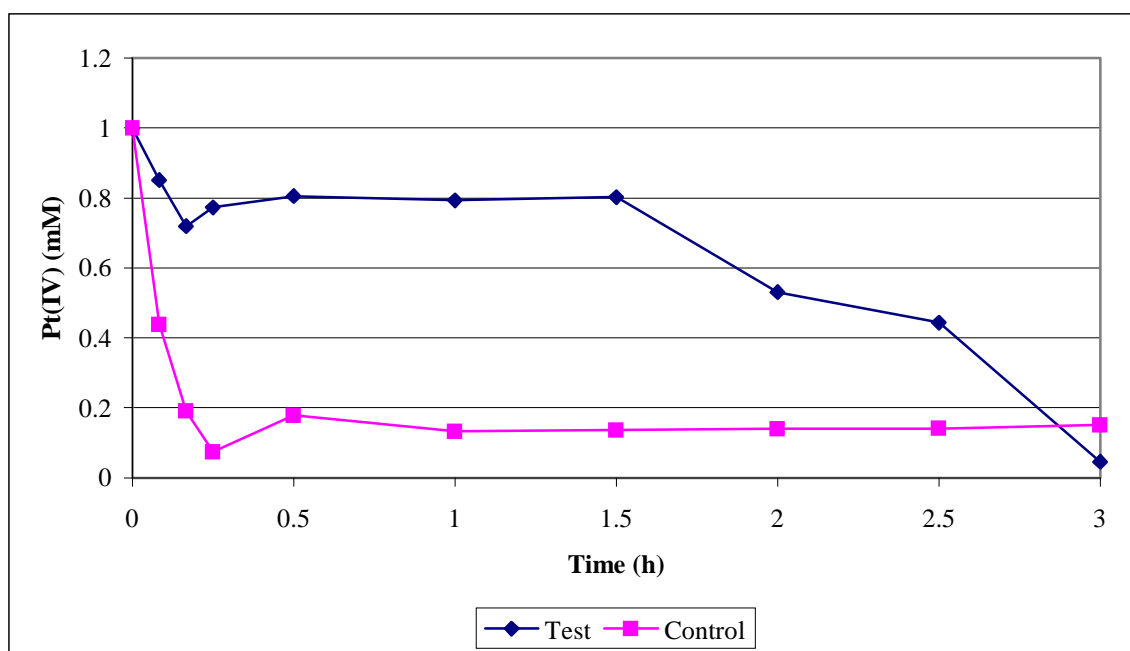


**Figure 2.3:** Reduction of Pt(IV) in the presence of viable SRB cells and hydrogen. [Test: SRB cells + H<sub>2</sub>(g) + Pt(IV), Control: Cell-free + H<sub>2</sub>(g) + Pt(IV).]\*

Unexpectedly, both reactions showed Pt(IV) loss over the time period observed. In Fig 2.3, results illustrated that after 0.25 h, the cell-free control had begun to exhibit an unexpected colour change from yellow to clear with ~92.5 % of the Pt(IV) ion

\* All values shown have a standard deviation < 10 %

being reduced at a rate of  $3.7 \text{ mM}\cdot\text{hr}^{-1}$ . After a further 0.25 h a significant colour change had occurred to dark grey which became considerably darker to black over time. The colour change from grey to black correlated with a slight increase in absorbance at 261 nm. The origin of this particular interference was expected to be due to the formation of platinum nanoparticles in aqueous solution; literature states that their broad UV-Vis spectrum would most likely interfere with a wide range of absorbances (Henglein *et al.*, 1995; Mizukoshi *et al.*, 2001; Liu *et al.*, 2004). This interference that resulted in a false increase in Pt(IV) concentration, dropped slightly after 1 h and subsequently held steady throughout the rest of the time period, indicating partial instability of the particles in solution (Henglein *et al.*, 1995). These results clearly demonstrate an abiotic reaction occurring between hydrogen gas and the platinum salt  $\text{H}_2\text{PtCl}_6$ , where the platinum(IV) metal-ion rapidly became reduced to platinum black, Pt(0) colloid at room temperature. A black precipitate was observed to collect on the bottom of the tube after the reaction was terminated supporting the suggestion that the nanoparticles were not stable in the experimental solution as mentioned above.

In the case of the SRB test sample (Fig 2.3), a slower reduction mechanism was observed where a small loss of Pt(IV) of ~28 % occurred within the first 10 min at a rate of  $1.68 \text{ mM}\cdot\text{hr}^{-1}$ . Pt(IV) loss stabilised over a stationary reduction period, and only showed further reduction after 1.5 h. The stationary reduction period observed by the cells correlates to the lag phase required for re-activation of the periplasmic  $\text{H}_{\text{ase}}$  enzyme, by hydrogen, after exposure to oxygen. Lissolo and colleagues (1984) demonstrated how hydrogen could be utilised to reactivate a  $\text{H}_{\text{ase}}$  enzyme which had become deactivated by oxidic conditions. Low levels of oxygen have been shown to reversibly inhibit this enzyme. The reduction of the Pt(IV) ion resumed between 1.5-3 h at a slower rate of  $0.50 \text{ mM}\cdot\text{hr}^{-1}$ , where a colour-change to grey was noticed after 2.5 h. When the cell containing samples were centrifuged, the supernatant was clear indicating that most of the reduced platinum was present within/on the cells which would be later confirmed by TEM analysis.

These results initially indicated the involvement of a biotic two-step mechanism for Pt(IV) reduction. First a rapid uptake of a small percentage of Pt(IV) by the cells via passive biosorption, second an active, induced mechanism, most likely involving the



periplasmic H<sub>ase</sub> with hydrogen acting as the electron donor, as shown by Rashamuse and Whiteley (2007) and/or the abiotic involvement of H<sub>2</sub>(g) in the independent reduction of Pt(IV) (Fukuoka *et al.*, 2006; Bönemann *et al.*, 2007). Literature search regarding Pt(IV) reduction by hydrogen revealed a number of cases where hydrogen was in fact used in the chemical synthesis of platinum nanoparticles by the abiotic reduction of Pt(IV) (Henglein *et al.*, 1995) and Pt(II) salts (Henglein & Giersig, 2000). This information further cast doubt on hydrogen as a suitable electron donor in these experiments.

In the research conducted by Rashamuse and Whiteley (2007), the reductive properties of hydrogen were not fully taken into consideration, though its effect cannot be ignored. The abiotic effect of hydrogen poses the question of whether the cells themselves are utilising hydrogen as an electron donor for an enzymatic reduction mechanism or whether they are merely passively adsorbing the particles, formed by the abiotic reduction mechanism. Therefore a new experiment was developed to determine the effect of hydrogen at a much lower concentration.

#### *2.3.2.2. Effect of low hydrogen concentration on Pt(IV) reduction*

As mentioned above, this experiment was conducted in order to investigate whether lower hydrogen concentrations would have the same rapid, reductive ability as previously observed and to test whether the consortium was capable of reducing Pt(IV) in the absence of hydrogen.

Due to regular sampling and a non-continuous addition of hydrogen or nitrogen, strict anaerobic conditions could not be maintained, though exposure to oxygen/air was kept to a minimum.

The amount of Pt(IV) concentration calculated from the samples taken at various timed intervals is shown (Fig 2.4 I). As the cells were challenged with a 1 mM solution of Pt(IV), the initial starting concentration in all samples was expected to be 1 mM (+/-0.03 mM) at 0 h, however directly after addition of the cells the heat-killed cell sample exhibited a 13.6 % drop in Pt(IV) concentration, while the live cells with an electron donor (i.e. hydrogen) whether present or absent, exhibited a greater decrease in Pt(IV) concentration of ~56 % and ~60 % for these samples respectively.

A colour change from yellow to brown was observed by the samples containing viable cells indicating the formation of Pt(0).

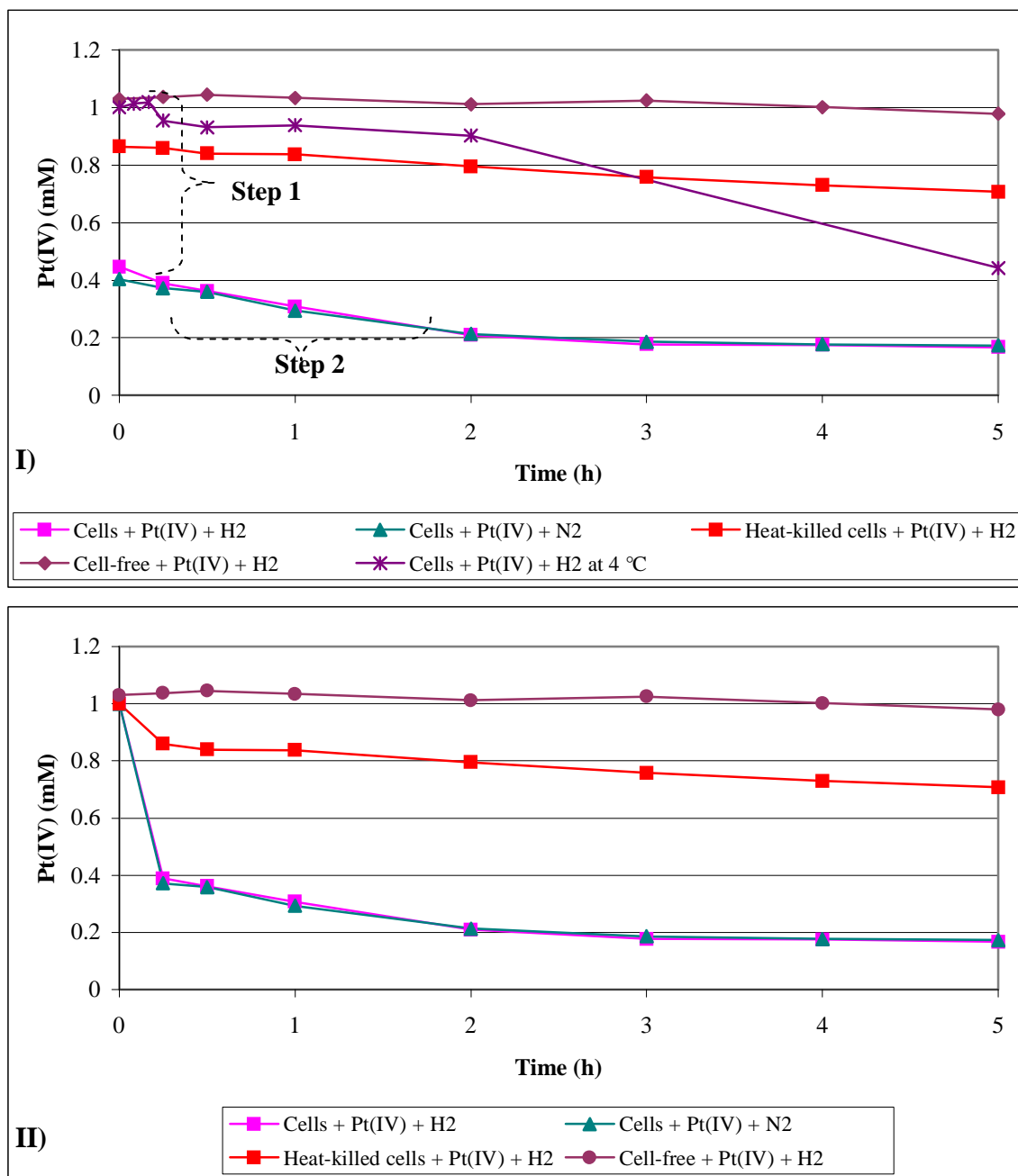


**Figure 2.4:** Bioreduction of Pt(IV) by SRB cells [I] Pt(IV) reduced by SRB consortium over time. II) Normalised data illustrating the amount of Pt(IV) reduced by an SRB consortium over time.]\*

It was theorised that the significant drop in Pt(IV), observed in the viable cell-samples either in the presence or absence of an electron donor (Fig 2.4 I), may be part of a separate mechanism to that observed in section 2.3.2.1, possibly in response to higher

\* All values shown have a standard deviation < 10 %

levels of oxygen due to non-continuous addition of the electron donor and regular sampling. As the heat-killed cells exhibited a far lower potential for Pt(IV) reduction, with only ~30 % of the Pt(IV) being reduced via passive biosorption after 5 h, this “new” mechanism was also hypothesised to be a two-step process. Step 1, an initial active, rapid reduction, followed by Step 2, a slower step of passive biosorption or active transport as a result of the cells responding to higher levels of oxygen.

Opperman and van Heerden (2007) demonstrated that two separate mechanisms for Cr(IV) reductase are observed under anaerobic versus aerobic conditions in the thermophilic bacterium *Thermus scotoductus*. The anaerobic mechanism was found to occur under non-growth conditions and required lactate as the electron donor (Möller & van Heerden, 2006). The aerobic mechanism was demonstrated to occur both under growth or non-growth conditions via the Cr(IV) reductase action of a soluble, constitutively expressed cytoplasmic, NADH-dependant enzyme, either in the presence or absence of an exogenous electron donor. The rate of reduction however was increased significantly in the presence of exogenous electron donor. Opperman and van Heerden (2007) go on to explain that it is not uncommon for bacteria to maintain their metal reductase activity in the absence of an exogenous electron donor. Since, bacteria produce and store high-energy carbohydrate polymers under normal growth conditions, these polymers will become metabolised in times of metabolic starvation, thereby releasing the stored energy for general cell maintenance while simultaneously producing an endogenous store of electrons for use in metal reductase activity.

In order to further investigate this theory, the reduction of Pt(IV) by viable cells at 4 °C, was undertaken. The cells were incubated on ice for 5 min prior to the investigation and maintained on ice for the duration in order to lower the metabolic rate of the resting cells. It was expected that if the initial step was an active mechanism, the lower temperature should sufficiently slow down this process by lowering enzymatic activity. The results showed that for cells at 4 °C in the presence of hydrogen (Fig 2.4 I), the initial reduction period (Step 1) slowed considerably, with the expected amount (1 mM) of Pt(IV) present at 0 h and only 56 % of Pt(IV) being reduced, after ~5 h. This result further supports the hypothesis that the majority of the Pt(IV) reduction observed in Step 1, was due to an active process. Since the Pt(IV)

ion cannot be accurately measured upon addition of cells at room temperature, “0 h” will always reflect the expected starting concentration (1 mM) from this point forward.

Other differences observed in the results of Fig 2.4 I, was the lack of a stationary reduction period that was previously seen in Figure 2.3, suggesting that the  $H_{ase}$  responsible for the reductase activity in 2.3.2.1, may not be the same  $H_{ase}$  responsible for this oxygen-tolerant mechanism. For example, the  $H_{ase}$  in section 2.3.2.1 seems to be intolerant to oxygen, requiring anaerobic conditions for activity, while the  $H_{ase}$  in section 2.3.2.2 was fairly stable in low levels of oxygen. It is well documented that SRB contain a variety of  $H_{ase}$  enzymes both cytoplasmic and periplasmic, either free or membrane-bound capable of hydrogen uptake or hydrogen evolution (Postgate, 1965; De Lacy *et al.*, 2000). De Luca and colleagues (2001) demonstrated that an oxygen-tolerant [NiFe]- $H_{ase}$  isolated from the periplasm of *Desulfovibrio fructosovorans* was responsible for Tc(VIII) reduction. Oxygen did not inhibit the reduction although hydrogen, acting as an electron donor, was a requirement. From these results, the role of the oxygen-sensitive cytoplasmic  $H_{ase}$  could be excluded.

It should also be considered that complete reduction (100 %) of the Pt(IV) ion was not attained (unlike in section 2.3.2.1) possibly due to toxicity effects of oxygen and/or the metal salt in solution. Alternatively, the total amount of Pt(IV) may be unavailable to the reduction mechanism due to passive sequestration/biosorption as ~20 % of Pt(IV) ion was reduced by the heat-killed cells after 2 h (Fig 2.4 II).

The cell-free control exhibited relative stability of the Pt(IV) ion at the hydrogen concentration used. Low hydrogen concentrations were employed due to the reductive potential of this gas on the Pt(IV) and Pt(II) ions in aqueous solution (Fukuoka *et al.*, 2006; Bönnemann *et al.*, 2007) and illustrated in section 2.3.2.1, Fig 2.3 (Control).

Another unusual observation in Fig 2.4 I, was the similarity in reduction potential of the control experiment lacking an electron donor, with that of the sample using exogenous hydrogen as an electron donor. These results indicated that this viable, environmental culture of a sulfate-reducing consortium was capable of reducing the Pt(IV) ion without such an exogenous electron donor. Certain SRB's, such as

*D. desulfuricans* are capable of metal-reduction via the oxidation of organic compounds, that is not coupled to growth, and often results in the production of endogenous hydrogen or formate (Lloyd *et al.*, 2001; Madigan *et al.*, 2000; De Luca *et al.*, 2001), though the mechanism for this is not fully understood. This has major advantages as this would exclude the possibility of the exogenous electron donor interfering in the reaction, as high concentrations of hydrogen were observed to.

At 0 h, the pH for the viable cell-samples, either in the presence or absence of hydrogen, was lower than expected at pH 7.45 but remained stable throughout the investigation. The pH of the heat-killed sample was pH 7.6 at 0 h, which was the expected starting pH of the Tris-HCl buffer (200 mM, pH 7.6). The lower pH observed for the viable cells correlates to the lower Pt(IV) and higher Pt(II) concentrations resulting from Cycle 1 of Pt(IV) reduction. Similarly, the pH of the heat-killed sample continued to decrease slowly reaching pH 7.51 after 5 h. The drop in pH was due to the generation of a total of 6 HCl molecules from the reduction of one molecule of H<sub>2</sub>PtCl<sub>6</sub> and subsequent deposition of a single Pt(0) atom (Equation 5) (Koebel *et al.*, 2008), however due to the presence of the Tris-HCl buffer, the pH change was kept to a minimum. The reaction was expected to proceed as follows via the catalytic action of a periplasmic H<sub>ase</sub>:



When comparing the same results in Fig 2.4 I - with the exception of the cells incubated at 4 °C and including the expected starting concentration (1 mM) for Pt(IV) - the evidence for a two step reduction process for Pt(IV) to Pt(II) was even more convincing, and is illustrated in Fig 2.4 II. In viable cells, Step 1 occurs between 0-0.25 h while Step 2 occurs from 0.25–2 h, after which there were no further significant changes observed.

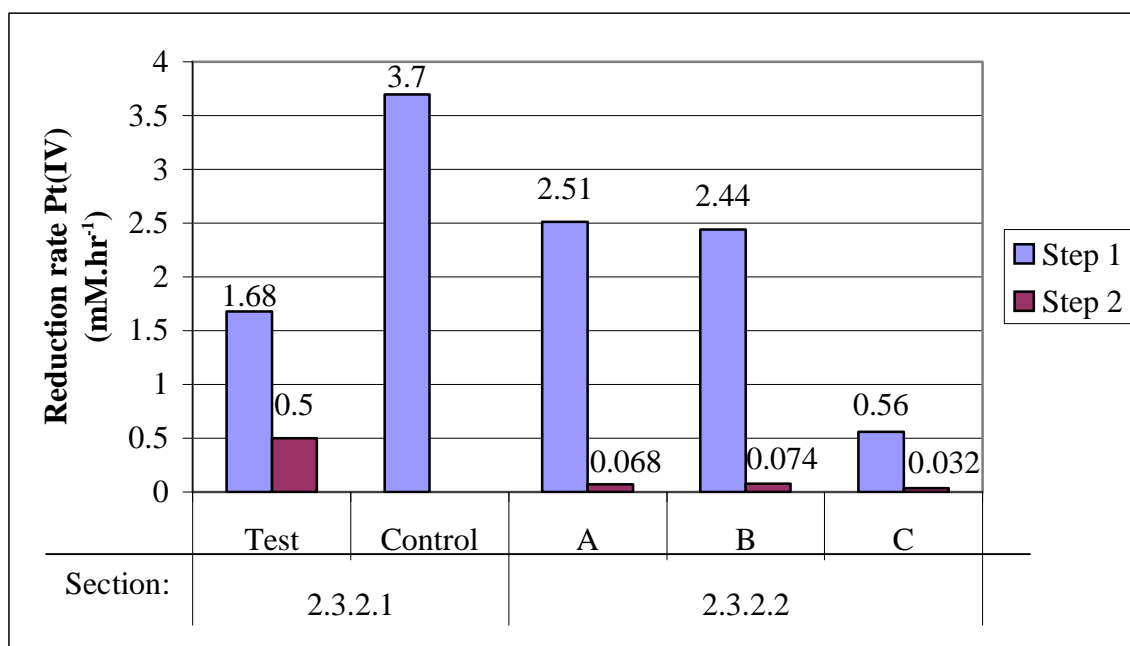


**Figure 2.5:** Comparison of the reduction rates of Pt(IV). [Section 2.3.2.1: Test) Cells + Pt(IV) + H<sub>2</sub>(g) bubbled through, Control) Cell-free + Pt(IV) + H<sub>2</sub>(g) bubbled through. Section 2.3.2.2: A) Cells + Pt(IV) + H<sub>2</sub>(g), B) Cells + Pt(IV) + N<sub>2</sub>(g), C) Heat-killed cells + Pt(IV) + H<sub>2</sub>(g).] \*

The test sample (section 2.3.2.1) (Fig 2.5), shows that under anaerobic conditions, there was an initial rapid Pt(IV) reduction step (Step 1) followed by a slower secondary reduction (Step 2) after induction of H<sub>ase</sub> activity by hydrogen. The initial reductase activity was shown to increase significantly in the presence of oxygen (section 2.3.2.2.) while the second step was decreased, but could be improved by exogenous hydrogen. Very little activity was seen in the case of the heat-killed sample. These results further demonstrate the possibility that two separate mechanisms are involved in the reduction of Pt(IV) including an oxygen-sensitive H<sub>ase</sub> and a ‘novel’ oxygen-tolerant Pt(IV) reductase as observed in sections 2.3.2.1 and 2.3.2.2 respectively.

It was hypothesised (Riddin *et al.*, 2006) that the overall Pt(IV) reduction to Pt(0) by biological action occurs via a two-cycle mechanism where Pt(II) is the intermediate (section 1.3.3, Fig 1.5). To investigate this, the absorbance values of the same samples in section 2.3.2.2 tested for Pt(IV) at 261 nm were tested for Pt(II) at 230 nm (Fig 2.6).

\* All values shown have a standard deviation < 10 %

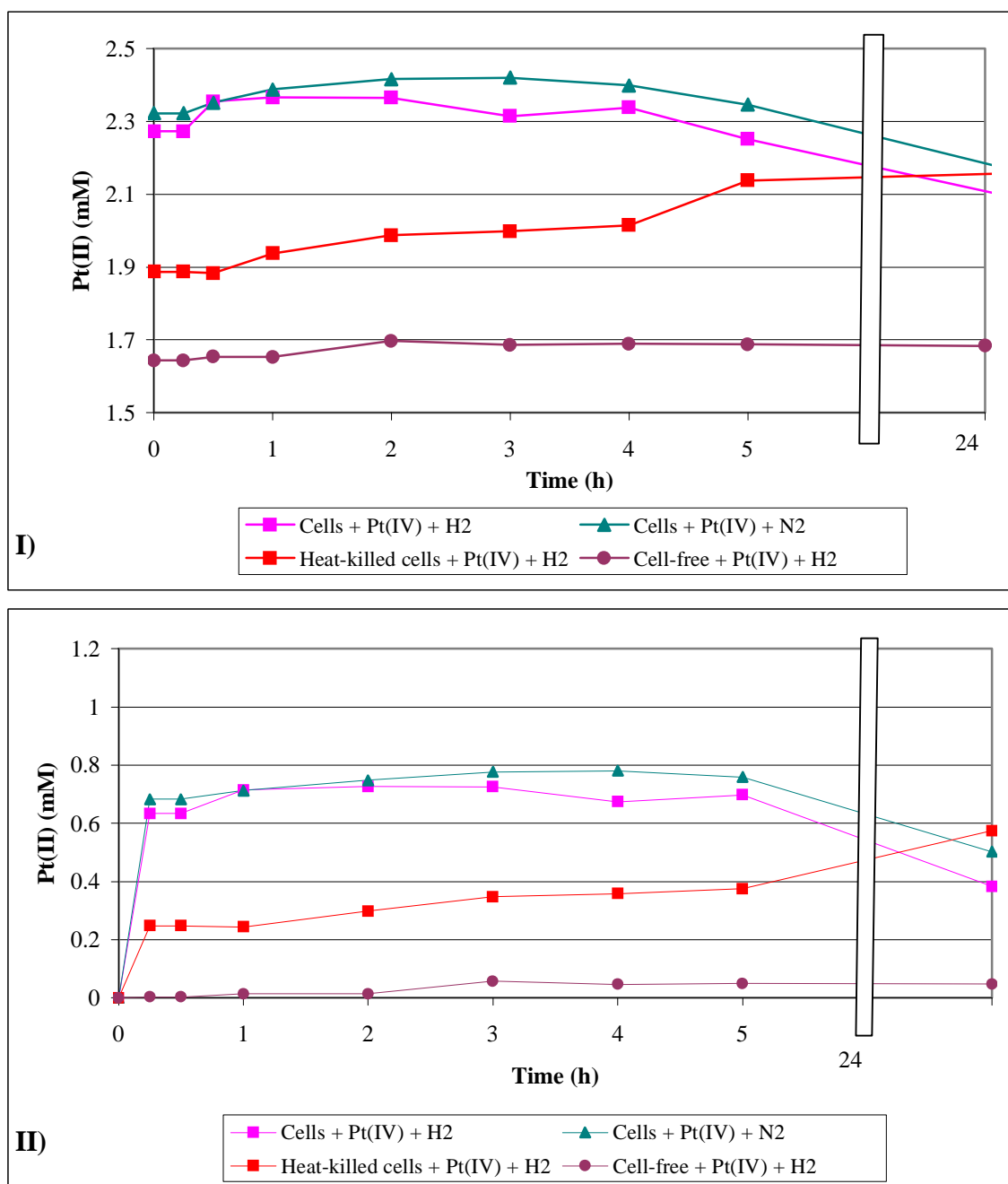


**Figure 2.6:** Bioreduction of Pt(II) by SRB cells. **I)** Formation and subsequent reduction of Pt(II) by SRB consortium over time. **II)** Normalised data for the formation and subsequent reduction of Pt(II) by SRB consortium over time.] \*

Since the Pt(IV) ion also absorbed at 230 nm, Fig 2.6 I illustrates the complications that arose. The initial starting concentrations of the Pt(II) ion were all far greater than expected due to the residual absorbance of the Pt(IV) ion at this wavelength (Appendix E). This, in turn, made it difficult to determine the true Pt(II) ion

\* All values shown have a standard deviation < 10 %

concentration. From the 1 mM Pt(IV) cell-free control, an apparent Pt(II) concentration of 1.64 mM was observed at 0 h. As no cells were present to account for any Pt(IV) reduction, this value was taken to represent the point where no Pt(II) ions had yet been formed from the bioreduction of Pt(IV). Therefore, in all subsequent calculations, the data was normalised by deducting this value (1.64 mM) from the apparent Pt(II) concentrations observed in Fig 2.6 I, and the Pt(II) concentration at 0 h was taken to be 0 mM. When analysing the results for the Pt(II) ion in Fig 2.6 II, the concentration of this ion was shown to exhibit an initial rapid increase in concentration. This correlates strongly to Fig 2.4 II, which illustrates an initial rapid decrease in Pt(IV) concentration in the samples containing viable cells. To our knowledge, this is the first evidence of a two-cycle reduction mechanism of Pt(IV) becoming reduced to Pt(0) via the intermediate ion Pt(II) by a biological organism, as hypothesised by Riddin *et al.* (2006).

As mentioned above for Fig 2.6 II, the concentration of Pt(II) increases rapidly within 1 h, eventually reaching a maximum at 4 h for the cell sample lacking an electron donor (under nitrogen), after which the concentration decreases slowly reaching a concentration of ~0.50 mM Pt(II) after 24 h. In the presence of exogenous hydrogen, a slightly higher rate of Pt(II) reduction was observed where it reached a concentration of ~0.38 mM Pt(II) after 24 h. These results indicate that the Pt(IV) ion must be fully reduced before reduction of the Pt(II) ion will begin.

In the heat-killed sample, a steady increase in Pt(II) formation was observed over time. As there is no direct UV-Vis spectroscopy evidence of any reduction or re-oxidation of the Pt(II) ion occurring in this sample, these results further indicate that an active/enzymatic process is responsible for Cycle 2 of this mechanism [i.e. Pt(II) --> Pt(0)]. While partial reduction of Pt(IV) has been shown to be able to occur passively, the passive reduction of Pt(II) cannot be completely ruled out without further investigation.

The reduction of Pt(IV) ---> Pt(II) was rapid in viable cells in the presence of low levels of oxygen and as previously mentioned in section 2.3.2.2, was observed to occur via a two-step process, Fig 2.4 II(Cells + Pt(IV) + H<sub>2</sub> & Cells + Pt(IV) + N<sub>2</sub>). Step 1, an initial rapid reduction of the majority of Pt(IV) ions by an active



mechanism followed by Step 2, a slower, possibly passive process involving biosorption. The fact that the heat-killed cells exhibit a much lowered capacity of ~30 % reduction/removal of Pt(IV) ions from solution after 5 h, further supports this theory.

The reduction of Pt(II)  $\rightarrow$  Pt(0) occurs in a single step at a much slower rate than that of Pt(IV)  $\rightarrow$  Pt(II) and was observed to be incomplete after 24 h in the presence of viable cells (Fig 2.6 II). The reduction of Pt(II) was however increased in the presence of low levels of exogenous hydrogen. An active mechanism of Pt(II)  $\rightarrow$  Pt(0) reduction is further supported by the apparent lack of this step in heat-killed cells (Fig 2.6 II) indicating that an active, enzymatic/protein based process – most likely the  $H_{ase}$  enzyme (Rashamuse & Whiteley, 2007) - is involved. As neither Cycle 1 [Pt(IV)  $\rightarrow$  Pt(II)] nor Cycle 2 [Pt(II)  $\rightarrow$  Pt(0)] of the overall reduction mechanism was inhibited by the presence of low levels of oxygen or absence of an electron donor, the  $H_{ase}$  is expected to be at least partially oxygen tolerant capable of utilising endogenous stores of electron donors for metal reduction. Certain species of SRB, such as *D. desulfuricans*, are capable of producing endogenous electron donors, such as hydrogen, from the oxidation of organic compounds (i.e. lactate) during stationary phase metabolism in the absence of sulfate (Fig 1.7 A) (Lloyd *et al.*, 2001).

In this investigation, the independent reductive ability of  $H_2(g)$  has been negated by the low exogenous concentration of this gas present in this experiment. The results for the cell-free sample illustrated in Fig 2.6 II shows a loss of only ~5 % Pt(IV) after 24 h which may be attributed to chemical reduction.

#### 2.3.2.3. *Effect of oxic conditions with no exogenous electron donor*

This experiment was conducted in order to determine the effect of atmospheric oxygen concentration on the reductive mechanism of Pt(IV) in the absence of an exogenous electron donor, by the present consortium of sulfate-reducing bacteria.

On addition of the cells, a rapid reduction of Pt(IV) was observed (Fig 2.7), which continued and slowed after time with ~80 % being reduced after 2 h with no further change. A colour change of the cells from light yellow to brown was observed over

this period, most likely due to the formation of Pt(0) which is brown to black in colour.

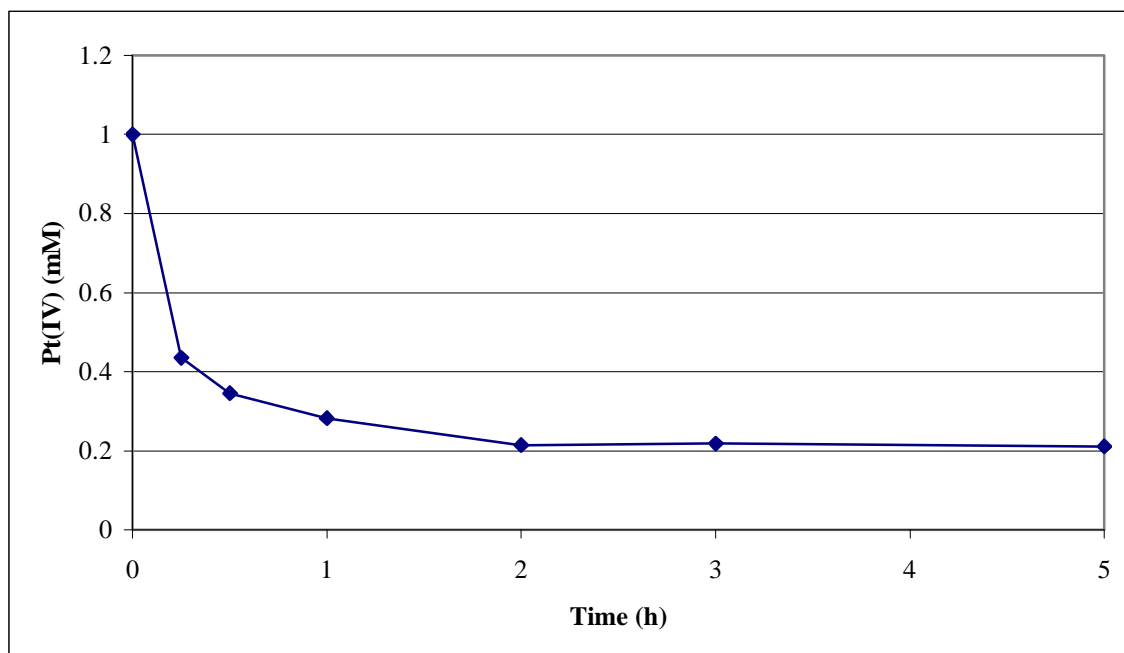


**Figure 2.7:** Reduction of Pt(IV) over time by the current consortium of SRB under an aerobic atmosphere with no exogenous electron donor . \*

The Pt(IV) reduction path was very similar to those observed under partially anaerobic conditions. These results correlate to those in the previous section which suggested that the mechanism was oxygen tolerant. Once again, complete reduction (100 %) of the Pt(IV) ion was not attained, possibly due to the reasons mentioned previously in section 2.3.2.2.

Although SRB are generally classified as strict anaerobes, containing oxygen-sensitive  $H_{ase}$  enzymes - that have previously been cited as the major cause of metal-reductase activity within SRB – a number of species have been found to be surprisingly oxygen tolerant, containing oxygen-tolerant  $H_{ase}$ 's (De Lacy *et al.*, 2000; Fournier *et al.*, 2004). Some SRB have even been shown to be capable of replacing sulfate with oxygen in respiration for ATP synthesis (Cypionka, 2000).

The pH remained relatively constant throughout the investigation only decreasing by 0.1 pH units from 7.61 to 7.51. The pH was seen to decrease over time following a

\* All values shown have a standard deviation < 10 %

similar trend as seen for the reduction rate. This is explained by the release of HCl into solution from the reduction of  $\text{H}_2\text{PtCl}_6$  as explained in section 2.3.2.2.

### 2.3.3. *Elucidating the mechanism*

The results from the previous experiments were combined to produce the following graphs (Fig 2.8 A & B), with Pt(0) calculated as the difference between the Pt(IV) and Pt(II) concentrations assuming stoichiometric chemistry. These graphs show the stoichiometric relationship of Pt(IV)  $\rightarrow$  Pt(II)  $\rightarrow$  Pt(0) during bioreduction by the SRB consortium in the presence (Fig 2.8 A) and absence (Fig 2.8 B) of hydrogen as the electron donor. These results prove the hypothesis as suggested by Riddin *et al.* (2006) that the bioreduction of Pt(IV) reduction to Pt(0) is a two-cycle mechanism with Pt(II) as the intermediate.

The reduction rates of the Pt(IV) ion in Fig 2.8 A and B, are almost identical with a subtle difference that arises in the reduction of the Pt(II) ion and subsequent formation of Pt(0). The sample with an external electron donor shows a noticeably faster rate in both cases. In both graphs, the reduction of the Pt(II) ion exhibits a stationary reduction phase much like that observed in Fig 2.3, section 2.3.2.1 for the reduction of the Pt(IV) ion. This further suggests that the reduction of the Pt(II) ion is an active process, possibly due to a periplasmic  $\text{H}_{\text{ase}}$ , while the reduction of Pt(IV) to Pt(II) is due to a second oxygen-tolerant Pt(IV) reductase.

From the results obtained in the prior investigations, three suggested mechanisms are put forward to further explain the bioreduction of Pt(IV)  $\rightarrow$  Pt(0) by a consortium of SRB under anaerobic/aerobic conditions

#### Mechanism 1:

**“During anaerobic reduction of the Pt(IV) ion observed in section 2.3.2.1. Fig 2.3 (Test), an oxygen-sensitive periplasmic  $\text{H}_{\text{ase}}$  is responsible for the reduction of Pt(IV) to Pt(0) in the presence of hydrogen acting as the electron donor.”**

There is also evidence to suggest that hydrogen itself is partly responsible.

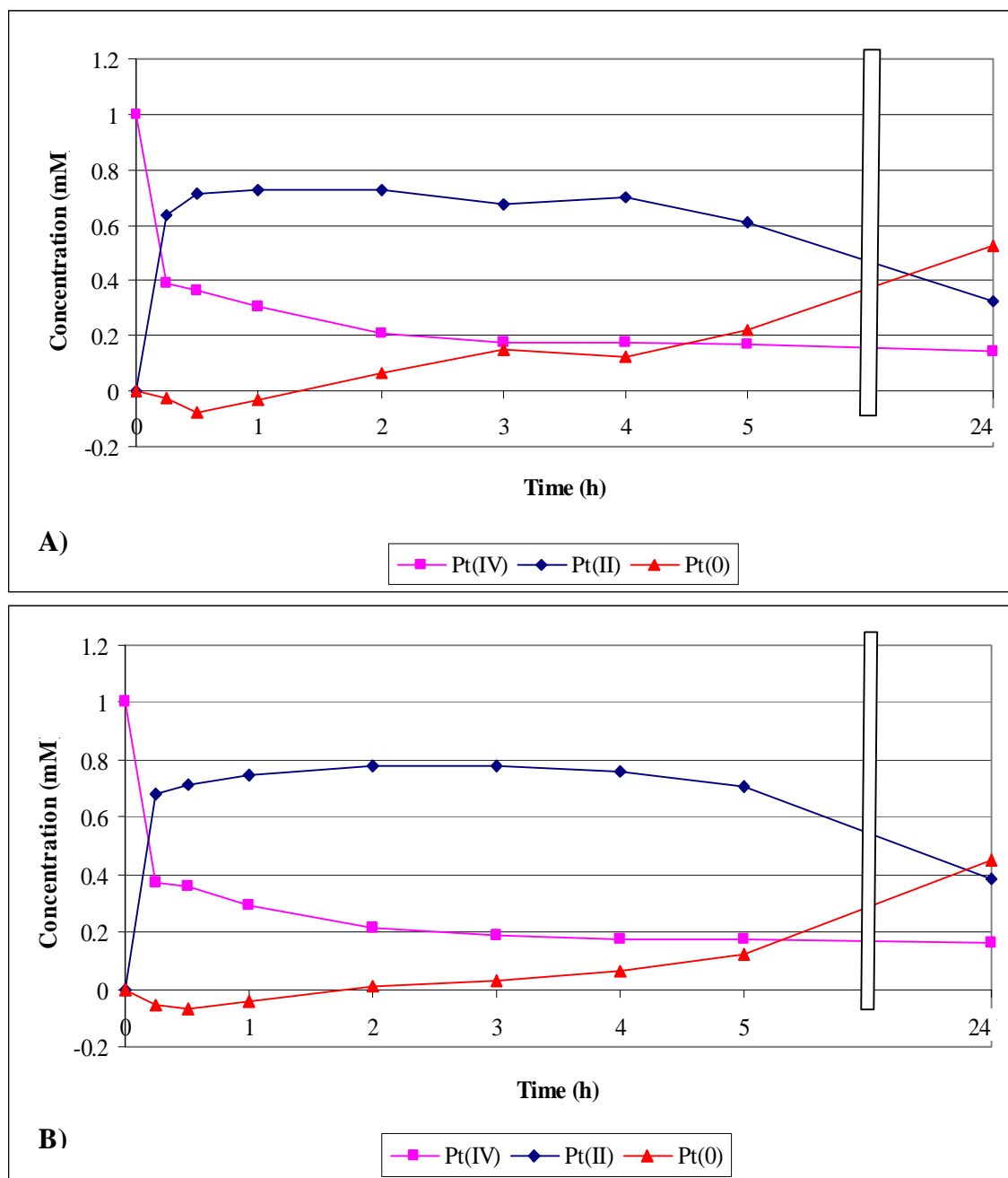


**Figure 2.8:** Conversion of Pt(IV)  $\rightarrow$  Pt(II)  $\rightarrow$  Pt(0) over time for the sample with **A)** hydrogen as the exogenous electron donor and **B)** no exogenous electron donor. \*

### Mechanism 2:

**“In the presence of oxygen, the mechanism is more complex and is seen to differ from that observed under anaerobic conditions.”**

\* All values shown have a standard deviation < 10 %

Fournier *et al.* (2004) demonstrated that in *Desulfovibrio vulgaris* Hildenborough, the activity of the periplasmic [Fe]-H<sub>ase</sub> was increased significantly in the presence of oxygen, indicating its involvement in a protective mechanism against oxidative stress. The [Fe]-H<sub>ase</sub> is also classified as being responsible for the evolution of hydrogen in anaerobic bacteria (Das *et al.*, 2006). Therefore, under the more oxic conditions of section 2.3.2.2 (Fig 2.4 II), the activity of the periplasmic [Fe]-H<sub>ase</sub> was increased, stimulated rather than inhibited by the presence of oxygen. It is proposed that the production of the endogenous electron donor (hydrogen) by this [Fe]-H<sub>ase</sub> rapidly increases to sufficient levels to activate the more oxygen sensitive periplasmic membrane-bound [NiFe]-H<sub>ase</sub>, responsible for hydrogen uptake (Das *et al.*, 2006). This H<sub>ase</sub> then utilizes the evolved hydrogen as an electron donor resulting in the higher initial reductase activity of the Pt(IV) ion (Step 1 of Pt(IV) reduction) observed in samples containing viable cells, section 2.3.2.2, Fig 2.4 II.

### Mechanism 3:

**“Under non-growth conditions, the electrons utilized by the H<sub>ase</sub> for metal reduction are produced via the respiration of oxygen, by the metabolism of endogenous polyglucose and/or other organic compounds accumulated within the cell during normal growth.”**

A number of possible reasons exist for the presence of the lag phase observed in the reduction of the Pt(II) ion (Fig 2.8 A & B). First, the lag phase occurs due to the competitive nature existing between the Pt(IV) and Pt(II) ions where the [NiFe]-H<sub>ase</sub>'s has a higher affinity for Pt(IV). Therefore, Pt(II) reduction will only proceed once Pt(IV) has been fully reduced and for the same reason will occur at a slower rate.

Second, the endogenous production of hydrogen/electrons via the oxidation of organic compounds, evolved by [Fe]-H<sub>ase</sub> or oxygen respiration, would most likely be rapid initially, slowing down as the finite store of organic compounds/substrate becomes limiting. Therefore the amount of endogenous hydrogen/electrons produced would decrease as substrate becomes further limited resulting in most of the H<sub>ase</sub> activity being utilised for Pt(IV) reduction with less being available for Pt(II) reduction.

Third, the decreased reductase activity observed in Step 2 of Pt(IV) reduction may be due to oxygen toxicity. Even though the SRB seem to be readily oxygen tolerant, oxidative stress would become deleterious after a significant amount of exposure (Fournier *et al.*, 2004). The activity of [Fe]- periplasmic H<sub>ase</sub> in *D. vulgaris* Hildenborough was also increased by the addition of chromate which increased the redox potential much like the addition of hexachloroplatinate would (Fournier *et al.*, 2004).

#### 2.3.4. TEM & SEM-EDAX analysis

With SEM analysis, due to their high atomic number, metals appear as areas of light/white highlighted against a dark background as they reflect more electrons (Sriamornsak & Thirawong, 2003), under back-scattering conditions. With this in mind, spots of interest with expected metal content were chosen and analysed for the presence of Pt(0). It is important to note that under the conditions employed for SEM-EDAX analysis, the following results are not quantitative.

##### 2.3.4.1. Control SRB experiment in the absence of Pt(IV)

The control was prepared in the same way as the other samples with the exception of the cells not being challenged with Pt(IV). From the TEM images, no areas of notable electron density in the variety of cells was observed (Figure 2.9 A<sub>1+2</sub>). With regards to the SEM-EDAX analysis Fig 2.9 B, there were a number of other elements present such as phosphorus (P), oxygen (O), nitrogen (N) and sulfur (S), all which would be expected to be present due to their associations in amino acids, proteins, and the structural elements of cells. The vertical black lines indicate where the platinum peaks would be expected to appear.

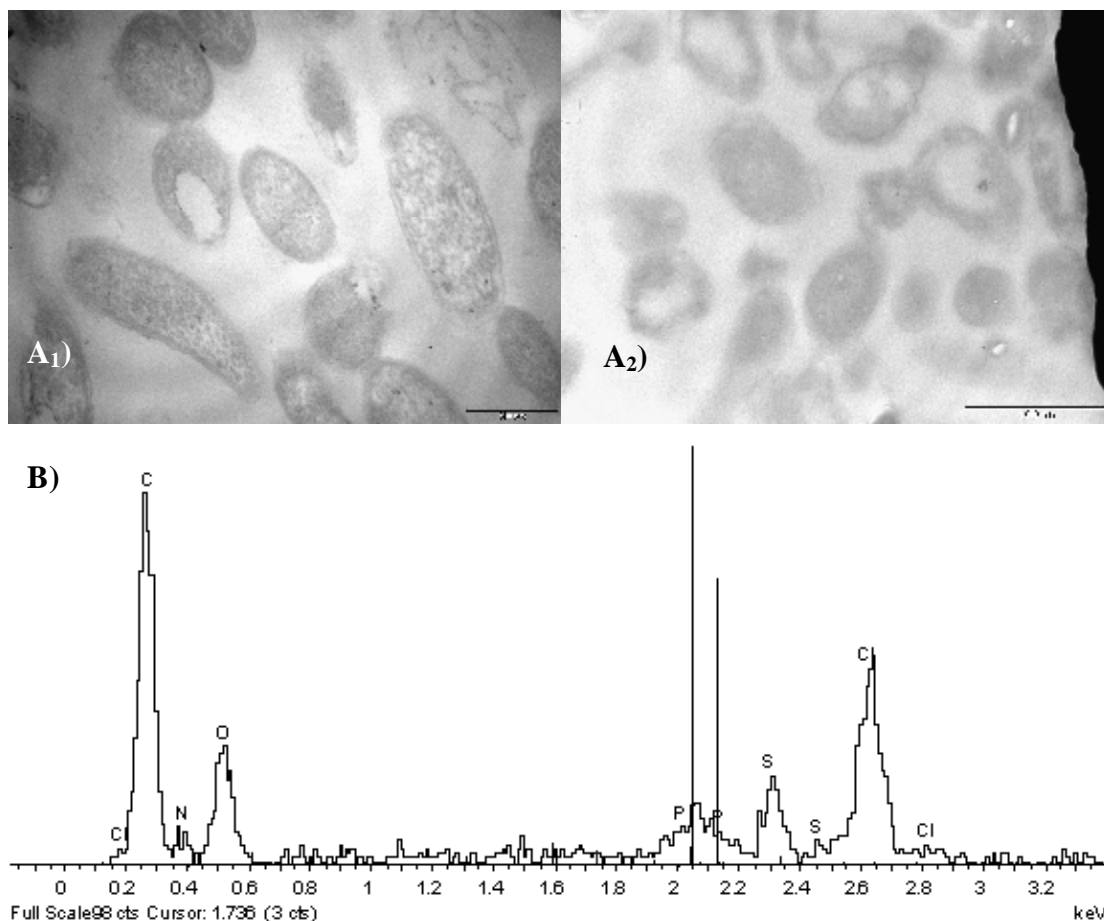


**Figure 2.9:** Control cells not challenged with Pt(IV). [A<sub>1</sub>) + A<sub>2</sub>): TEM images of control cell sample. Scale bars = 500 nm and 1000 nm respectively. B) SEM-EDAX spectrum of control sample.

#### 2.3.4.2. Cell-free Pt(IV) control in the presence of high levels of hydrogen

From the cell-free control of section 2.3.2.1, a number of electron dense Pt(0) particles were observed in the TEM image (Fig 2.10 A<sub>1+2</sub>). Fig 2.10 A<sub>2</sub> is an enlargement of Fig 2.10 A<sub>1</sub> and clearly shows electron dense particles, mostly rounded-irregular in nature and ranging in size from 10-50 nm. Fig 2.10 B shows the EDAX graph obtained from the same sample, clearly indicating the presence of Pt(0) as illustrated by the platinum peaks.

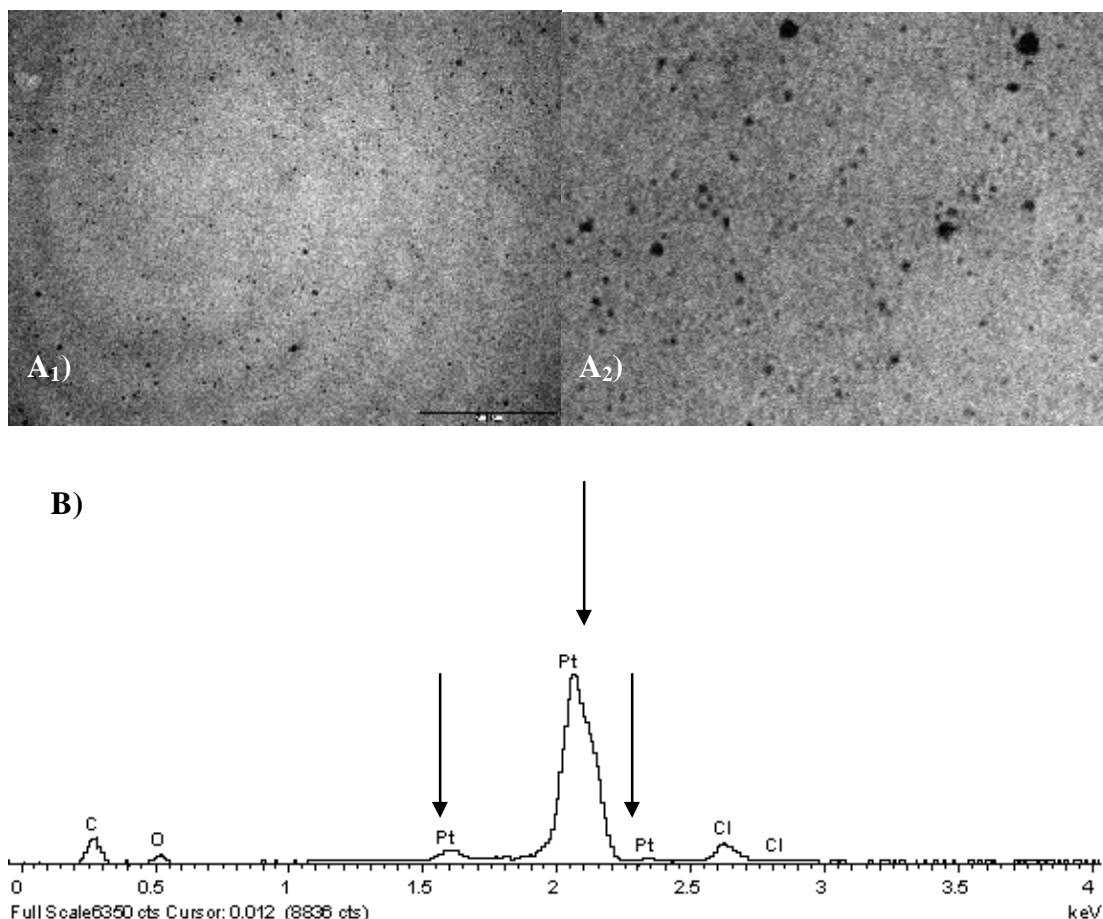


**Figure 2.10:** Cell-free control from section 2.3.2.1., incubated with Pt(IV) under high hydrogen concentration. [A<sub>1</sub>] A TEM image illustrates the presence Pt(0) particles formed by the abiotic reduction of Pt(IV) by hydrogen. Scale bar = 500 nm. A<sub>2</sub>) enlarged version of A<sub>1</sub>. B) The EDAX spectrum obtained from a sample of the cell-free control.]

#### 2.3.4.3 SRB sample challenged with Pt(IV) in the presence of high hydrogen levels

The test sample from section 2.3.2.1 shows a number of cells with electron dense platinum deposits located mainly within the periplasm, the area between the inner and outer membranes of the cells (Fig 2.11 A<sub>1+2</sub>), as illustrated by the black arrows. The TEM image on the right (A<sub>2</sub>) shows a number of cells, some of which exhibit areas of metal precipitation while others do not. This indicates that Pt(IV) reduction is a selective mechanism with not all cells present in the consortium containing the required Pt(IV) reductase mechanism. Figure 2.11 B – shows an EDAX graph of the same sample, clearly indicating the presence of Pt(0), among other biologically relevant elements.



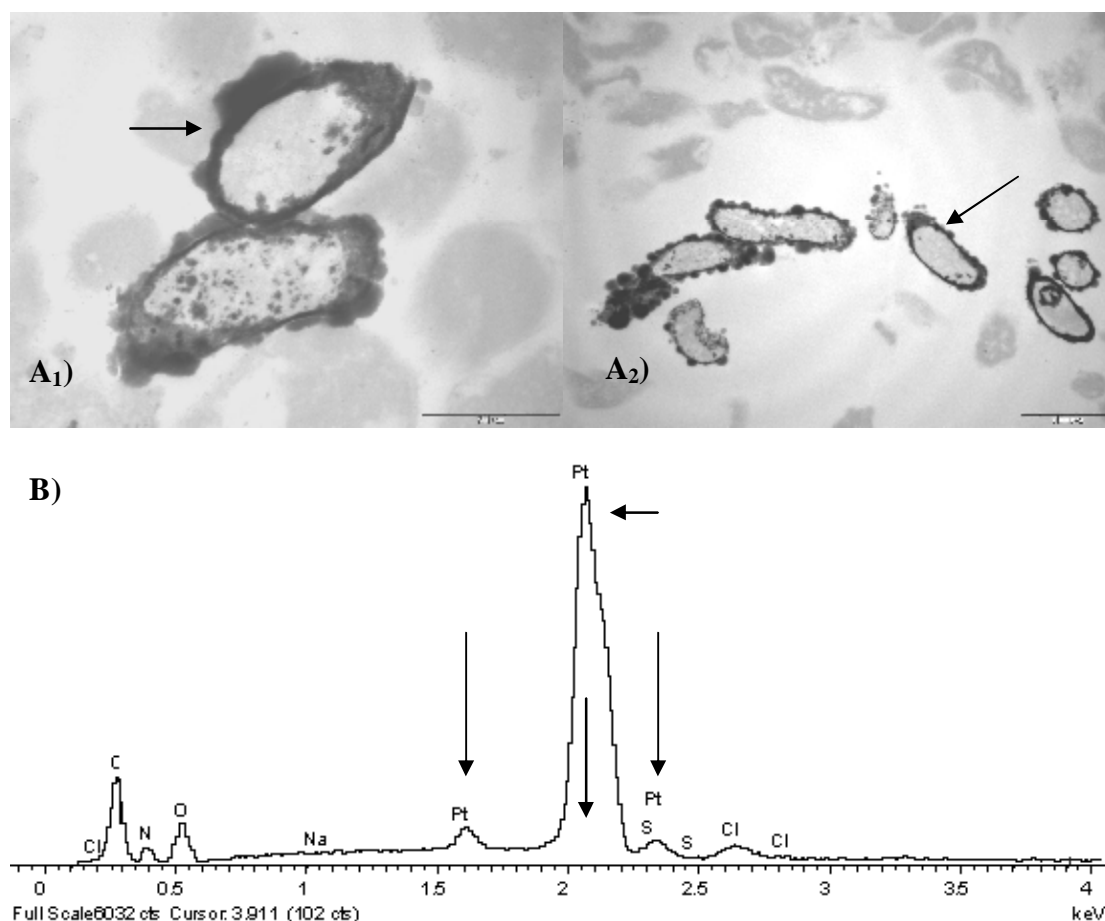


**Figure 2.11:** Cells incubated in Pt(IV) with hydrogen bubbled through as electron donor. [A<sub>1</sub>) TEM image of cells with platinum deposits in the periplasm. Scale bar = 500 nm. A<sub>2</sub>) Image showing selective Pt(0) uptake. Scale bar = 1000 nm. B) EDAX graph of this sample indicating presence of platinum.]

#### 2.3.4.4. SRB cells challenged with Pt(IV) in the absence of hydrogen

In the sample containing no additional electron donor (Fig 2.12 A<sub>1+2</sub>), a number of cells were observed to exhibit electron density within the periplasmic regions. From the image on the left (A<sub>1</sub>), it is also evident that the uptake of Pt(IV) is once again a selective mechanism as not all the bacteria in the consortium are shown to exhibit metal precipitation. The metal precipitate is mainly observed to be located within the periplasm with a small percent located on the cell surface (A<sub>2</sub>). These results further support the involvement of a H<sub>ase</sub> enzyme as well as a passive immobilisation mechanism in the Pt(IV) reductase activity of this sample - under partially oxic conditions. These cells do, however exhibit a lower amount of Pt(0) precipitation than those observed under anaerobic conditions with exogenous hydrogen. This suggests

that the anaerobic mechanism is observed to be more efficient than the aerobic mechanism.

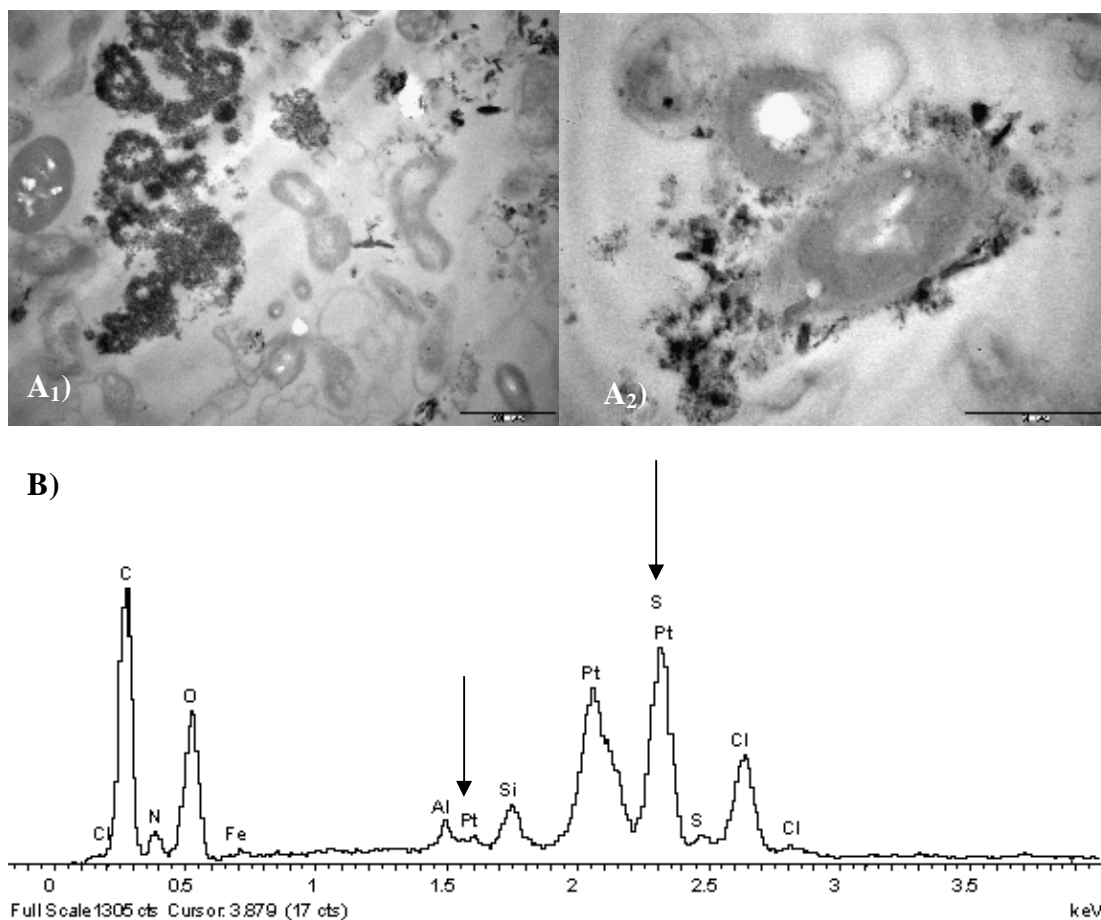


**Figure 2.12:** A<sub>1</sub>) TEM image of SRB consortium with no exogenous hydrogen. Scale bar = 1000 nm. A<sub>2</sub>) SRB cell showing electron dense deposits in the periplasm. Scale bar = 500 nm. B) EDAX spectrum of sample with no exogenous hydrogen.

The above spectrum (Fig 2.12 B) was obtained from the same sample without an exogenous electron donor (section 2.3.2.2). A number of elements are present including carbon (C), oxygen (O) and nitrogen (N) which, as described previously would be expected to be present in any carbon-based life form. Pt(0) is clearly present indicating that this sample is capable of reducing Pt(IV) to Pt(0), with no exogenous electron donor under partially oxic conditions. Chlorine (Cl) is also present and most likely originated from the platinum salt. The presence of sulfur (S) may either be due to the growth medium which is unlikely since the cells were washed multiple times and resuspended in a non-sulfur containing buffer and is therefore more likely to be due to cysteine residues from proteins and/or FeS compounds. The presence of iron

(Fe) may further support the growing evidence for the involvement of a  $H_{ase}$  enzyme as iron is part of the periplasmic  $H_{ase}$  active site. Small amounts of aluminium (Al) and silica (Si) are also present from unknown sources.

These results prove that the SRB consortium is capable of reducing Pt(IV) both with and without an exogenous electron donor under partially/fully oxic conditions although the mechanism under anaerobic conditions is more efficient.

#### 2.3.4.5. Heat-killed SRB cells challenged with Pt(IV) with low levels of hydrogen

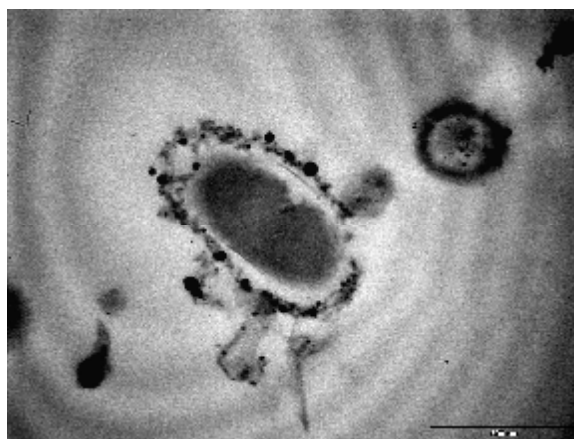


**Figure 2.13:** TEM image of heat-killed SRB cell with surface localised platinum deposits. [Scale bar = 500 nm.]

The heat-killed samples also showed a degree of electron dense deposits but they were all located on the external surface of the bacterial cell wall, not within the periplasm, indicating that only a passive reductive mechanism is involved in this case (Fig 2.13). The platinum concentration was not sufficient for EDAX analysis but may be inferred by the presence of the electron dense deposits observed in the TEM image.

## 2.4. Summary & Conclusions

- The present consortium of SRB are capable of reducing Pt(IV) to Pt(0)
- Exogenous sources of hydrogen, or any other electron donor is not required for the reduction of Pt(IV) although the rate of reduction is improved in the presence of exogenous electron donor (hydrogen).
- The reduction of Pt(IV)  $\rightarrow$  Pt(II) occurs via a two-step mechanism, an initial rapid reduction step followed by a slower reduction rate.

- Oxygen does not inhibit the reduction of Pt(IV)  $\rightarrow$  Pt(0) by the current consortium of SRB but is observed to occur via a separate, less efficient mechanism, than observed under anaerobic conditions
- Pt(IV) becomes reduced to Pt(0) via the intermediate cation Pt(II) in a two-cycle reduction mechanism
- Reduction of Pt(II) occurs at a slower rate than that of Pt(IV)
- Several H<sub>ase</sub> enzymes may be responsible for Pt(IV) metal reduction.

## CHAPTER THREE

### Periplasmic hydrogenase:

### Role in the bioreductive mechanism of Pt(IV) to Pt(0)

---

---

#### 3.1. Introduction

Sulfate-reducing bacteria (SRB) are present in a variety of anaerobic environments. Once thought to be strict anaerobes, the discovery of their existence in oxic environments has since refuted this report. SRB exhibit a number of responses to oxygen, which are often but not necessarily species specific. First, certain species such as *Desulfobacter*, migrate via chemotaxis, to metabolically acceptable levels, of oxygen concentration, within a microbial mat. Second, some SRB aggregate together, thereby forming a more oxygen tolerant microenvironment, while others (i.e. *Desulfovibrio*) have even been observed to reduce oxygen, often at respiration rates exceeding their aerobic cousins, either under growth or non-growth conditions (Cypionka, 2000; Fournier *et al.*, 2004).

*Desulfovibrio vulgaris* Hildenborough has been shown to possess four periplasmic hydrogenases ( $H_{ase}$ 's), namely a membrane bound [NiFeSe]- $H_{ase}$ , two membrane-bound [NiFe]- $H_{ase}$ 's and a soluble [Fe]- $H_{ase}$ . It is still unknown why this microbe would require such redundancy. A number of suggestions have been made mostly around the basis that it is a survival mechanism. The redundancy would allow the microbe to cope with a number of deleterious conditions including the presence of  $H_{ase}$  inhibitors, as well as fluxes in environmental metal and hydrogen concentrations. It is also thought that they may be involved in separate metabolic pathways (Caffrey *et al.*, 2007).

During oxygen respiration in aerobic micro-organisms, a number of highly activated oxygen radicals (i.e. superoxide  $O_2^-$ ) are produced. Left unattended, these undesirable molecules would result in massive oxidative damage, eventually resulting in cell death.

Superoxide dismutase (SOD) and superoxide reductase (SOR) are both involved in the removal of such unwanted oxygen anions from the system of aerobic microbes, and have recently been identified in *Desulfovibrio* species (Davydova *et al.*, 2006) with the highest concentrations of these proteins being found during the stationary growth phase (Davydova & Sabirova, 2002).

Fournier *et al.* (2004) described the unexpected oxygen tolerance of the abundant periplasmic [Fe]-H<sub>ase</sub> in *D. vulgaris* Hildenborough and suggested the involvement of SOD and/or SOR in a protective mechanism of this typically oxygen-sensitive enzyme. This particular H<sub>ase</sub>, has been shown to possess a high concentration of iron-sulfur clusters [4Fe-4S] which in turn makes it susceptible to superoxide inhibition, since this radical tends to destabilise these clusters. Fournier and colleagues (2004) demonstrated that in the presence of pure oxygen both the wild-type and an SOD-deleted mutant showed an increase in H<sub>ase</sub> activity due to the up-regulation of the [Fe]-H<sub>ase</sub> gene. The wild-type cells, however exhibited a higher H<sub>ase</sub> activity than the SOD-deleted mutant, thereby proving their theory that SOD has a protective function in relation to this H<sub>ase</sub>. The up-regulation of this particular [Fe]-H<sub>ase</sub> under oxic conditions also suggests that it, too, may have a protective function against oxidative-stress for the cell in general. This is supported by the work of Baumgarten and colleagues (2001) where oxygen reduction in *D. vulgaris* Marburg was shown to be the result of action by the periplasmic [Fe]-H<sub>ase</sub> and a cytochrome.

H<sub>ase</sub> enzymes play a major role in hydrogen cycling within anaerobic organisms. The [Fe]-H<sub>ase</sub> was the first to be purified to homogeneity and sequenced in *D. vulgaris* and demonstrates exceptional turn-over rates that far surpass those of the related nitrogenase enzymes. It is known to have bidirectional functionality in anaerobic hydrogen metabolism, since these particular metalloenzymes are capable of H<sub>2</sub> uptake during normal growth conditions and H<sub>2</sub> evolution, by scavenging excess electrons produced during fermentative metabolism, in the absence of sulfate (Das *et al.*, 2006).

Voordouw (2002) demonstrated that a) an [Fe]-H<sub>ase</sub> is very likely to be involved in endogenous hydrogen production via pyruvate oxidation in this organism, and b) that hydrogen and other fermentation products accumulated during the initial growth stages of *D. vulgaris* Hildenborough. This metabolic “accumulation” is known as the “hydrogen/fermentation burst” which occurs when electrons released from the oxidation of organic acids exceed the rate of sulfate reduction by these electrons. Odom and Peck (1981) first proposed that the *Desulfovibrio spp.* produced molecular H<sub>2</sub> via a cytoplasmic H<sub>ase</sub> that scavenges these excess electrons. The hydrogen then disperses through the cell to the periplasm where it becomes available for use by the periplasmic H<sub>ase</sub>. There are, however, a number of issues associated with this hypothesis, namely the fact that a cytoplasmic H<sub>ase</sub> has yet to be identified in *D. vulgaris* and the fact that hydrogen production from lactate oxidation is an energetically unfavorable reaction (Voordouw, 2002).

It is therefore exceedingly possible that endogenous electrons are produced during fermentative metabolism and/or accumulated during the hydrogen burst, via an [Fe]-H<sub>ase</sub>. This enzyme is both protected from oxidative stress by SOD and up-regulated in the presence of oxygen. The endogenous electrons become utilised during non-growth conditions, in the absence of sulfate, for the reduction of the platinum metal-ions by other periplasmic H<sub>ase</sub>'s protected from oxidative stress by the [Fe]-H<sub>ase</sub> and SOD. As demonstrated in Chapter 2, the Pt(IV) ion becomes reduced via a two-cycle, biologically dependant process to elemental platinum (Pt0) via the intermediate cation, Pt(II), in the presence or absence of an exogenous electron donor. An exogenous electron donor is not necessary since electrons are being produced endogenously. The mechanism is furthermore expected to be an active, enzymatic process which includes the activity of a periplasmic located, oxygen-tolerant/protected H<sub>ase</sub> enzyme(s), but this has yet to be confirmed.

The results in Chapter 2, demonstrated that there are separate mechanisms responsible for this bioreduction under anaerobic and aerobic conditions respectively. Under aerobic conditions, an exogenous electron donor was shown to be non-essential, but did result in

an increased reduction rate of the Pt(II) ion when present. The involvement of an oxygen-tolerant/protected H<sub>ase</sub> enzyme(s) is further supported by the evidence that the reduction of the Pt(II) ion does not go to completion in the absence of an exogenous electron donor, most likely due to limited availability.

Since the anaerobic mechanism of Pt(IV) reductase activity with hydrogen acting as the electron donor has been previously reported by Rashamuse and Whitely (2007), the aerobic mechanism will form the focus of subsequent investigations.

The objectives of Chapter 3 are to:

- i) Inhibit the periplasmic H<sub>ase</sub> (s) in whole cells by incubation with Cu(II), a known irreversible inhibitor.
- ii) Confirm, via an adapted methyl-viologen H<sub>ase</sub> assay for whole cells, that the inhibitor has resulted in lowered/loss of periplasmic H<sub>ase</sub> activity post incubation with inhibitor.
- iii) Determine this enzyme(s) involvement in the two cycles of aerobic Pt(IV) bioreduction to Pt(0) via the Pt(II) intermediate.
- iv) Investigate any Pt(II) reductase activity of the inhibited and uninhibited whole cells on the Pt(II) ion.



## 3.2. Materials & Methods

### 3.2.1. Materials

All materials and reagents used were of analytical grade and purchased from Sigma-Aldrich (South Africa) or Merck (South Africa) unless otherwise stated. All gases were purchase from Afrox, South Africa.

### 3.2.2. Methods

#### 3.2.2.1. Growth and culture of SRB consortium

The SRB consortium was sub-cultured from BR1 and grown anaerobically as described in Chapter 2, with lactate acting as the major carbon source. Cells were harvested for use after reaching stationary phase (after day 7), washed twice in ddH<sub>2</sub>O to remove any interfering sulfate and/ sulfide and resuspended in minimal Tris-HCl buffer (200 mM, pH 7.6) (50 ml).

#### 3.2.2.2. Preparation of cells for Cu(II) inhibition studies

Prior to metal reduction experiments, the resuspended cells were incubated in varying concentrations of CuCl<sub>2</sub>.6H<sub>2</sub>O (0.5 mM/5 mM), a known irreversible inhibitor of the periplasmic H<sub>ase</sub> (De Luca *et al.*, 2001), under oxic conditions, in the dark at room temperature for 20 minutes. The cells were once again washed twice in ddH<sub>2</sub>O to remove any residual CuCl<sub>2</sub>.6H<sub>2</sub>O [Cu(II)] and resuspended in Tris-HCl buffer (200 mM, pH 7.6).

#### 3.2.2.3. Metal salt reduction experiments

Experimental conditions were similar to those described in Chapter 2. Each separate investigation was performed in a Frasco Rescado screw cap bottle. SRB cells (19.2 g.L<sup>-1</sup>), previously incubated in either 0.5 mM or 5 mM CuCl<sub>2</sub>.6H<sub>2</sub>O, were resuspended in Tris-HCl buffer (200 mM, pH 7.6) to a final volume of 5 ml, and placed at room temperature, in the dark. These cells were then challenged with 1 mM solutions of either Pt(IV) or Pt(II) salts from H<sub>2</sub>PtCl<sub>6</sub> and Na<sub>2</sub>PtCl<sub>4</sub> respectively. Investigations took place under normal atmospheric conditions with no exogenous electron donor. Controls included native cells that had not been pretreated with CuCl<sub>2</sub>.6H<sub>2</sub>O, cell-free and heat-killed cells.

To heat-kill cells, the cell samples were placed at 148 °C for 20-25 min in a Spectroquant® Nova 60 (Merck, South Africa), while cell-free samples contained extra Tris-HCl buffer (200 mM, pH 7.6) in place of the cell volume. Aliquot samples (100 µl) were collected and analysed by UV-Vis spectroscopy as previously described in Chapter 2. All sampling was performed in triplicate.

#### 3.2.2.4. Hydrogenase assay of whole cells

A simplified method for assaying  $H_{ase}$  activity in whole cells of *Enterobacter aerogenes* was adapted for use with the current consortium of SRB (Ren *et al.*, 2005). Uninhibited or inhibited cells were incubated in a 0.1 % (w/v) solution of Triton X-100 overnight at 4 °C to increase permeability of the cell walls to allow access of the electron transfer mediator, methyl viologen (MV), to the intracellular  $H_{ase}$ . The reduction of the methyl-viologen cation (electron acceptor) in Tris-HCl buffer (20 mM, pH 7.60) by the  $H_{ase}$  enzyme(s) could be followed spectrophotometrically by observing the change in absorbance at 604 nm ( $\epsilon_{604nm} = 13.9 \text{ mM}^{-1}\text{cm}^{-1}$ ) with  $H_2$  (99.9 %) acting as the electron donor by purging the headspace for the duration of the assay. The assay was performed in a normal 1 cm UV-cuvette, fitted with a rubber stopper to maintain anaerobic conditions and to allow for injection of samples. The assay had a final volume of 2600 µl consisting of: 2500 µl (1 mM) pre-activated methyl-viologen, and pre-activated whole-cell sample (100 µl) which was added to initiate the reaction. Pre-activation entails bubbling with  $H_2$  (99.9 %) for 15 min in the case of MV and 60 min for the whole cells. One unit of  $H_{ase}$  activity was defined as the amount of  $H_{ase}$  that catalyses the reduction of 1 µmol of methyl-viologen per min in the presence of excess hydrogen.

#### 3.2.2.5. TEM analysis

Cells were collected during sampling, fixed and prepared for TEM analysis and imaging as previously described in Chapter 2.

#### 3.2.2.6. SEM-EDAX analysis

Cell samples were prepared and analysed as previously described in Chapter 2.

### 3.3. Results & Discussion

Cu(II) is a known irreversible inhibitor of the periplasmic  $H_{ase}$ , while the cytoplasmic  $H_{ase}$  is unaffected (Lloyd *et al.*, 1999). Previous work (Rashamuse *et al.*, 2008) demonstrated that 95 % of the  $H_{ase}$  activity, relative to a sample free of inhibitor, was lost in the presence of 1 mM Cu(II). The mechanism of periplasmic  $H_{ase}$  inhibition by metal salts such as Zn(II) and Cu(II) is expected to occur via the irreversible binding of these metal ions to the iron (Fe) and/or nickel (Ni) active sites, although this mechanism has yet to be fully elucidated.

#### 3.3.1. Pt(IV) bioreduction

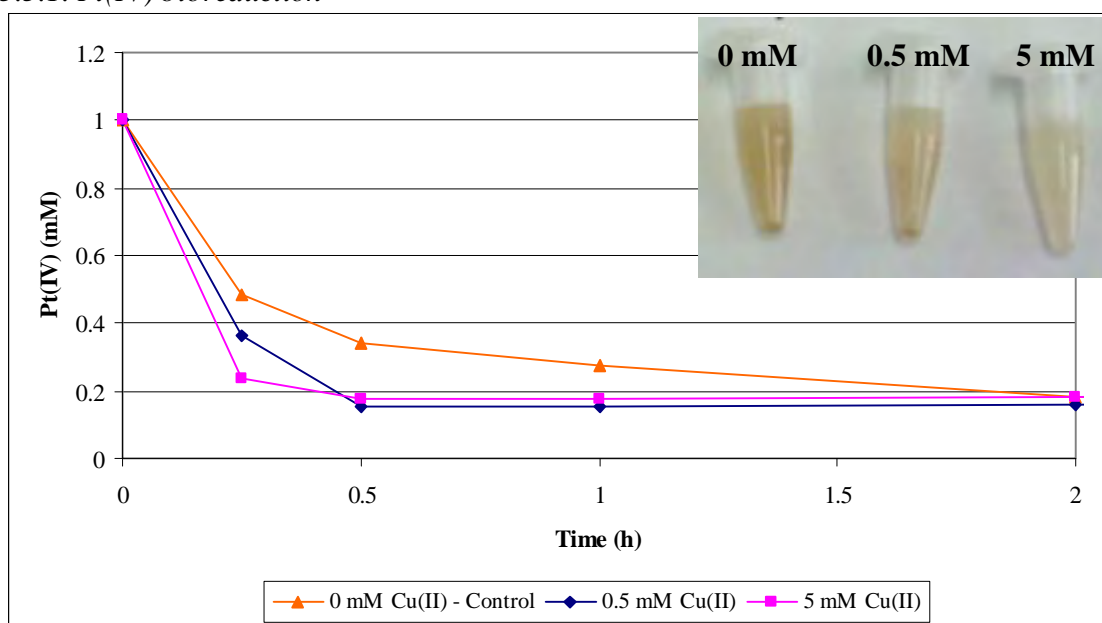


**Figure 3.1:** Bioreduction of Pt(IV) by whole cells pretreated with  $CuCl_2 \cdot 6H_2O$ . [Inset - Image of samples post bioreduction.] \*

It has been well documented (De Luca *et al.*, 2001) that the reduction of a number of metals by a periplasmic  $H_{ase}$  is completely inhibited in SRB cells pre-treated with Cu(II).

Since it was anticipated that the periplasmic  $H_{ase}$  (s) is/are involved in this mechanism, it was expected that the reduction of both platinum ions [(IV) and (II)], would be inhibited by pre-treatment of the cells with Cu(II). The results, however demonstrated an

\* All values shown have a standard deviation < 10 %

increasing Pt(IV) reduction rate, with increasing levels of the inhibitor (Fig 3.1). The concentration of Pt(IV), in each sample decreased from an initial 1 mM to 0.18 mM within 2 h after which no further decrease was noted. This strongly suggests that the periplasmic  $H_{ase}$  is not involved in the reduction of this ion under aerobic conditions as previously thought, but that another mechanism, which is positively influenced by the presence of Cu(II) ions is in operation.

Since heat-killed cells [section 2.3.2.2, Fig 2.4 II] exhibited a far lower Pt(IV) reduction potential than native cells, the reduction step of Pt(IV) to Pt(II) is still expected to be an active enzymatic process, coupled with slow, passive biosorption. As the cytoplasmic  $H_{ase}$  is unaffected by pre-treatment with Cu(II) (Lloyd *et al.*, 1999) the role of this particular  $H_{ase}$  enzyme in Pt(IV) bioreduction cannot be ruled out, without further investigations. It is proposed that the Pt(IV) ion may become reduced in the cytoplasm, by the cytoplasmic  $H_{ase}$ , to Pt(II) where it diffuses out to the periplasm and becomes reduced to Pt(0) by one or more of the periplasmically located  $H_{ase}$ 's.

The inset image in Fig 3.1 shows pictures taken post bioreduction for the samples as indicated. These images clearly illustrate that the overall bioreductive mechanism has been compromised in the presence of Cu(II). Even though Pt(IV) reduction is occurring, the colour change to brown, indicating formation of Pt(0) (Lin *et al.*, 2006), is decreased with increasing inhibitor concentration. This suggests that the reduction step of Pt(II) to Pt(0) is being compromised in some way, and is therefore dependant on a periplasmic  $H_{ase}$ .

To further investigate this proposal, the formation and subsequent reduction of Pt(II) from Pt(IV) reduction was studied. It was hypothesised that because the Pt(IV) reduction rate increased in the presence of Cu(II), and that Pt(II) is formed from the bioreduction of Pt(IV), the Pt(II) ion would follow a similar formation rate. The results observed in Fig 3.2 however, did not correlate as expected. The formation of the Pt(II) ion from Pt(IV) reduction, and the subsequent reduction thereof, over a time period of 8 h, is illustrated. In both samples containing pre-treated cells, the apparent Pt(II) formation rate

is far lower than expected. Similarly, the apparent Pt(II) concentration of the control sample is also unexpectedly lower than those observed with viable cells under less aerobic conditions (section 2.3.2.2, Fig 2.6 II). It is proposed that in the presence of high oxygen levels, the periplasmic [Fe]-H<sub>ase</sub> becomes upregulated in response to oxidative stress (section 3.1), this in turn results in the Pt(II) reduction cycle to Pt(0) foregoing the stationary reduction period observed in section 2.3.2.2. The earlier onset of Pt(II) reduction results in the lower than expected Pt(II) concentrations observed in Fig 3.2.

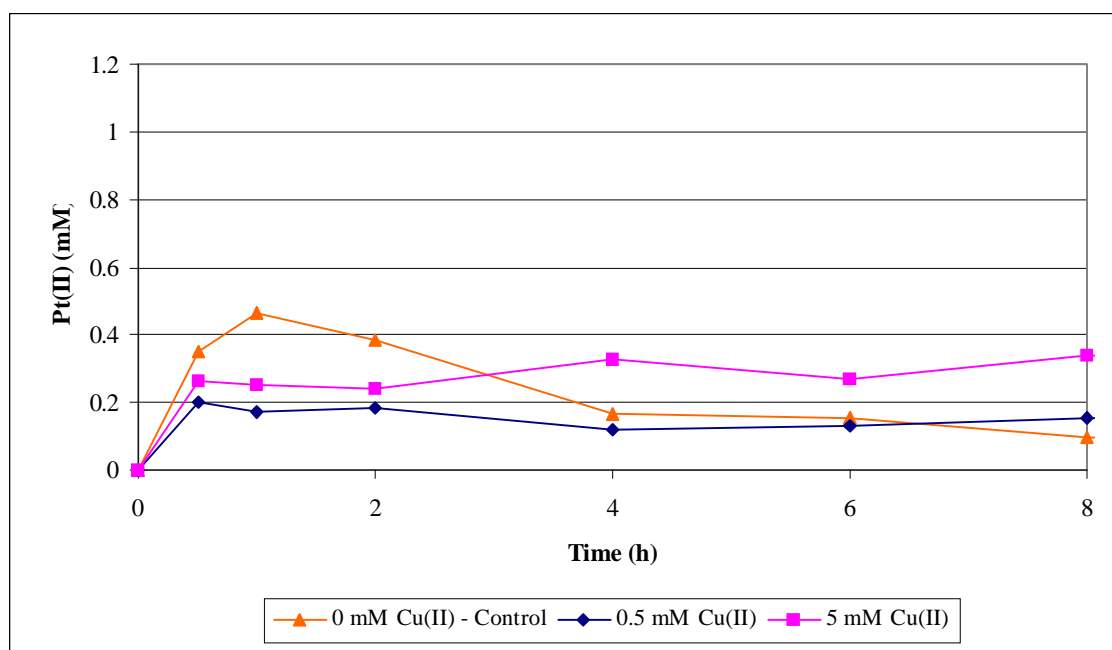


**Figure 3.2:** Formation and subsequent reduction of Pt(II) from Pt(IV). \*

With regards to the reduction of the Pt(II) ion, Fig 3.2 illustrates that the presence of the inhibitor is indeed affecting the reduction of the Pt(II) ion. The control sample continues to reduce Pt(II) up to 8 h while the pre-treated samples exhibit a cessation of Pt(II) reductase activity after just 2 h, at varying concentrations that correlate to the extent of Cu(II) pre-treatment. The fact that the Pt(II) concentration is not observably stoichiometric to the Pt(IV) ion indicates that Pt(II), under aerobic conditions, becomes reduced and/or passively adsorbed upon production, i.e. there is no stationary reduction phase while Pt(IV) becomes completely reduced before Pt(II) reduction begins.

\* All values shown have a standard deviation < 10 %

It is unclear why the Pt(II) concentration of the pre-treated cells was far lower than that of the control sample. It is hypothesised that either a) a number of periplasmic H<sub>ase</sub> enzymes are present, much like those in *D. vulgaris* Hildenborough (section 3.1), which may have provided temporary protection of the H<sub>ase</sub> (s) against the inhibitor in the pre-treated cells (Caffrey *et al.*, 2007) while still being upregulated in response to oxidative stress, or b) it may have been due to passive biosorption as observed with the Pt(IV) ion in relation to the heat-killed cells (Fig 2.4 II). The degree of biosorption may have been positively influenced by the pre-treatment of the cells with Cu(II), although further investigation is required to confirm this

These results indicate that a periplasmic H<sub>ase</sub> is largely responsible for the reduction of Pt(II) to Pt(0).

### 3.3.2. Pt(II) bioreduction

To further understand the role of the periplasmic H<sub>ase</sub> in Pt(IV) bioreduction, the two-cycle mechanism of Pt(IV) reduction to Pt(0) via Pt(II) was 'short circuited' by challenging the cells with the Pt(II) ion from Na<sub>2</sub>PtCl<sub>4</sub>.

The starting concentration of the Pt(II) ion was calculated as 1 mM at 0 h for all samples (Fig 3.3). A small yet rapid reduction period was observed in all samples between 0-1 h, with slower reduction rates observed in samples pre-treated with increasing Cu(II) concentrations. It was also clear from this graph, that the reduction of the Pt(II) ion had not gone to completion after 8 h. This further supports the hypothesis that a limited, endogenous electron donor is being utilised which results in a less efficient mechanism than would be expected in the presence of an exogenous electron donor. The sample that had been treated with 5mM Cu(II) showed a marked loss in reduction potential with only ~0.18 mM Pt(II) reduced after 8 h, while the control and the 0.5 mM Cu(II) sample exhibited very similar reduction curves with ~0.37 mM Pt(II) becoming reduced after 8 h. These results indicate that at low levels of Cu(II), there is a mechanism in place which provides temporary protection against the inhibitor, most probably by redundancy of H<sub>ase</sub> enzymes. At higher Cu(II) concentrations however, Pt(II) reduction is compromised.

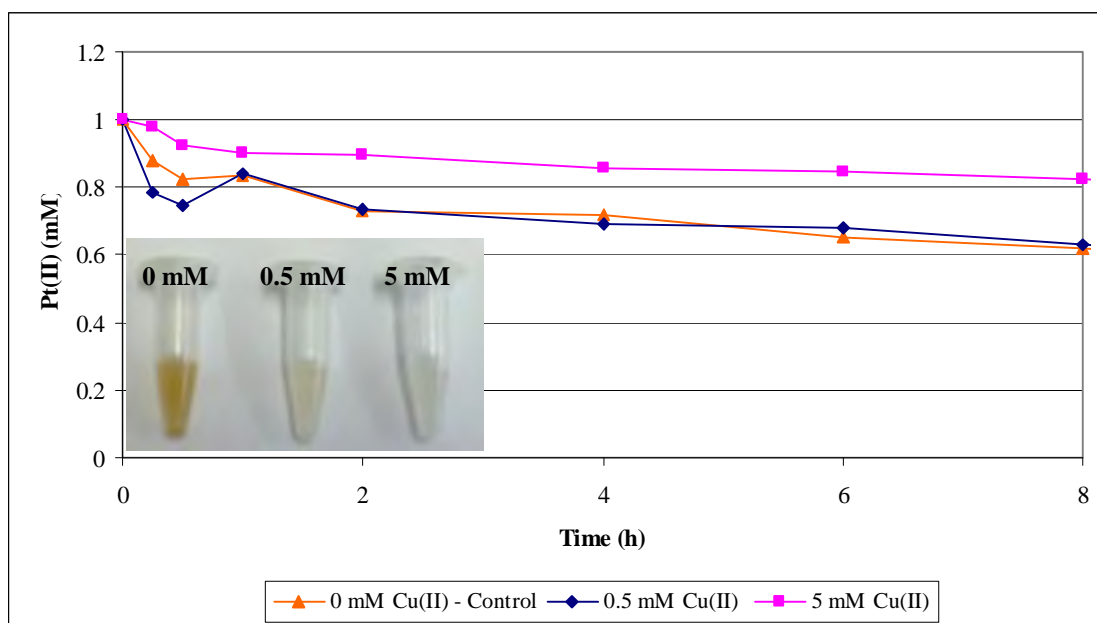


**Figure 3.3:** Bioreduction of Pt(II) salt  $\text{Na}_2\text{PtCl}_4$  by whole cells pre-treated with Cu(II) [Inset: Samples post bioreduction.]\*

These results demonstrate that 0.5 mM Cu(II) is not a sufficient inhibitor concentration for complete inhibition of the periplasmic  $\text{H}_{\text{ase}}$  within this consortium, while 5 mM Cu(II) is shown to significantly compromise the reductase activity. To support this statement, Fig 3.3 (inset) shows images of the samples post bioreduction. The samples containing pre-treated cells (0.5 mM and 5 mM) exhibit a fairly insignificant colour change from light yellow to brown indicating that Pt(0) formation has been affected, and since the reduction of the Pt(IV) ion is increased in the presence of Cu(II), the rate limiting step in this case is that of Pt(II) to Pt(0).

Any abiotic effect of the buffer on the Pt(II) starting ion was investigated and illustrated in Fig 3.4 I. The cell-free control sample, shows that Pt(II) is somewhat unstable under the experimental conditions with  $\sim 0.22$  mM Pt(II) lost after 8 h. The ion, however does seem to be more stable in the presence of cells. The heat-killed cells exhibited a decreased reductive potential for this ion, due to denaturation of the  $\text{H}_{\text{ase}}$  enzymes, and mirrors the Pt(II) reduction curve of the cells pre-treated with 5 mM Cu(II) (Fig 3.3).

\* All values shown have a standard deviation < 10 %

This suggests that the ‘bioreduction’ observed in both cases is most likely due to passive biosorption and not due to  $H_{ase}$  action.

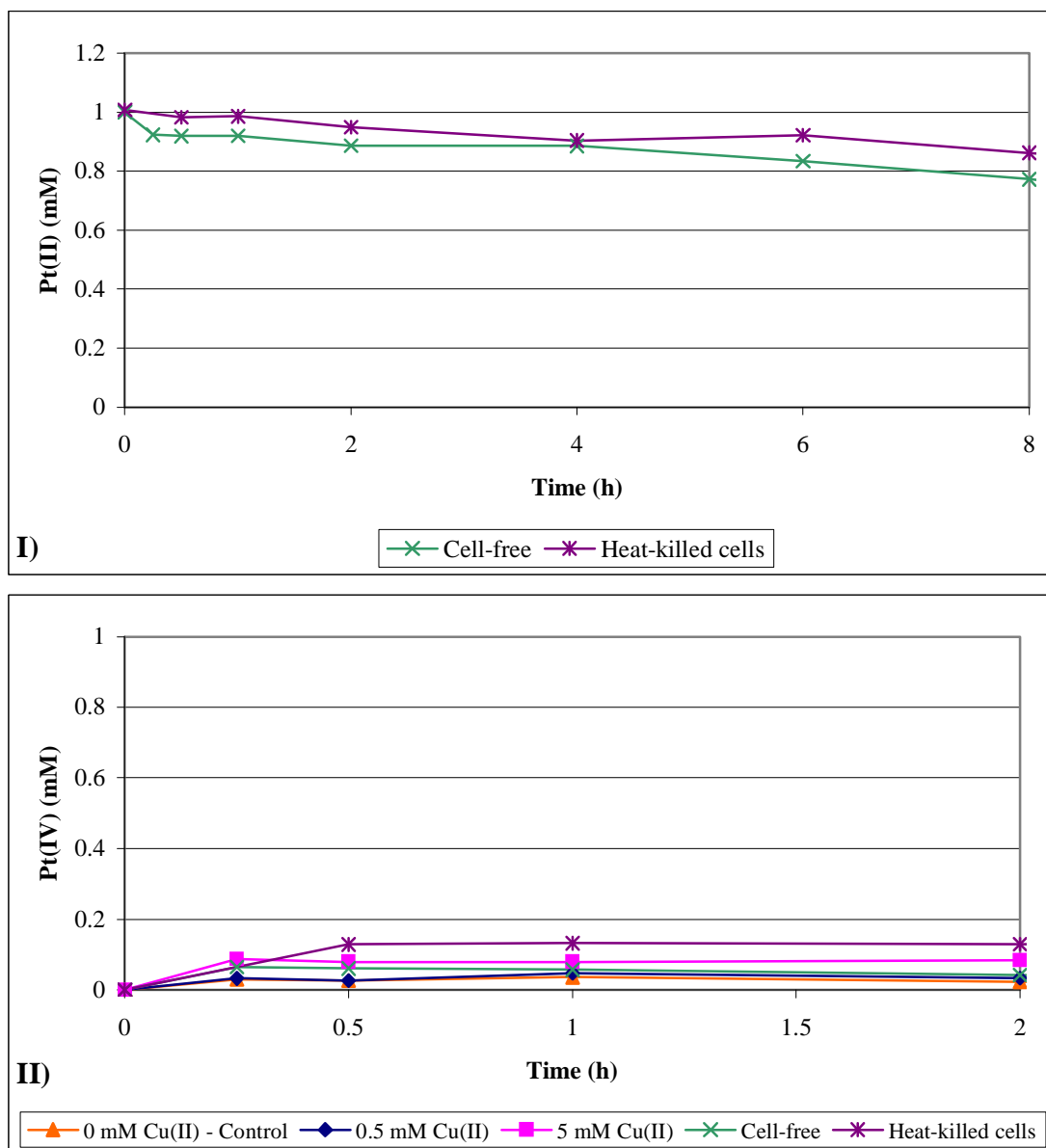


**Figure 3.4:** Bioreduction of Pt(II). [I) Abiotic reduction of Pt(II) salt  $Na_2PtCl_4$  II) Graph showing small percentage of re-oxidation of Pt(II) back to Pt(IV).] \*

These results all confirm that an active mechanism involving a periplasmic  $H_{ase}$  using limited, endogenously produced electrons, is responsible for the second cycle of the

\* All values shown have a standard deviation < 10 %



overall reductive mechanism [i.e. Pt(II)  $\rightarrow$  Pt(0)], yet it is still unclear which enzyme(s) is/are responsible for the initial reduction of Pt(IV) to Pt(II).

Fig 3.4 II illustrates that only a minimal percentage of the Pt(II) starting ion becomes reoxidised to Pt(IV). The heat-killed control and 5 mM Cu(II) sample exhibit the most reoxidation producing 0.1- 0.17 mM Pt(IV), while the rest of the samples all show Pt(IV) concentrations less than 0.1 mM Pt(IV). These values are all well below those observed in the investigations containing cells, indicating that any abiotic effects on this ion are negligible.

### 3.3.3. Hydrogenase assay of whole cells

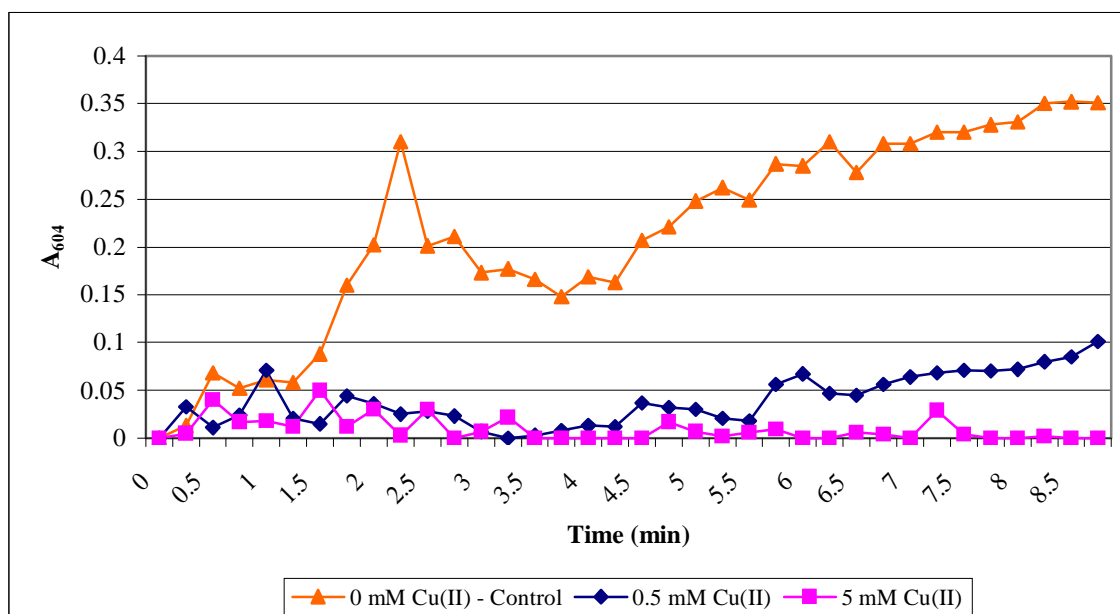


**Figure 3.5:** Reduction of the methylviologen ion by whole cells pre-treated with Cu(II).

A simplified method for assaying  $H_{ase}$  activity in whole cells of *Enterobacter aerogenes* was adapted for use with the current consortium of SRB. The cells were first pre-treated with Cu(II) to inhibit the periplasmic  $H_{ase}$ , as described previously. Cells were then incubated in 0.1 % solution of Triton X-100 overnight at 4 °C to increase permeability of the cell walls to allow access of the electron transfer mediator, methyl viologen (MV), to the intracellular  $H_{ase}$ . The assay protocol was followed as described in section 3.2.2.4.

Figure 3.5 displays the change in absorbance at 604 nm over time. As expected, the control sample (Fig 3.5) was observed to have the greatest  $H_{ase}$  activity ( $0.47 \mu\text{mol} \cdot \text{min}^{-1} \cdot \text{ml}^{-1}$ ) since this sample had not been pre-treated with the inhibitor. This also indicates that the cells used in this experiment are viable. The sample incubated in 0.5 mM Cu(II) was observed to require an induction period of  $\sim 5.5$  min before low  $H_{ase}$  activity was observed ( $0.18 \mu\text{mol} \cdot \text{min}^{-1} \cdot \text{ml}^{-1}$ ), approximately 38.3 % of the uninhibited cell activity, while the 5 mM sample did not show any activity over the time period analysed ( $0 \mu\text{mol} \cdot \text{min}^{-1} \cdot \text{ml}^{-1}$ ). This confirms that Cu(II) does in fact inactivate the periplasmic  $H_{ase}$  enzyme as stated in literature, however with this particular consortium, a concentration greater than 0.5 mM Cu(II) is required to completely abolish activity within the time period studied.

#### 3.3.4. TEM and SEM-EDAX analysis

##### 3.3.4.1. Control experiments

###### 3.3.4.1.1. SRB cells in the absence of Pt(IV)/Pt(II)

- See Chapter 2, Section 2.3.4.1.

The control sample that had not been challenged with platinum ions in solution did not undergo a colour change to brown, as is indicative of Pt(0) formation. Instead it remained a light yellow colour, exhibiting both a lack of electron dense regions under TEM analysis and the peaks characteristic of Pt(0) during EDAX analysis.

###### 3.3.4.1.2. Pt(IV) bioreduction with native SRB cells

To test for reductase activity under aerobic conditions with no exogenous electron donor, the native cells were challenged with Pt(IV) and the cells exhibited a colour change from yellow to brown indicating Pt(0) formation. The cells were prepared via standard fixing and embedding procedures and visualised using a JEM JEOL 1210 transmission electron microscope (TEM).

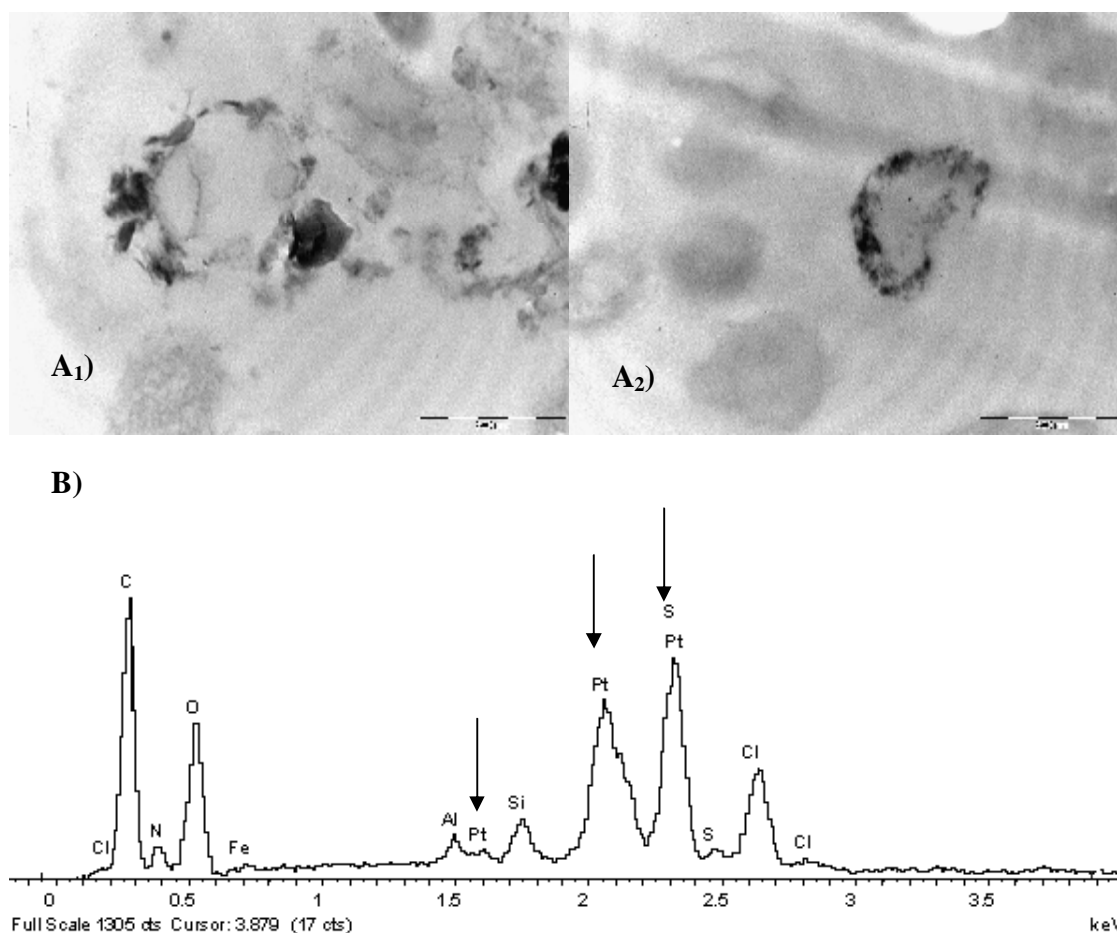


**Figure 3.6:** Screening for Pt(IV) reduction by native SRB cells. [A<sub>1+2</sub>) TEM images of cells with electron dense metal deposits within the periplasmic regions. Scale bars = 500 nm respectively. B) EDAX graph of sample clearly showing the presence of Pt(0).]

The images (Fig 3.6 A<sub>1+2</sub>) show the presence of electron dense areas in the periplasmic regions of the cells. This further supports the growing evidence that an oxygen-tolerant periplasmic H<sub>ase</sub> is involved in this mechanism. As mentioned in Chapter 2, the colour change to brown is indicative of Pt(0) formation, however this needed to be conclusively proven via EDAX. The EDAX graph in Fig 3.6 B, clearly shows the presence of Pt(0) along with small concentrations of sulfur and other biologically relevant elements. The presence of iron (Fe) is unexpected, but may be attributed to the presence of the [Fe]-H<sub>ase</sub> which is believed to be involved in platinum reductase activity within this consortium.

## 3.3.4.1.3. Pt(II) bioreduction with native SRB cells

As for the Pt(IV) ion, the native cells were challenged with a starting ion of Pt(II) under the experimental conditions described in section 3.2.2.3.

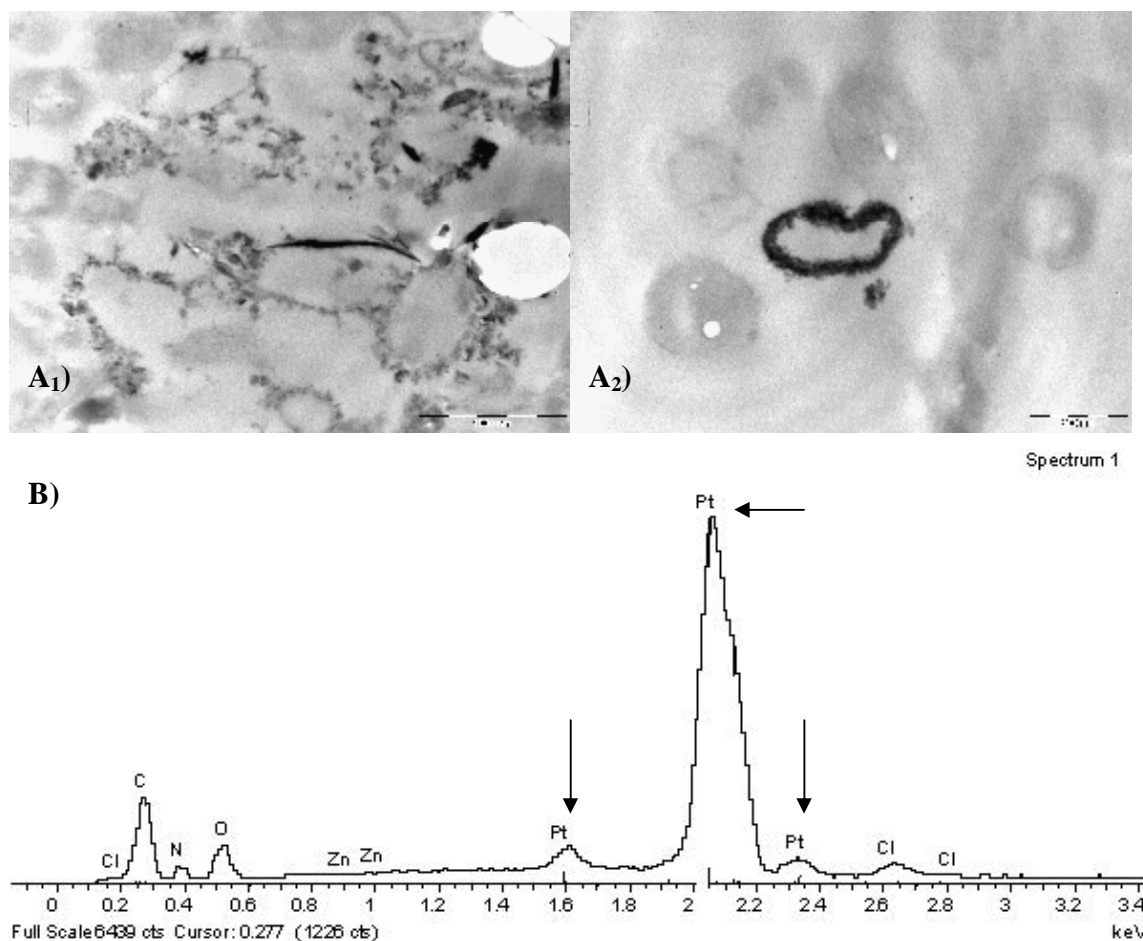


**Figure 3.7:** Screening for Pt(II) reduction by native SRB cells. [**A**<sub>1+2</sub>] TEM images of cells with electron dense metal deposits within the periplasmic regions. Scale bars = 1000 nm and 500 nm respectively. **B**) EDAX graph of sample clearly showing the presence of Pt(0).]

Once again a colour change of the cells from light yellow to brown was observed indicating Pt(0) formation which was later confirmed by EDAX analysis of the samples as shown in Fig 3.7 B. It is proposed that, the Pt(II) reductase activity is the result of a [NiFe]-H<sub>ase</sub> or [Fe]-H<sub>ase</sub> that becomes upregulated due to oxidative stress, while the Pt(IV) reductase activity is due to either a cytoplasmic H<sub>ase</sub>, or another non-H<sub>ase</sub> enzyme that becomes upregulated in the presence of Cu(II). The electron dense regions in the

periplasm of the cells, as visualised in the TEM images in Fig 3.7 A<sub>1+2</sub>, further supports the expected involvement of an oxygen-tolerant periplasmic H<sub>ase</sub> in the reduction of Pt(II) ---> Pt(0).

### 3.3.4.2. Metal reduction by SRB cells after pre-treatment with an inhibitor

To examine the effect of the inhibitor, Cu(II), on the bioreduction of the platinum ions, the SRB cells were challenged with varying concentrations of the inhibitor prior to incubation with the platinum salts.

#### 3.3.4.2.1. Bioreduction of platinum ions with cells incubated in 0.5 mM Cu(II)

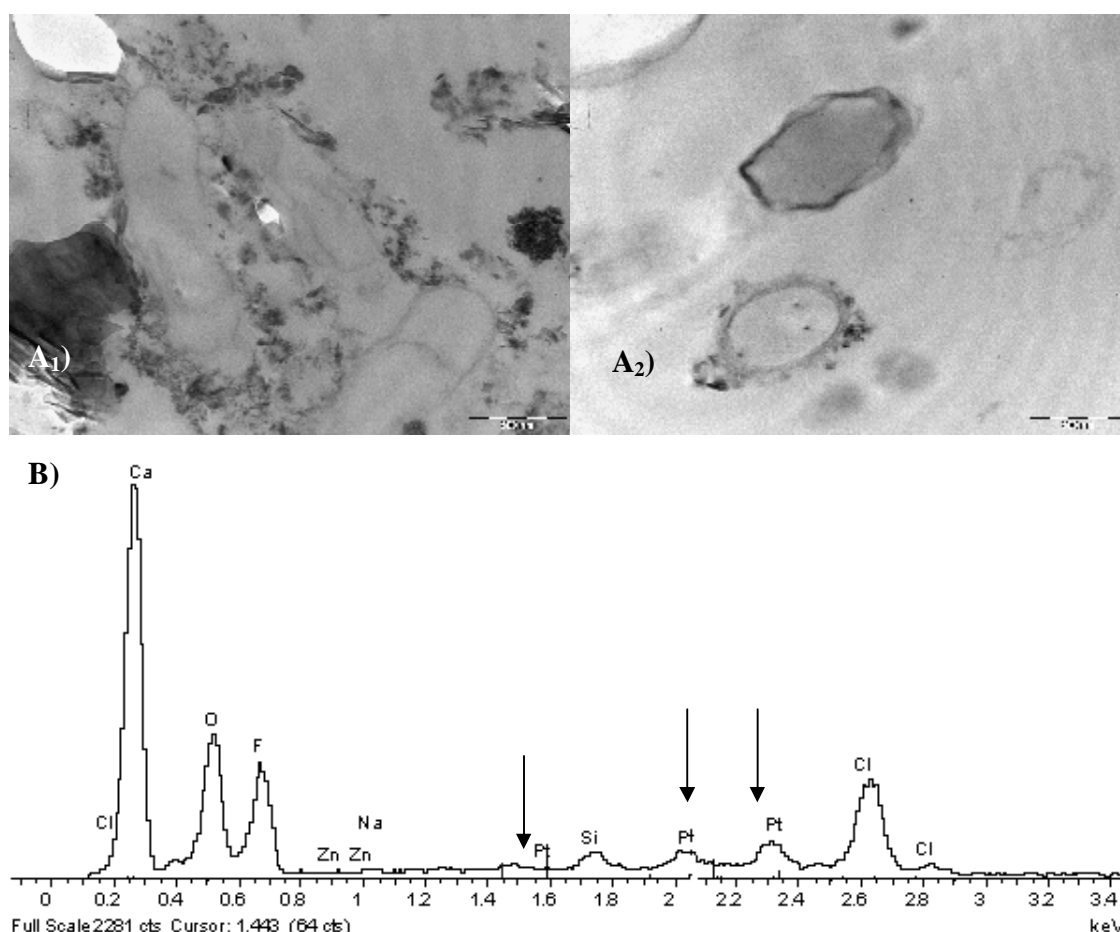


**Figure 3.8:** Screening for platinum ion reduction by SRB cells pre-treated with 0.5 mM Cu(II). [A<sub>1+2</sub>) TEM images of cells with low concentrations of electron dense metal deposits within the periplasmic regions, as well as on the cell surface. Scale bars = 500 nm respectively. B) EDAX graph of sample showing low levels of Pt(0).]

The sample containing 0.5 mM Cu(II) exhibited a significantly lower amount of Pt(0) as observed in the TEM images (Fig 3.8 A<sub>1+2</sub>). This is supported by the visual observations of the insignificant colour changes occurring in the pretreated samples (Fig 3.1 and 3.3 insets).

The electron dense regions are mainly located on the surface of the cells, indicating passive biosorption, with a very small percentage located within the periplasm. This is confirmed by the low levels of elemental platinum observed in the EDAX graph (Fig 3.8 B). It was previously shown (section 3.3.3) that a 0.5 mM Cu(II) was not sufficient to completely abolish the activity of the periplasmic H<sub>ase</sub>, as ~38.3 % of the native activity remained. These results indicate that the majority of the active mechanism has been abolished with metal immobilisation occurring via passive biosorption by structural moieties on the cell walls.

#### 3.3.4.2.2. Bioreduction of platinum ions with cells incubated in 5 mM Cu(II)

In this sample the cells were challenged with 5 mM Cu(II), a ten fold increase in the inhibitor concentration as compared to section 3.3.4.2.1.

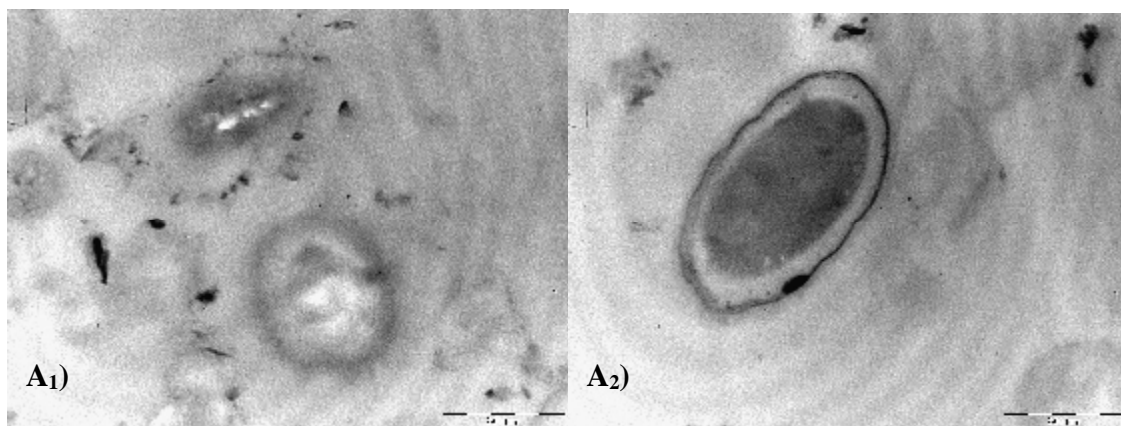


**Figure 3.9:** Screening for platinum ion reduction by SRB cells pre-treated with 5 mM Cu(II). [A<sub>1+2</sub>) TEM images of cells with particularly low concentrations of electron dense metal deposits within the periplasmic regions. Majority of the metal is located on the cell surfaces. Scale bars = 500 nm respectively.]

A barely perceptible colour change was observed in this sample indicating that the formation of Pt(0) had been largely inhibited. This was supported by the TEM images (Fig 3.9 A<sub>1+2</sub>) that showed very little metal precipitation, with the majority of the electron dense deposits located on the surface of the cells and none located within the periplasm. The Pt(0) concentration was below detectable limits for EDAX analysis, but its presence may be inferred by the electron dense deposits on the cell walls which have previously been confirmed to be elemental platinum.

### 3.4. Summary & Conclusions

- Cu(II) inhibits the periplasmic H<sub>ase</sub> in this consortium of SRB as expected.
- A periplasmic H<sub>ase</sub> is not responsible for the reduction of the Pt(IV) ion as initially expected. A separate unknown active mechanism is involved, that is up-regulated in the presence of the Cu(II) ion.
- A periplasmic H<sub>ase</sub> is responsible for the reduction of the Pt(II) ion.
- The native cells possess Pt(II) and Pt(IV) reductase activity both resulting in the formation of Pt(0).

## **CHAPTER FOUR:**

### **Screening an SRB cell-free crude extract for Pt(IV) reductase activity and metal nanoparticle synthesis**

---

---

#### **4.1. Introduction**

The preparative techniques for nanoparticles (NP's) can generally be classified into two categories; either the 'top-down' approach where larger particles are reduced in size to nanoscale particles; or the 'bottom-up' approach, building upwards from the atomic/molecular scale to the nanoscale (Chan *et al.*, 2004). Even though top-down approaches, such as lithographic and bonding techniques are generally far more expensive and time-consuming than the bottom-up methods, they do tend to produce more well-defined NP's. Currently, combinations of these two methods are being investigated and are showing a great deal of promise (Mijatovic *et al.*, 2005).

Solutions of metal nanoparticles, or colloids, often exhibit distinct absorption bands in the ultraviolet-visible (UV-Vis) wavelengths due to interband transitions or the excitation of their surface plasmons (Creighton & Eadon, 1991). Platinum NP's, unlike those of gold and silver that possess specific absorbance peaks at 510-540 nm (Mandal *et al.*, 2005; He *et al.*, 2007) and 400-450 nm (Ahern & Garrell, 1991; Shankar *et al.*, 2001) respectively, generally exhibit a broad spectrum with no specific maxima that stretches throughout the UV-Vis spectrum, increasing in intensity towards the UV wavelengths (Creighton & Eadon, 1991). Where the gold and silver colloids vary greatly in colouration from red to blues, purples and yellows, the platinum colloid is generally either a black-brown colour or occasionally a golden hue due to the oscillations of their surface plasmons (Fu *et al.*, 2002; Konishi *et al.*, 2007). This also makes them inherently more difficult to study as the absorbance spectra of the precursor ions are masked by the increasing NP spectrum.

Since the spectrum of silver and gold NP's are greatly influenced by a number of factors such as particle size, shape, environment and degree of particle aggregation, it is possible to estimate the NP size distribution from the data obtained from the



spectrum. In contrast to this, it is not possible to approximate the size of NP's from the spectrum of colloidal platinum, as it is not affected by particle size (Kim & Kim, 2004; Zhang *et al.*, 2007). Kim and Kim (2004) suggest that the apparent independence of the Pt(0) spectrum to this factor is due to the minimal contribution of the surface plasmons to the overall absorption of the colloid. From this, it may be concluded that the only factors affecting the Pt(0) spectrum are particle concentration and aggregation.

Metal colloids are often hindered by stability issues in aqueous solutions that result in particle aggregation due to the attractive van der Waal's forces that are exaggerated in NP's (Singhal *et al.*, 1999; Tripp *et al.*, 2002; Hakim *et al.*, 2005). For this reason a number of synthetic additives or 'capping agents', such as polyvinylpyrrolidone (PVP) (Ahmadi *et al.*, 1996; Sun & Xia, 2002) or sodium polyacrylate (Lee *et al.*, 2004), are currently in use that adsorb to the surface of the NP, thereby sterically stabilising the NP and preventing this aggregation from occurring with an additional advantage of morphology control (Chen *et al.*, 1999; Sun & Xia, 2002). There are, however, a number of drawbacks to the use of these synthetic stabilisers, such as total inhibition of particle growth if bound too tightly to the particle (Hou *et al.*, 2005), particle deformation (Mijatovic *et al.*, 2005) and reduced catalytic activity (Chan *et al.*, 2004). For this reason, more natural routes are being sought where biological molecules such as proteins (BSA) and amino acids (L-cysteine) are being used to the same effect, negating the need for synthetic polymers (Zhang *et al.*, 2007).

Zhang and colleagues (2007) described the production of apoferritin-stabilised gold NP's. They demonstrated that in order to maintain both particle stability and solubility within an aqueous system, apoferritin was required during the reduction step where the particles became adsorbed to the external surface of the protein, preventing particle precipitation.

Metal NP's in aqueous solution have an overall weak positive charge and will therefore adsorb to proteins at greater degrees when the pH value is equal to, or slightly more basic, than the pI of the constituent proteins in solution since a) at the pI, protein solubility is at its lowest, and b) the electrostatic repulsion between proteins is minimised due to an overall neutral charge (Ahern & Garrell, 1991).

The rate of NP synthesis using chemical methods has been shown to have significant effects on the overall size of the NP's produced. A rapid reduction rate generally results in a higher concentration of NP's that are smaller in size, and vice versa due to the effect on primary and secondary nucleation. Larger particles form from a slower reduction rate that corresponds to a slower primary nucleation step. This occurs due to the formation of fewer nuclei that collide with, and join to, other nuclei resulting in a low concentration of larger particles. Conversely, in the presence of a more rapid reduction rate, more nuclei are formed at one time during the primary nucleation phase. This depletes the precursor salt before particle growth can progress in the secondary nucleation phase, thereby generating a higher concentration of smaller particles (Zhu *et al.*, 2004; Iwamoto *et al.*, 2005; Basu *et al.*, 2008).

The results in Chapter 3 demonstrated that elemental platinum was becoming reduced by an active, oxygen-tolerant, enzymatic process within viable SRB cells, and immobilised as amorphous deposits within the periplasmic space. It is proposed that in the absence of the spatial restrictions imposed by the cell, a cell-soluble extract (CSE) will result in a similar reduction mechanism as determined in Chapters 2 and 3, with the additional advantage of producing stable, geometric nanoparticles.

The objectives of Chapter 4 are to:

- i) Screen the cell-soluble extract crude protein solution for Pt(IV) reductase activity.
- ii) Determine the effect of  $\text{H}_2\text{PtCl}_6$  concentration on the bioreduction mechanism and nanoparticle morphology.
- iii) Determine the effect of a buffer on the bioreduction mechanism and nanoparticle morphology.
- iv) Attempt to 'short-circuit' the two-cycle bioreductive mechanism by starting with the Pt(II) ion.

## 4.2. Materials & Methods

### 4.2.1. Materials

All chemicals, which were of analytical grade, were obtained from Sigma-Aldrich (South Africa) or Merck (South Africa) unless otherwise stated. All gases were purchased from Afrox (South Africa).

### 4.2.2. Methods

#### 4.2.2.1. Preparation of Crude Soluble Extract (CSE)

The SRB cells were cultured under anaerobic conditions and harvested as described previously in Chapter 2. The cell pellet obtained was washed twice in ddH<sub>2</sub>O to remove any sulfide or sulfate which could result in the precipitation of the platinum salt in solution as a metal sulfide. The cells were resuspended in minimal volume ddH<sub>2</sub>O (50 ml) and sonicated using a Vibracell sonicator (Sonics and Materials Inc., USA) at 10 W for 4 min (30 sec intervals) at 4 °C to rupture the cells and release the cell contents. To solubilise the membrane proteins, 2 % sodium cholate was added to the homogenate and stirred overnight at 4 °C. Next, the homogenate was centrifuged (18 000g, 20 min, 4 °C) to remove the cell debris and the resulting supernatant was dialysed overnight at 4 °C against ddH<sub>2</sub>O using Snakeskin<sup>®</sup> Pleated Dialysis tubing (MWCO 10 kDa) to remove the salts, any residual sulfates/sulfides and small molecular weight proteins. To prevent bacterial growth the CSE solution was kept at 4 °C and 100 µg.ml<sup>-1</sup> ampicillin and 25 µg.ml<sup>-1</sup> tetracycline-hydrochloride were added periodically.

#### 4.2.2.2. Platinum reduction experiments

##### 4.2.2.2.1. Effect of H<sub>2</sub>PtCl<sub>6</sub> concentration

Prior to experimental set-up and pH adjustment, the CSE crude solution was incubated on ice for 10 min to slow any enzymatic activity. A total volume of 5 ml, consisted of 250 µg.ml<sup>-1</sup> protein from the CSE, H<sub>2</sub>PtCl<sub>6</sub> concentrations ranging from 0.35 mM – 3 mM. The pH was adjusted to 9.0 with 1 M NaOH and the final volume was made up with ddH<sub>2</sub>O. '0 h' was taken as the point after pH adjustment while still on ice. After pH adjustment the samples were placed in an incubator at 65 °C in the dark, where triplicate samples (300 µl) were taken at regular intervals (0, 0.5, 1, 2, 4,

6, 8 h). Controls were set-up as above with the exception of the CSE volume being replaced by ddH<sub>2</sub>O.

#### 4.2.2.2.2 *Effect of a sodium-bicarbonate buffer(200 mM, pH 9.0)*

The experimental set-up was as described in section 4.2.2.2.1. with the exception of ddH<sub>2</sub>O being replaced with a sodium-bicarbonate buffer (200 mM, pH 9.0).

#### 4.2.2.2.3. *Effect of a Pt(II) starting ion*

The experimental set-up was similar as that described in section 4.2.2.2.1 with the exception of the platinum salt, H<sub>2</sub>PtCl<sub>6</sub>, being replaced by a 0.75 mM solution of Na<sub>2</sub>PtCl<sub>4</sub>.

#### 4.2.2.3. *Sample analysis and platinum ion determination*

All samples underwent analysis by UV-Vis spectroscopy. Endpoint readings, using a PowerWave (Bio-Tek, Instrumental Inc., USA), were taken at 230 nm, 261 nm and 334 nm to analyse for Pt(II), Pt(IV) and Pt(0) respectively. Absorbance values for the Pt(II) and Pt(IV) ions were converted to platinum ion concentrations using the standard curves in Appendix D. Pt(0) concentration could not be assayed directly due to the inherent problems associated with nanoscale platinum materials resulting in a lack of an appropriate standard curve. Hence, an absorbance of 334 nm was chosen as an ‘indicator’ of nanoparticle formation over time (section 4.3.1.2). Samples were diluted appropriately in ddH<sub>2</sub>O prior to analysis and blanked against ddH<sub>2</sub>O.

#### 4.2.2.4. *Spectrum (UV-Vis) scanning of reduction samples*

As previously mentioned in section 4.1, platinum nanoparticles do not exhibit a single absorbance maximum as is observed in the case of silver and gold nanoparticles. Instead, a wide absorbance spectrum stretching from UV to the visible wavelengths, increasing towards the UV region is seen to be characteristic of platinum nanoparticles in aqueous solutions. In order to identify the presence of platinum nanoparticles by their unusual spectrum, a UV-Vis spectrum scan of all samples was performed from 200 – 550 nm (2 nm intervals) blanked against ddH<sub>2</sub>O.

#### 4.2.2.5. Bradford assay

The samples were assayed for protein concentration using the Bradford protocol (Bradford, 1976) (Appendix C).

#### 4.2.2.6. Native-Polyacrylamide gel electrophoresis (Native-PAGE)

The CSE samples, both pre- and post-bioreduction, from an investigation challenging CSE with 0.75 mM Pt(IV) (65 °C, pH 9), were concentrated ~ten-fold using an Ultracel YM-10 ultrafiltration membrane (MWCO 10 kDa). Approximately 50 µg.ml<sup>-1</sup> protein was loaded in separate lanes for each sample and run concurrently on a 7.5 % continuous native-PAGE gel constructed according to the MiniGel recipe in Appendix F. The gel was run at 130 V for 60 min and stained via the Coomassie method.

#### 4.2.2.7. TEM analysis

For TEM analysis, 2 µl of the sample was pipetted onto a carbon-coated, copper TEM grid and allowed to settle for ~2 min, after which any excess liquid was carefully removed with filter paper and allowed to air-dry further over night in the dark.

#### 4.2.2.8. SEM-EDAX analysis

For EDAX analysis, a sample of a solution post bioreduction was concentrated ~ten-fold using an Ultracel YM-10 ultrafiltration membrane (MWCO 10 kDa). The retentate was placed on a carbon strip attached to an SEM brass support and air-dried at 65 °C overnight. Samples were analysed as previously described in Chapter 3.

### 4.3. Results & Discussion

#### 4.3.1. Effect of Pt(IV) concentration in ddH<sub>2</sub>O

##### 4.3.1.1. Cell-free controls

For all control samples (i.e. lacking CSE), the Pt(IV) concentration remained reasonably constant over 8 h (Fig 4.1 A). In addition none of the controls exhibited a colour change indicative of the formation of Pt(0) NP's (Fig 4.1 C<sub>1+2</sub>). This confirms that the reduction of the platinum ion is due to the presence of biological components in solution and not due to any abiotic mechanism.

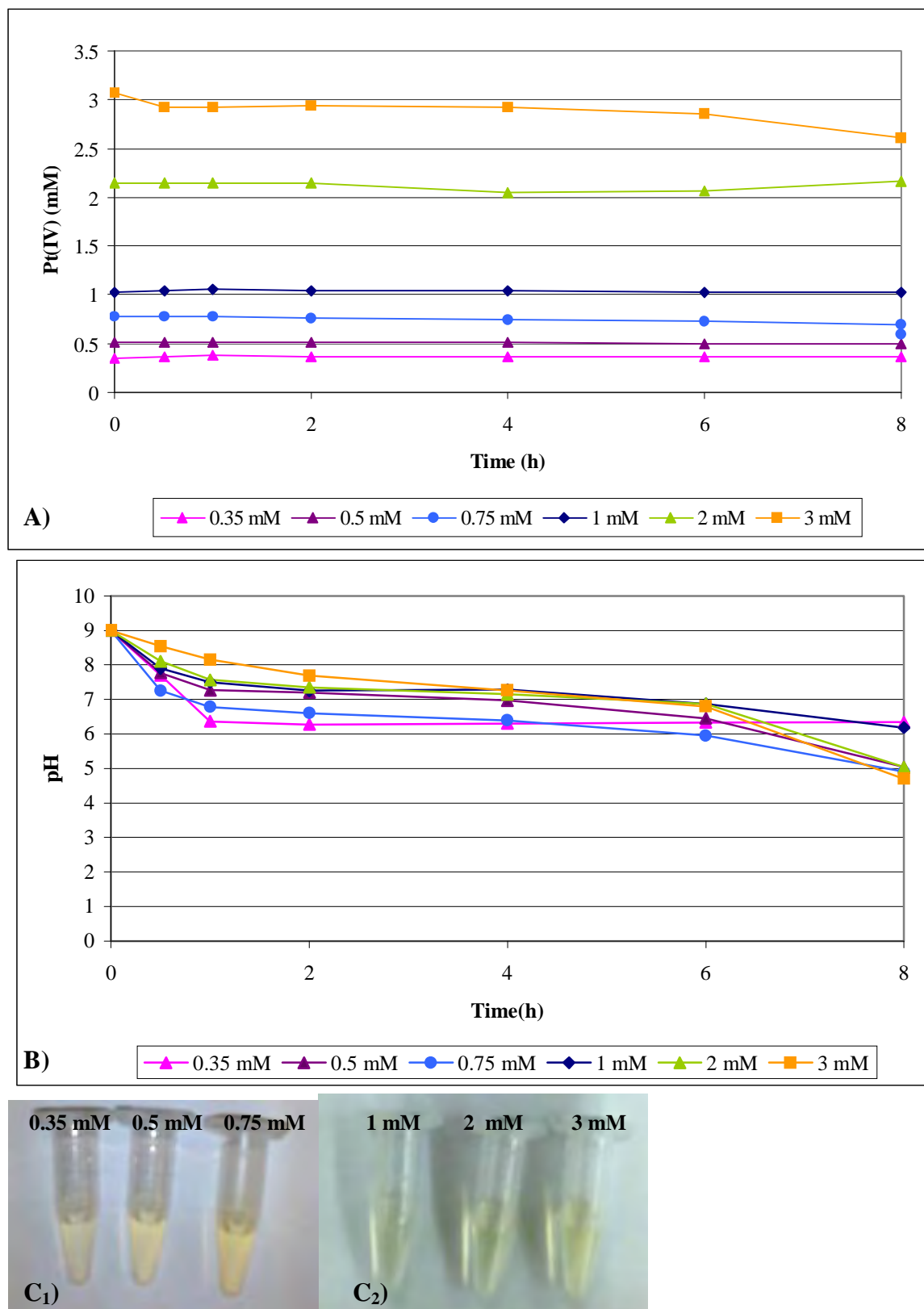


**Figure 4.1:** Cell-free control samples [A) Pt(IV) at various concentrations, B) pH over time for control samples, C<sub>1+2</sub>) Images of control sample post-bioreduction.]\*

\* All values shown exhibit a standard deviation < 10%

The pH of the control experiments decreased over time most likely due to the hydrolysis of  $\text{H}_2\text{PtCl}_6$  where  $\text{Cl}^-$  ligands are replaced by  $\text{H}_2\text{O}$  in basic, aqueous solutions. The octahedral Pt(IV) complex, however remains exceptionally stable under a wide range of conditions (Spieker *et al.*, 2002). After 8 h, none of the solutions exhibited a pH below pH 4.5.

#### 4.3.1.2. Pt(IV) < 1 mM

This experiment was conducted to determine whether varying the Pt(IV) concentration would have an effect on the overall bioreductive mechanism by the SRB consortium and the resulting nanoparticle morphology.

It was initially expected that the reduction of the two platinum ions Pt(IV) and Pt(II) would be observed much in the same way they were observed in Chapter 2 and 3, i.e. by following their absorbances at 261 nm and 230 nm, respectively. The results however, exhibited a different trend. The samples with Pt(IV) concentrations less than 1 mM (0.35 mM – 0.75 mM) showed an initial reduction period between 0-0.5 h, as was expected. This however, was followed by an unusual trend of, what appeared to be, increasing Pt(IV) concentration over the remaining period (Fig 4.2 A).

Literature states that Pt(0) nanoparticles in aqueous solution, unlike gold or silver nanoparticles, which exhibit specific absorbance maxima (Shankar *et al.*, 2001; He *et al.*, 2007), possess a wide absorbance spectrum that stretches throughout the ultraviolet-visible regions, increasing towards the UV wavelengths (Creighton & Eadon, 1991). The formation of Pt(0) nanoparticles and their resulting absorbance spectrum would then be expected to interfere in the determination of the Pt(IV) and Pt(II) ions at 261 nm and 230 nm, respectively. Since a reduction curve was not available, the rate of Pt(IV) reduction could not be calculated from these results.

To determine whether the formation of nanoparticles (NP's) in solution were indeed the cause for the false increase in Pt(IV) concentration, a spectrum scan was performed on the samples and an example is shown in Fig 4.2 B. The spectrum at 0 h, represents the Pt(IV) ion at a concentration of 0.5 mM, containing  $250 \mu\text{g}\cdot\text{ml}^{-1}$  CSE. Over 0.5 h, the peak at 261 nm, representative of the Pt(IV) ion, is seen to decrease markedly. Over time however, the absorbance at this wavelength, as well as other

wavelengths along the UV-Vis spectrum are observed to increase. This increasing absorbance spectrum was also seen to correlate to a colour change from light yellow to brown, which as mentioned previously, is indicative of the formation of Pt(0) nanoparticles in solution (Creighton & Eadon, 1991; Konishi *et al.*, 2007).

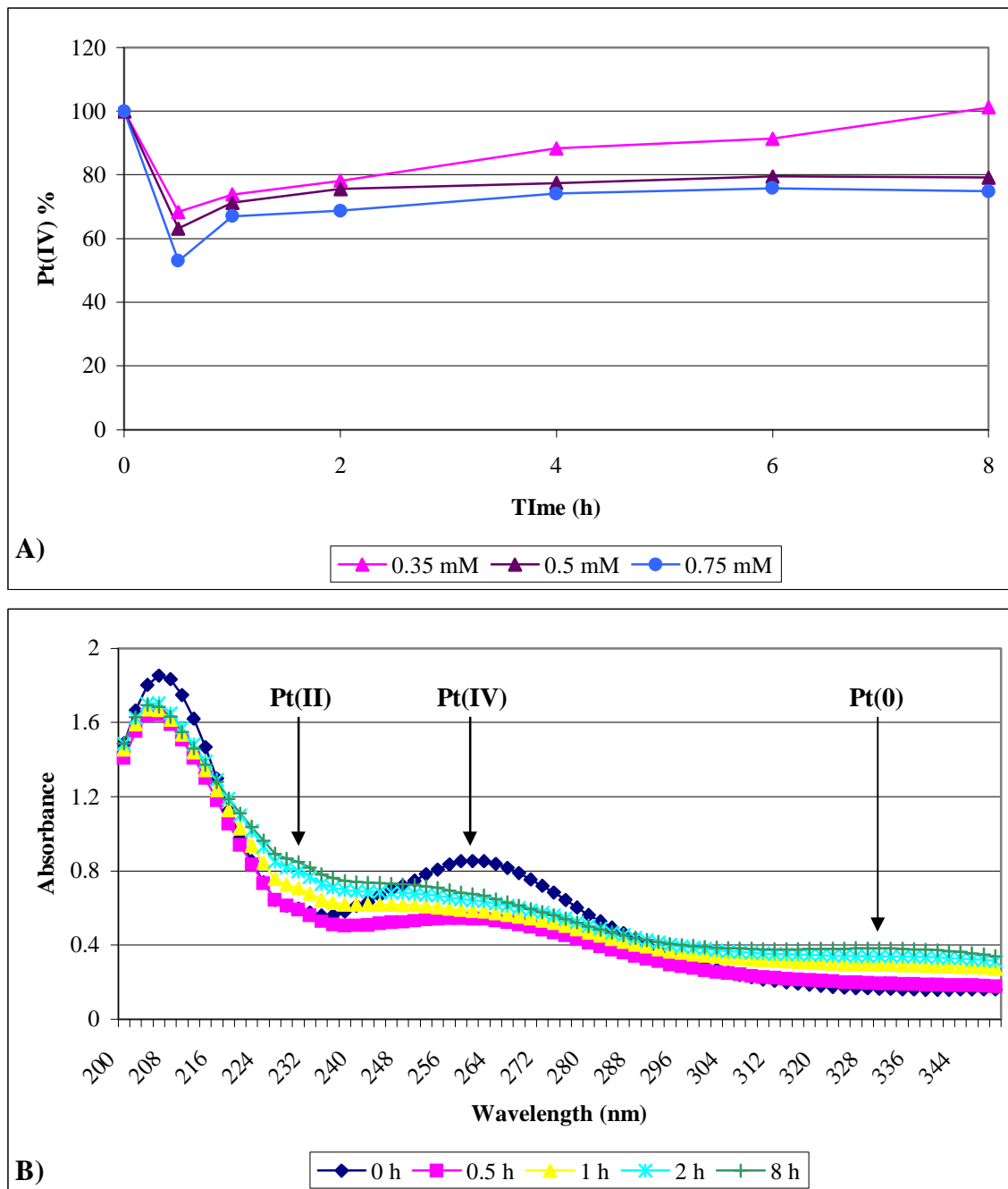


**Figure 4.2:** Bioreduction of Pt(IV) < 1 mM by CSE. [A) Pt(IV) reduction curve, B) Spectrum scan of a 0.5 mM sample over 8 h.] \*

\* All values shown exhibit a standard deviation < 10%



These results support the proposal that the unexpected increase in Pt(IV) concentration was due to interference by Pt(0) NP's forming freely in solution. This phenomenon was not observed in the samples containing whole cells, due to the fact that the elemental platinum was confined to the cells that were pelleted out prior to analysis of the supernatant, while in the case of CSE, the particles are free in solution. Since the relative concentrations of the Pt(IV) or Pt(II) ions could not be determined experimentally, the wavelength of 334 nm was chosen as a non-quantitative indicator of Pt(0) formation, Fig 4.3.

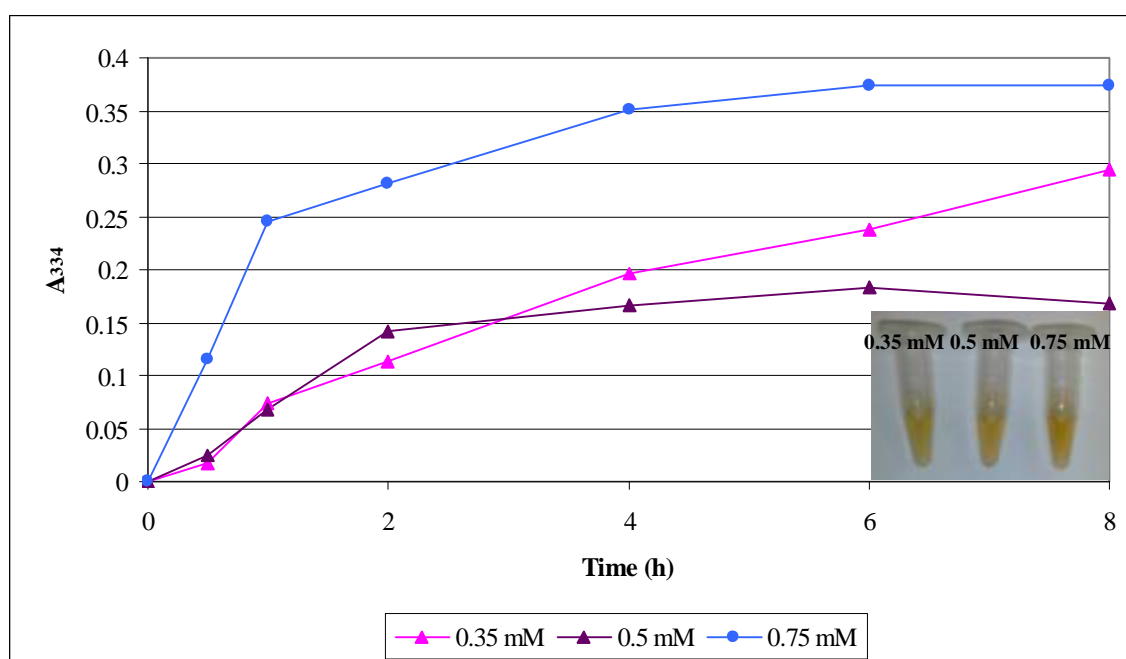


**Figure 4.3:** Pt(0) formation over time at 334 nm. [Inset: Image of samples post bioreduction.]\*

When comparing the normalised absorbance results for the different samples at 334 nm (Fig 4.3), an inverse of the expected reduction curve for Pt(IV) ions was observed. Initially in all cases, formation rates were observed to increase with increasing Pt(IV) concentration. After 3 h however, the 0.35 mM sample unexpectedly began out-competing the 0.5 mM sample, most likely due to differences in particle morphology. Due to the lack of a suitable standard curve, the Pt(0) concentration could not be accurately calculated, however this absorbance (334 nm) is still a suitable indicator of NP formation over time. The inset image (Fig 4.3), shows the degree of colour change that each sample had undergone after the completion of the reduction reaction, with the 0.75 mM sample having the most significant change.

\* All values shown exhibit a standard deviation < 10 %

The pH (Fig 4.4) decreased over time in varying degrees for all samples. The sample containing 0.35 mM Pt(IV) exhibited the least significant pH drop, where the 0.5 mM and 0.75 mM samples exhibited a very similar trend. Unexpectedly, the controls (Fig 4.1 B) were observed to have reached lower pH levels than those of the test samples, indicating that the protein solution is acting as its own buffering agent by resisting small changes in pH. The drop in pH is once again attributed to the generation of HCl from the bioreduction of  $\text{H}_2\text{PtCl}_6$  as discussed in section 2.3.2.2.

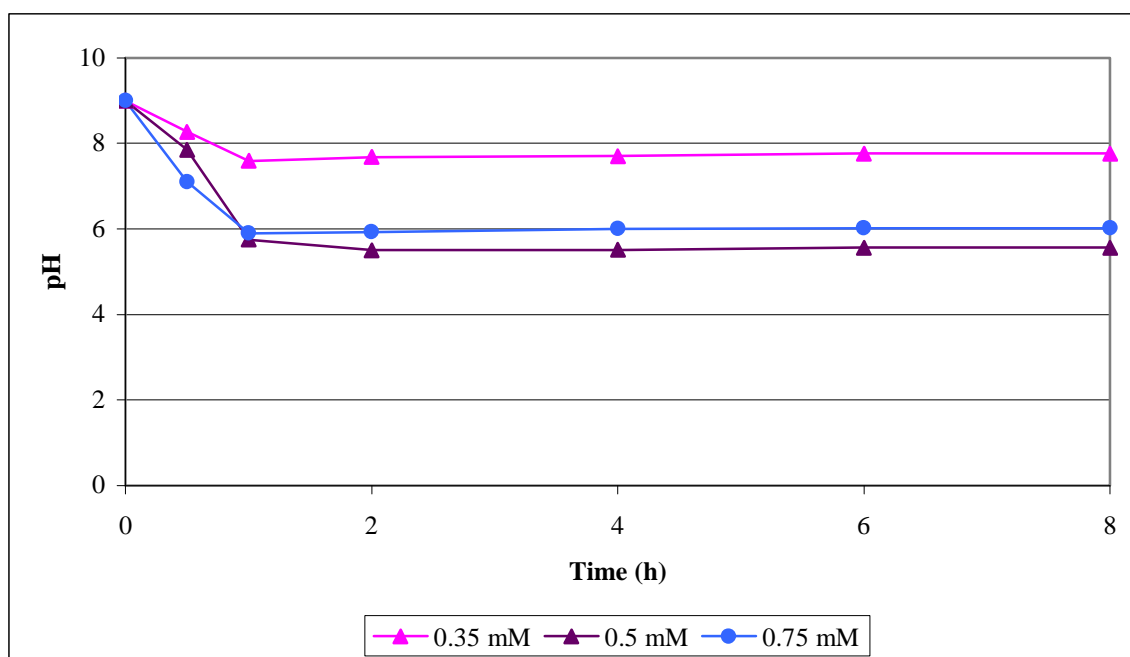


**Figure 4.4:** pH of the bioreductive samples over time.\*

#### 4.3.1.3. $\text{Pt(IV)} \geq 1 \text{ mM}$

All samples containing a Pt(IV) concentration greater than or equal to 1 mM, exhibited an exponential reduction curve over time (Fig 4.5 A). The reduction rate is seen to decrease in relation to increasing Pt(IV) concentration, opposite to the trends observed in section 4.3.1.2.

The exponential nature of the reduction curves mentioned above was confirmed by their linearisation by the semi-log plot, “ $\ln(y)$  vs  $x$ ” (Fig 4.5 B). All  $R^2$  values were greater than 0.97 indicating an adequate fit of the data to the trend line. The reduction rates of the exponential equations were obtained from these linearised graphs to be  $0.4637 \text{ mM}\cdot\text{h}^{-1}$ ,  $0.2334 \text{ mM}\cdot\text{h}^{-1}$  and  $0.1923 \text{ mM}\cdot\text{h}^{-1}$  for the 1 mM, 2 mM and 3 mM

\* All values shown exhibit a standard deviation < 10 %

samples respectively, indicating an inverse relationship between reduction rate and Pt(IV) concentration.

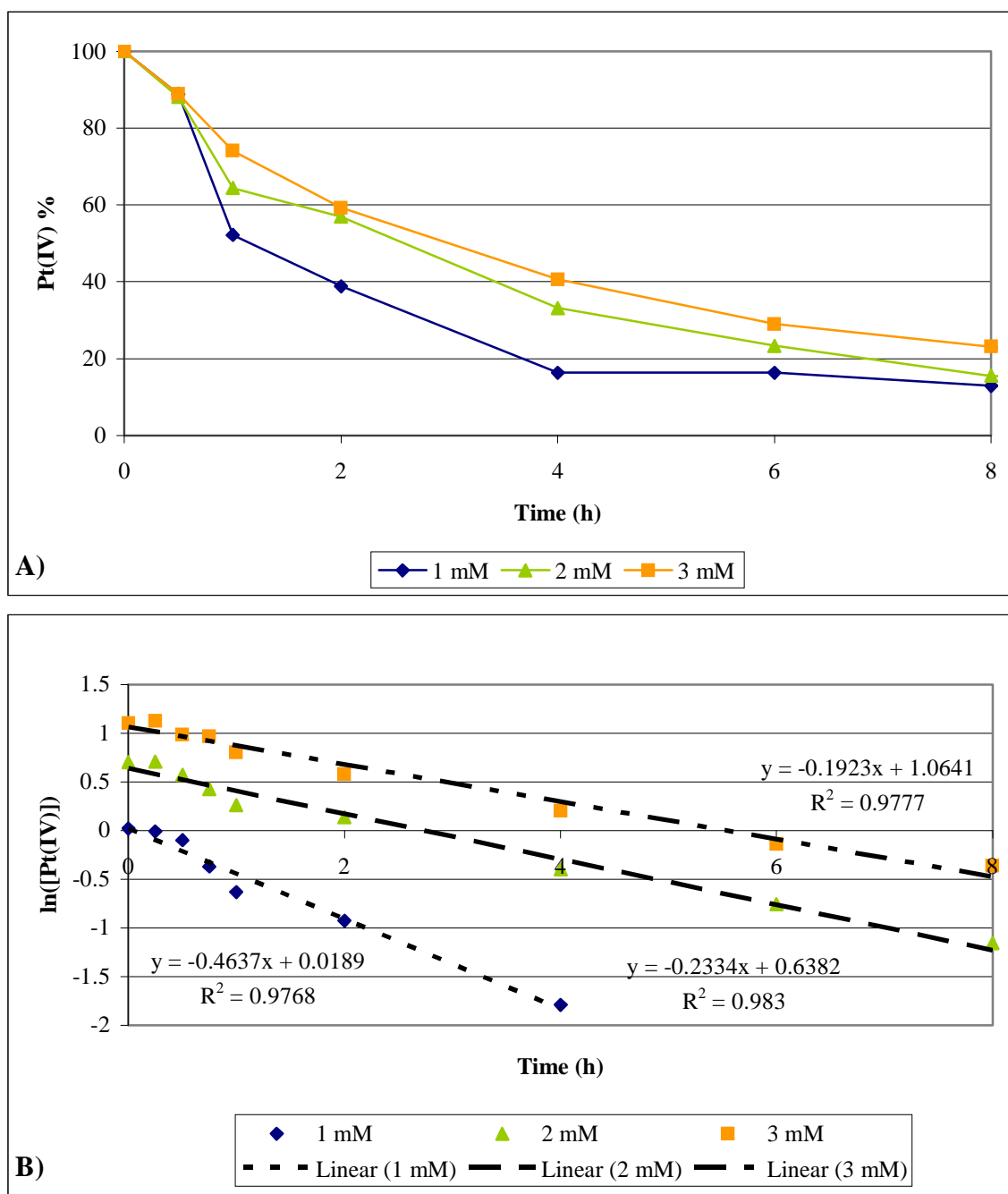


**Figure 4.5:** Effect of Pt(IV) concentration  $\geq 1$  mM. [A ) Pt(IV) reduction curve, B) Linearised reduction curve of samples  $\geq 1$  mM.]\*

Due to the results observed in section 4.3.1.2, it was uncertain as to why, in this case, with a higher concentration of Pt(IV) (i.e.  $\geq 1$  mM) the reduction of the Pt(IV) ion at 261 nm could be observed. A colour change to brown was observed indicating that

\* All values shown exhibit a standard deviation  $< 10\%$

the Pt(0) nanoparticles were forming over time, however the absorbance results indicated that the NP's were no longer interfering with the determination of the Pt(IV) ion. To further investigate this phenomenon, a closer look was taken at the absorbance readings at 334 nm (Fig 4.6).

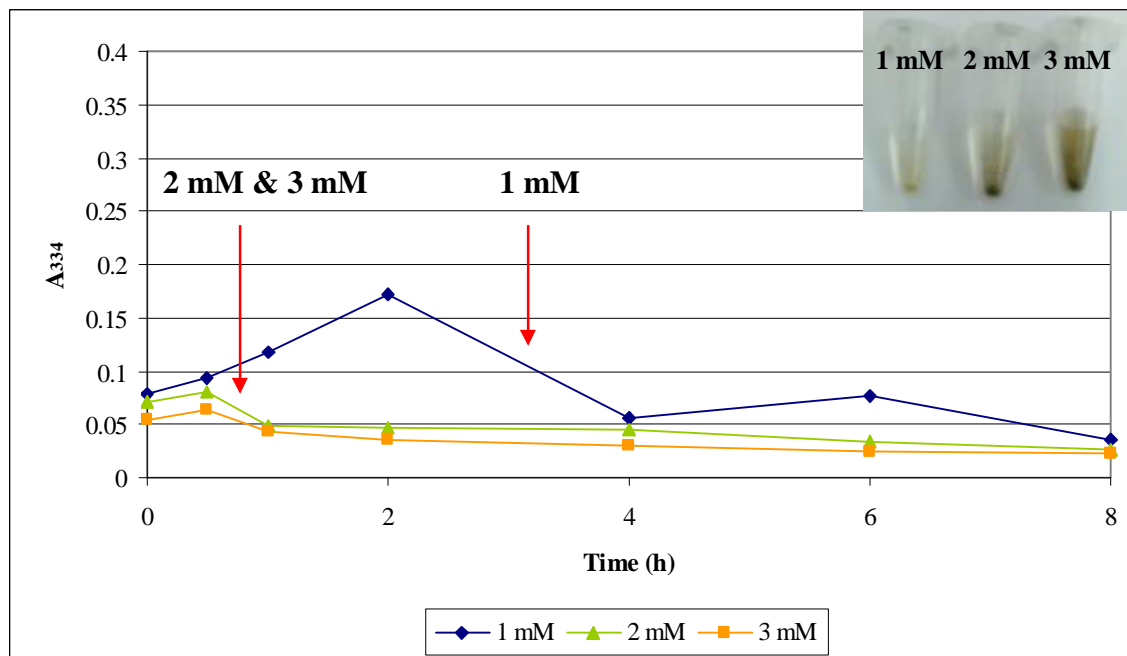


**Figure 4.6:** A<sub>334</sub> readings for samples  $\geq 1$  mM Pt(IV) [Inset: Image of samples post bioreduction.]\*

All three samples with a Pt(IV) concentration  $\geq 1$  mM showed an initial increase in absorbance at this wavelength (334 nm) indicating the formation of Pt(0) nanoparticles. The colour of the solutions also exhibited a colour change to brown, which correlates to the initial increase in absorbance at this wavelength. This increase was followed by a rapid decrease in absorbance between 2-4 h for the 1 mM sample and 0.5-1 h for the 2 mM and 3 mM samples respectively. Visual observations at these times showed the development of a brown precipitate while the supernatant of the solution became a pale yellow colour once more (Fig 4.6 Inset).

The moment when a sample exhibited a drop in absorbance, followed by the formation of a precipitate, could both be correlated to the point in time where the pH of the samples decreased below pH 4 (Fig 4.7). At this point, it is proposed that the unfavourable acidic pH resulted in the denaturation of a high percentage of the

\* All values shown exhibit a standard deviation  $< 10\%$

soluble protein that then precipitated out of solution. This was further substantiated through a Bradford protein assay of the samples (Fig 4.8)

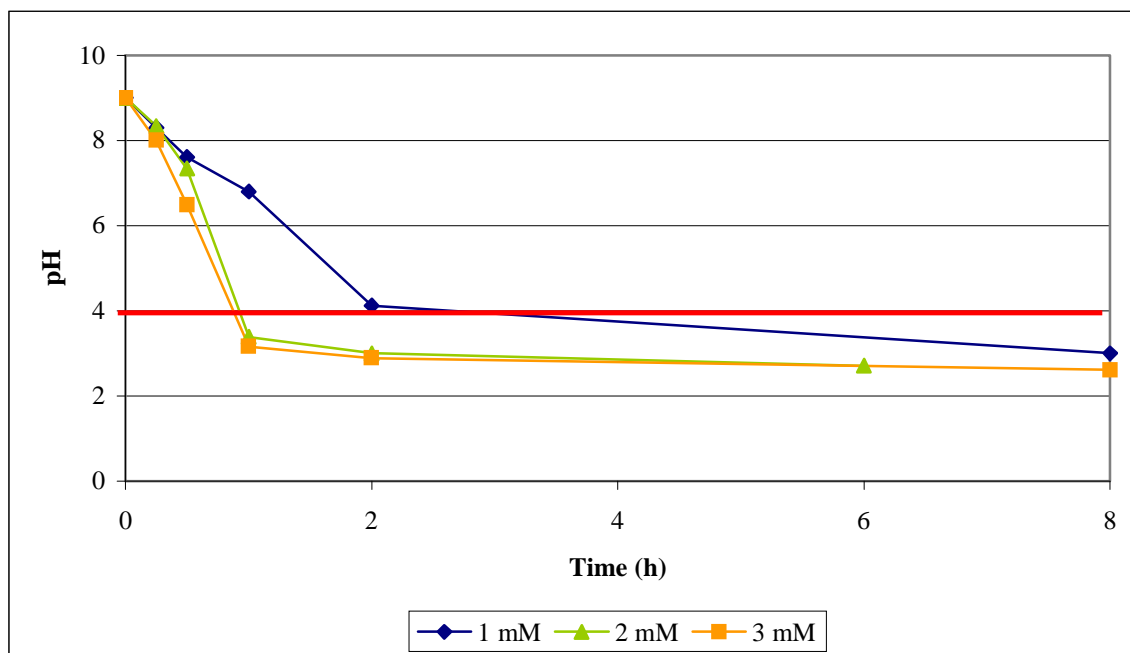


**Figure 4.7:** Change in pH of samples over time.\*

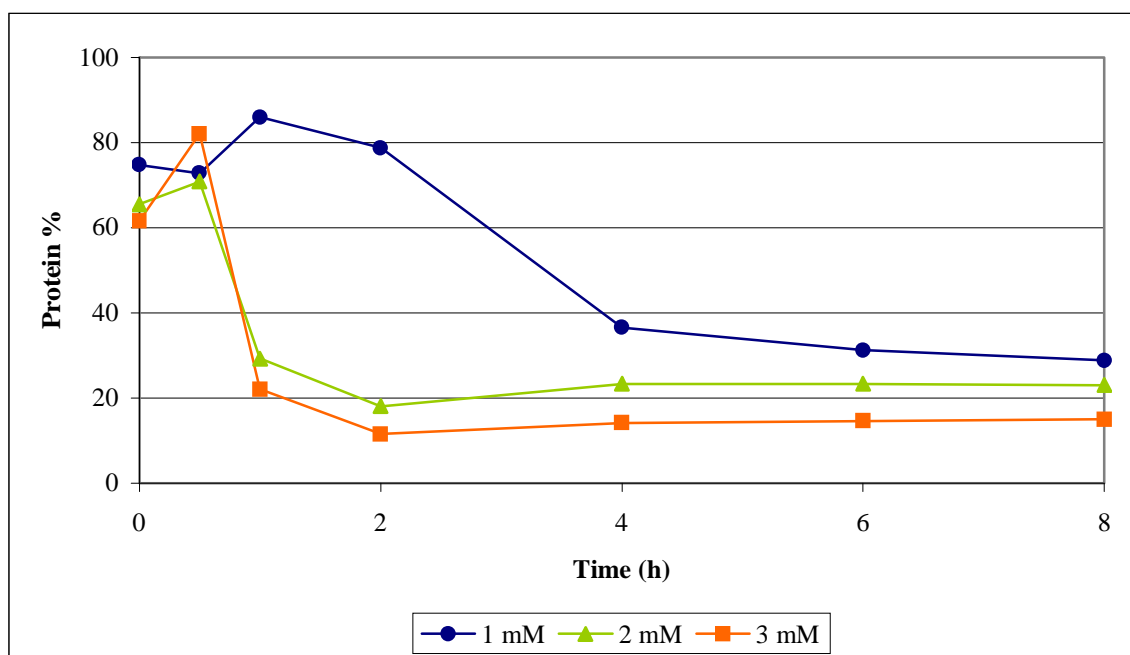


**Figure 4.8:** Change in protein concentration of samples over time.\*

The results from the Bradford protein assay (Fig 4.8) correlated precisely to those of the absorbance results at 334 nm (Fig 4.6) where an initial increase in ‘apparent’

\* All values shown exhibit a standard deviation < 10 %

protein concentration is observed - most likely due to the interference of the NP's absorbance spectrum – followed by a rapid decrease in protein concentration at the time intervals mentioned before. These results clearly show that protein precipitation had occurred due to denaturation caused by unfavourable acidic conditions.

The fact that the moment of protein precipitation correlated with the moment of decrease of absorbance at 334 nm strongly indicates that the NP's are being stabilised by the general, soluble protein in solution. When comparing the Bradford assay results (Fig 4.8) to those of pH over time (Fig 4.7), it becomes clear that at the point where the pH drops below pH 4.0, protein precipitates out of solution, co-precipitating the NP's with it, hence the brown colour of the precipitate, and the clear appearance of the supernatant.

It is significant to note that in all samples *post protein precipitation*, reduction of the Pt(IV) ion continued with only ~30-40 %, ~20 % and ~15 % of the protein remaining in solution for samples 1 mM, 2 mM and 3 mM respectively. The unexpected results observed in Fig 4.5 A, illustrating an inverse relationship between reduction rate and Pt(IV) concentration, may be explained by the following proposal. Greater amounts of protein precipitated in the presence of higher Pt(IV) concentrations, due to the acidic pH caused by greater yields of HCl being released by the reduction of H<sub>2</sub>PtCl<sub>6</sub>. This in turn resulted in a slower reduction rate due to a lower percentage of soluble protein present in the experimental solution. The fact that the reduction continued in all test cases, with the NP's bound to the protein, indicates that the NP's are not bound in such a way so as to inhibit the native activity of the remaining protein. This further suggests that the NP's are not covalently bound to the protein but are more likely adsorbed through electrostatic interactions.

In some cases, the binding of gold NP's to enzymes have unexpectedly shown to increase the catalytic activity and thermal stability of the protein, but in turn has also prevented reuse of the bioconjugate due to the difficulty in separating the bound constituents (Mandal *et al.*, 2005). This may explain the wide range of reductive activities observed for the CSE solution under the various conditions of pH, and temperature investigated.

The synthesis of stable, biogenic Pt(0) NP's, produced in the absence of synthetic polymers and without additional functionalisation steps has been demonstrated. Under the experimental conditions described, the NP's were found to be both stable in aqueous solution and do not negatively affect the catalytic activity of the proteins/enzymes to which they adsorb. These results may prove to have far reaching ramifications in the field of particle functionalisation.

#### 4.3.1.4. CSE protein analysis by Native-PAGE

The 7.5 % continuous native-PAGE gel (Fig 4.9), illustrates the differences in the native protein prior and post bioreduction of the Pt(IV) ion by the CSE, from the SRB consortium. In general terms, since native-PAGE separates proteins on the basis of charge and size, the smaller, acidic proteins would be located at the bottom of the gel while the larger, more basic proteins would be positioned at the top of the gel (Wilson & Walker, 2000). Equivalent amounts of protein ( $\sim 50 \mu\text{g}.\text{ml}^{-1}$ ) were loaded in each lane for each sample.

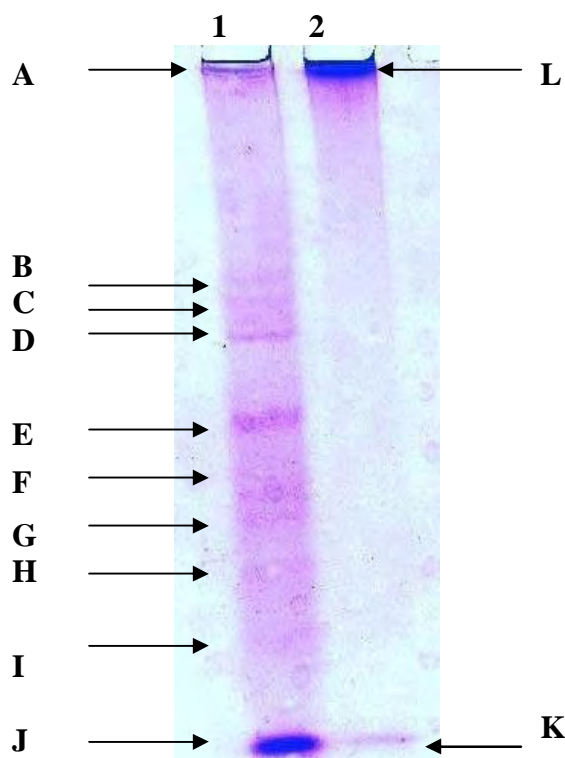


**Figure 4.9:** Continuous native-PAGE gel (7.5 %) of crude CSE solution. 1) pre and 2) post bioreduction of 0.75 mM Pt(IV). [The arrows A-J indicate the major protein bands from the CSE solution prior bioreduction, while the arrows L and K indicate the only protein bands visible post bioreduction.]

Lane 1, CSE prior bioreduction, clearly shows a number of native protein bands labelled A – J. The large band at “J” is expected to contain a number of small molecular weight, acidic proteins. Post bioreduction (Lane 2), a number of changes were obvious, namely the protein band at ‘K’ that was much smaller than that observed prior bioreduction (J), and similarly, the bands that should correspond to those labelled B-I in Lane 1 are no longer present in Lane 2. There is, however a large protein band in Lane 2, just below the well, indicating a large/aggregated, highly basic protein(s), that corresponds to a much lighter band (A) in Lane 1. This result suggests that the nanoparticles have bound to all soluble protein, specifically at the negative, acidic residues, thereby masking these charges and providing all protein with a general basic charge. In addition, the binding of the nanoparticles to the protein has had a possible aggregating effect, since the majority of the protein only just entered the pores of the gel. These results also strongly suggest that the overall charge of Pt(0) NP’s in aqueous solution is positive, correlating to literature (Ahern & Garrell, 1991).

#### 4.3.1.5. SEM-EDAX analysis

This EDAX spectrum (Fig 4.10) of a CSE sample post Pt(IV) bioreduction, depicts a number of peaks that are characteristic of elements contained within carbon-based life-forms; such as sodium (Na), calcium (Ca), nitrogen (N) and oxygen (O). Low levels of sulfur (S) are also present and most likely due to the presence of proteins as mentioned previously (section 2.3.4.4).

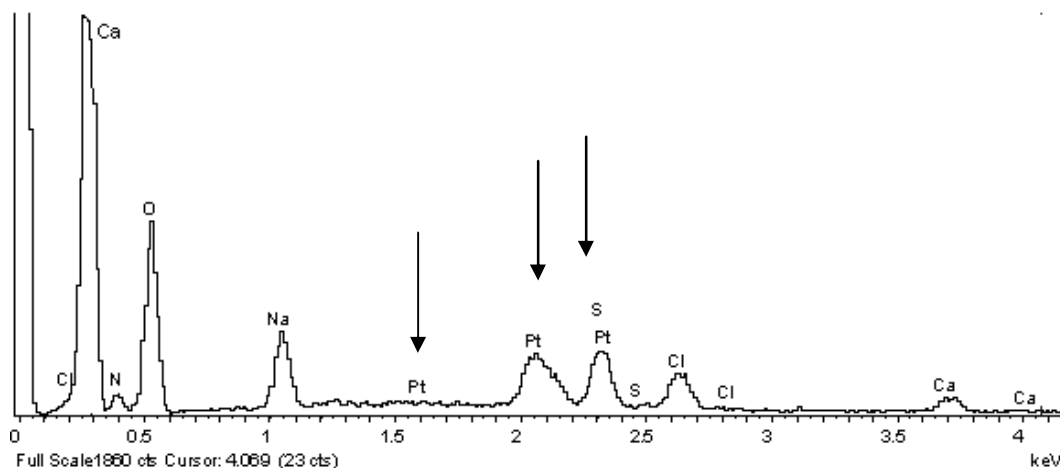


**Figure 4.10:** EDAX spectrum of CSE sample post bioreduction of Pt(IV).



The presence of the characteristic peaks of Pt(0), indicated by the arrows, prove that platinum is present in the sample and furthermore that Pt(IV) does in fact become reduced to elemental platinum, utilising the CSE from the current SRB consortium.

#### 4.3.2. Effect of Pt(IV) concentration in a sodium-bicarbonate buffer (200 mM, pH 9.0)

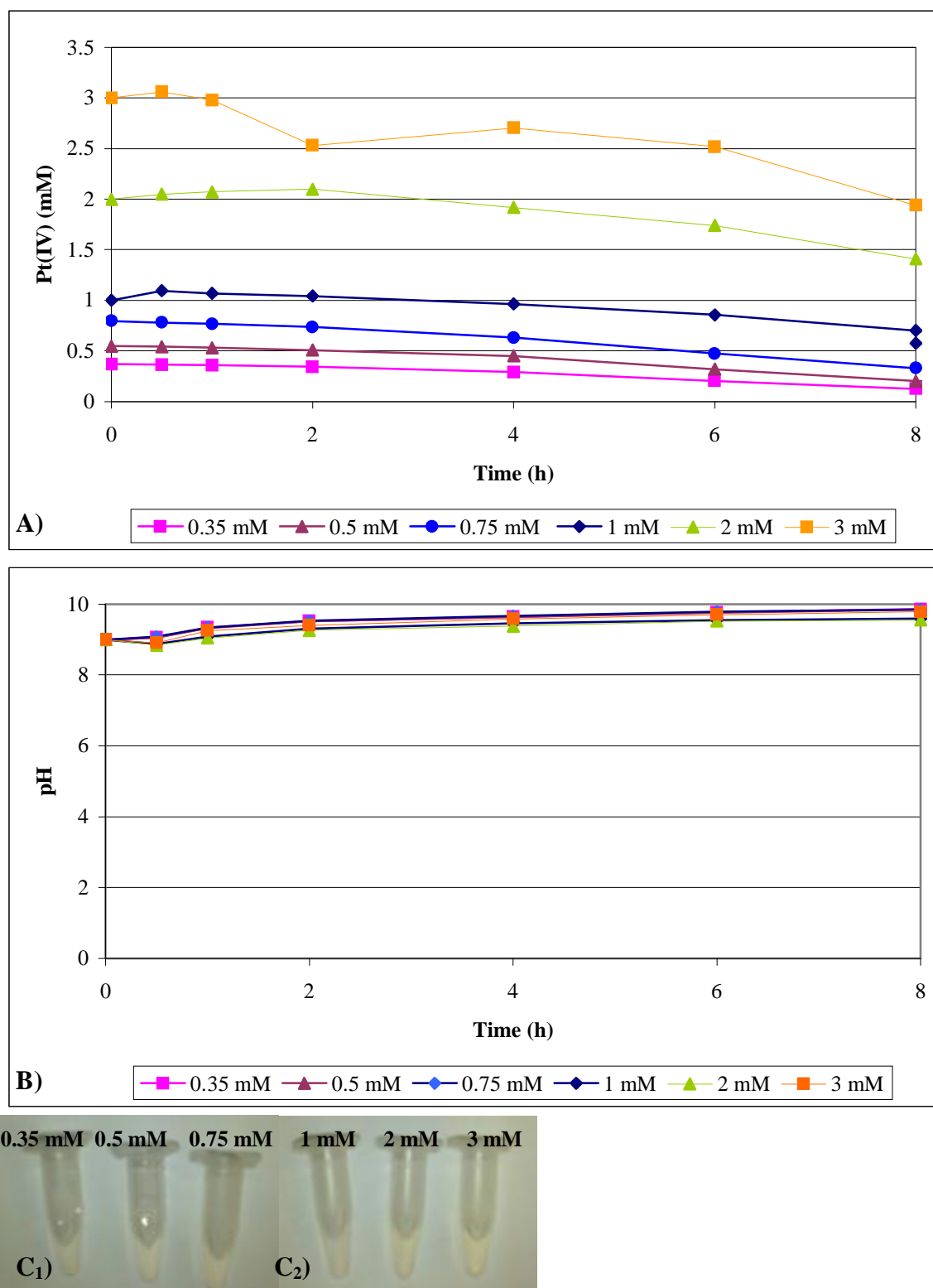
##### 4.3.2.1. Cell-free controls

In contrast to the previous experiments conducted in water (section 4.3.1) the controls in the presence of a sodium-bicarbonate (SBC) buffer (Fig 4.11 A), reflected an instability of the Pt(IV) ion. This is most likely due to the basic conditions (pH 9) of the SBC buffer, which tends to favour the hydrolysis of the  $\text{H}_2\text{PtCl}_6$  complex and the subsequent formation of hydroxide complexes (Bel'skaya & Duplyakin, 2007), though further investigation needs to be conducted to confirm this proposal.

Unexpectedly, the pH for all the control samples (Fig 4.11 B) increased slightly over time, in contrast to the investigations in water, where the pH decreased rapidly (Fig 4.1 B). Although statistically insignificant, this result was most likely due to the following equation (Equation 6) where the HCl produced from  $\text{H}_2\text{PtCl}_6$  reduction becomes neutralised by the buffer:

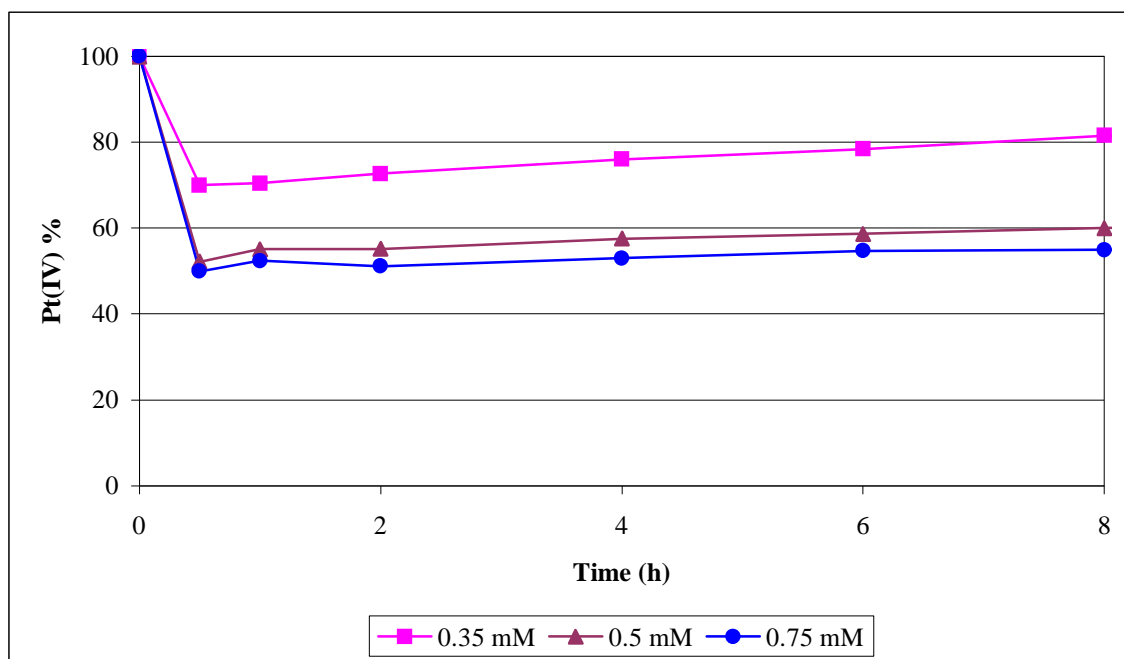


The images in Fig 4.11 C<sub>1+2</sub>, illustrate the lack of any colour change to brown in all control samples, confirming that the platinum nanoparticles are not formed due to any abiotic involvement of the sodium-bicarbonate buffer.



**Figure 4.11:** Control samples in sodium-bicarbonate buffer (200 mM, pH 9). [A] Pt(IV) concentration over time; B) pH over time for control samples, C<sub>1+2</sub>) Images of controls post bioreduction.]\*

\* All values shown exhibit a standard deviation < 10 %

4.3.2.2.  $Pt(IV) < 1 \text{ mM}$ 

**Figure 4.12:** Investigating the effect of a sodium-bicarbonate (200 mM, pH 9.0) buffer on the bioreductive mechanism. \*

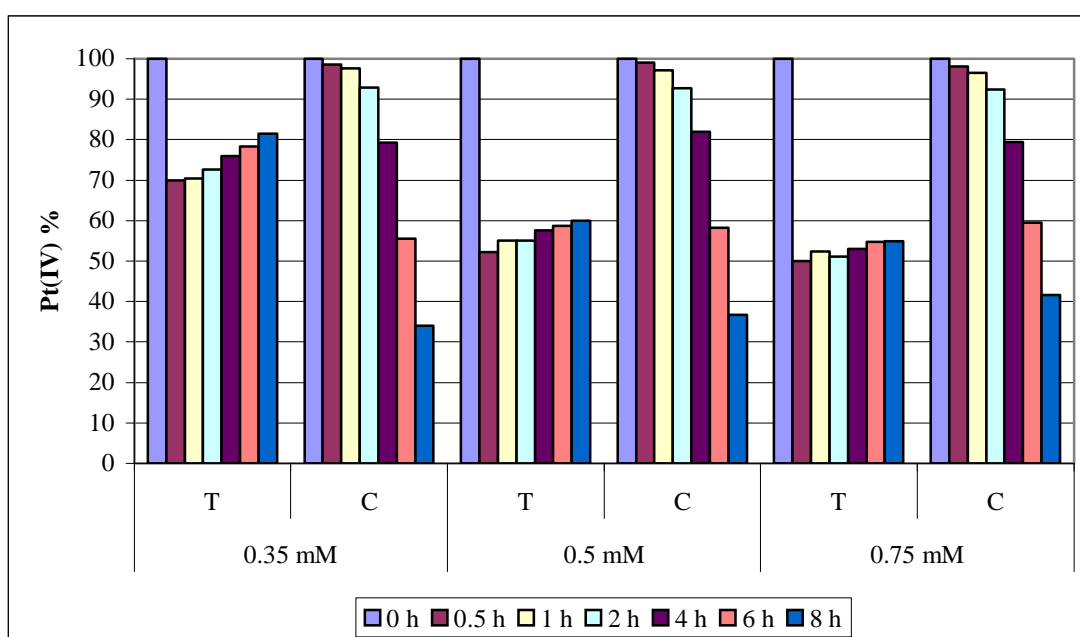


**Figure 4.13:** Comparison of Pt(IV) concentration in test (T) versus control (C) experiments. \*

Once again, the Pt(IV) ion exhibited the now expected trend of an initial reduction step followed by a period of apparent increase in concentration (Fig 4.12). This, as

\* All values shown exhibit a standard deviation < 10 %

shown previously in section 4.3.1.2, is due to interference caused by the increasing absorbance spectrum, characteristic of Pt(0) NP formation in aqueous solution.

When comparing the control experiments (i.e. lacking CSE) to the test experiments (Fig 4.13), the control samples in the presence of the sodium-bicarbonate buffer (200 mM, pH 9.0) were observed to exhibit an instability of the Pt(IV) ion, which readily underwent hydrolysis. The exact reason for this has yet to be elucidated. In the test samples however, the Pt(IV) ion was reduced at a far more rapid rate initially (0-0.5 h) indicating that the biological extract is actively involved in the reduction mechanism.

It is also apparent (Fig 4.13) that the unexpected increase in Pt(IV) concentration only appears in the test samples, with a greater percentage of Pt(IV) becoming reduced between 0-0.5 h, at higher Pt(IV) concentrations. The controls exhibited a very similar rate of reduction for all sample concentrations investigated (Fig 4.13). Since no colour change or NP spectrum was observed in the control samples (Fig 4.11 C<sub>1+2</sub>), it may be concluded that the formation of Pt(0) NP's is directly related to the presence of CSE and not due to an abiotic, non-enzymatic mechanism.

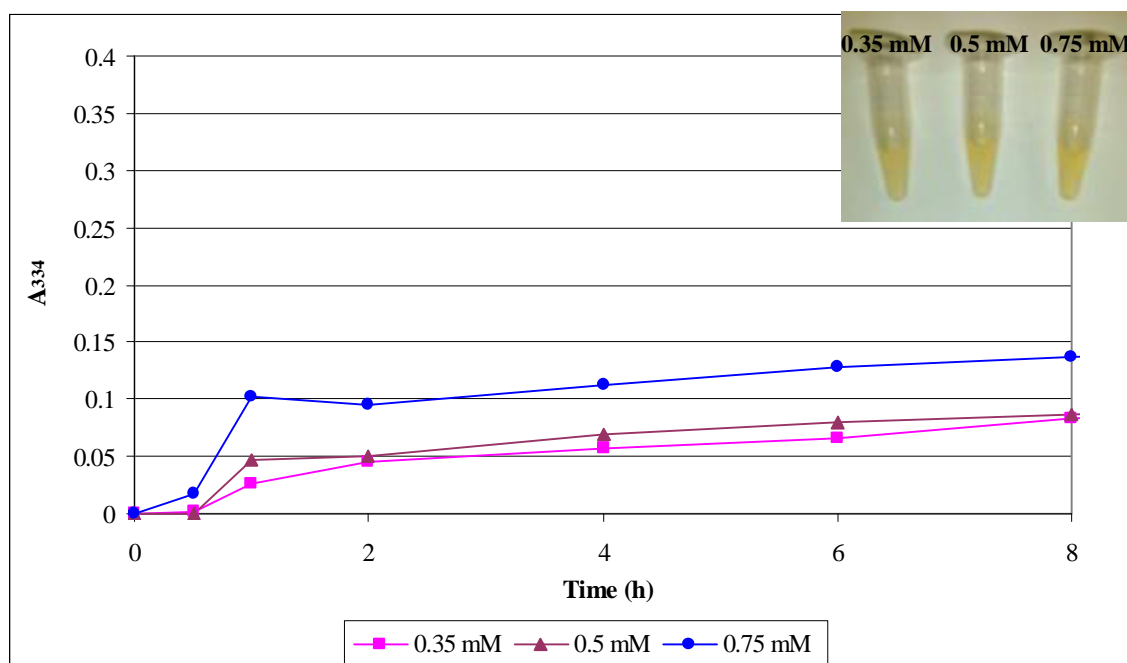


**Figure 4.14:** Pt(0) formation over time. [Inset: Image of samples post bioreduction.]\*

\* All values shown exhibit a standard deviation < 10 %

Since the Pt(IV) ion could not be determined, due to the interference from the Pt(0) NP spectrum, the absorbance at 334 nm was once again taken as a non-quantitative, indicator of Pt(0) NP formation over time as described in section 4.3.1.2. When comparing the rate of change in absorbance at 334 nm for these samples, Fig 4.14 showed a correlation between increasing Pt(IV) concentration and a higher Pt(0) formation rate. The 0.75 mM sample revealed the greatest Pt(0) formation rate as previously determined in section 4.3.1.2.

The colour change from yellow to brown, however was considerably less in the presence of the buffer (Fig 4.14 Inset) with a more golden hue forming over time. This was unexpected since the initial reduction rate of Pt(IV) was observed to increase (Fig 4.13). This correlates to the absorbance results observed in Fig 4.14 that show a very low change in absorbance when compared to the same samples in water (Fig 4.3). Since the Pt(0) spectrum is independent of particle size, as previously discussed in section 4.1, it is proposed that a drastic change in NP shape, concentration or aggregation is responsible for this trend, due to the presence of the sodium-bicarbonate (SBC) buffer.

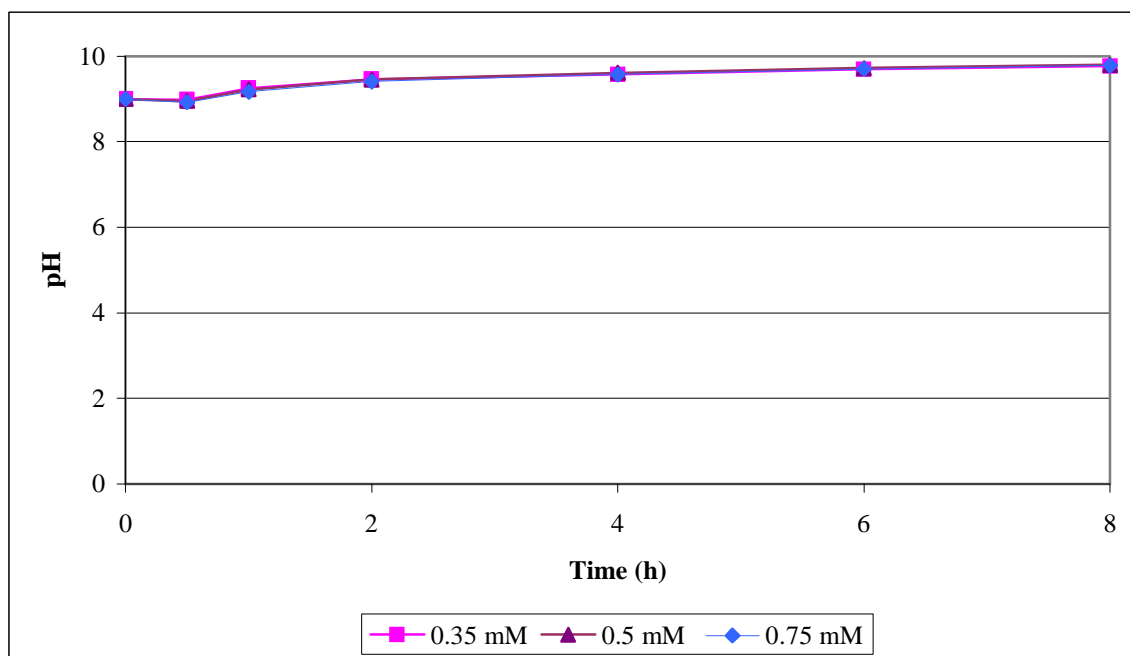


**Figure 4.15:** pH of samples over time. \*

\* All values shown exhibit a standard deviation < 10 %

As observed for the control samples, a very similar trend of increasing pH was seen for all samples over time (Fig 4.15). The samples initially showed a minor drop in pH to ~8.9 after 0.5 h followed by a slight increase to ~9.5 after 2 h. Here the pH began to level off reaching a maximum of ~9.8 after 8 h. In all cases the increase in pH is relatively insignificant and as mentioned previously, is most likely due to the neutralisation of the HCl generated from the reduction of the  $\text{H}_2\text{PtCl}_6$  complex (section 4.3.2.1).

#### 4.3.2.3. *Pt(IV)* $\geq 1 \text{ mM}$

The Pt(IV) ion was shown to decrease slowly over time in the controls (Fig 4.1 A), however a rapid reduction was observed in the test samples between 0-1 h followed by an increase and subsequent levelling-off of the apparent Pt(IV) concentration (Fig 4.16 A). It is also clear from these results that the reduction rate increased in the presence of a higher Pt(IV) concentration, as would be expected.

These results indicated that the presence of the buffer, had stabilised the pH at pH ~9, preventing the formation of the unfavourable acidic conditions described in section 4.3.1.3. This was further supported by the reduction rates increasing in relation to increasing Pt(IV) concentration, due to the protein remaining in its native, soluble and active state (Fig 4.16 B). The rates of Pt(IV) reduction for the first hour in all samples was calculated as  $0.841 \text{ mM}\cdot\text{h}^{-1}$ ,  $1.142 \text{ mM}\cdot\text{h}^{-1}$  &  $1.317 \text{ mM}\cdot\text{h}^{-1}$  for 1 mM, 2 mM and 3 mM respectively. This shows nearly a two-fold increase in reduction rate for the 1 mM sample conducted in section 4.3.1.3 in water of  $0.4637 \text{ mM}\cdot\text{hr}^{-1}$ . The rates for the 2 mM and 3 mM samples cannot be readily compared to those in section 4.3.1.3, due to the high percentage of protein precipitation that had occurred in the samples, being the most likely cause for the lowered reduction rates observed (Fig 4.5 B). Hence, a true representation of the overall reduction rates, in the presence of the original starting protein concentration of CSE, could not be determined due to the protein precipitation that had occurred.

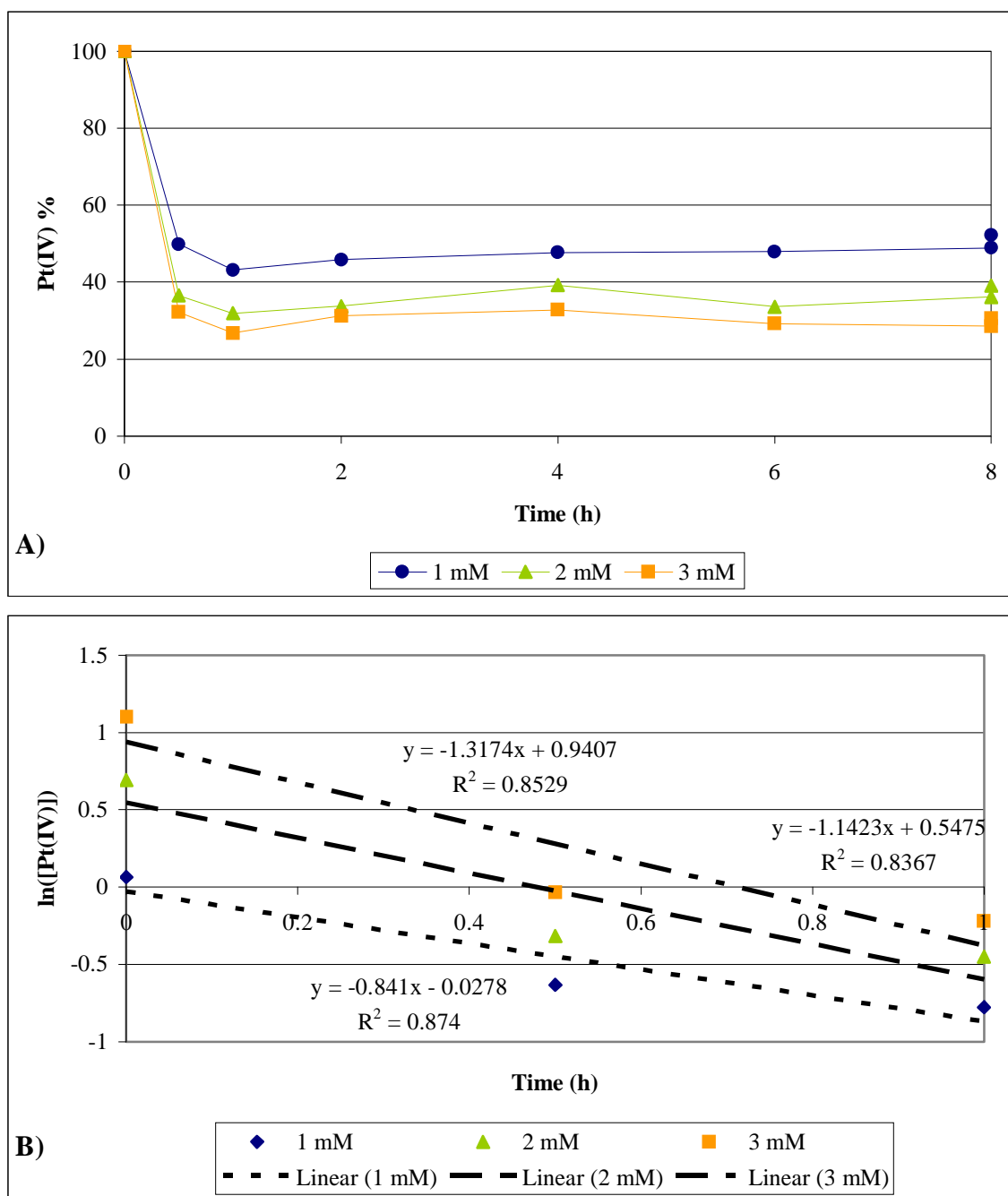


**Figure 4.16:** Bioreduction of Pt(IV). [A) Pt(IV) concentration over time, B) Pt(IV) reduction rate.] \*

In Fig 4.17, the 2 mM & 3 mM samples show a rapid increase in  $A_{334}$  between 0-4 h due to the formation of Pt(0) NP's. This was unexpectedly followed by a decrease in absorbance between 4-6 h, which could not be correlated to any decrease in pH (Fig 4.18) or protein precipitation as seen previously in section 4.3.1.3. It is proposed,

\* All values shown exhibit a standard deviation < 10 %

however that this decrease in absorbance may be due to instability and/or aggregation of the NP's in solution due to the presence of the buffer salts.  $A_{334}$  was then observed to increase somewhat in the 2 mM sample between 6-8 h but remained constant in the 3 mM sample. No unexpected decreases in  $A_{334}$  were observed in the 1 mM sample, as it exhibited a general trend of increasing  $A_{334}$  over the 8 h time period.

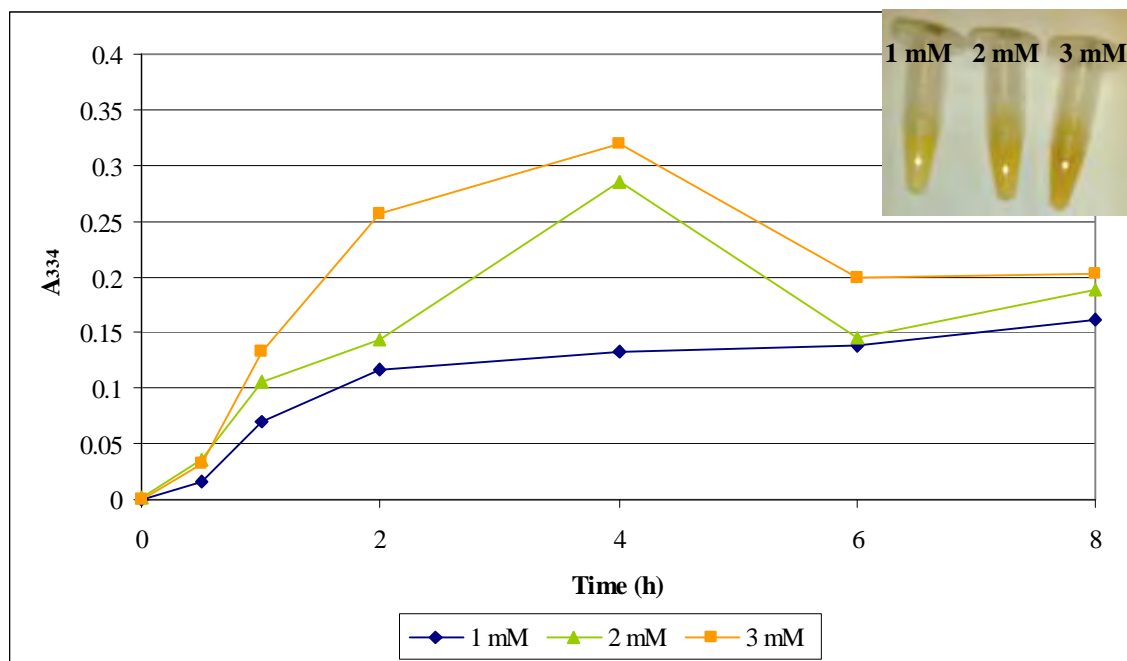


**Figure 4.17:** Formation of Pt(0) over time. [Inset: Image of samples post bioreduction.]\*

The visual observations of the samples over time (Fig 4.17 Inset) exhibited no protein precipitation. A colour change from light yellow to a dark, golden-yellow was also observed (Fig 4.17 Inset), indicating Pt(0) NP formation, however the degree of colour change was less than that observed in the investigations conducted in water (section 4.3.1.3, Fig 4.6 Inset). As mentioned previously, it is proposed that this may be due to changes in particle morphology due to the presence of the buffer salts.

In Fig 4.18, a similar trend in pH was observed as seen in the samples < 1 mM (Fig 4.15), an insignificant increase in pH was observed with an initial drop occurring between 0-0.5 h, that becomes slightly exaggerated in the higher Pt(IV) concentrations. For all samples, the pH begins increasing where it reaches a level of pH 9.5 after 8 h for the 1 mM sample while the 2 mM and 3 mM samples both exhibit an increasing trend of pH beyond that observed at 8 h.

\* All values shown exhibit a standard deviation < 10 %



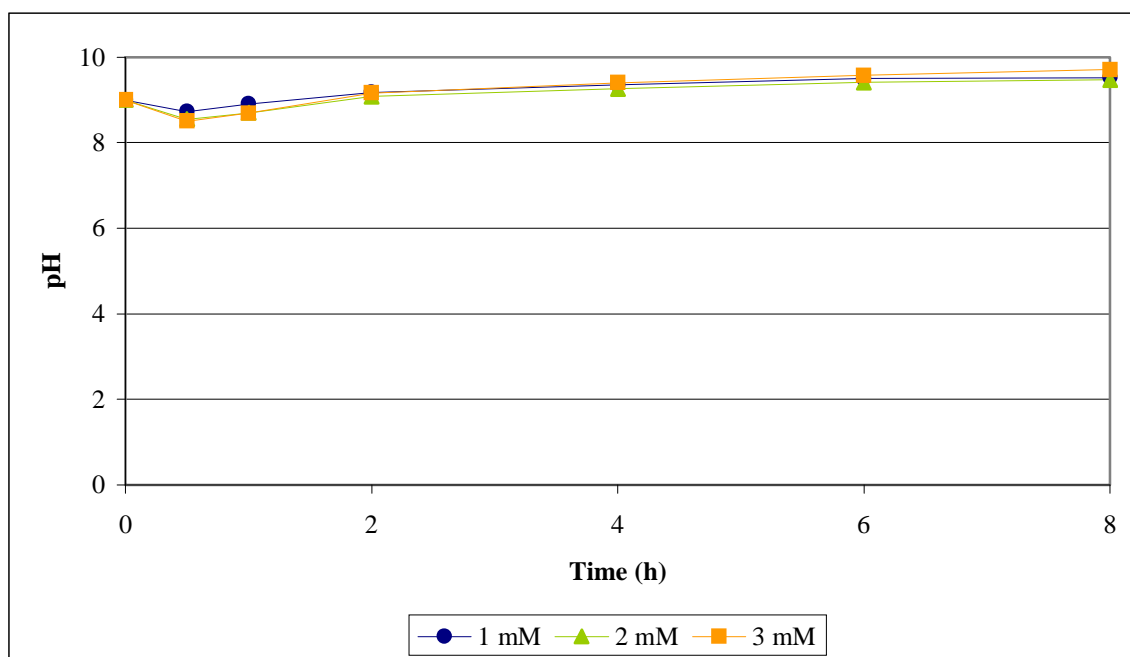


**Figure 4.18:** pH of samples over time. \*

#### 4.3.2.4. Comparing the effect of a sodium-bicarbonate (SBC) buffer (200mM, pH 9.0) versus ddH<sub>2</sub>O

The presence of the buffer results in a slight increase in reduction rate between 0-0.5 h when compared to the samples < 1 mM in water (Fig 4.19 I). The most significant observation, however is seen by the interference of the NP spectrum (1-8 h) in Pt(IV) ion determination which is exaggerated in the absence of the buffer. It is not known why this is the case, though it is proposed that it may be due to the morphological effects of the buffer salts on the NP's in solution.

In Fig 4.19 II, the addition of the buffer resulted in a significant increase in the Pt(IV) reduction rate when comparing the samples  $\geq 1$  mM. The initial percentage of Pt(IV) reduced in water for all samples  $\geq 1$  mM was ~12 % after 0.5 h. When comparing these values to that of the buffered samples over the same time period, it was observed that the percentage of Pt(IV) reduced had increased to 50, 54 & 58 % respectively for samples, 1 mM, 2 mM & 3 mM. At this point (0-0.5 h) for the Pt(IV) samples in water, no protein precipitation had yet occurred, therefore these points in time may be compared to the samples in buffer.

\* All values shown exhibit a standard deviation < 10 %

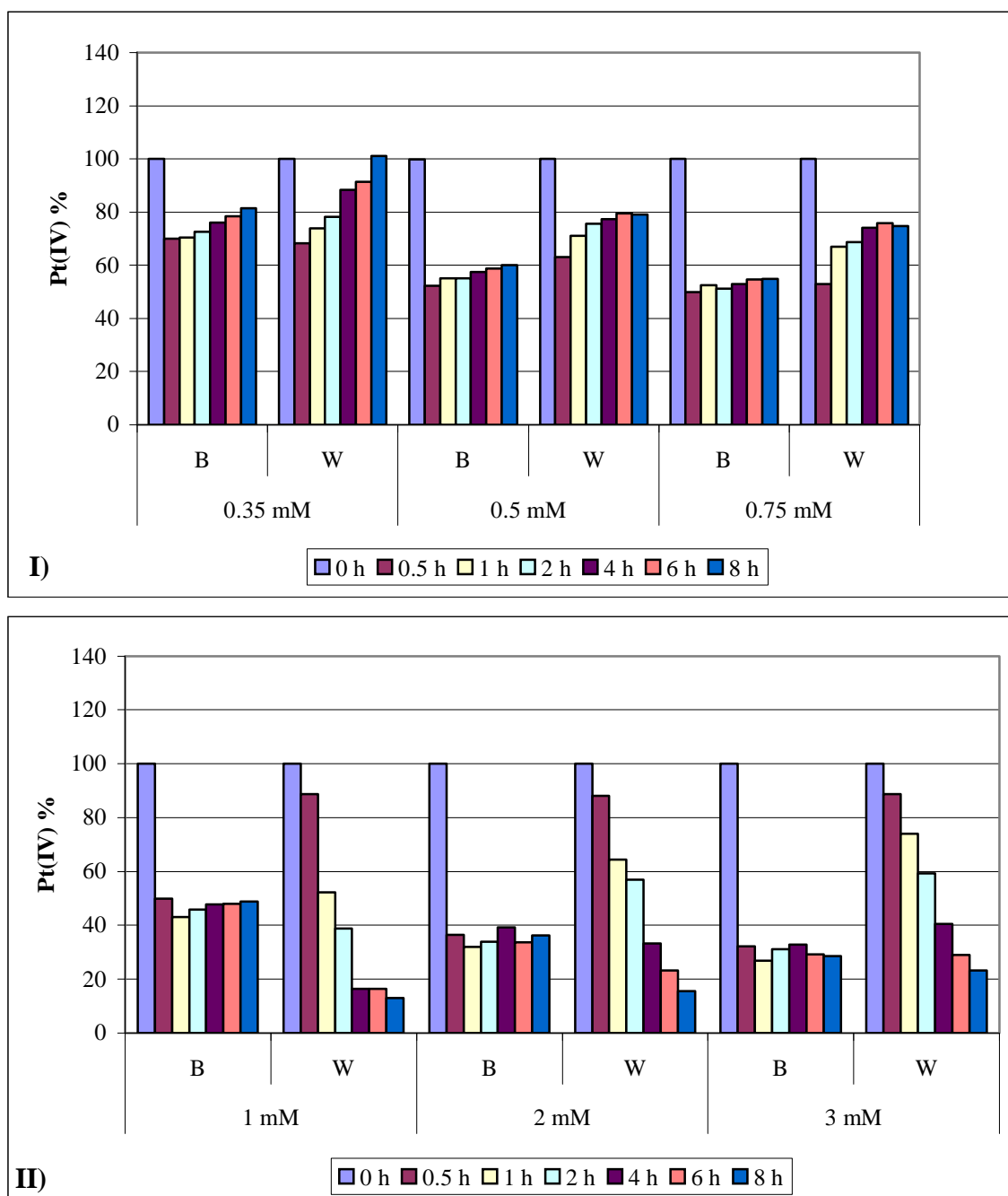


**Figure 4.19:** Comparing the reduction of the Pt(IV) ion **I)** < 1 mM Pt(IV) and **II)** >= 1 mM in **B)** sodium-bicarbonate buffer (200 mM, pH 9) and **W)** in ddH<sub>2</sub>O.]\*

In water, the Pt(IV) reduction rate decreases with increasing Pt(IV) concentration (Fig 4.19 II). The reduction of the Pt(IV) ion at 261 nm could be followed due to nanoparticle-protein precipitation, arising from the formation of acidic conditions as discussed in section 4.3.1.3, removing the NP interference. In comparison, the SBC samples >= 1 mM exhibit a slightly increasing reduction rate between 0-0.5 h in

\* All values shown exhibit a standard deviation < 10 %

regards to increasing Pt(IV) concentration. Since the buffer stabilised the pH > 4.0 (i.e. ~pH 9), the majority of the protein remained in solution thereby preventing the nanoparticle-protein precipitation observed in section 4.3.1.3. The formation of the NP's in solution hence resulted in the interference of the Pt(IV) and Pt(II) ion determinations caused by the characteristic UV-Vis spectrum of these particles.

#### 4.3.3. TEM analysis

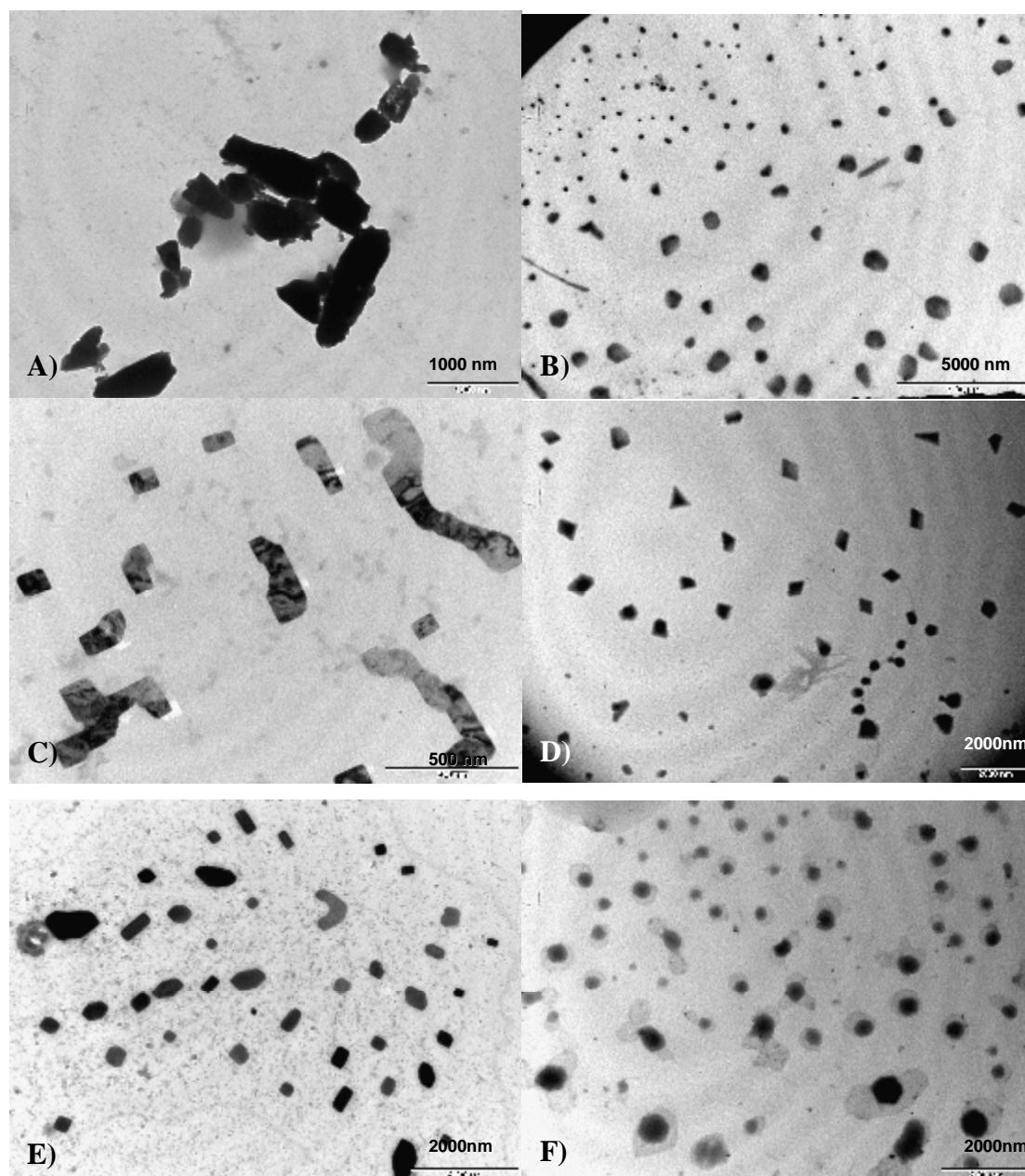


**Figure 4.20:** TEM images comparing the particles (<1 mM) post bioreduction in water versus SBC. [A) 0.35 mM in ddH<sub>2</sub>O. Scale bar = 1000 nm, B) 0.35 mM in SBC. Scale bar = 5000 nm, C) 0.5 mM in ddH<sub>2</sub>O. Scale bar = 500 nm, D) 0.5 mM in SBC. Scale bar = 2000 nm, E) 0.75 mM in ddH<sub>2</sub>O. Scale bar = 2000 nm, F) 0.75 mM in SBC. Scale bar = 2000 nm.]

The samples were analysed by TEM to determine and compare the morphology of the particles produced by the cell-free, CSE bioreductive mechanism. Fig 4.20 illustrates the differences observed in the morphology of the particles in the Pt(IV) samples less than 1 mM in water and buffer.

In the 0.35 mM Pt(IV) sample in water (Fig 4.20 A), a number of large (200-1000 nm), irregular, electron dense particles were observed, of which a high degree had become aggregated. The same sample in SBC (Fig 4.20 B) exhibited very different particles, all with straight, flat edges and the majority exhibiting a hexagonal or irregular morphology with a size range of 50-750 nm.

In the 0.5 mM sample in water (Fig 4.20 C), there were particles (100-500 nm) that were more reminiscent of geometric shapes such as rectangles and squares. These tended to form end-on-end aggregates that resulted in unusual 'step-like' structures. In SBC (Fig 4.20 D), the 0.5 mM sample exhibited individual, sharp-edged particles, the majority of which were four-sided shapes with hexagons, triangles and irregular morphologies also present. The majority of the particles fell in the size range of 100-350 nm with some larger outliers present.

The particles observed in the 0.75 mM sample in water (Fig 4.20 E) ranged in size from 200-800 nm and were more geometric in nature, often four-sided with clean, straight edges. There was also greater monodispersity in this sample compared to others in water, however there were still a number of irregular particles present. In SBC, the 0.75 mM sample (Fig 4.20 F) generally exhibited irregular particles with irregular edges, surrounded by a water-mark effect. It also demonstrated a generally smaller size distribution (i.e. 100-350 nm), than the 0.35 mM & 0.5 mM samples.

The presence of the SBC buffer appears to reduce the size of the NP's by increasing the reduction rate of the first reduction cycle of Pt(IV) to Pt(II). It has yet to be elucidated how this occurs, however it is proposed that the buffer maintains the optimum conditions required for the catalytic action of the unknown Pt(IV) reductase, identified in Chapter 3. This is further supported by the fact that the optimum conditions for hydrogenase activity, which was previously demonstrated in Chapter 3 to be involved in the second reduction cycle of Pt(II) to Pt(0), is approximately

pH 7.5-8.0 (Rashamuse *et al.*, 2008). Hence, under the current conditions, one would expect lowered activity. This is difficult to demonstrate however, due to the presence of the NP's in solution interfering with the determination of Pt(IV) ions. The fact that the colour development and change in absorbance at 334 nm appeared to be hindered in the presence of SBC, suggests that there was a lower concentration of particles. This would indicate that the second reduction cycle of Pt(II) to Pt(0) was compromised, supporting the evidence for the involvement of a periplasmic H<sub>ase</sub>.

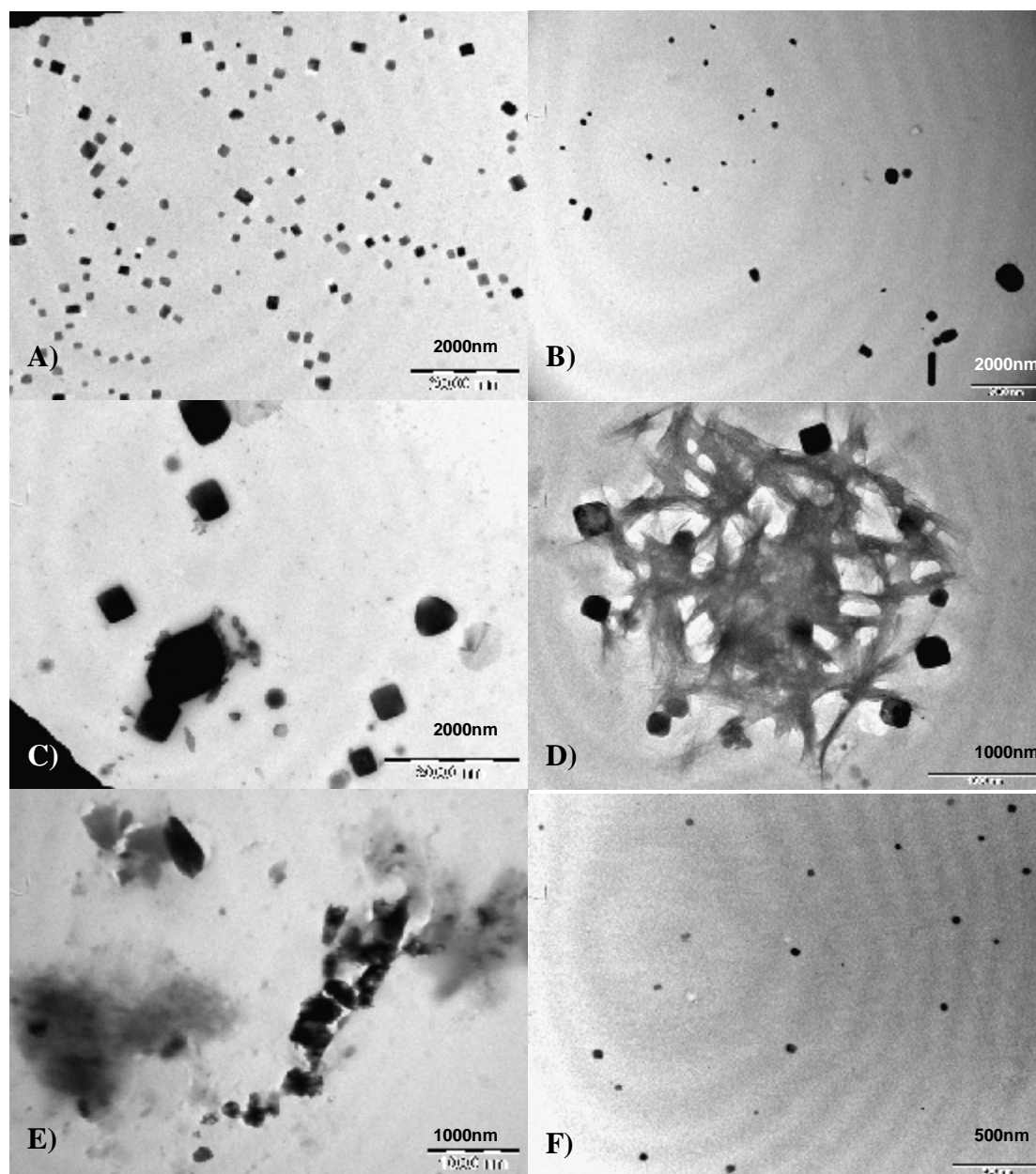


**Figure 4.21:** TEM images comparing the particles ( $\geq 1$  mM) post bioreduction in water vs SBC [A) 1 mM in ddH<sub>2</sub>O. Scale bar = 2000 nm, B) 1 mM in SBC. Scale bar = 2000 nm, C) 2 mM in ddH<sub>2</sub>O. Scale bar = 2000 nm, D) 2 mM in SBC. Scale bar = 1000 nm, E) 3 mM in ddH<sub>2</sub>O. Scale bar = 1000 nm, F) 3 mM in SBC. Scale bar = 500 nm.]

For the samples  $\geq 1$  mM identified in water (Fig 4.21 A, C & E), due to the nanoparticle-protein precipitation that arose from the acidic conditions generated by  $\text{H}_2\text{PtCl}_6$  reduction, a very low concentration of these particles remained soluble. This issue was not relevant for the particles identified in SBC.

In the 1 mM sample in water (Fig 4.21 A), the nanoparticles were highly geometric in shape, with the majority exhibiting square or rectangular conformations in the size range of 50-300 nm. There was a high degree of monodispersity with little aggregation observed. The results for 1 mM in SBC (Fig 4.21 B) showed monodisperse particles with a slightly wider size distribution of 50–350 nm with a few larger particles. The morphologies were generally irregular or rounded square/rectangular.

In the 2 mM sample in water (Fig 4.21 C), a very low number of large (400-1000 nm) electron dense, geometric particles were observed. The results for the 2 mM sample in SBC (Fig 4.21 D) showed square particles of a much narrower size distribution i.e. 50-150 nm. This image also clearly shows the particles adsorbed to an electron dense matrix, that is believed to be either buffer salt crystals or protein.

Last, the 3 mM sample in water (Fig 4.21 E) showed large amounts of amorphous electron dense deposits, while the 3 mM sample in SBC (Fig 4.21 F) showed small rounded-square NP's with a narrow size distribution of 10-80 nm, and a high degree of monodispersity.

It appears that in water, the mechanism favours a higher Pt(IV) concentration for more regular, geometric particle conformations. The resulting acidic pH however, hinders the amount of particles that could be used due to the particles precipitating out of solution adsorbed to the denatured proteins. For this reason, the effect of an SBC buffer on the reduction rate and subsequent nanoparticle morphologies was investigated. The presence of the buffer maintained the integrity of the native proteins by preventing the formation of acidic conditions. In addition, the buffer resulted in an increased, initial Pt(IV) to Pt(II) reduction rate in all samples. This in turn generated particles that not only decreased in size in relation to this increased reduction rate, but also exhibited drastically altered morphologies when compared to those particles

produced in water. These results suggest that the buffer salts have a morphological effect on the particles size, either a) directly; by binding to various facets of the growing crystal or b) indirectly; by increasing the rate of reduction of the platinum ions by creating optimal conditions for the increased activity of the unknown Pt(IV) reductase, identified in Chapter 3.

Table 4.1 illustrates the general trend of decreasing nanoparticle size in relation to an increasing Pt(IV) concentration, hence increased reduction rate. The direction of the arrows indicates increasing average particle size. This correlates to trends observed during chemical synthesis of metal nanoparticles where a more rapid reduction rate results in smaller particles and vice versa, as previously discussed in section 4.1. It should be noted here that there is no size distribution for the 3 mM sample in water due to the formation of non-crystalline, amorphous deposits.

**Table 4.1:** Comparison of the size distributions for various samples.

Pt(IV) (mM)	Size distribution (nm)	
	ddH <sub>2</sub> O	SBC
0.35	200-700	50-750
0.5	100-500	100-350
0.75	200-800	100-350
1	50-300	50-350
2	400-1000	150-150
3	N/A – Amorphous deposits	10-80

Due to the effects that the buffer exerts on the particle morphology, and the fact that this mechanism has yet to be elucidated, it was decided for the sake of simplicity, that subsequent investigations would be conducted in water to minimise this complication. The Pt(IV) concentration of 0.75 mM was chosen as it was the highest Pt(IV) concentration that was possible without nanoparticle-protein precipitation occurring.

The results illustrate, that in the absence of the cellular restrictions, both in the presence and absence of a buffer system, biogenic NP's that vary greatly in size and shape, are synthesised via the reductive mechanism elucidated in Chapters 2 and 3.

#### 4.3.4. Investigating the effect of the bioreductive mechanism on Pt(II) reduction

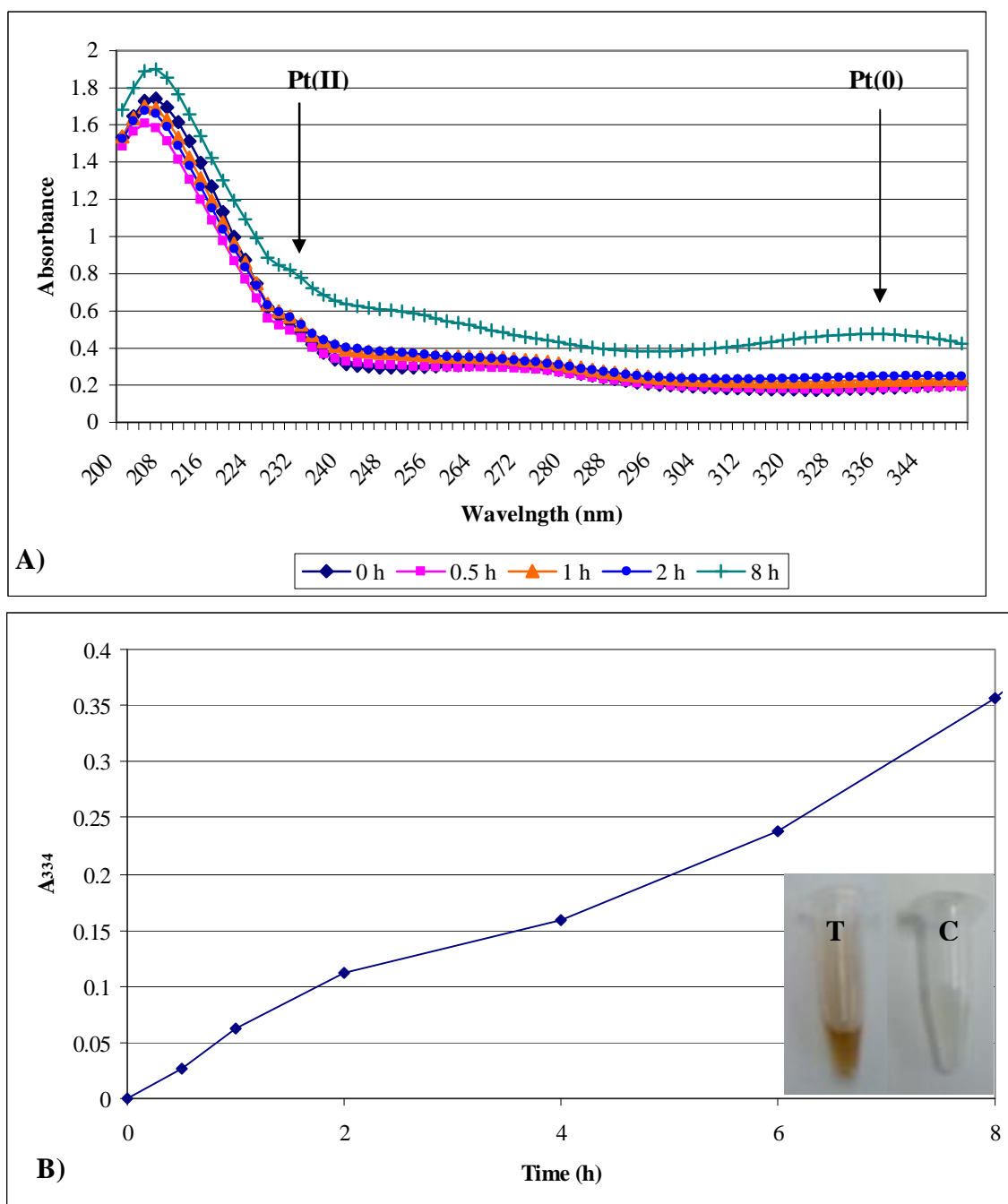


**Figure 4.22:** The bioreduction of the Pt(II) ion by CSE over time. [A) Spectrum scan showing interference from NP spectrum, B) Formation of Pt(0) at 334 nm; Inset – Image of the test sample (T) and control (C) post-bioreduction.]\*

\* All values shows exhibit a standard deviation < 10 %



This experiment was conducted in order to determine whether the two-cycle mechanism of bioreduction from Pt(IV) to Pt(0) via Pt(II) elucidated in Chapters 2 and 3, could be 'short-circuited' through the use of an initial Pt(II) starting ion from  $\text{Na}_2\text{PtCl}_4$  in the presence of CSE. This experiment was conducted in water to avoid the inherent complications arising through the use of a buffer, as demonstrated in the previous section.

The spectrum scan (Fig 4.22 A) illustrates the shifting spectrum of Pt(II) during bioreduction by CSE. The Pt(II) sample at '0 h' clearly lacks the characteristic peak of Pt(IV) at 261 nm, but is seen to exhibit a shoulder at 230 nm indicative of the Pt(II) ion.

As expected, it was not possible to follow the reduction of the Pt(II) ion at 230 nm due to the interference of the NP spectrum that became more and more prevalent over time. Fig 4.22 B, represents the production of Pt(0) NP's as followed spectrophotometrically at 334 nm. The formation of Pt(0) follows a more linear relationship when compared to those produced from the bioreduction of Pt(IV) as the starting ion (Fig 4.3) in water. This indicates that a) the reduction of the Pt(II) ion is inherently slower than that of the Pt(IV) ion and b) the presence of the Pt(IV) ion has an upregulating effect on the formation of Pt(0) from the reduction of the intermediate Pt(II) ion. The formation of a peak at 334 nm is also more pronounced in this sample than has been observed in previous investigations, most likely due to alterations in the particle morphology, overall NP concentration or aggregation. The particle morphology will be investigated further in the following section.

#### 4.3.4.1. TEM analysis

The particles observed in this sample exhibited both geometric and irregular morphologies. In Fig 4.23 A, the particles are shown to be adsorbed to what is assumed to be a protein matrix. These NP's are larger and more geometric in nature, possessing clean, straight edges, compared to those smaller, more irregular particles observed free in solution (Fig 4.23 B). These results suggest that the protein, acting as an adsorbent in this case, is influencing the shape and size of the particles produced.

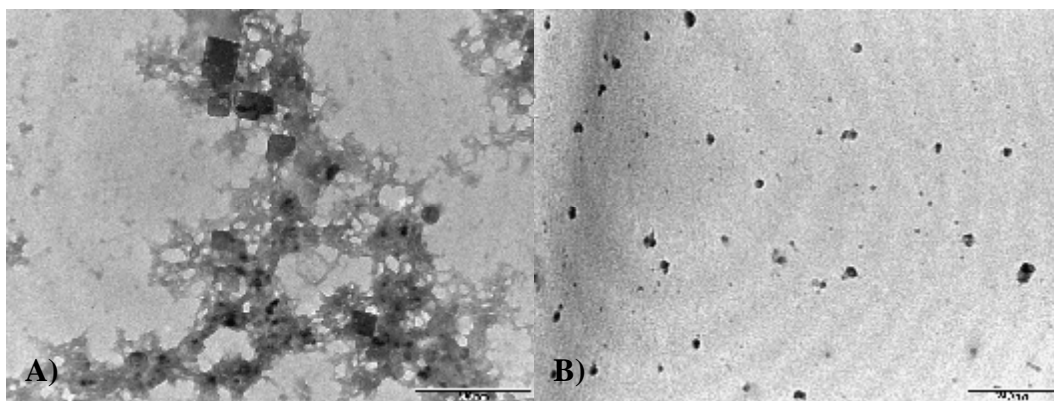


**Figure 4.23:** Examples of particles from the bioreduction of Pt(II) [A) Particles bound to protein matrix, B) Irregular particles free in solution. Scale bar = 500 nm in both cases.]

Similarly, as for the investigations involving Pt(IV), the formation of crystalline NP's were observed when the restrictions imposed by the cell had been eliminated.

#### 4.4 Summary & Conclusions

- Pt(0) is formed from the enzymatic bioreduction of Pt(IV) by CSE
- NP's are stabilised in solution by protein
- Free Pt(0) NP's interfere in the determination of the Pt(IV) and Pt(II) ions
- NP formation can be followed by the change in absorbance at  $A_{334}$
- The absence of the spatial restrictions of the cell allows for the formation of crystalline NP's, exhibiting both irregular and geometric morphologies
- Particles reduce in size with increasing reduction rate and *vice versa*
- SBC results in an increased Pt(IV) reduction rate, and a decrease in particle size by an unknown mechanism
- CSE contains Pt(II) reductase activity, where the Pt(0) formation rate is slower than that of the formation rate from Pt(IV) reduction
- NP's bound to protein exhibit larger, more geometric morphologies than those that remain unbound.

## **CHAPTER FIVE:**

### **Effects of experimental factors on biogenic nanoparticle morphology**

---

---

#### **5.1. Introduction**

Transition metal nanoparticles (NP's) of various shapes and sizes have been shown to be able to catalyse various reactions by lowering the activation energy required for the reaction to proceed. NP's of different morphologies, however, tend to differ in their catalytic activity (El-Sayed, 2001; Narayan & El-Sayed, 2008). Pd(0) and Pt(0) NP's are capable of catalysing the Suzuki reaction, which couples arylboronic acid with aryl-halides to produce biaryls, as well as electron transfer (Narayan & El-Sayed, 2005) and hydrogenation reactions (Nadgeri *et al.*, 2008). Narayan and El-Sayed (2005) determined that the percentage of surface atoms on the corners and edges of Pt(0) and Pd(0) NP's correlated to the degree of catalytic activity of the general colloid. Hence, the catalytic behaviour of metal NP's is due to a high surface-to-volume ratio where a high percentage of the total atoms composing the particle are located on the surface (El-Sayed, 2001). With this in mind, Narayan and El-Sayed (2005), demonstrated that tetrahedral NP's of transition metals, displayed the greatest catalytic activity, followed by spherical NP's, with cubic NP's exhibiting the lowest catalytic potential. These results further substantiated the need for a more accurate control of morphological synthesis.

The requirement for particle stabilisation and shape controlled nanoparticle synthesis has led to the use of numerous 'capping agents' (CA's). These range from the biological to the synthetic and have had a number of positive outcomes with regards to morphology control. Popular synthetic polymers include polyvinylpyrrolidone (PVP) (Ahmadi *et al.*, 1996; Sun & Xia, 2002) and sodium polyacrylate (Lee *et al.*, 2004) while a common biological CA, is bovine serum albumin (BSA) (Mitra & Bhaumik, 2007). The exact

mechanism by which the capping agent controls size and shape is still not fully understood. It has been hypothesised that the CA binds to various crystallographic planes, thereby preventing crystal growth in that direction by inhibiting the addition of atoms on that particular plane (Sun & Xia, 2002). CA's have also been employed to stabilise the particles in solution by steric hindrance, also known as steric stabilisation, thereby preventing particle flocculation (Narayanan & El-Sayed, 2008).

PVP is a neutral polymer that binds to nanoparticles via a "train-loop-tail" model. Certain segments of the polymer are in contact with the particle via hydrophobic interactions (train) while other parts are in-between (loop) and extending into the solution (tail) preventing other particles, which may be attracted by mutual van der Waal's forces, from aggregating together (Chen *et al.*, 1999). PVP as a CA, has a number of advantages, namely; it is metabolically inactive, inert and has excellent stability and complexation properties (LaCount *et al.*, 1997). The major drawback arises from the possibility that by binding to and encapsulating the nanoparticle, PVP, or any other CA for that matter, may result in a reduction of the effective catalytic activity of the colloid by blocking the active sites on the surface of the individual particles (Elechiguerra *et al.*, 2005; Ershov *et al.*, 2006).

Basu and colleagues (2008) investigated the effects of pH and temperature on the morphology of gold NP's in the presence of BSA with ascorbic acid acting as an additional reducing agent. They found that an increase in temperature resulted in a subsequent increase in reduction rate of the Au(III) ion, which in turn resulted in smaller NP's being produced. They stated that by increasing the reduction rate, one is effectively increasing the rate of primary nucleation and slowing the rate of secondary nucleation. Smaller, more irregular particles are formed since fewer ions are available for the second nucleation step, while the reverse is also applicable. Next, they investigated the effect of three different pH's namely pH 3, pH 7 and pH 10 on gold NP morphology by BSA reduction. They found that in the presence of this protein, the reduction of gold ions and subsequent formation of Au(0) nanotriangles only occurred at pH 3. They proposed that at this pH, BSA would be denatured and in a more linear conformation, possibly

exposing a number of disulfide regions, which may be acting as a template for the formation of triangular Au(0) NP's. Hence, a specific protein conformation is necessary before reduction will proceed.

In the case of chloroplatinic acid (CPA) or  $H_2PtCl_6$ , this transition metal complex exists as a number of equilibrium complexes in aqueous solutions. During CPA hydrolysis in aqueous solutions, the chloride ligand is often substituted with either hydroxide (OH<sup>-</sup>), aqua (H<sub>2</sub>O) or a combination of aqua-hydroxide complexes, which can differ in both charge and ligand constitution. The degree of CPA hydrolysis is highly dependant on the pH of the solution since, at low pH, CPA hydrolysis is minimised with maximum coordination of the chloride ligand occurring and formation of aqua-complexes being favoured. At high pH, CPA undergoes extensive hydrolysis with hydroxide-complexes predominating (Spieker *et al.*, 2002; Bel'skaya & Duplyakin, 2007). Variation in pH may therefore also have a secondary role in NP morphology. As enzymatic, bioreductive mechanisms are likely to be dependant on metal-ion-active-site interactions, the dependence of the precursor metal-ion complex on the solution pH, may have a significant effect on the morphology of the resultant particle.

The results in Chapter 4 demonstrated that the crystalline NP's formed, in the absence of the spatial restrictions imposed by the cell, were stabilised by general soluble protein in the CSE. The particles observed, however, exhibited a wide range of shapes with broad size-distributions that is not ideal for a synthetic process.

The objectives of Chapter 5 are to:

- i) Compare and contrast the effects of a synthetic capping agent (i.e. PVP) on the reduction rate of Pt(IV) in SRB cells and a CSE solution.
- ii) Determine the mechanistic and morphological effects of PVP, CSE protein as a biological capping agent, temperature and pH on the bioreductive mechanism and biogenic NP's.
- ii) Determine the hydrogenase ( $H_{ase}$ ) activity of the CSE solution, pre- and post-bioreduction.

## **5.2. Materials & Methods**

### **5.2.1. Materials**

All chemicals were of analytical grade and obtained from Sigma-Aldrich (South Africa) or Merck (South Africa) unless otherwise stated. All gases were obtained from Afrox (South Africa).

### **5.2.2. Methods**

#### *5.2.2.1. Cell harvesting and preparation of SRB cells for experiments*

The SRB cells were cultured and harvested according to the protocol described in Chapter 2.

#### *5.2.2.2. Analysis of platinum ions*

Prior to analysis of whole cell samples by UV-Vis spectroscopy, the aliquot fractions collected during the timed intervals (0, 0.5, 1, 2, 4, 6, 8 h) for each experiment were centrifuged (13 000g, 2 min, RT) to separate the supernatant fractions, which would proceed for further analysis, from the cell pellet. For all samples undergoing spectrophotometric analysis, absorbance readings were taken at 261 nm, 230 nm and 334 nm, as previously described in section 4.2.2.3, to follow the changes in Pt(IV), Pt(II) and Pt(0) respectively.

#### *5.2.2.3. Morphology control*

### **Part A: SRB whole cell investigation**

#### *5.2.2.3.1. Effect of PVP on Pt(IV) reduction by SRB cells*

The experimental set-up consisted of 30 ml Frasco Rescado screw-cap bottles with a final experimental volume of 5 ml consisting of an SRB cell concentration of 19.2 g.L<sup>-1</sup> (wet weight), 1 mM H<sub>2</sub>PtCl<sub>6</sub>, and two different concentrations of PVP (10 000 Da) (20 mg.ml<sup>-1</sup> PVP or 100 mg.ml<sup>-1</sup> PVP) with the final volume made up with Tris-HCl buffer (200 mM, pH 7.6). A number of controls were set up namely; a control including cells but excluding PVP (PVP-free), and two separate cell-free controls including PVP at the two concentrations mentioned above (CF20 and CF100). The investigations were conducted

in the dark, under normal atmospheric conditions with no exogenous electron donor provided. Aliquot fractions (300  $\mu$ l) were collected in triplicate at regular intervals (0, 0.5, 1, 2, 4, 6, 8 h) and kept on ice until further analysis.

### **Part B: Cell-soluble extract (CSE) investigations**

#### *5.2.2.3.2. Effect of PVP on Pt(IV) reduction by the CSE*

The experimental set-up was similar to that described in section 4.2.2.2.1. Prior to experimental set-up and pH adjustment, the CSE solution was incubated on ice for 10 min to slow any enzymatic activity. A total experimental volume of 5 ml, after pH adjustment to 9.0 with 1 M NaOH, consisted of 250  $\mu$ g.ml<sup>-1</sup> protein from the CSE and 0.75 mM H<sub>2</sub>PtCl<sub>6</sub>. Different amounts of PVP were dissolved in two separate experimental solutions to give final concentrations of 20 mg.ml<sup>-1</sup> PVP and 100 mg.ml<sup>-1</sup> PVP respectively. Controls were set-up to include a sample excluding CSE with the CSE volume replaced by ddH<sub>2</sub>O (CSE-free) and a sample including CSE but excluding PVP (PVP-free). '0 h' was taken as the point after pH adjustment while still on ice. The experimental samples were placed in an incubator at 65 °C in the dark, where triplicate aliquots (100  $\mu$ l) were taken at regular intervals and analysed as described in section 4.2.2.3.

#### *5.2.2.3.3. Effect of CSE protein as a biological capping agent*

The experimental conditions were maintained as described in section 5.2.2.3.2, with the exception of various CSE protein concentrations (50, 250 and 500  $\mu$ g.ml<sup>-1</sup>) being challenged with a 0.75 mM H<sub>2</sub>PtCl<sub>6</sub> solution at a starting pH of 9.0 in the dark at 65 °C. Samples were collected and analysed as described in section 5.2.2.3.2.

#### *5.2.2.3.4. Effect of temperature*

The experimental set-up was identical to that described in section 5.2.2.3.2 with the exception of the experimental samples being incubated at fixed temperatures (25, 45 and 65 °C). CSE-free controls were set-up, and samples were collected and analysed as previously mentioned in section 5.2.2.3.2.

#### *5.2.2.3.5. Effect of pH*

The experimental set-up was identical to that described in section 5.2.2.3.2 with the exception of the experimental samples being incubated at various starting pH's (7.6, 9.0 and 11.0). CSE-free controls were set-up, and samples were collected and analysed as previously mentioned in section 5.2.2.3.2.

#### *5.2.2.4. Investigating the hydrogenase activity of the CSE*

The hydrogenase activity of the CSE solution was determined by modification of the protocol described in section 3.2.2.4. Three different samples were assayed for hydrogenase activity; first, a CSE sample, prior bioreduction, that had been pre-activated under H<sub>2</sub> for 1 h (CSE + H<sub>2</sub>), second a CSE sample, prior bioreduction, that had not been pre-activated under H<sub>2</sub> but rather kept under N<sub>2</sub> for 1 h (CSE + N<sub>2</sub>), and third a CSE sample, post bioreduction of Pt(IV), that had not been pre-activated by H<sub>2</sub> but rather kept under N<sub>2</sub> for 1 h (CSE/Pt + N<sub>2</sub>). Methyl viologen (MV) was pre-activated by bubbling with H<sub>2</sub> for 15 min. In a 1cm quartz cuvette, with H<sub>2</sub> added to the headspace for the duration of the assay, 100 µl of a 500 µg.ml<sup>-1</sup> protein solution from one of the CSE samples described above was added to 2500 µl of pre-activated MV to give a final protein concentration of 19.23 µg.ml<sup>-1</sup> in 2600 µl. The change in absorbance at 604 nm was measured over time at 15 sec intervals.

#### *5.2.2.5. TEM analysis*

Whole cells and CSE samples were prepared and visualised as described in Chapter 2 and Chapter 4 respectively.

#### *5.2.2.6. SEM-EDAX analysis*

Whole cells and CSE samples were prepared and analysed for Pt(0) as described in Chapter 2 and Chapter 4 respectively.



### 5.3. Results & Discussion

#### 5.3.1. Morphology control

##### Part A: SRB whole cell investigations

##### 5.3.1.1. Effect of PVP on Pt(IV) reduction by SRB cells

The cell-free control samples (Fig 5.1 CF20 & CF100) indicate a level of instability of the Pt(IV) ion due to the presence of PVP, however the rate of reduction in the other samples containing cells is far more rapid in all cases, indicating that the majority of Pt(IV) reduction is due to the presence of the viable SRB cells.

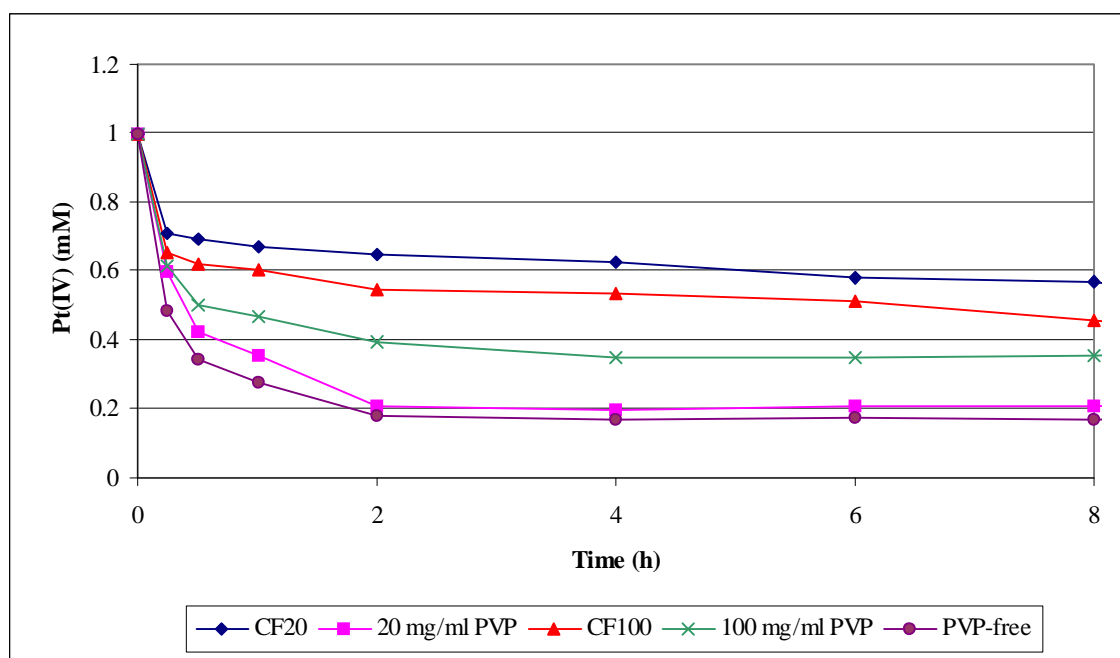


**Figure 5.1:** Effect of PVP on the reduction rate by SRB cells \*

In the case of the PVP-free control, the reduction of Pt(IV) occurs more rapidly between 0-2 h than in the samples containing PVP (Fig 5.1). After this time, no significant change was observed. The concentration of Pt(IV) decreased over 0-2 h for all samples, with the sample containing the highest PVP concentration (100 mg.ml<sup>-1</sup> PVP) exhibiting the lowest reduction rate and the PVP-free control exhibiting the highest reduction rate. These results illustrate that the addition of PVP to the experimental solution appears to compromise the reduction of Pt(IV).

\* All values shown exhibit a standard deviation < 10 %

Throughout the reduction reaction, the cells began exhibiting a colour change to brown, indicative of Pt(0) formation. It is interesting to note that the initial reduction period between 0-0.5 h, is roughly identical for both the 20 mg.ml<sup>-1</sup> PVP and the 100 mg.ml<sup>-1</sup> PVP samples, resulting in ~40 % Pt(IV) reduction. The PVP-free sample, however exhibited a ~52 % reduction in the Pt(IV) ion, a 12 % increase over the same time period. The initial drop (0-0.5 h) in Pt(IV) concentration is due to either passive biosorption or active uptake by the biomass.

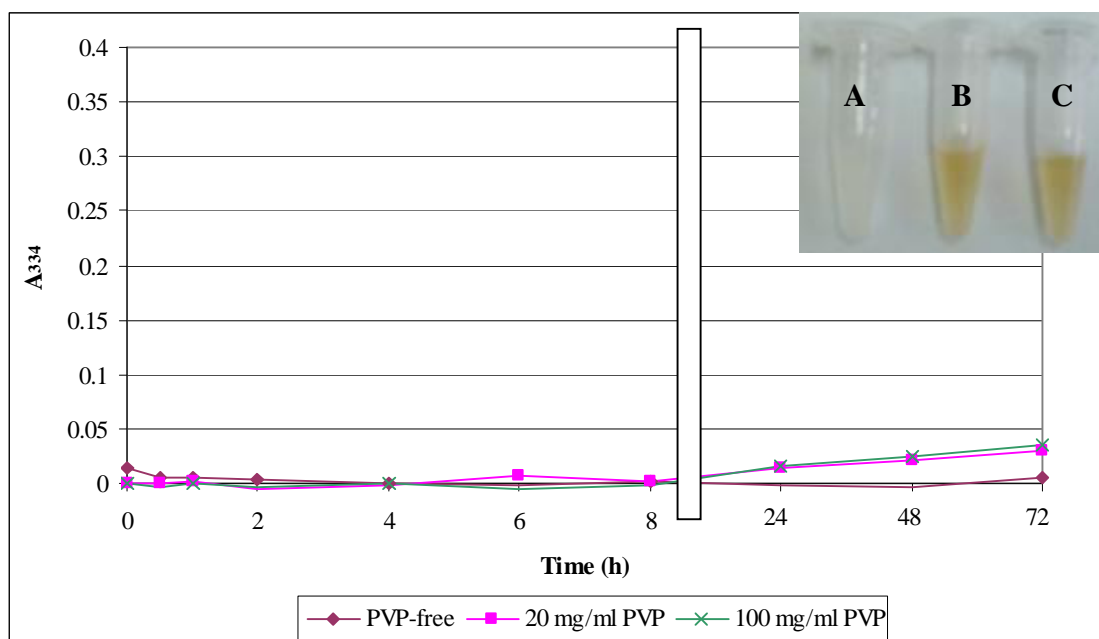


**Figure 5.2:** Formation of Pt(0) NP's in the extracellular solution, in the presence of SRB cells, challenged with Pt(IV) in the presence of PVP [Inset: Supernatant of samples post bioreduction A) PVP-free, B) 20 mg.ml<sup>-1</sup> PVP, C) 100 mg.ml<sup>-1</sup> PVP.]\*

The results suggest that either; a) PVP becomes adsorbed to the external areas of the cell wall, thereby blocking the sites upon which biosorption may occur, hence a sample with a higher PVP concentration would have a lower initial drop in Pt(IV) and *vice versa*, and/or b) that since PVP lowers the potential for passive biosorption by binding to the outer cell wall, it may, for the same reason, have a similar effect on the active uptake of Pt(IV) by blocking the uptake pores, resulting in the inverse relationship of reduction rate to PVP concentration observed in Fig 5.1.

\* All values shown exhibit a standard deviation < 10 %

Over the 8 h period, the colour of the cells darkened from pale yellow to brown, indicating the deposition of Pt(0) within/on the cells. Approximately 16 h post bioreduction (24 h), a visual observation was made in the whole cell samples incubated in various PVP concentrations. The colour of the supernatant, separated from the cell pellet of the various cell fractions collected throughout the investigation, began exhibiting a colour change to light-brown (Fig 5.2 Inset). This colour change was not observed in the PVP-free control, nor had it been observed in any of the prior investigations in Chapter 2 or 3. The presence of the brown colour, as mentioned before is a clear indicator of Pt(0) NP formation in aqueous solution, and is substantiated by the increase in  $A_{334}$  in Fig 5.2 after 24 h. This suggests that the presence of PVP is either; a) resulting in the stabilisation of an extracellular protein with Pt(IV) reductase activity, or b) preventing the binding of the NP's to the cells, which results in their passive diffusion or active transport out of the cell, into the extracellular environment. To confirm this, further investigations are required. LaCount and colleagues (1997) demonstrated that genetically manipulated cells of *Nicotinana tabacum* in the presence of PVP, resulted in a 35-fold increase in the concentration of a previously unstable, extracellular heavy-chain monoclonal antibody (HC MAb) while the intracellular concentration remained unchanged. This proved that PVP was capable of stabilising and thereby increasing the production of a protein from a cellular origin.

#### 5.3.1.2. TEM and SEM-EDAX analysis of SRB cells

##### 5.3.1.2.1. Control experiment: PVP-free

- See Chapter 3, section 3.3.4.1.2.

##### 5.3.1.2.2. SRB cells with $20 \text{ mg.ml}^{-1}$ PVP

The supernatant isolated from this sample at 24 h exhibited a light brown colour indicating a low concentration of NP's in this extracellular solution. This was supported by the TEM images (Fig 5.3  $A_{1+2}$ ) illustrating the electron dense regions within the periplasmic area of the cells. The Pt(0) deposits exhibited a more structured, plate-like morphology unlike the amorphous deposits observed in the PVP-free control experiment, (section 3.3.4.1.2). In addition, there appears to be a lower concentration of Pt(0)

depicted by the lighter grey colouration of the deposits in the TEM image, indicating thinner regions of electron density. Although the EDAX spectrum (Fig 5.3 B) for this sample is non-quantitative, it does appear to suggest the presence of lower Pt(0) concentrations than were previously observed in the PVP-free control (section 3.3.4.1.2). This demonstrates that PVP, effectively slows the bioreductive mechanism thereby affecting Pt(0) crystal growth.

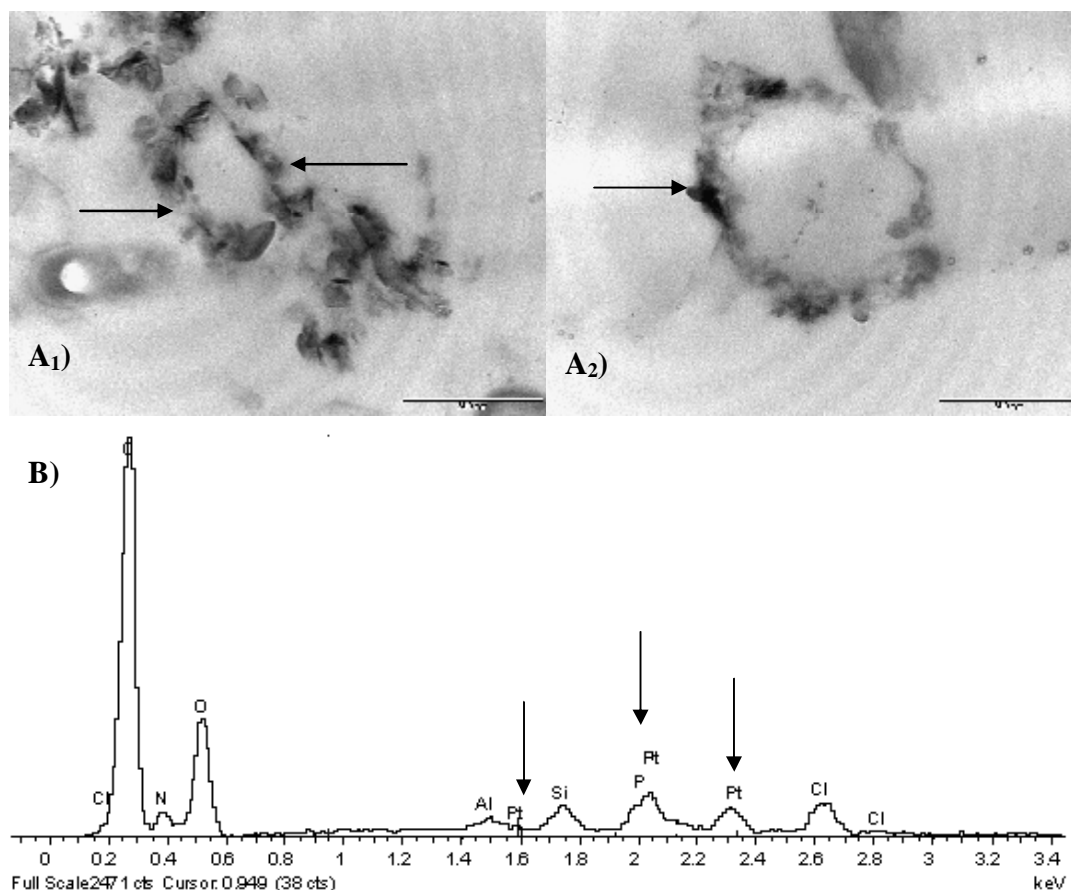


**Figure 5.3:** SRB cells challenged with Pt(IV) in the presence of 20 mg.ml<sup>-1</sup> PVP [A<sub>1+2</sub>) TEM images of cells with plate-like platinum deposits in the periplasmic space. Scale bars = 500 nm in both cases. B) Small platinum peaks on the EDAX graph suggest low amounts of Pt(0) present.]

#### 5.3.1.2.3. SRB cells with 100 mg.ml<sup>-1</sup> PVP

The supernatant of this sample after 24 h, exhibited a slightly darker brown colour than that of the sample containing 20 mg.ml<sup>-1</sup> PVP. This indicates that a higher concentration of NP's, are present in the extracellular solution of this sample. When comparing the

TEM images of the 20 mg.ml<sup>-1</sup> and 100 mg.ml<sup>-1</sup> PVP samples (Fig 5.3 A<sub>1+2</sub> and Fig 5.4 A<sub>1+2</sub>) to the control (Fig 3.6 A), it was observed that after 24 h, the cells in the PVP samples exhibited a much lower concentration of electron dense metal deposits within the periplasm, than were observed in the PVP-free sample (section 3.3.4.1.2), with the majority of the Pt(0) located extracellularly, with increasing PVP concentration. This suggestion is supported by the unexpectedly low Pt(0) peaks observed in the EDAX spectrum for both samples containing PVP (Fig 5.3 B & 5.4 B).

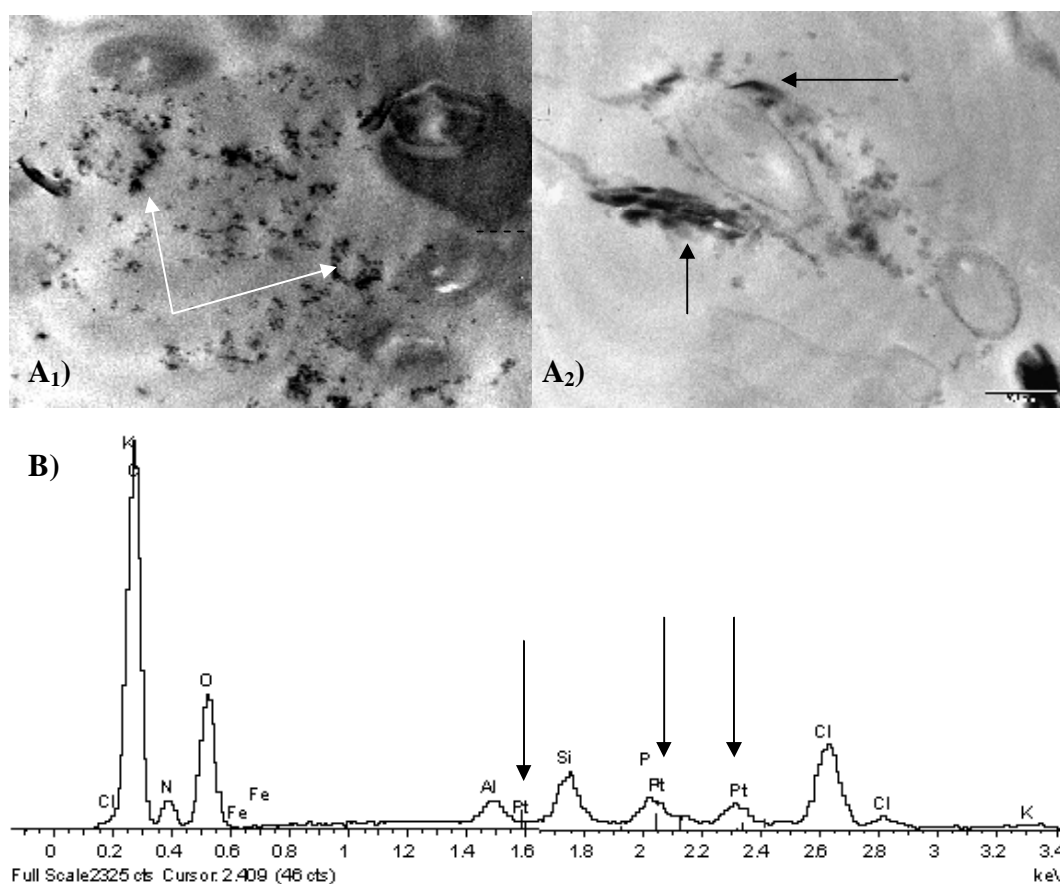


**Figure 5.4:** SRB cells challenged with Pt(IV) in the presence of 100 mg.ml<sup>-1</sup> PVP [A<sub>1</sub>] TEM images of samples with extracellular platinum deposits, and A<sub>2</sub>) Cells with a low concentration of platinum deposits in the periplasmic space. Scale bars = 500 nm in both cases. B) Small platinum peaks on the EDAX graph suggest low amounts of Pt(0) present.]

These results suggested that the higher PVP concentration not only resulted in further inhibition of the reduction mechanism, but had also prevented the particles from binding to the cells. To summarise, NP's were produced via the nucleation of Pt(0) atoms

synthesised by the two-cycle mechanism of Pt(IV) bioreduction elucidated in Chapters 2 and 3. They were however, unable to bind to the cell in the presence of PVP, resulting in the NP's becoming exported - either passively/actively - to the external milieu, which in turn resulted in the visual colour change of the supernatant from pale-yellow to brown.

### *5.3.1.3. TEM analysis of SRB cell supernatants in the presence of PVP*

#### *5.3.1.3.1. Supernatant of 20 mg.ml<sup>-1</sup> PVP*

An attempt was made to visualise the free NP's in the supernatant solution as had previously been completed in Chapter 4 for the CSE investigations. In the 20 mg.ml<sup>-1</sup> PVP supernatant solution, a most unusual and unexpected phenomenon was observed. It was possible to dynamically observe electron dense NP's forming upon contact of the sample with the electron beam. A number of shapes and sizes were formed, with the majority of the smaller particles being rounded-irregular in shape while the larger particles exhibited more geometric conformations [rectangle, rod, square, triangle]. An example is shown below in Fig 5.5 A.

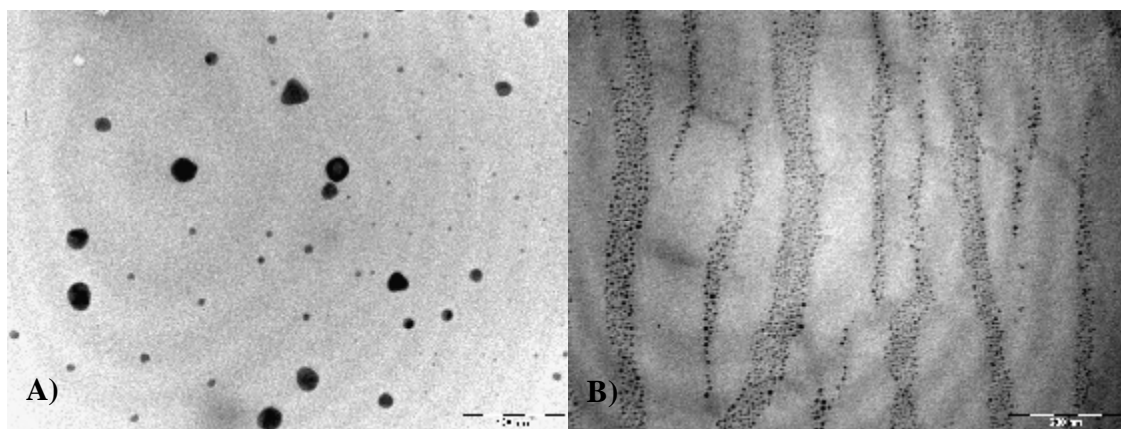


**Figure 5.5:** TEM images of the 20 mg.ml<sup>-1</sup> PVP supernatant solution after 24 h. [A) Image depicting various conformations of NP's formed by irradiation with the TEM electron beam. Scale bar = 100 nm. B) Image illustrating the formation of NP's within grooves of the carbon coated TEM grid. Scale bar = 200 nm.]

This phenomenon only occurred in the presence of a Tris-HCl buffer, and not in water or a sodium-bicarbonate buffer as investigated in Chapter 4. Since Tris [2-Amino-2(hydroxymethyl)-1,3-propanediol] contains an amine and hydroxyl groups, it is likely

that it will bind with metal-ions and thereby form buffer-metal complexes, which in turn may lead to experimental results dependant on the said buffer (Fischer *et al.*, 1979). This suggests that a Tris-Pt complex with a high reduction potential may have formed that became reduced to elemental Pt(0) upon contact with the electron beam from the TEM. This suggestion was further supported by the visual evidence that illustrates NP's forming within grooves on the carbon coating of the TEM grid, where the platinum salt solution would have pooled when wet and hence dried at a higher concentration (Fig 5.5 B). It may also be possible that very small NP's (< 5 nm) are present that could not be visualised, due to the limitations of the TEM equipment used. Upon contact with the electron beam, these small particles may have become excited, resulting in particle growth by Ostwald ripening, though this could only have been confirmed with further investigation. With extended irradiation times, the as-formed particles migrated towards each other and coalesced or sintered into larger particles.

A similar situation was previously reported by Ito *et al.* (1999) and Li *et al.* (2005) who observed the dynamic formation of copper and silver oxide NP's respectively, and subsequent particle sintering by electron beam irradiation in a TEM. Ito and colleagues (1999) stated that this particular mechanism of particle growth was not attributable to Ostwald ripening, but rather due to the induction of an electrical field within the electron microscope. In some cases, under extended irradiation by the beam, the particles collapsed and dissipated, leaving behind an imprint in the carbon coating. An example is illustrated in Fig 5.6 A-D, which illustrates the effect of electron beam irradiation on a rectangular particle over 60 sec. The particle begins as electron dense, upon irradiation by the electron beam smaller particles are generated that grow out of the larger rectangular particle. The large particle, in turn becomes less electron dense as the atoms diffuse outwards forming the smaller particles. Eventually, the large rectangular particle, and the smaller particles begin to collapse upon themselves as dissipation continues, leaving an imprint in the carbon coating where the original particle was once supported. Tanaka *et al.* (2002), stated that when the energy from the electron beam, exceeds that of the cohesion energy of a particle, the particle diffuses out, essentially collapsing. The cohesion energy of a substance may be roughly estimated by the melting point of the

element involved. This suggests that the structural changes observed may have been due to heat generated by the TEM beam especially since the operating voltage was below 100 kV.<sup>1</sup>

The TEM is a vital tool for the study of nanoparticle morphology and aggregation. As a technique however, it possesses a number of drawbacks. In order to visualise the particles, the basic principle requires the interaction of electrons from the electron beam with the NP's in the sample.

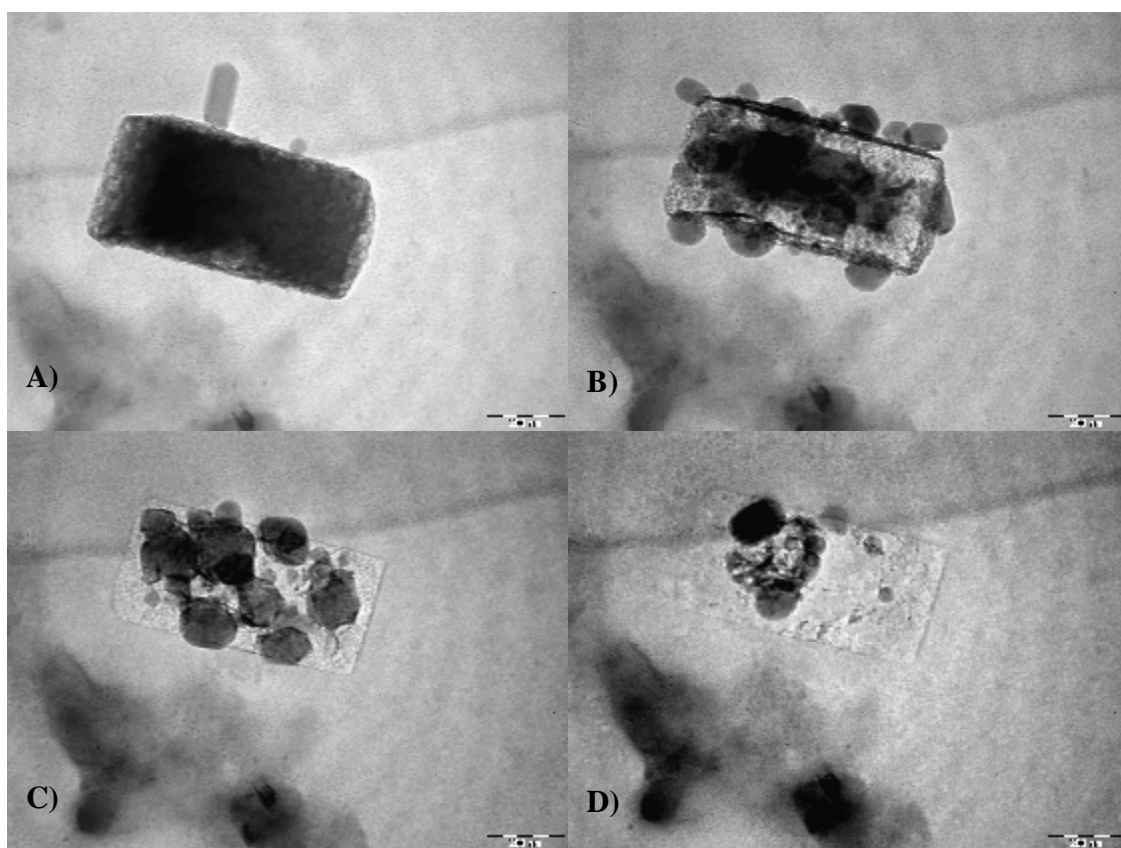


**Figure 5.6:** Sequence of TEM images illustrating the dissipation and collapse of a rectangular NP after 60 sec irradiation under the TEM electron beam. [A) 0 sec, B) 20 sec, C) 40 sec D) 60 sec. Scale bar = 200 nm in all cases.]

This interaction often results in structural and molecular changes (Tanaka *et al.*, 2002) of the particles that are being studied, skewing the visual results. The exact mechanism by

---

<sup>1</sup> Private communication with Mintek, South Africa



which this phenomenon occurs is still unknown, however, a number of theories are up for debate attempting to explain these structural fluctuations, such as heating of the sample by the electron beam; electron knock-on or Coulomb explosion (Klimenkov *et al.*, 2001; Tanaka *et al.*, 2002; Braidy *et al.*, 2008).

#### *5.3.1.3.2. Supernatant 100 mg.ml<sup>-1</sup> PVP*

The phenomenon of dynamic NP formation due to irradiation by the electron beam, mentioned in section 5.3.1.3.1 for the 20 mg.ml<sup>-1</sup> PVP sample, did not occur with the 100 mg.ml<sup>-1</sup> PVP sample. It is proposed that the higher PVP concentration (5-fold increase) is capping the smaller particles - whose presence was suggested in the previous section - but cannot, due to limitations of the magnification of the current TEM equipment, be visualised. The capping agent thereby prevents growth induced by the electron beam, resulting in NP's that are too small to observe.

### **Part B: Cell-soluble extract (CSE) investigations**

#### *5.3.1.4. Effect of PVP on the Pt(IV) bioreductive mechanism of CSE*

Between 0-0.5 h, the reduction of the Pt(IV) ion followed the expected trend for both PVP samples (Fig 5.7). The subsequent formation of Pt(0) NP's in solution began interfering with the determination of this ion at 261 nm, between 0.5-8 h. This interference gave the appearance of an increasing Pt(IV) concentration during this period, as previously observed in Chapter 4. The spectrum scan of the 100 mg.ml<sup>-1</sup> PVP sample at 0, 0.5 and 8 h, from 200-350 nm clearly shows the increasing interference at 261 nm, caused by the formation of the wide UV-Vis spectrum of Pt(0) NP's (Fig 5.7, inset). The NP spectrum is caused by the surface plasmon absorption resulting from the oscillation of free electrons on the particle's surface. This in turn, results in the different colours observed for colloidal metal nanoparticles in aqueous solutions (El-Sayed, 2001).

A colour change from yellow to brown was also observed in both these samples indicating the formation of Pt(0) NP's and is illustrated in the images of the samples post bioreduction (Fig 5.8 - Inset). These results are substantiated by the absorbance results in Fig 5.8, illustrating the change in absorbance of this sample at 334 nm over 8 h.

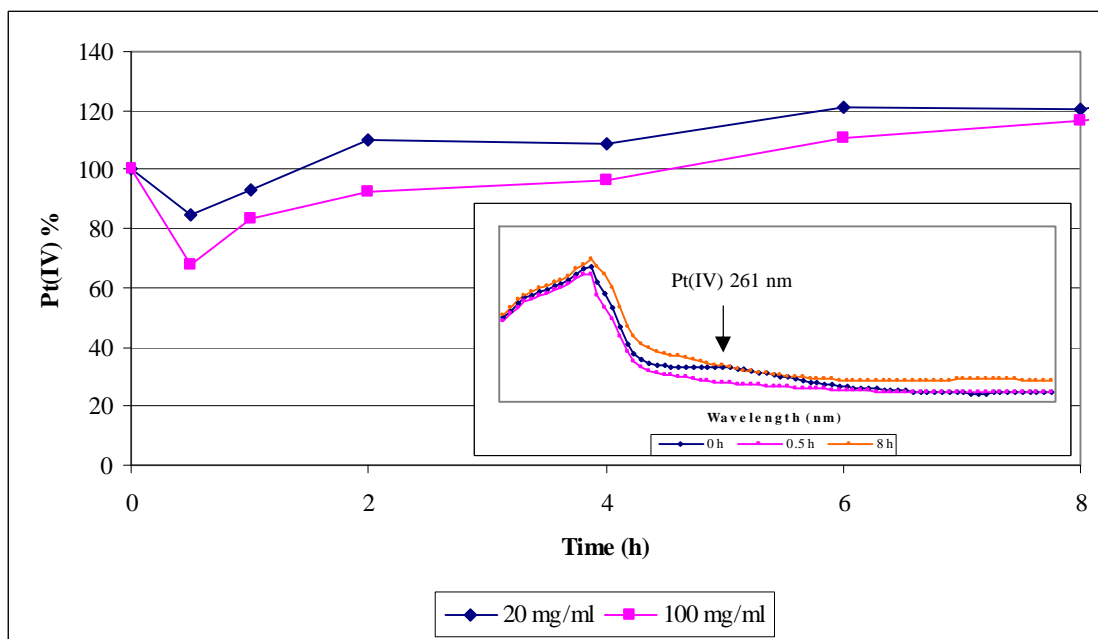


**Figure 5.7:** Interference of Pt(0) NP's in the determination of the Pt(IV) ion. [Inset: Spectrum scan showing formation of NP spectrum interfering with determination of Pt(IV) ion at 261 nm. Blue line) 0 h, Pink line) 0.5 h, Orange line) 8 h.]\*

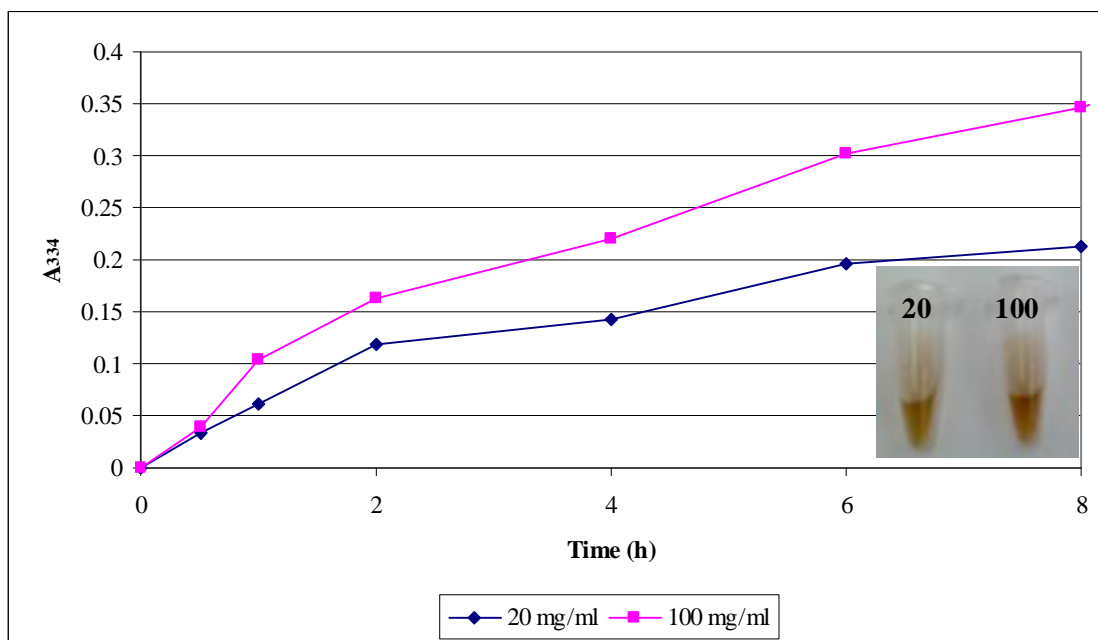


**Figure 5.8:** Bioreduction of Pt(IV) and NP formation by CSE in the presence of PVP. [Inset: Image of 20 mg.ml<sup>-1</sup> PVP sample and 100 mg.ml<sup>-1</sup> PVP sample post bioreduction.]\*

\* All values shown exhibit a standard deviation < 10 %

This wavelength was chosen as a non-quantitative indicator of Pt(0) NP formation over time, as described previously in section 4.3.1.2. The absorbance increased over time indicating the formation of NP's free in solution for both samples. A greater rate of change in absorbance was observed in the 100 mg.ml<sup>-1</sup> PVP sample than the 20 mg.ml<sup>-1</sup> sample at 334 nm indicating that a greater concentration of NP's had formed with the 100 mg.ml<sup>-1</sup> PVP sample. This correlated to the fact that a higher concentration of PVP, or any capping agent, would result in a higher concentration of smaller NP's and was further substantiated by the greater degree of colour change exhibited by the 100 mg.ml<sup>-1</sup> PVP sample.

### 5.3.1.5. Effect of crude CSE protein as a biological capping agent

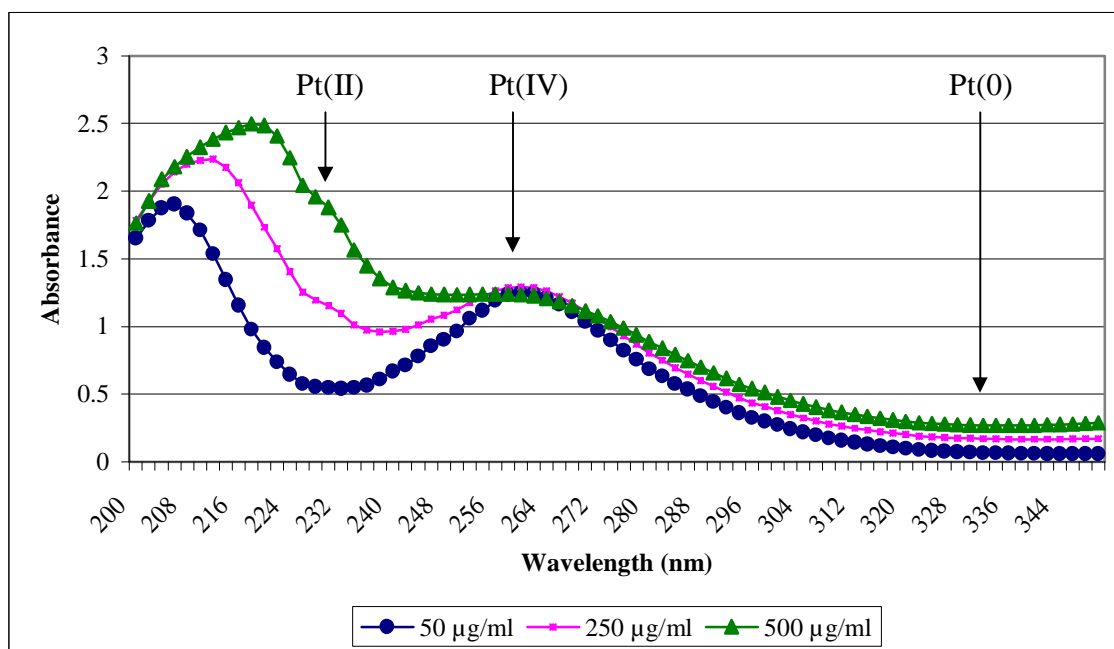


**Figure 5.9:** Initial spectra at 0 h, for various CSE concentrations.

The effect of an increasing protein concentration on the spectrum scan of a 0.75 mM Pt(IV) solution at 0 h is illustrated (Fig 5.9). It is clear that the amount of protein present has no effect on the absorbance at 261 nm, for Pt(IV) determinations, though there is an increasing trend in absorbance around 334 nm, which is used as a non-quantitative indicator of Pt NP's. Hence, for the 334 nm graphs, the values are always normalised (i.e. initial absorbance at 0 h, is subtracted from all subsequent absorbances) to remove this

effect. Similarly, the protein concentration has a drastic effect on the determination of the Pt(II) ion at 230 nm, which made it impossible to accurately gauge the concentration of this ion since it not only increases in concentration over time, but also decreases during reduction of Pt(II) to Pt(0).

The Pt(IV) results for the 250  $\mu\text{g}\cdot\text{ml}^{-1}$  and 500  $\mu\text{g}\cdot\text{ml}^{-1}$  CSE sample (Fig 5.10 A), correlated to those observed previously for CSE investigations in the presence (section 5.3.1.4) and absence of PVP (section 4.3.1.2). The Pt(IV) ion for both these samples, exhibited an initial drop in concentration (0-1 h) that subsequently appeared to increase over the remaining time period. This false increase in Pt(IV) concentration was determined, in Chapter 4 and section 5.3.1.4, to be the result of the Pt(0) NP spectrum, which develops in relation to particle concentration. As the NP concentration increases, so does the UV-Vis interference of the NP spectrum on the determination of the Pt(IV) ion at 261 nm. The samples also exhibited a colour change to brown which correlated to the increase in absorbance at 334 nm (Fig 5.10 B), both of which are indicators of Pt(0) NP formation in aqueous solution.

For the 250  $\mu\text{g}\cdot\text{ml}^{-1}$  and 500  $\mu\text{g}\cdot\text{ml}^{-1}$  samples, the first evidence of NP formation occurred between 0-1 h where an increase in  $A_{334}$  was observed. In contrast to these results, the 50  $\mu\text{g}\cdot\text{ml}^{-1}$  sample, exhibited a decrease in Pt(IV) concentration (similar to that observed in section 4.3.2.2; Pt(IV) concentration  $\geq 1$  mM in water) over time and this trend continued up to 8 h where the Pt(IV) concentration appeared to stabilise at approximately 35 %. Since no precipitate was observed, these results suggested that the NP's were forming in lower concentration and at a much slower rate. The first significant evidence of NP formation, in this sample, occurred between 0.5-2 h, where an increase in  $A_{334}$  was observed (Fig 5.10 B). Very little change in absorbance at  $A_{334}$  was observed after this period, possibly due to the low protein concentration and prior incubation on ice inhibiting further bioreduction.

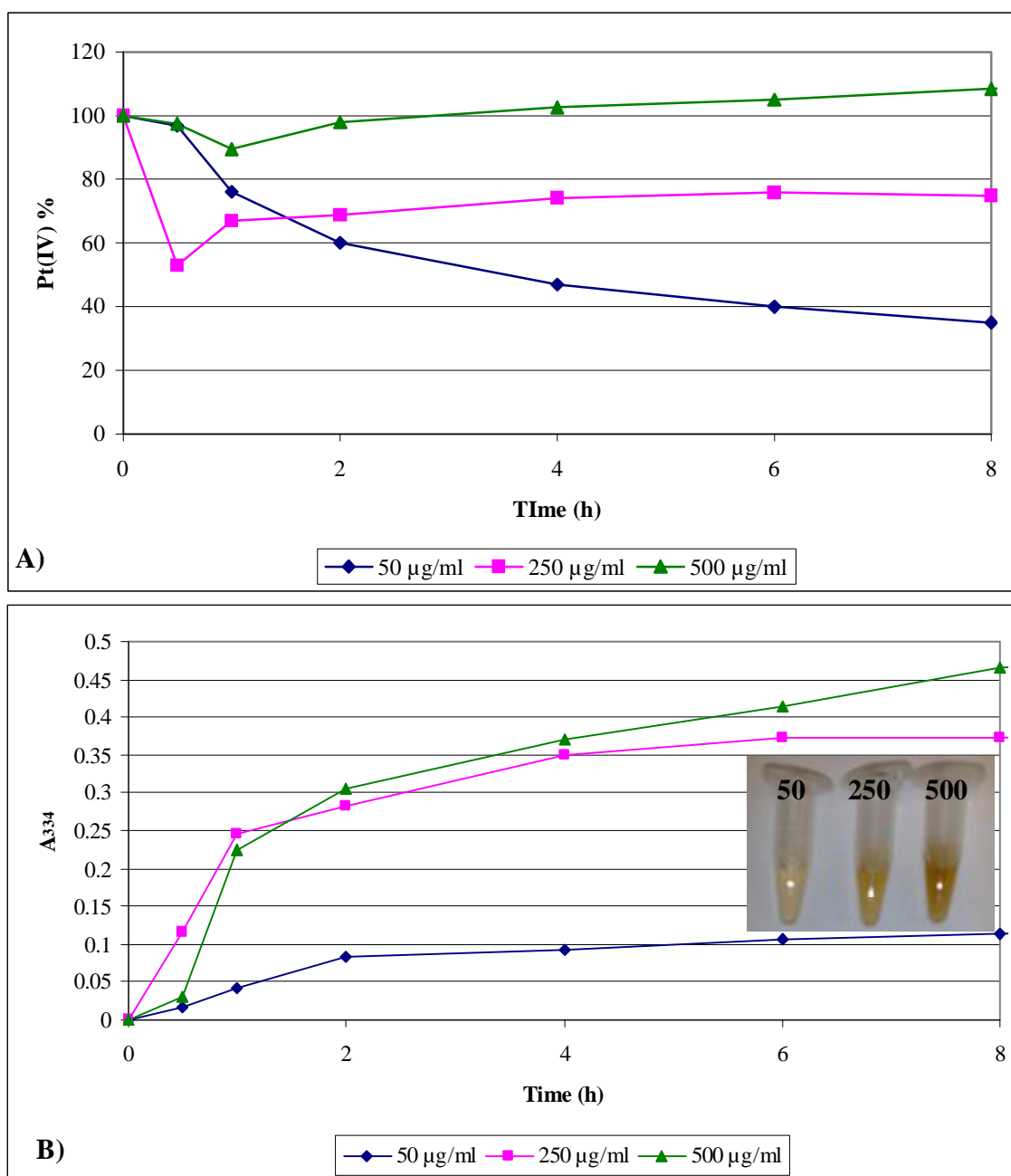


**Figure 5.10:** Bioreduction of Pt(IV) in the presence of varying CSE protein concentration. **A)** Pt(IV) reduction and interference by Pt(0) NP's. **B)** Formation of Pt(0) NP's over time. **Inset:** 50 µg.ml<sup>-1</sup>, 250 µg.ml<sup>-1</sup>, 500 µg.ml<sup>-1</sup> post bioreduction.]\*

These results were all supported by the visual evidence illustrated in the images (Fig 5.10 B – Inset) that depicts the samples under varying degrees of colour change to brown.

\* All values exhibit a standard deviation of < 10 %

After bioreduction, the 50  $\mu\text{g}\cdot\text{ml}^{-1}$  sample exhibited the least significant colour change while the 500  $\mu\text{g}\cdot\text{ml}^{-1}$  sample exhibited the greatest colour change to brown. This may simply be explained by a higher CSE protein concentration resulting in a more rapid rate of NP formation, which in turn would effectively increase the NP concentration. These results followed the expected trend as an increase in general protein concentration would effectively increase the concentration of the specific enzymes involved [i.e. Pt(IV) reductase; hydrogenase] in this mechanism which subsequently would result in an increase in reduction rate.

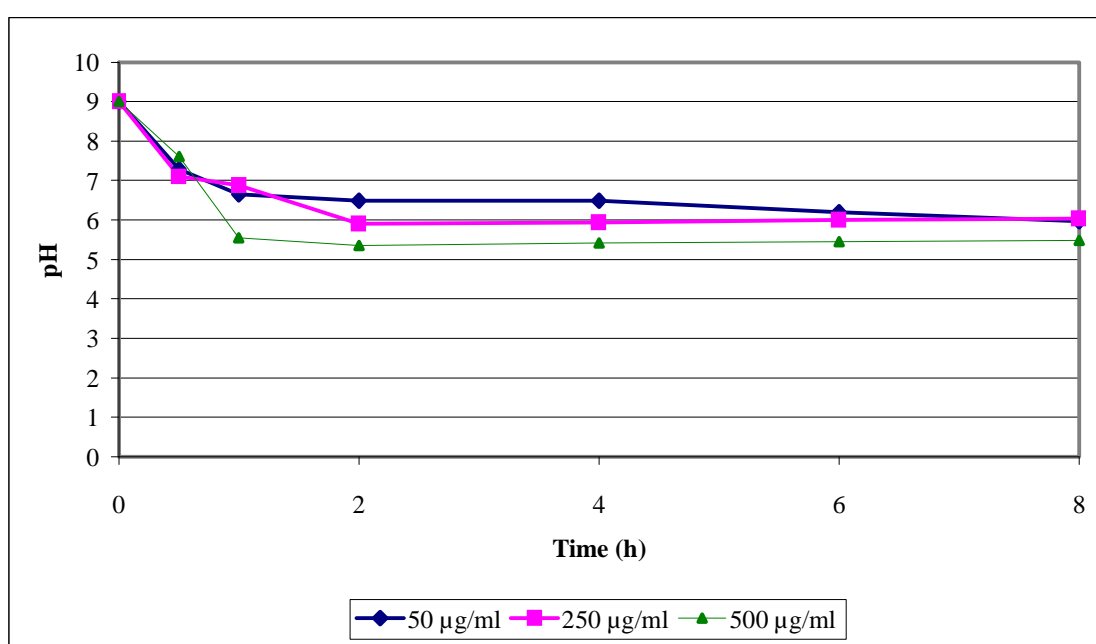


**Figure 5.11:** Change in pH over time.\*

As expected, the starting pH (Fig 5.11) for all samples was 9.0 but decreases considerably over the first 0-2 h for all samples. The greater the reduction rate, the more rapid the release of HCl into solution will be (section 2.3.2.2), resulting in a greater drop in pH. Hence, the 500  $\mu\text{g}\cdot\text{ml}^{-1}$  sample exhibited the greatest decrease in pH and vice versa for the 50  $\mu\text{g}\cdot\text{ml}^{-1}$  sample. The pH does not drop below pH 5 in all cases, hence no precipitation of the protein-NP bioconjugates was visually observed in any of these samples.

\* All values exhibit a standard deviation < 10 %.

5.3.1.5.1. *TEM analysis of CSE as a biological capping agent*

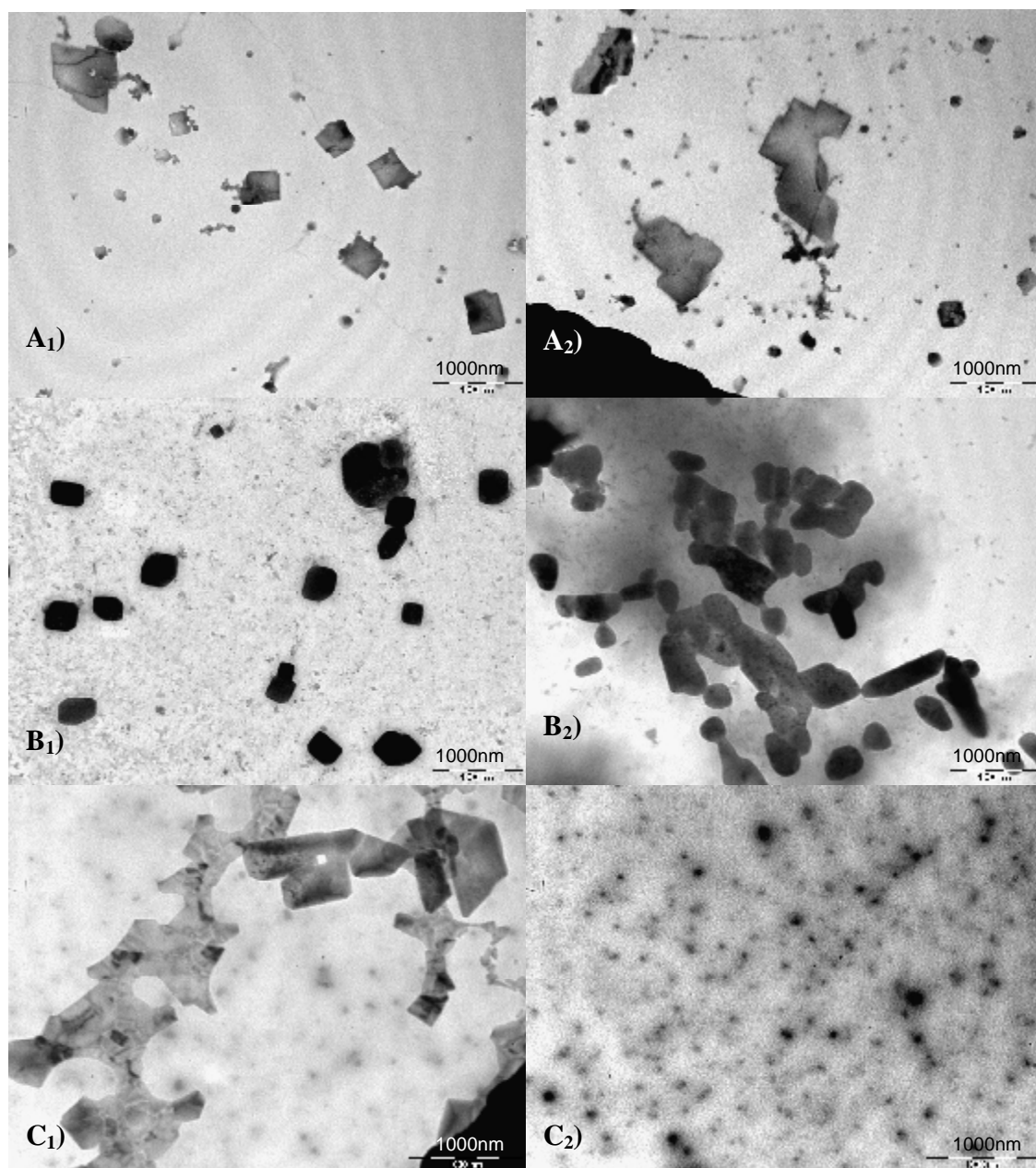


**Figure 5.12:** TEM images of CSE samples. [A<sub>1+2</sub>) 50 µg.ml<sup>-1</sup> CSE protein, B<sub>1+2</sub>) 250 µg.ml<sup>-1</sup> CSE protein, C<sub>1+2</sub>) 500 µg.ml<sup>-1</sup> CSE protein. Scale bar = 1000 nm in all cases.]

The 50 µg.ml<sup>-1</sup> sample (Fig 5.12 A<sub>1+2</sub>) exhibited large particles with geometric shapes such as squares and rectangles in addition to smaller irregular shaped particles. The NP's had clean, straight edges but tended to aggregate together. The smaller irregular particles

appear to be binding to and becoming incorporated by the larger particles. This phenomenon is known as Ostwald ripening and results in particle growth which effectively lowers particle concentration (Lameiras, 1999; Sepulveda-Guzman *et al.*, 2007). The 250  $\mu\text{g}\cdot\text{ml}^{-1}$  sample (Fig 5.12 B<sub>1+2</sub>) produced slightly smaller particles that were more electron dense than those observed in Fig 5.12 A. These NP's were also aggregated, although the individual particles could still be differentiated within the larger aggregate. The 500  $\mu\text{g}\cdot\text{ml}^{-1}$  sample displayed a combination of very small particles of unknown morphology (Fig 5.12 C<sub>1</sub>), due to the restrictions of magnification imposed by the current TEM, and very large aggregates with clean, straight edges indicative of geometric shapes. In some cases, the individual particles could still be identified within the larger aggregate (Fig 5.12 C<sub>2</sub>).

In general, the particle size is seen to have an inverse relationship to the protein concentration of the CSE solution. This may be due to capping effects by the general protein in solution, or may simply be the result of a more rapid reduction rate due to the presence of a higher concentration of specific enzymes. It is therefore difficult to differentiate between the two possibilities without further investigations.

#### *5.3.1.6. Bioreductive mechanism and nanoparticle morphology*

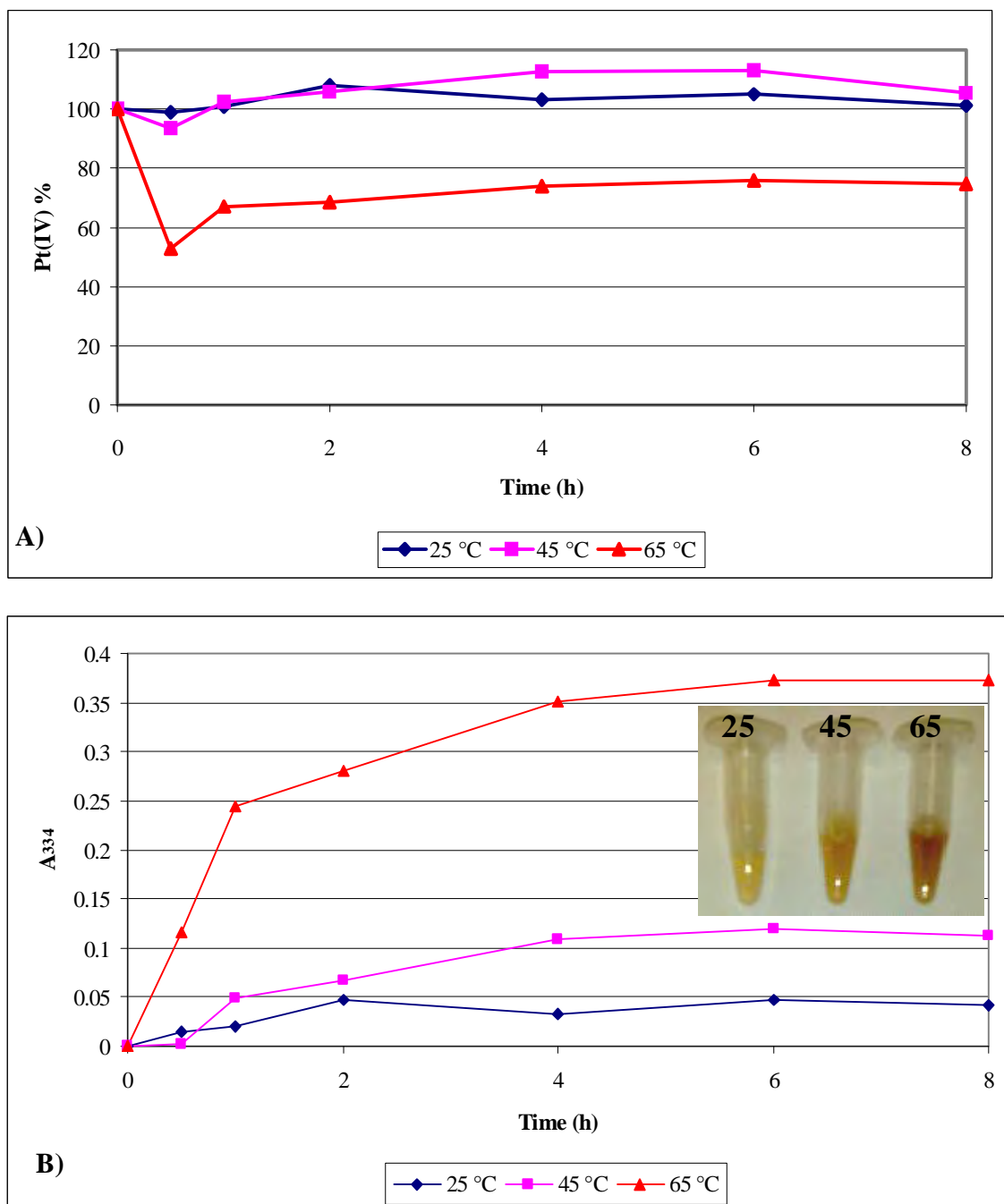
##### *5.3.1.6.1. Effect of temperature*

Fig 5.13 A, demonstrates that the bioreduction of Pt(IV) by CSE was optimal at a temperature of 65 °C. In all cases a decrease in Pt(IV) was observed followed by an apparent increase due to the interference of Pt(0) NP's in solution. The absorbance at A<sub>334</sub> (Fig 5.13 B) of the sample at 65 °C exhibits a far more rapid increase in absorbance at 334 nm, followed by the sample at 45 °C and last, the sample at 25 °C.

In correlation to the A<sub>334</sub> results, the colour change of the samples (Fig 5.13 B Inset) demonstrates that the sample at 65 °C exhibited the most prominent colour change while the sample at 25 °C exhibited the least significant colour change. These results correlate to the work published by Riddin and colleagues (2006) who demonstrated, via a



statistical, surface response methodology, that 65 °C was the optimum temperature for Pt(IV) bioreduction, using a *Fusarium oxysporum* fungal strain.



**Figure 5.13:** Effect of temperature on the bioreductive mechanism. [A) Pt(IV) reduction and interference by NP's. B) Formation of Pt(0) NP's over time. Inset: Images of samples post bioreduction.]\*

\* All values exhibit a standard deviation < 10 %

Since the optimal temperature for hydrogenase activity is 36 °C (Rashamuse & Whiteley, 2007), this further supports the results from Chapter 3, which demonstrated that an unknown Pt(IV) reductase was responsible for Cycle 1 [Pt(IV)  $\rightarrow$  Pt(II)] of the overall bioreductive mechanism of Pt(IV) while a periplasmic hydrogenase was responsible for Cycle 2 [Pt(II)  $\rightarrow$  Pt(0)]. Therefore, at 65 °C, one would expect the hydrogenase activity to be low. It has been demonstrated however, that noble metal NP's such as gold have had the effect of increasing catalytic activity and temperature stability of various enzymes (Mandal *et al.*, 2005). This may explain why Cycle 2 [i.e. Pt(II)  $\rightarrow$  Pt(0)] was not significantly compromised by the high temperature.

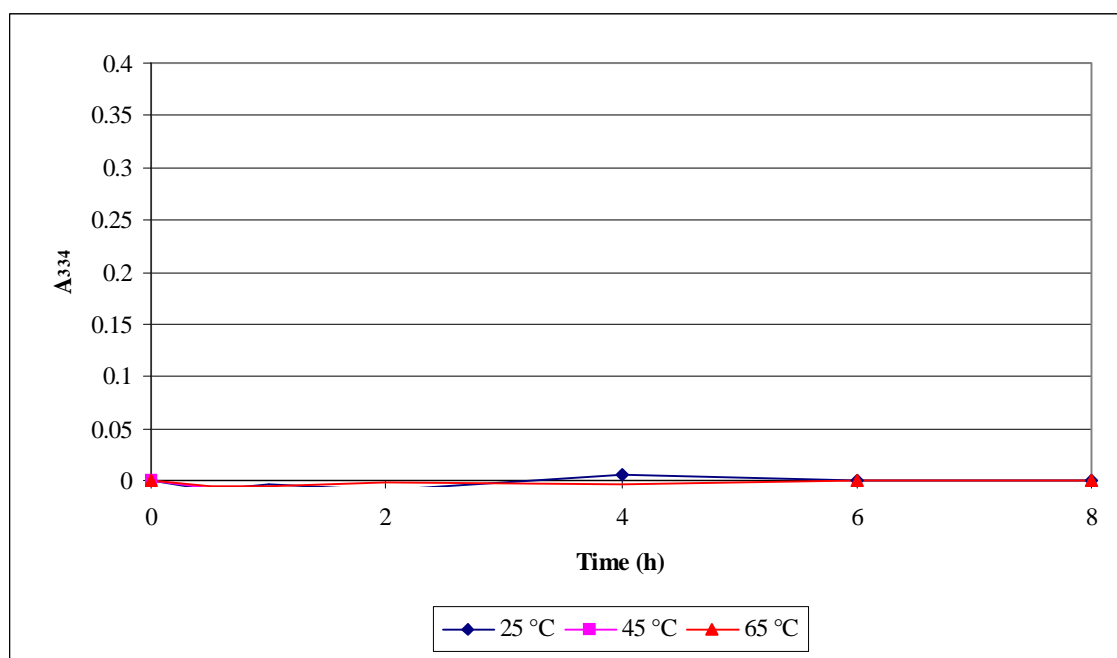


**Figure 5.14:** Change in A<sub>334</sub> of control samples.\*

The results of the control experiments, where the CSE volume was replaced with extra ddH<sub>2</sub>O (Fig 5.14), exhibited no significant change in absorbance for any of the samples. This supported the fact that the production of Pt(0) NP's is an active, enzymatic process – as determined in Chapters 3 and 4, and not merely due to experimental, or other abiotic conditions.

\* All values exhibit a standard deviation < 10 %

5.3.1.6.2. TEM analysis of temperature samples

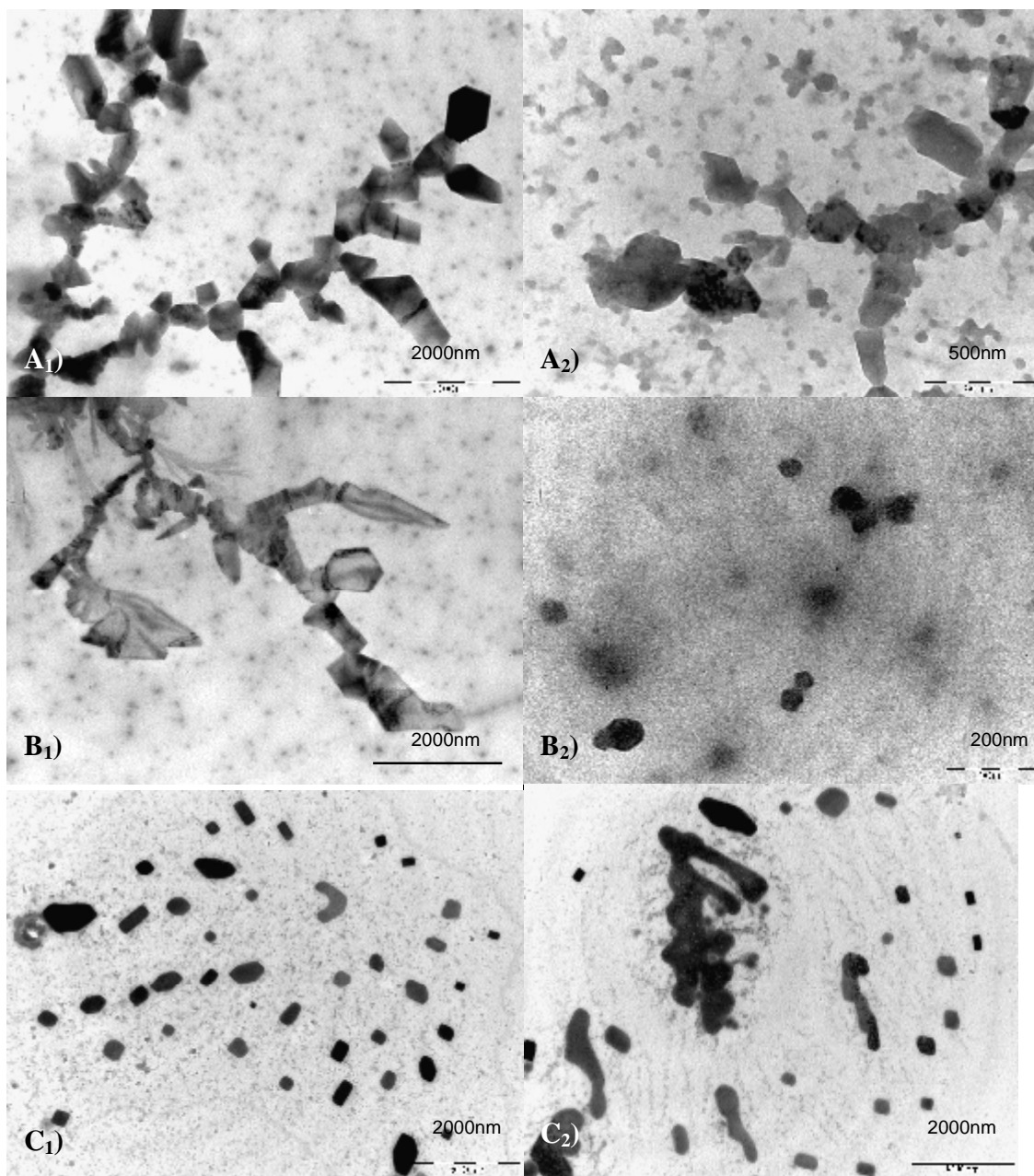


**Figure 5.15:** TEM images of samples exposed to various temperatures. [**A<sub>1+2</sub>**) 25 °C. Scale bar = 2000 nm & 500 nm, **B<sub>1+2</sub>**) 45 °C. Scale bar = 2000 nm & 200 nm. **C<sub>1+2</sub>**) 65 °C. Scale bar = 2000 nm & 2000 nm.]

The particles observed in the 25 °C sample (Fig 5.15 A<sub>1</sub>) exhibited a number of different morphologies, with the majority being geometric in nature (i.e. hexagons, pentagons and squares). These particles demonstrated a tendency to aggregate end-on-end forming large,

dendritic-like structures. The individual particles are clearly visible indicating that coalescence had not yet occurred. In addition, this sample (Fig 5.15 A<sub>2</sub>) possessed a number of smaller, irregular particles that appeared to be coated in a biological material, which was assumed to be protein from the CSE solution. These particles became adsorbed and incorporated by the larger, more geometric particles, as previously observed in section 5.3.1.5.1.

The 45 °C sample (Fig 5.15 B<sub>1</sub>) exhibited similar particles to those observed at 25 °C, however the aggregates had fused to form single large particles in the micrometer range, with clean, sharp edges indicative of geometric shapes. Smaller (< 100 nm), electron dense particles (Fig 5.15 B<sub>2</sub>) were also present that exhibited both regular and quasi-geometric morphologies.

Finally, the sample at 65 °C possessed a number of geometric particles, the majority appearing to be four-sided with clean, straight edges and rounded corners. The degree of monodispersity was greatest in this sample with only a low percentage of particles becoming aggregated. The particles appeared to be highly electron dense due to their dark black colour. The NP's in this sample were far smaller than those observed in the previous two samples and exhibited the best monodispersity and morphology control, however a number of irregular particles were still present.

In conclusion, higher temperatures result in smaller, more monodisperse particles, most likely due to the effect on the reduction rate of the metal-ion.

#### *5.3.1.6.3. Effect of pH*

The apparent change in Pt(IV) concentration over time at pH 7.6, 9 and 11 is illustrated (Fig 5.16 A). Initially (0-0.5 h), the concentration drops in all samples correlating to the reduction of Pt(IV) to Pt(II). The formation of Pt(0) NP's in solution however, results in what appears to be an increase in Pt(IV) concentration due to the increasing NP spectrum interfering with the determination of this ion as previously shown in Chapter 4 and section 5.3.1.4.

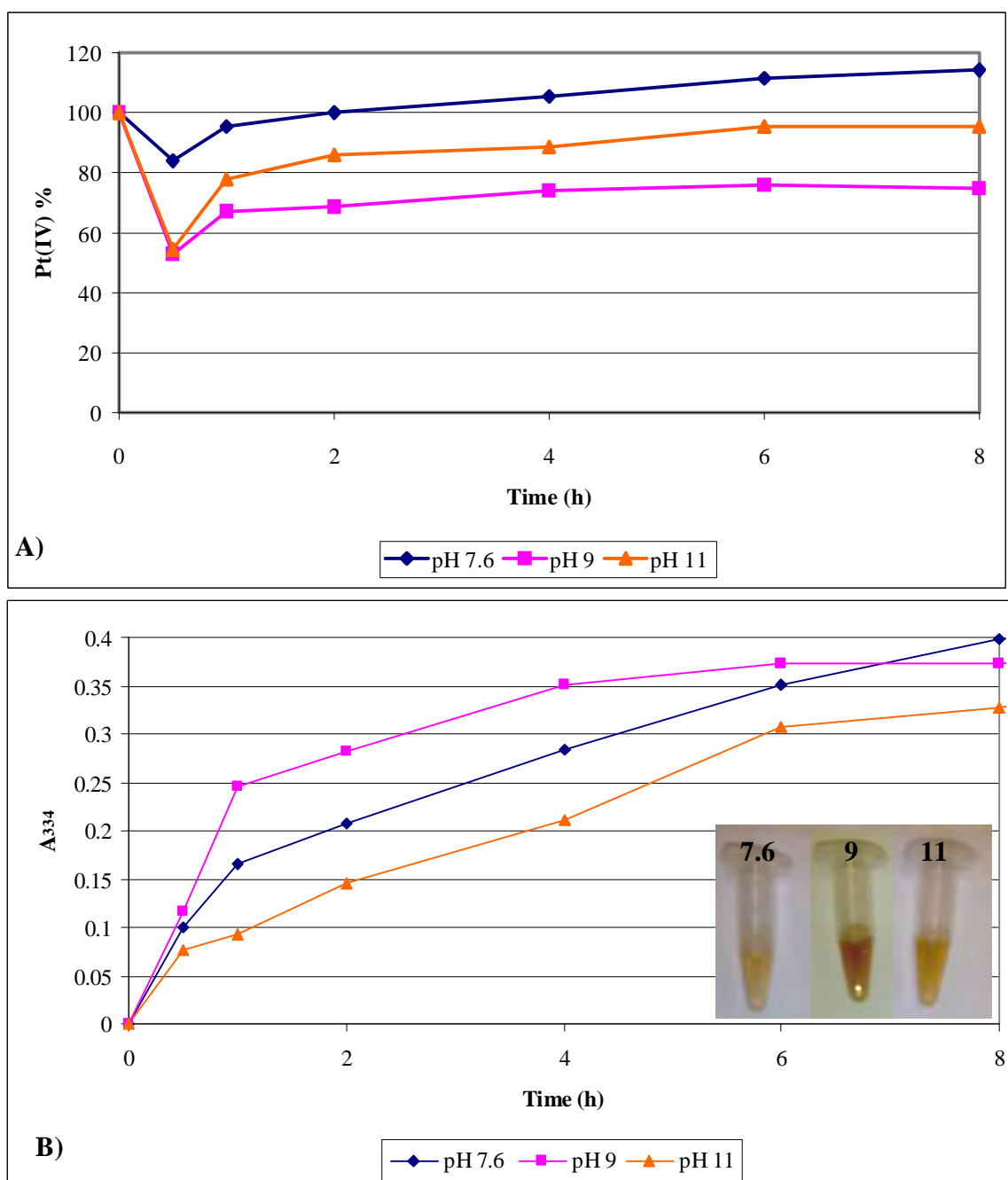


**Figure 5.16:** Effect of pH on the bioreductive mechanism. [A] Pt(IV) reduction and interference by NP's. B) Formation of Pt(0) NP's over time. **Inset:** Images of samples post bioreduction.]\*

The extreme, basic conditions in the pH 11 sample showed the lowest rate of particle formation at A<sub>334</sub> (Fig 5.16 B). The optimum pH for Pt(IV) bioreduction by the CSE

\* All values exhibit a standard deviation < 10 %

solution was demonstrated to be pH 9. When observing the formation of the Pt(0) NP's by  $A_{334}$ , it was clear that the sample at pH 9 showed the greatest change in absorbance indicating a greater concentration of NP's and optimal conditions for Pt(IV) bioreduction. Equilibrium was also reached earlier at 6 h in this sample.

The pH optimum determined in this investigation correlates to the results published by Riddin and colleagues (2006) in that pH 9, was the optimum pH for the bioreduction of the Pt(IV) ion by an extracellular protein solution isolated from a *Fusarium oxysporum* fungal strain.

The second greatest rate of NP formation was observed in the sample at pH 7.6 (Fig 5.16B). This is the optimum pH for the hydrogenase enzyme (Rashamuse & Whiteley, 2007) which has been shown in Chapter 3, to be responsible for Cycle 2 [i.e. Pt(II)  $\rightarrow$  Pt(0)] of the overall Pt(IV) reduction mechanism. These results lend further credence to the results obtained in Chapter 3, which demonstrated that an unknown enzyme, proposed to be a Pt(IV) reductase that becomes upregulated in the presence of Cu(II) and has a pH optimum of pH 9.0, was responsible for Cycle 1 [i.e. Pt(IV)  $\rightarrow$  Pt(II)]. The hydrogenase enzyme would still be active at pH 9, although its activity should be compromised, while the reverse would occur at pH 7.6 with regards to the Pt(IV) reductase activity.

The colour change for all samples (Fig 5.16 B - Inset) correlated well to the data discussed above. The sample at pH 9 exhibited the greatest colour change while the samples at pH 11 and pH 7.6 exhibiting the lowest degree of colour development.

All control samples (Fig 5.17) however, showed no change in absorbance at  $A_{334}$  indicating that Pt(0) NP's were not forming due to the experimental conditions alone and that CSE was required for the bioreductive mechanism of Pt(IV) to Pt(0) to occur. In direct correlation to these results, no colour change was observed for the control samples, indicating that the temperatures investigated, could not abiotically reduce the Pt(IV) ion.

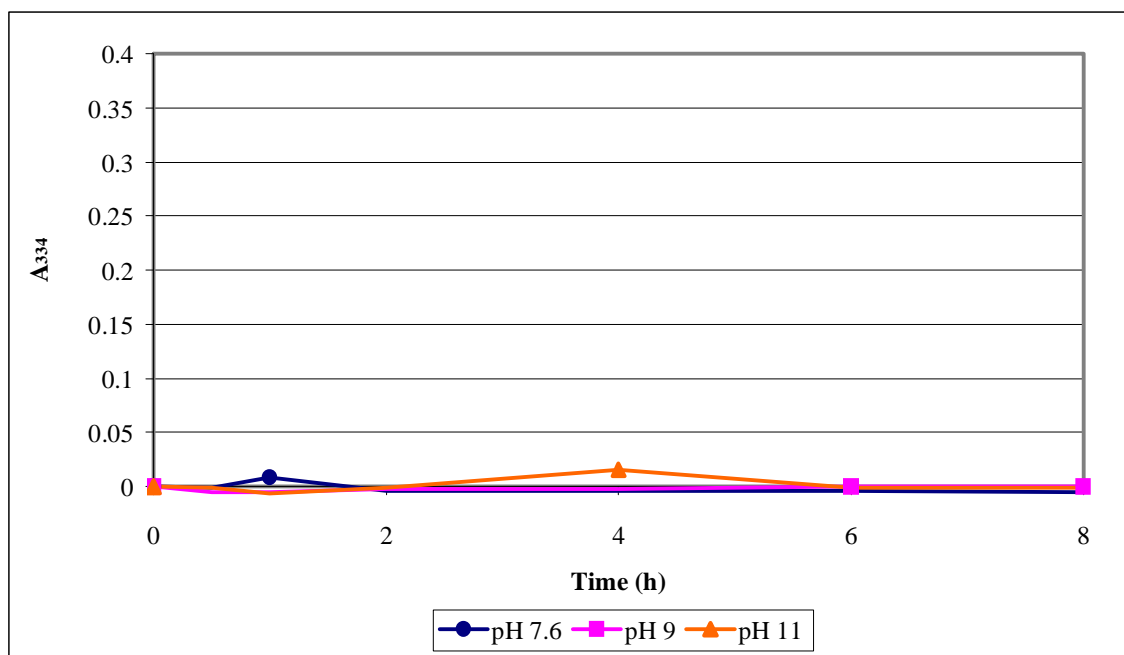


**Figure 5.17:** Change in absorbance at A<sub>334</sub> for the control samples. \*

#### 5.3.1.6.4. TEM analysis of pH samples

In the pH 7.6 sample (Fig 5.18 A<sub>1+2</sub>), a number of different shapes and sizes were observed ranging from geometric to irregular. Some of the particles exhibited a layer of material adsorbed to the surface of the particle (Fig 5.18 A<sub>2</sub>) that was expected to be the stabilising protein layer described in Chapter 4.

The NP's observed in the pH 9 sample (Fig 5.18 B<sub>1+2</sub>) are as described for the 65 °C temperature sample in Fig 5.15 C<sub>1+2</sub>, due to the overlap of experimental conditions and comparison of the same sample.

The NP's contained within the pH 11 sample exhibited a wide variety of morphologies ranging from the small (< 100 nm) irregular (Fig 5.18 C<sub>1</sub>), to the large (> 500 nm) geometric particles arranged in chain/dendritic-like aggregates (Fig 5.18 C<sub>2</sub>).

\* All values exhibit standard deviations < 10 %.

As mentioned in section 5.1, the pH of the experimental solution plays a significant role in the morphology of the NP's produced during chemical synthesis. These results clearly show the same is true for biogenic NP's. In contrast to the NP's produced under various temperatures (section 5.3.1.6.1), there does not appear to be a clear trend of particle size or shape development in relation to pH.

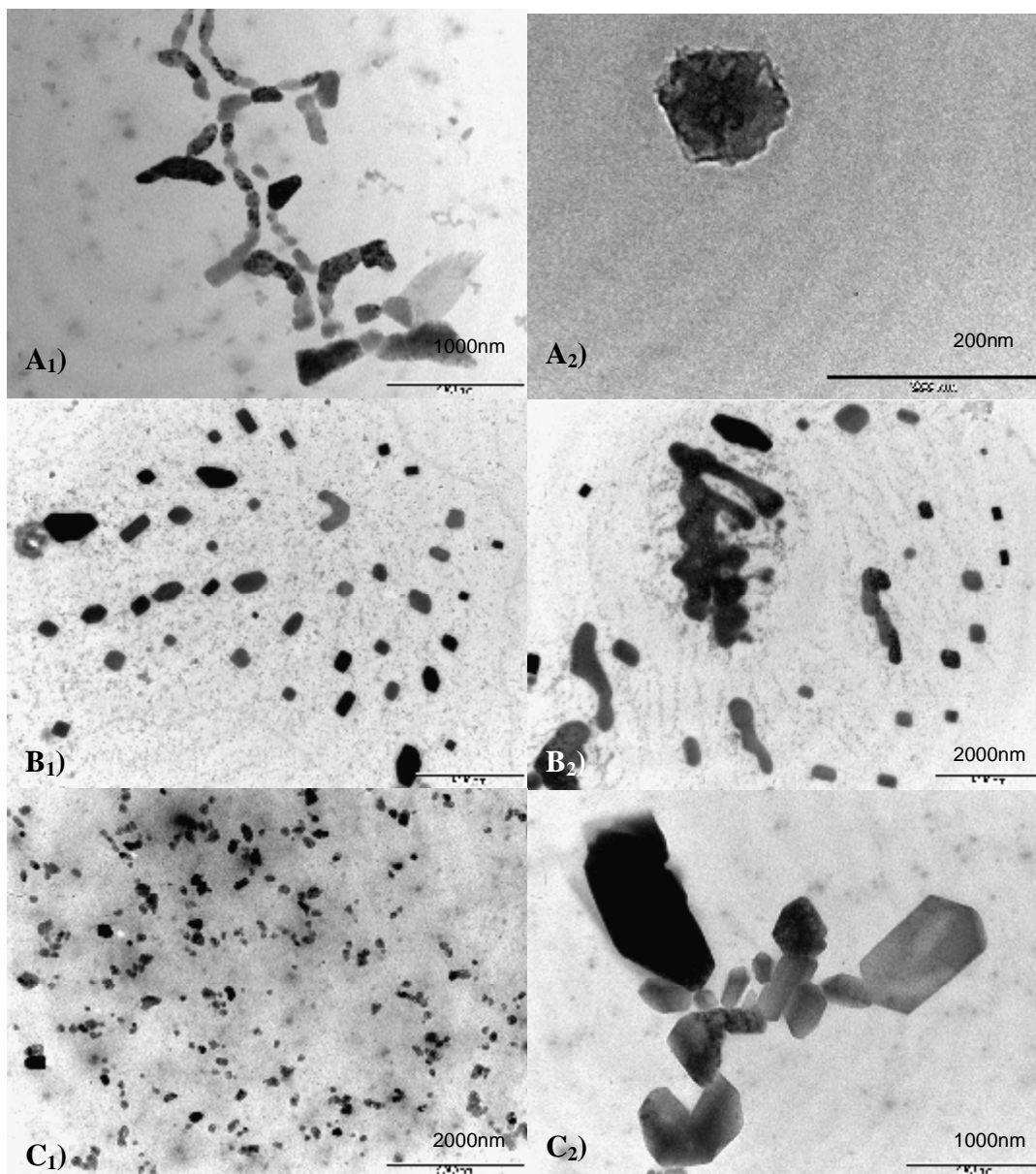


**Figure 5.18:** TEM images of samples. [A<sub>1+2</sub>) pH 7.6. Scale bar = 1000 nm & 200 nm, B<sub>1+2</sub>) pH 9. Scale bar = 2000 nm & 2000 nm. C<sub>1+2</sub>) pH 11. Scale bar = 2000 nm & 1000 nm.]



5.3.1.7. Investigating the hydrogenase activity of CSE

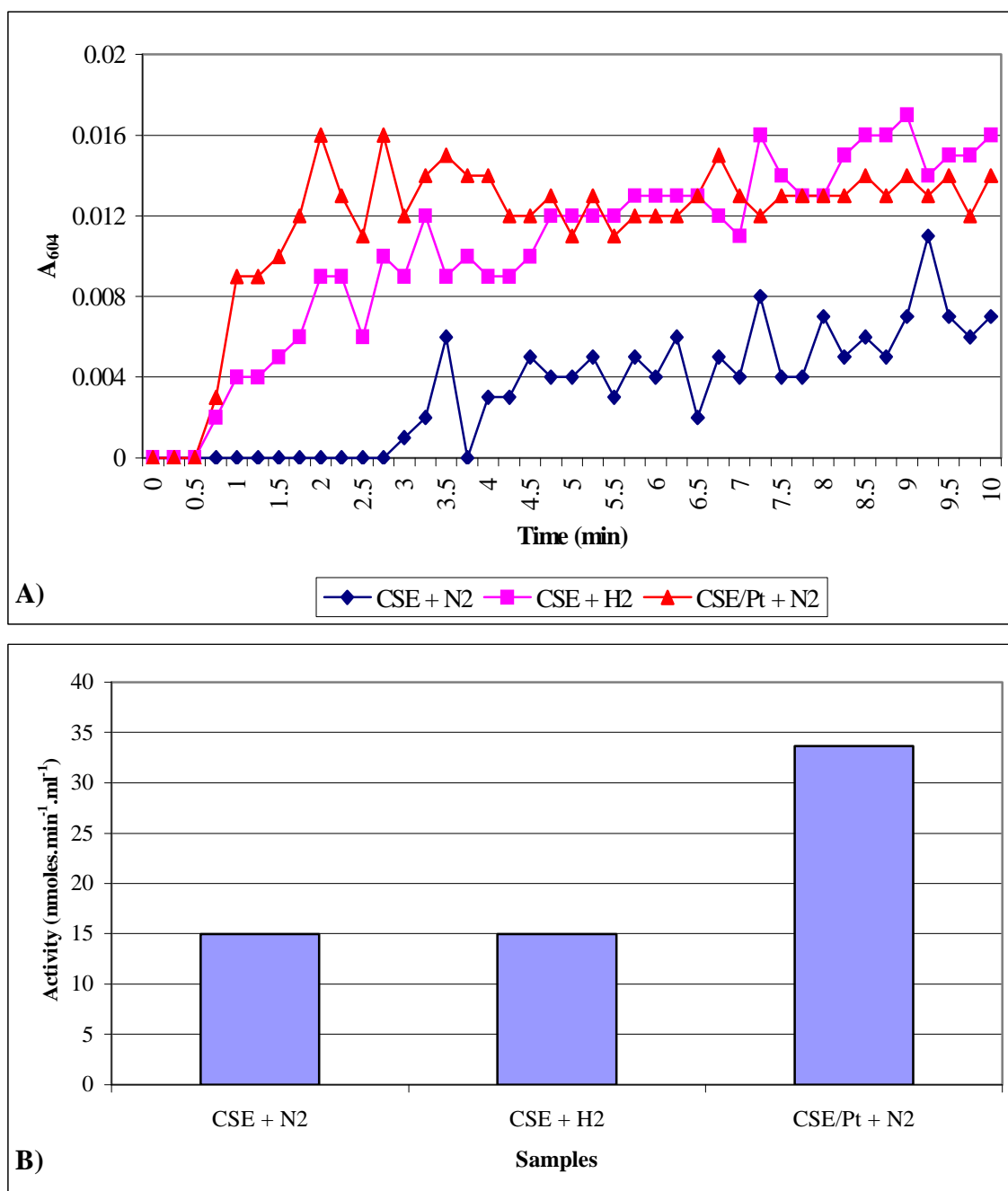


**Figure 5.19:** Hydrogenase activity of CSE samples [A) Change in A<sub>604</sub> over time, B) Activity of CSE samples (nmoles.min<sup>-1</sup>.ml<sup>-1</sup>). CSE + N<sub>2</sub>) CSE prior bioreduction not pre-activated, kept under N<sub>2</sub>, CSE + H<sub>2</sub>) CSE prior bioreduction preactivated under H<sub>2</sub>, CSE/Pt + N<sub>2</sub>) CSE post bioreduction of Pt(IV) not pre-activated, kept under N<sub>2</sub>.]

A modified hydrogenase assay, as described in section 5.2.2.4, was performed on three different CSE samples. First, a CSE sample, prior bioreduction, that had been pre-activated under H<sub>2</sub> for 1 h (CSE + H<sub>2</sub>); second a CSE sample, prior bioreduction, that had not been pre-activated under H<sub>2</sub> but rather kept under N<sub>2</sub> for 1 h (CSE + N<sub>2</sub>), and third a CSE sample, post bioreduction of Pt(IV), not pre-activated under H<sub>2</sub> but kept under N<sub>2</sub> for 1 h (CSE/Pt + N<sub>2</sub>). The final, total CSE protein concentration for all samples was 19.23 µg.ml<sup>-1</sup>. The change in absorbance at 604 nm was observed over a 10 min time period. For all samples, an initial induction period under the hydrogen atmosphere was required before any activity was observed. The sample prior bioreduction, kept under nitrogen [Fig 5.19 A (CSE + N<sub>2</sub>)], exhibited the longest induction period of ~3 min, after which very low activity was observed (14.96 nmoles.min<sup>-1</sup>.ml<sup>-1</sup>). The other samples [(Fig 5.19) (CSE + H<sub>2</sub> & CSE/Pt + N<sub>2</sub>)], showed a much shorter induction period of 0.5 min each. It was interesting to note that the CSE sample post bioreduction and lacking pre-activation (CSE/Pt + N<sub>2</sub>), exhibited an activity of 33.67 nmoles.min<sup>-1</sup>.ml<sup>-1</sup> (a 2.25-fold increase) when compared to the CSE sample prior bioreduction (CSE + H<sub>2</sub>) activated under hydrogen (14.96 nmoles.min<sup>-1</sup>.ml<sup>-1</sup>) (Fig 5.19 B). Comparing the activity of the two samples prior bioreduction revealed identical activities of 14.96 nmoles.min<sup>-1</sup>.ml<sup>-1</sup> although the induction period was greatly reduced in the pre-activated (CSE + H<sub>2</sub>) sample.

Metal NP's bound to certain enzymes/proteins have resulted in pH and temperature related stabilisation of the bound protein as well as enhanced catalytic activity of enzymes (Mandal *et al.*, 2005; Li *et al.*, 2007). This may explain the wide range of activity of the CSE solution observed over the various pH's and temperatures tested. The increased activity observed in the sample post bioreduction (CSE/Pt + N<sub>2</sub>) is most likely due to catalytic action of the NP's bound to the protein in the CSE sample since the methyl-viologen assay has also been used to test the catalytic efficiency of Pt(0) NP's (Rudoy *et al.*, 2005).

These results indicate that the Pt(0) NP's formed by the two-cycle bioreduction of Pt(IV) to Pt(0) via the Pt(II) intermediate, results in NP's that are catalytically active even

though bound to general protein in solution. These NP's may in turn be stabilising the enzymes involved in the bioreductive mechanism of Pt(IV) allowing them to function over a wider range of experimental conditions than they otherwise would be able to.

#### **5.4. Summary & Conclusions**

- The presence of PVP, during Pt(IV) bioreduction by SRB cells, results in a decreased Pt(IV) reduction rate. Results indicated that PVP adsorbs to the surface of the cell, thereby interfering with passive biosorption as well as active uptake of the Pt(IV) ions in solution.
- The presence of PVP during Pt(IV) bioreduction by SRB cells results in the formation/exportation of Pt(0) NP's to the extracellular medium.
- Irradiation of an air-dried, supernatant sample of a Pt(IV) solution post bioreduction in a Tris-buffer, results in the dynamic formation of electron dense NP's of various shapes and sizes – this phenomenon was not observed in ddH<sub>2</sub>O or a sodium-bicarbonate buffer nor in the presence of a high PVP concentration.
- Irradiation of NP's with the TEM electron beam resulted in structural changes of the particles.
- In the presence of CSE, the PVP-free control exhibits the greatest rate of NP formation, however in relation to the two PVP samples of differing concentration, the 100 mg.ml<sup>-1</sup> PVP sample exhibited a more rapid rate of NP formation than the 20 mg.ml<sup>-1</sup> PVP sample most likely due to the formation of smaller NP's.
- An increase in CSE concentration was shown to increase the Pt(0) NP formation rate, however it could not be determined whether the effect on particle morphology was due to the CSE protein or the altered reduction rate.
- Increase in temperature results in an increase in the Pt(0) NP formation rate leading to a subsequent decrease in NP size.
- pH was shown to have a significant effect on NP morphology and Pt(0) NP formation rate, yet no obvious trend in NP size or shape evolution was observed.
- Biogenic Pt(0) NP's, produced by the bioreductive mechanism of the CSE solution from SRB, exhibit catalytic activity in the methyl-viologen assay.

## CHAPTER SIX:

### General discussion and conclusions

---

---

#### 6.1. Introduction

Transition metal nanoparticles (NP's), particularly platinum and palladium, are in great demand for the production of more efficient fuel-cell catalysts (Liu *et al.*, 2006), and other emerging technologies. Current chemical methods of NP synthesis are costly, complicated and produce toxic substances which are hazardous to the environment and human health (Gamez *et al.*, 2003). A 'green-friendly' method of NP synthesis is therefore being sought. A number of micro-organisms, including fungi, bacteria and yeasts, have been screened to contain various metal-ion reductase activities (Ahmad *et al.*, 2003; Mukherjee *et al.*, 2003; Sastry *et al.*, 2003). Although this mechanism has not yet been fully elucidated, the majority of the metal reductase activities in micro-organisms tend to be attributed to the redox active hydrogenase enzymes (Lloyd *et al.*, 2001; Payne *et al.*, 2002; Rashamuse & Whiteley, 2007; Govender *et al.*, 2008). The use of microbes for metal NP synthesis overcomes the negative aspects of chemical methods as it provides the possibility of a cheaper, more environmentally friendly protocol. In addition to this, once the mechanism of biological NP synthesis has been fully elucidated, it will provide the means of being able to control the morphology of the NP's produced, simply by manipulating the experimental conditions.

Sulfate-reducing bacteria (SRB) have been identified to contain a number of metal reductase activities ranging from the noble metals (Au) (Lengke & Southam, 2006), to the transition metals (Pd, Pt) (Lloyd *et al.*, 1998, Rashamuse & Whiteley, 2007) and the radionuclides (Tc) (Lloyd *et al.*, 2001). They are also capable of removing metal-ions from solution by forming insoluble metal sulfides with the metabolic product, hydrogen sulfide (Liamleam & Annachhatre, 2007). SRB have also been shown to contain a

number of hydrogenase enzymes, with some species, such as *Desulfovibrio vulgaris* Hildenborough containing six  $H_{ase}$ 's in total (Caffrey *et al.*, 2007), all of which make them ideal candidates for studies into metal NP synthesis. SRB consortiums have been known to be far more robust than the purer cultures as they are capable of preventing the growth of contaminant species by the production of toxic metabolic products, which by a serendipitous turn of events, enhance their own growth (Gibson, 1990). An additional benefit is provided by the syntrophic relationships formed within consortiums, which endows the constituted species with a higher degree of oxygen tolerance (Bade *et al.*, 2000).

## **6.2. Elucidating the bioreductive mechanism of Pt(IV) by an unknown consortium of sulfate-reducing bacteria**

Prior work by Rashamuse and Whiteley (2007) showed that resting cells of a mixed consortium of SRB were capable of Pt(IV) reduction to elemental platinum under anaerobic conditions, in the presence of an electron donor, such as hydrogen. They determined the metal reductase activity to be attributed to the action of an oxygen-sensitive periplasmic hydrogenase ( $H_{ase}$ ). In contrast, the results from this investigation in a similar resting, SRB consortium, demonstrated the presence of a separate, although less efficient, aerobic, enzymatic reduction mechanism, which was not dependant on an exogenous electron donor. Since Pt(IV) was shown to become abiotically reduced to Pt(0) by hydrogen (section 2.3.2.1, Fig 2.3) , an experimental approach independent of this reducing gas was favored.

In 2006, Riddin and colleagues proposed a two-step mechanism for Pt(IV) bioreduction, by micro-organisms (section 1.3.3, Fig 1.5), to Pt(0) which included the intermediate cation, Pt(II). The UV-Vis spectroscopy results of this chapter demonstrated the basis of this hypothesis to be true. By observing the reduction of the Pt(IV) cation at 261 nm (Liu *et al.*, 2004), and subsequently following the change in absorbance at 230 nm - experimentally determined to be relevant for Pt(II) and substantiated by Henglein and colleagues (1995) – it became clear that a stoichiometric relationship was occurring where Pt(IV) was becoming reduced to Pt(II) over time (section 2.3.3, Fig 2.8 A & B).

Further observation of the Pt(II) cation demonstrated that the reduction of this ion to Pt(0) was occurring at a far slower rate than that of its precursor ion, Pt(IV). It was proposed that endogenous hydrogen was being produced by the resting consortium of SRB in the absence of sulfate, via the fermentative pathway or by a  $H_{ase}$  enzyme capable of hydrogen evolution (i.e. [Fe]- $H_{ase}$ ). Once reaching acceptable limits, the endogenous electron donor would either a) be used by an oxygen tolerant [Fe]- $H_{ase}$ , previously shown to become upregulated in the presence of oxygen (Fournier *et al.*, 2004), which would subsequently lead to the reduction of the Pt(IV) ion; or b) activate the less oxygen tolerant  $H_{ase}$ 's which in turn would result in the reduction of Pt(IV). Since endogenously produced hydrogen would be limited and in low concentration, the majority of the electron stores would be utilised in the reduction of the Pt(IV) ion, with little left over for the final reduction step of Pt(II) to Pt(0). This would explain the slower reduction rate observed for Pt(II) when compared to that of Pt(IV). It is therefore proposed, that several  $H_{ase}$  enzymes may be responsible for this reduction mechanism, some more tolerant to aerobic conditions than others and/or having a higher affinity for Pt(IV) than Pt(II).

### **6.3. Periplasmic hydrogenase: Role in the bioreductive mechanism of Pt(IV) to Pt(0)**

The mechanism for Pt(IV) reduction to Pt(0), as proposed by Riddin and colleagues (2006) was partially elucidated in Chapter 2, to be a two-cycle reduction mechanism with Pt(II) acting as the intermediary. Further proof, however, was required with regards to the role of the  $H_{ase}$  enzyme in this mechanism.

Inhibition studies, involving the use of Cu(II), a known irreversible inhibitor of the periplasmic  $H_{ase}$  (De Luca *et al.*, 2001), revealed the true mechanistic action of the  $H_{ase}$  in the bioreduction of Pt(IV) under aerobic conditions. The SRB cells were pre-treated with varying concentrations of the inhibitor and subsequently challenged with a Pt(IV) solution. The results demonstrated that, with increasing concentrations of Cu(II), the reduction rate of Pt(IV) increased unexpectedly. To further substantiate the action of the inhibitor on the periplasmic  $H_{ase}$ , a modified hydrogenase assay was performed on the cells. The assay proved that Cu(II) did in fact inhibit the periplasmic  $H_{ase}$  as expected, with a concentration greater than 0.5 mM required for complete inhibition of activity. In

conjunction, these results clearly prove that under the aerobic conditions described - and using the current SRB consortium - that the bioreduction of the Pt(IV) ion to Pt(II) is not due to reductase action by a periplasmic  $H_{ase}$ , but rather by an unknown, oxygen-tolerant enzyme that becomes up-regulated in the presence of Cu(II), henceforth termed 'Pt(IV) reductase'. Further investigations revealed that cells pre-treated with Cu(II) exhibited a compromised reductive potential of the Pt(II) starting ion, relative to the concentration of the inhibitor. This indicates that, although the initial reductive cycle of Pt(IV) to Pt(II) is not due to  $H_{ase}$  action, the second cycle of Pt(II) to Pt(0) is dependant on a periplasmic  $H_{ase}$ . This would explain the lower reduction rate of Pt(II) in relation to Pt(IV) due to the low concentration of endogenous hydrogen that would be available for  $H_{ase}$  action, by fermentative metabolism.

A new mechanism for the bioreduction of Pt(IV) to Pt(0) is proposed (Fig 6.1):

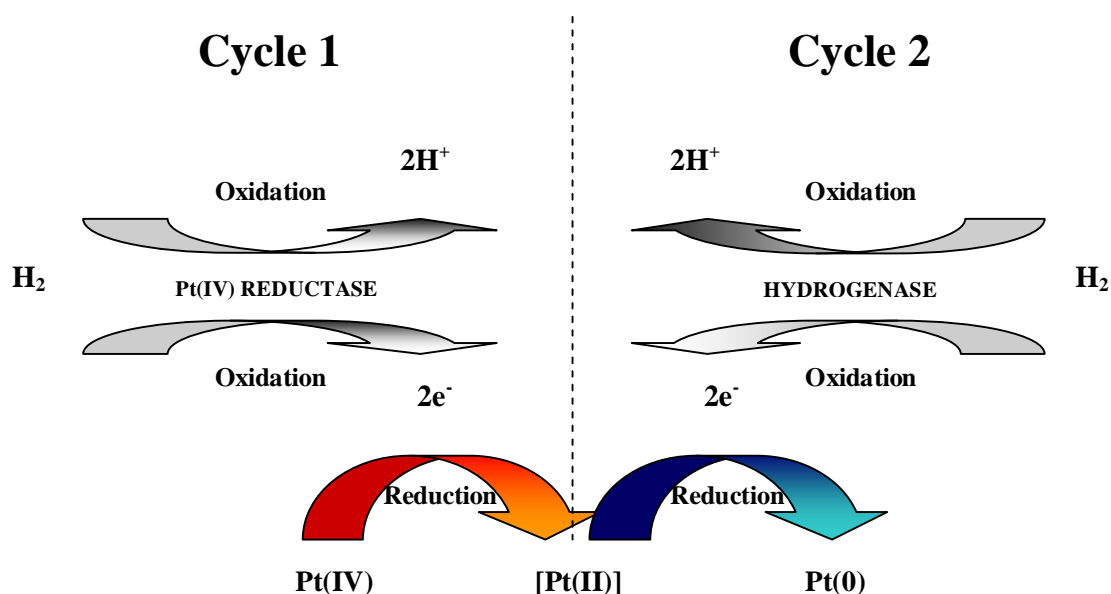


**Figure 6.1:** Newly proposed mechanism of Pt(IV) reduction by micro-organisms.

The reduction of the Pt(IV) ion in Cycle 1, has been shown to be more complicated than originally thought, involving the action of an oxygen-tolerant enzyme, Pt(IV) reductase, which becomes up-regulated in the presence of Cu(II). The reduction of the Pt(II) ion occurs via an active mechanism involving a periplasmic  $H_{ase}$ , most likely a [Fe]- $H_{ase}$  or

[NiFe]-H<sub>ase</sub>. Though passive biosorption is also involved, it is only responsible for a small percentage of the total bioreduction observed.

#### **6.4. Screening an SRB cell-free crude extract for Pt(IV) reductase activity and metal nanoparticle synthesis**

It was proposed that by removing the spatial restrictions imposed by the cell on the bioreductive mechanism, the formation of crystalline, geometric Pt(0) NP's would result in place of the amorphous deposits observed thus far.

The SRB cells were lysed by sonication to release the contents of the cells into solution, which was termed the 'cell soluble extract' (CSE). Previous work by Riddin and colleagues (2006) had determined the optimal experimental conditions for Pt(0) NP synthesis by an extracellular, fungal protein solution to be pH 9 and 65 °C. Hence, these were the initial experimental conditions tested to screen for Pt(IV) reductase activity in the CSE.

The effect of a range of Pt(IV) concentrations, on the bioreductive mechanism and NP synthesis, was investigated. Samples with a concentration less than 1 mM Pt(IV) (0.35 mM, 0.5 mM, 0.75 mM) initially exhibited a drop in Pt(IV) concentration as previously demonstrated in whole cells in Chapter 2. After 0.5 h however, it falsely appeared as though the Pt(IV) concentrations were increasing in all three samples. This false increase in Pt(IV) concentration correlated to the visual observation of the solutions turning from pale yellow to brown. Literature states that Pt(0) NP's in colloidal dispersion exhibit a brown-black colour in aqueous solutions, which is due to their wide UV-Vis spectrum with no specific maxima. When examining the change in UV-Vis spectrum from 200 - 350 nm over 8 h, the formation of a Pt(0) NP spectrum is evident and the wavelength of 334 nm was chosen as an indicator of NP formation over time. The formation of the NP spectrum interferes with the determination of the Pt(IV) and Pt(II) ions at 261 nm and 230 nm respectively, making accurate estimations on the concentrations of these ions impossible using UV-Vis methods.



The effect of Pt(IV) concentrations greater than, or equal to 1 mM (1 mM, 2 mM and 3 mM) was also investigated. In contrast to the results observed for the samples less than 1 mM, the reduction of the Pt(IV) ion could be observed at 261 nm. Visual observations of the samples showed an initial colour change from pale yellow to brown, indicating formation of Pt(0) NP's. At various times for each sample, however, a brown precipitate would begin collecting at the bottom of the flask. This was later confirmed to be the precipitation of the protein bound-NP bioconjugate due to acidic conditions resulting from the higher Pt(IV) concentrations. The precipitation of the NP's in turn removed the interfering spectrum caused by the particles in solution, allowing the Pt(IV) ion to be analysed at 261 nm. This proved that the NP's were binding to and being stabilised by the general CSE protein in solution.

As predicted, the removal of the spatial restrictions of the cell on the bioreductive mechanism resulted in the formation of geometric and irregular NP's. The particles were observed, via TEM analysis, to reduce in size in relation to an increasing reduction rate and *vice versa*. This correlates to trends observed in chemical synthesis methods in regards to the principles of particle nucleation.

In an attempt to overcome the precipitation of the protein-NP bioconjugate in higher Pt(IV) concentrations, the effect of a sodium-bicarbonate (SBC) buffer at pH 9.0 was investigated. The buffer was shown to maintain the pH within the desired range but had an effect on the reduction rate and NP morphology. In the presence of the SBC buffer, the Pt(IV) reduction rate increased when compared to the same experiments conducted in water. This lends further credence to the results indicating that: the reduction of Pt(IV) to Pt(II) is not due to a periplasmic hydrogenase - that has an optimal pH at ~7.6 - but rather to a novel Pt(IV) reductase with a pH optimum of 9.0, that is upregulated by Cu(II). Once again, the increase in the reduction rate resulted in a decreasing trend for particle size. The morphology of the particles was also affected. Although the exact mechanism by which SBC controls particle morphology is still unknown, it is proposed that the buffer salts bind to various crystallographic plains of the particle during the initial nucleation

step, thereby preventing further growth in the direction of that particular plane, much in the same way as the function of capping agents.

The bioreductive mechanism was capable of being 'short-circuited' by the addition of Pt(II) as the starting ion. The CSE solution was shown to reduce the Pt(II) ion to Pt(0), though when comparing the rates of Pt(0) NP formation at 334 nm, the NP formation rate resulting from Pt(II) reduction was slower than that in the presence of the Pt(IV) starting ion. This suggests that the enzymes involved have a greater affinity for the Pt(IV) ion than the Pt(II) ion, most probably due to the molecular interaction of the ions with the active site of the enzymes responsible. This would further explain why the Pt(IV) reduction rate is far more rapid than that of the Pt(II) ion.

### **6.5. Effects of experimental factors on biogenic nanoparticle morphology**

PVP has been used extensively within chemical synthesis methods to control the size and shape of the nanoparticles produced (Ahmadi *et al.*, 1996; Sun & Xia, 2002). It was proposed, therefore, that PVP would function in a similar capacity when added to a biological reductive mechanism.

The results demonstrated that in the presence of PVP, the reduction of Pt(IV) by the SRB cells was compromised. It was hypothesised that the capping agent was adsorbing to the surface of the cell, thereby interfering with both passive and active uptake mechanisms. In addition, the presence of PVP also resulted in an unusual phenomenon. First, the supernatants of the cell samples began exhibiting a colour change to brown. Second, an increase in  $A_{334}$  was observed. Both these results are indicative of Pt(0) NP's in aqueous solution suggesting the presence of extracellular NP's. This phenomenon was not observed in the absence of PVP. The precise mechanism by which extracellular NP's are formed in the presence of PVP has yet to be elucidated. However, it is proposed that either a) the PVP is binding to cellular and proteinaceous components that would otherwise be binding the NP's formed on an intracellular level, or b) the PVP is increasing the production and stabilising an extracellular protein with metal reductase activities. To confirm the presence of extracellular NP's, the supernatant samples were

analysed by TEM. Unexpectedly, the dynamic formation of electron dense NP's, of various morphologies, could be observed upon irradiation of the samples with the electron beam. This phenomenon was only observed to occur in the presence of a Tris-HCl buffer and not in a sodium-bicarbonate buffer or water nor in the presence of a high PVP concentration ( $100 \text{ mg.ml}^{-1}$ ). Under extended irradiation times, the dynamically formed particles underwent structural fluctuations.

In the cell-soluble extract (CSE) samples, the control sample in the absence of PVP was shown to exhibit the greatest rate of Pt(0) NP formation. In the presence of PVP however, the  $100 \text{ mg.ml}^{-1}$  PVP sample exhibited a more rapid rate of NP formation than the  $20 \text{ mg.ml}^{-1}$  PVP sample most likely due to the formation of smaller NP's by the action of the capping agent.

The general CSE protein was investigated for its potential as a biological capping agent. It was demonstrated that the NP formation rate increased in relation to increasing CSE protein concentration. This in turn resulted in the formation of increasingly smaller NP's. It could not be determined, however, whether this result was due to the increased reduction rate or due to the capping effect of the protein.

The effect of temperature and pH on the bioreductive mechanism and resulting NP morphology was also investigated. The results demonstrated that a) an increase in temperature lead to a decrease in particle size due to an increased reduction rate, while b) pH had a significant effect on both the reduction rate and NP morphology, however no obvious trends in relation to pH could be elucidated.

When comparing the hydrogenase activity of CSE samples both pre and post bioreduction, the results showed that the CSE sample post bioreduction, containing protein-NP bioconjugates, exhibited the greatest activity even without preactivation under hydrogen. This suggests that a) the NP's are catalytically active, and b) the NP's may be stabilising the hydrogenase enzymes by binding to them.

**6.6. Future work**

- i) Screen the SRB consortium, under the optimal conditions determined by this research, for other metal-ion reductase activities.
- ii) Isolate, purify and identify the Pt(IV) reductase, from this SRB consortium, responsible for Pt(IV) reduction to Pt(II).
- iii) Screen pure cultures of SRB identified, by bioinformatics techniques, to contain the above-mentioned enzyme for metal-ion reductase activities.
- iv) Further investigate methods of NP morphology control by exploring the possibility of using molecular imprinting techniques.
- v) Investigate the possibility of a template-like action, of the purified enzymes responsible for Pt(IV) reduction to elemental platinum, on NP synthesis.

---

---

## REFERENCES

---

---

Ahalya N, Ramachandran TV and Kanamadi RD (2003), "Biosorption of Heavy Metals", *Research Journal of Chemistry and Environment*, **7**(4):71-79

Ahern AM and Garrell RL (1991), "Protein-metal interactions in protein-colloid conjugates probed by surface-enhanced raman spectroscopy", *Langmuir*, **7**:254-261

Ahmad A, Senapati S, Khan MI, Kumar R, Ramani R, Srinivas V & Sastry M (2003), "Intracellular synthesis of gold nanoparticles by a novel alkalotolerant actinomycete, *Rhodococcus* species", *Nanotechnology*, **14**(7):824-828.

Ahmadi TS, Wang ZL, Green TC, Henglein A and El-Sayed MA (1996), "Shape-Controlled Synthesis of Colloidal Platinum Nanoparticles", *Science, New Series*, **272**(5270):1924-1926

Aitken RJ, Kreely KS and Tran CL (2004), "Physical characteristics/properties of nanoparticles. In *Nanoparticles: An occupational hygiene review*", pp 7-18, Edinburgh: Crown copyright.

Akamatsu K, Nakahashi K, Ikeda S & Nawafune H (2003), "Fabrication and structural characterization of nanocomposites consisting of Ni nanoparticles dispersion in polyimide films", *Eur. Phys. J. D.*, **24**:377-380.

Akerman ME, Chan WC, Laakkonen P, Bhatia SN & Ruoslahti E (2002), "Nanocrystal Targeting In Vivo", *PNAS*, **99**:12617-12621.

Alexander M (1973), "Microorganisms and Chemical Pollution", *BioScience*, **23**(9):509-515.

Atlas RM (1978), "Microorganisms and Petroleum Pollutants", *BioScience*, **28**(6):387-391.

Bade K, Manz W, Szewzyk U (2000), "Behavior of sulfate-reducing bacteria under oligotrophic conditions and oxygen stress in particle-free systems related to drinking water", *FEMS Microbiol Ecol.*, **32**:215– 23.

Basu N, Bhattacharya R and Mukherjee P (2008), "Protein-mediated autoreduction of gold salts to gold nanoparticles", *Biomed. Mater.*, **3**:1-6.

Battersby NS, Malcolm SJ, Brown CM and Stanley SO (1985), "Sulphate reduction in oxic and sub-oxic North East Atlantic sediments", *FEMS Microbiol. Ecol.*, **31**:225-228.

Baumgarten A, Redenius I, Kranczoch J and Cypionka H (2001), "Periplasmic oxygen reduction by *Desulfovibrio* species", *Arch. Microbiol.*, **176**(4):306-309.

Beard MC, Turner GM & Schmuttenmaer CA (2002), "Size-Dependent Photoconductivity in CdSe Nanoparticles as Measured by Time-Resolved Terahertz Spectroscopy", *Nano Lett.*, **2**(9):983-987.

Bedell GW and Darnall DW (1990), "Immobilisation of non-viable biosorbent algal biomass for the recovery of metal ions. Biosorbents and Biosorption recovery of heavy metals". Volesky B (ed), CRC Press, Boca Raton, Florida, pp 313-326.

Bel'skaya OB and Duplyakin VK (2007), Molecular mechanism of formation of supported platinum catalysts of the Pt/Al<sub>2</sub>O<sub>3</sub> family", *Russ. J.Gen. Chem.*, **77**(12):2232-2242.

Beveridge TJ and Doyle RJ (1989), "Metal ions and Bacteria", Wiley-Interscience, pg 32-52, New York.

Bollag DM, Rozycki MD, and Edelstein SJ (1996), "Protein Methods", 2<sup>nd</sup> Edition, Chapter 6, pp 155-169, Wiley-Liss, Inc. New York. USA.

Bolotin KI, Keummeth F, Pasupathy AN, Ralph DC (2004), "Metal-nanoparticle single-electron transistors fabricating using electromigration", *Appl. Phys. Lett.*, **84**:3154.

Bönneman H, Khelashvili G, Behrens S, Hinsch A, Skupien K and Dinjus E (2007), "Role of the platinum nanoclusters in the iodide/triiodide redox system of dye solar cells", *J. Clust. Sci.*, 18(1):141-155.

Bradford MM (1976), "A rapid and sensitive method for the quantitation of microgram quantities of protein utilizing the principle of protein-dye binding", *Anal. Biochem.*, 72(1-2):248-254.

Braidy N, Jakubek ZJ, Simard B, Botton GA (2008), "Quantitative Energy Dispersive X-ray Microanalysis of Electron Beam-Sensitive Alloyed Nanoparticles", *Microsc. Microanal.*, **14**:166-175.

Bridge TAM, White C and Gadd GM (1999), "Extracellular metal-binding activity of the sulphate-reducing bacterium *Desulfococcus multivorans*", *Microbiology*, **145**:2987-2995.

Bruchez MJ, Moronne M, Gin P, Weiss S & Alivisatos AP (1998), "Semiconductor Nanocrystals as Fluorescent Biological Labels", *Science*, **281**(5385):2013-2016.

Bruins MR, Kapil S and Oehme FW (2000), "Microbial Resistance to Metals in the Environment", *Ecotox. and Environ. Safe.*, **45**:198-207.

Caffrey SM, Park H, Voordouw JK, He Z, Zhou J and Voordouw G (2007), "Function of Periplasmic Hydrogenases in the Sulfate-Reducing Bacterium *Desulfovibrio vulgaris* Hildenborough", *J. Bacteriol.*, **189**(17):6159-6167.

Cao YC, Jin R & Mirkin CA (2002), "Nanoparticles with Raman Spectroscopic Fingerprints for DNA and RNA Detection", *Science*, **297**(5586):1536-1540.

Carpentier W, Sandra K, De Smet I, Brige A, De Smet L & Van Beeumen J (2003), "Microbial Reduction and Precipitation of Vanadium by *Shewanella oneidensis*", *Appl. Environ. Microb.*, **69**(6):3636-3639.

Chan K, Ding J, Ren J, Cheng S and T KY (2004), "Supported mixed metal nanoparticles as electrocatalysts in low temperature fuel cells", *J. Mater. Chem.*, **14**:505-516.

Chardin B, Giudici-Orticoni MT, De Luca G, Guigliarelli B and Bruschi M (2003), "Hydrogenases in sulphate-reducing bacteria function as chromium reductase", *Appl. Microbiol. Biotechnol.*, **63**:315-321.

Chatelus C, Carrier P, Saignes P, Libert MF, Merlier Y, Lespinat PA, Fauque G and Legall J (1987), "Hydrogenase activity in aged, nonviable *Desulfovibrio vulgaris* cultures and its significance in anaerobic biocorrosion", *Appl. Environ. Microb.*, **53**(7):1708-1710.

Chen CW, Tano D and Akashi M (1999), "Synthesis of platinum colloids sterically stabilised by poly(N-vinylformamide) or poly(N-vinylalkylamide) and their stability towards salt.", *Colloid. Polym. Sci.*, **277**:488-493.

Choo H, He B, Liew KY, Liu H and Lin J (2006), "Morphology and control of Pd nanoparticles", *J. Mol. Catal. A-Chem.*, **244**: 217-228.

Clarke PH, Postgate JR, Duggleby CJ (1980), "Microbiology and Pollution: the Biodegradation of Natural and Synthetic Organic Compounds [and Discussion]", *Phil. Trans. R. Soc. Lond. B*, **290**(1040):355 -367.

Cohen RRH (2006), "Use of microbes for cost reduction of metal removal from metals and mining industry waste streams", *J. Clean. Prod.*, **14**:1146-1157.



Cox PM, Betts RA, Jones CD, Spall SA, Totterdell IJ (2000), "Acceleration of global warming due to carbon-cycle feedbacks in a coupled climate model.", *Nature*, **408**(6809):184-187.

Creighton JA and Eadon DG (1991), "Ultraviolet-visible absorption spectra of the colloidal metallic elements", *J Chem. Soc. Faraday Trans.*, **87**(24):3881-3891

Cypionka H (2000), "Oxygen respiration by desulfovibrio species", *Annu. Rev. Microbiol.*, 54:827-848.

Das D, Dutta T, Nath K, Kotayi SM, Das KAK and Veziroglu TN (2006), "Role of Fe-hydrogenase in biological hydrogen Production", *Curr. Sci.*, **90**(12):1627-1637.

Davydova M, Gorshkov O and Tarasova N (2006), "Periplasmic superoxide dismutase from *Desulfovibrio desulfuricans* 1388 is an iron protein", *Biochemistry (Moscow)*, **71**(1):68-72.

Davydova M and Sabirova RZ (2002), "Antioxidative enzymes of sulfate-reducing bacterium *Desulfovibrio desulfuricans*: Superoxide dismutase and peroxidases", *Biochemistry (Moscow)*, **67**(7):822-825.

De Lacy AL, Santamaria E, Hatchikian EC and Fernandez VM (2000), " Kinetic characterisation of *Desulfovibrio gigas* hydrogenase upon selective chemical modification of amino acid groups as a tool for structure-function relationships", *Biochim. Biophys. Acta*, **1481**:371-380.

De Luca G, De Philip P, Dermoun Z, Rousset M and Vermeglio A (2001), "Reduction of Technetium(VIII) by *Desulfovibrio fructosovorans* is mediated by the nickel-iron hydrogenase", *Appl. Environ. Microbiol.*, **67**(10):4583-4587.

Dilling W and Cypionka H (1990), "Aerobic respiration in the sulfate reducing bacteria", *FEMS Microbiol. Lett.*, **71**:123-128.

Dolla A, Fournier M and Dermoun Z (2006), "Oxygen defense in sulfate-reducing bacteria", *J. Biotechnol.* **126**:87-100.

Durán N, Marcato PD, Alves OL, De Souza GI & Esposito E (2005), "Mechanistic aspects of biosynthesis of silver nanoparticles by several *Fusarium oxysporum* strains", *Journ. Nanobiotech.*, **3**:8.

Earl B and Wilford LDR (1991), "Chemistry Data Book", Chapter 3: Elements of the Periodic Table, pp 71, Blackie and Son, Ltd., Great Britain.

Eccles H (1995), "Removals of heavy metals from effluent streams – Why select a biological process?", *Inter. Biodeterior. And Biodegrad*, **16**:5-17.

Eccles H (1999), "Treatment of metal-contaminated wastes: why select a biological process?", *Trends Biotechnol.*, **17**(12):462-465.

Elechiguerra JL, Burt JL, Morones JR, Camacho-Bragado A, Gao X, Lara HH and Yacaman MJ (2005), "Interaction of silver nanoparticles with HIV-1", *Journ. Nanobiotech.*, **3**:6.

El-Sayed MA (2001), "Some Interesting Properties of Metals Confined in Time and Nanometer Space of Different Shapes", *Accounts Chem. Res.*, **34**(4):257-265.

Ershov BG, Anan'ev AV and Sukhov NL (2006), "The effect of the concentration of platinum nanocolloid on the rate of catalytic reactions in aqueous solution.", *Colloid J+*, **68**(2):148-154.

Evans DJ and Pickett CJ (2003), "Chemistry and the hydrogenases", *Chem. Soc. Rev.*, **32**:268-275.

Fischer BE, Haring UK, Tribolet R and Sigel H (1979), "Metal Ion/Buffer Interactions. Stability of binary and ternary complexes containing 2-Amino-2(hydroxymethyl)-1,3-propanediol (Tris) and adenosine 5'-triphosphate (ATP)", *Eur. J. Biochem.*, **94**:523-530.

Fournier M, Dermoun Z, Durand MC and Dolla A (2004), "A New Function of the *Desulfovibrio vulgaris* Hildenborough [Fe] Hydrogenase in the Protection against Oxidative Stress", *J. Biochem.*, **279**(3):1787-1793.

Fu X, Wang W, Wu N, Gui L and Tang Y (2002), "Shape-selective preparation and properties of oxalate-stabilized Pt colloid", *Langmuir*, **18**(12):4619-4624.

Fude L, Harris B, Urrutia MM and Beveridge TJ (1994), "Reduction of Cr(VI) by a consortium of sulphate-reducing bacteria (SRBIII)", *Appl. Environ. Microb.*, **60**(5):1525-1531.

Fukuoka A, Higuchi T, Ohtake T, Oshio T, Kimura J, Sakamoto Y, Shimomura N, Inagaki S and Ichikawa M (2006), "Nanonecklaces of Platinum and Gold with High Aspect Ratios Synthesized in Mesoporous Organosilica Templates by Wet Hydrogen Reduction", *Chem. Mater.*, **18**(2):337-343.

Gadd GM (1993), "Interactions of Fungi with Toxic Metals", *New Phytol.*, **124**(1):25-60.

Gadd GM (1999), "Fungal production of citric and oxalic acid: Importance in metal speciation, physiology and biogeochemical processes", *Adv. Microb. Physiol.*, **41**:47-92.

Gadd GM (2000), "Bioremedial potential of microbial mechanisms of metal mobilisation and immobilisation", *Curr. Opin. Biotech.*, **11**:271-279.

Gadd GM and Griffiths AJ (1978), "Microorganisms and heavy metal toxicity", *Microb. Ecol.*, **4**:303-317.

Gadd GM and White C (1996), "A comparison of carbon/energy and complex nitrogen sources for bacterial sulphate-reduction: potential applications to bioprecipitation of toxic metals as sulphides", *J. Ind. Microbiol. Biot.*, **17**(2):116-123.

Gamez G, Gardea-Torresdey JL, Tiemann KJ, Parsons J, Dokken K & Yacaman J (2003), "Recovery of gold(III) from multi-elemental solutions by alfalfa biomass", *Adv. Environ. Res.*, **7**(2):563-571.

Gavel OY, Bursakov SA, Calvette JJ, Georg GN, Moura JJG and Moura I (1998), "ATP Sulphurylase from sulphate-reducing bacteria of the genus *Desulfovibrio*. A novel metalloprotein containing cobalt and zinc", *Biochemistry*, **37**:16225-16235

Georganopoulou DG, Chang L, Nam J, Thaxton CS, Mufson EJ, Klein WL & Mirkin CA (2005), "From The Cover: Nanoparticle-based detection in cerebral spinal fluid of a soluble pathogenic biomarker for Alzheimer's disease", *P. Nat. Acad. Sci-Biol.*, **102**(7):2273-2276.

Gibson GR (1990), "A Review: Physiology and ecology of the sulphate-reducing bacteria", *J. Appl. Bacteriol.*, **69**:769-797.

Govender Y, Riddin TL, Gericke M and Whiteley CG (2008), "Bioreduction of platinum salts into nanoparticles: a mechanistic perspective", *Biotechnol. Lett.*, DOI 10.1007/s10529-008-9825-z.

Guo C, Boullanger P, Jiang L and Liu T (2007), "Highly sensitive gold nanoparticles biosensor chips modified with a self-assembled bilayer for detection of Con A", *Biosens. Bioelectron.*, **22**(8):1830-1834.

Gwinn MR and Vallyathan V (2006), "Nanoparticles: Health Effects: Pros and Cons", *Environ. Health Persp.*, **114**(12):1818-1825.

Hakim LF, Portman JL, Casper MD and Weimer AW (2005), "Aggregation behavior of nanoparticles in fluidized beds", *Powder Technol.*, **160**:149-160.

Hamilton WA (1998), "Bioenergetics of sulphate-reducing bacteria in relation to their environmental impact", *Biodegradation*, **9**: 201–212.

He S, Guo Z, Zhang Y, Zhang S, Wang J and Gu N (2007), "Biosynthesis of gold nanoparticles using the bacteria *Rhodopseudomonas capsulata*", *Mater. Lett.*, **61**:3984-3987.

Henglein A, Ershov BG and Malow M (1995), "Absorption spectrum and some chemical reactions of colloidal platinum in aqueous solutions", *J. Phys. Chem.*, **99**:14129:14136.

Henglein A and Giersig M (2000), "Reduction of Pt(II) by H<sub>2</sub>: Effects of Citrate and NaOH and Reaction Mechanism", *J. Phys. Chem. B.*, **104**:6767-6772.

Hou Y, Kondoh H, Ohta T and Gao S (2005), "Size-controlled synthesis of nickel nanoparticles", *Appl. Surf. Sci.*, **241**:218–222.

Ibrahim Z, Ahmad A & Baba B (2001), "Bioaccumulation of Silver and the Isolation of Metal-Binding Protein from *P.diminuta*", *Brazil. Arch. of Biol. and Tech.*, **44**(3):223-225.

Ito Y, Jain H and Williams DB (1999), "Electron beam induced growth of Cu nanoparticles in silica glass matrix", *Appl. Phys. Lett.*, **75**(24):3793-3795.

Iwamoto M, Kuroda K, Kanzow J, Hayashi S and Faupel F (2005), "Size evolution effect of the reduction rate on the synthesis of gold nanoparticles", *Adv. Powder Technol.*, **16**(2):137-144.

Jain KK (2005), "Nanotechnology in clinical laboratory diagnostics", *Clin. Chim. Acta*, **358**(1-2):37-54.

Kim NH and Kim K (2004), " Surface-Enhanced Raman scattering at platinum nanoaggregates", *Chem. Phys. Lett.*, **393**:478-482.

Klimenkov M, Matz W, Nepijko SA and Lehmann M (2001), "Crystallisation of Ge nanoclusters in SiO<sub>2</sub> caused by electron irradiation in TEM", *Nucl. Instrum. Meth. B*, **179**(2):209-214.

Koebel MM, Jones LC and Somorjai GA, (2008), "Preparation of size-tunable, highly monodisperse PVP-protected Pt-nanoparticles by seed-mediated growth", *J. Nanopart. Res.*, **10**:1063–1069.

Kolmert A and Johnson DB (2001), "Remediation of acidic waste waters using immobilised, acidophilic sulfate-reducing bacteria", *J. Chem. Technol. Biot.*, **76**(8):836-843.

Konishi Y, Ohno K, Saitoh N, Nomura T, Nagamine S, Hishida H, Takashi Y, Uruga T (2007), "Bioreduction of platinum nanoparticles on the bacterium *Shewanella algae*", *J. Biotechnol.*, **128**:648-653.

Kubik T, Bogunia-Kubik K & Sugisaka M (2005), "Nanotechnology on Duty in Medical Applications", *Curr. Pharma. Biotech.*, **6**:17-33.

Kuyucak N and Volesky B (1988), "Biosorbents for the recovery of metals from industrial solutions", *Biotechnol. Lett.*, **10**(2):137-142.

LaCount W, An G and Lee JM (1997), "The effect of polyvinylpyrrolidone (PVP) on the heavy chain monoclonal antibody production from plant suspension cultures", *Biotechnol. Lett.*, **19**(1):93-96.

Lameiras FA (1999), "Ostwald Ripening: An Approach with Dynamical Systems", *Mater. Res.*, **2**(3):139-143.

LaVan DA, McGuire T & Langer R (2003), "Small-scale systems for in vivo drug delivery", *Nat Biotech.*, **21**(10):1184-1191.

Lee G, Shin S and Oh S (2004), "Preparation of silver dendritic nanoparticles using sodium polyacrylate in aqueous solution", *Chem. Lett.*, **33**(2):118.

Lemos RS, Gomes CM, Santana M, LeGall J, Xavier AV, Teixeira M (2001), "The 'strict' anaerobe *Desulfovibrio gigas* contains a membrane-bound oxygen-reducing respiratory chain", *FEBS Lett.*, **496**:40–3.

Lengke M and Southam G (2006), "Bioaccumulation of gold by sulphate-reducing bacteria cultured in the presence of gold(I)-thiosulphate complex", *Geochem. Cosmochim. Ac.*, **70**:3646-3661.

Li C, Robertson IM, Jenkins ML, Hutchison JL and Doole RC (2005), "In situ TEM observation of the nucleation and growth of silver oxide nanoparticles", *Micron.*, **36**:9-15.

Li D, He Q, Cui Y, Duan L and Li J (2007), "Immobilisation of glucose oxidase onto gold nanoparticles with enhanced thermostability", *Biochem. Biophys. Res. Commun.*, **355**(2):488-493.

Liamleam W and Annachhatre AP (2007), "Electron donors for biological sulfate reduction", *Biotechnol. Adv.*, **25**:452–463.

Lin C, Khan M and Lin SD (2006), "The preparation of Pt nanoparticles by methanol and citrate", *J. Coll. Interf. Sci.*, **299**(2):678-685.

Lin C and Lin K (1969), "Spoilage bacteria in canned foods", *Appl. Microbiol.*, **19**(2):283-286.

Lissolo T, Pulvin S and Thomas D (1984), "Reactivation of the hydrogenase from *Desulfovibrio gigas* by hydrogen. Influence of redox potential", *J. Biol. Chem.*, **259**(19): 11725-11729.

Liu Z, Hong L, Pun Tham M, Han Lim T and Jiang H (2006), "Nanostructured Pt/C and Pd/C catalysts for direct formic acid fuel cells", *J. Power Sources*, **161**(2):831-835.

Liu Z, Ling XY, Su X and Lee JM (2004), “Carbon-supported Pt and PtRu nanoparticles as catalysts for a direct methanol fuel cell”, *J. Phys. Chem. B.*, **108**:8234-8240.

Lloyd JR, Mabbett AN, Williams DR and Macaskie LE (2001), “Metal reduction by sulphate-reducing bacteria: physiology, diversity and metal specificity”, *Hydrometallurgy*, **59**:327-337.

Lloyd JR and Macaskie LE (1996), “A novel phosphorimager-based technique for monitoring the microbial reduction of technetium”, *Appl. Environ. Microbiol.*, **65**:578–582.

Lloyd JR, Ridley J, Khizniak T, Lyalikova NN and Macaskie LE (1999), “Reduction of Technetium by *Desulfovibrio desulfuricans*: Biocatalyst Characterization and Use in a Flowthrough Bioreactor”, *Appl. Environ. Microbiol.*, **65**(6):2691-2696.

Lloyd JR, Yong P and Macaskie LE. (1998), “Enzymatic recovery of elemental palladium by using sulphate-reducing bacteria”, *Appl. Environ. Microbiol.*, **64**(11):4607-4609.

Lojou E, Bianco P, and Bruschi M (1998), “Kinetic studies on the electron transfer between bacterial c-type cytochromes and metal oxides”, *J. Electroanal. Chem.*, **452**:167–177.

Lovely DR, Widman PK, Woodward JC and Phillips EJP (1993), “Reduction of Uranium by Cytochrome c<sub>3</sub> of *Desulfovibrio vulgaris*”, *Appl. Environ. Microbiol.*, **59**(11):3572-3576.

Macaskie LE, Baxter-Plant VS, Creamer NJ, Humphries AC, Mikheenko IP, Mikheenkko PM, Penfold DW and Yong P (2005), “Applications of bacterial hydrogenases in waste decontamination, manufacture of novel bionanocatalysts and in sustainable energy”, *Biochem. Soc. T.*, **33**(1):76-79.



Mack C, Wilhelmi C, Duncan JR and Burgess JE (2007), “Biosorption of precious metals”, *Biotechnol. Adv.*, **25**:264–271.

Madigan MT, Martinko JM and Parker J (2000), “Brock Biology of Microorganisms”, (9<sup>th</sup> Edition), pp 498-502, Prentice Hall International Inc, USA.

Mandal S, Phadtare S and Sastry M (2005), “Interfacing biology with nanoparticles”, *Curr. Appl. Phys.*, **5**:118-127

Michel C, Brugna M, Aubert C, Bernadac A, Bruschi M (2001), “Enzymatic reduction of chromate: comparative studies using sulfate-reducing bacteria. Key role of polyheme cytochromes c and hydrogenases”, *Appl. Microbiol. Biotechnol.*, **55**:95–100.

Michel C, Giudici-Ortoni MT, Baymann F and Bruschi M (2003), “Bioremediation of Chromate by sulphate-reducing bacteria, cytochromes c<sub>3</sub> and hydrogenases”, *Water Air Soil Poll.*, **2**:161-169.

Mijatovic D, Eijkel JCT, van den Berg A (2005), “Technologies for nanofluidic systems: top-down vs. bottom-up—a review”, *Lab Chip*, **5**:492–500.

Mills RL (2000), “The hydrogen atom revisited”, *Int. J. Hydrogen Energ.*, **25**:1171-1183.

Minz D, Fishbain S, Green SJ, Muyzer G, Cohen Y, Rittmann, BE, Stahl DA (1999), “Unexpected population distribution in a microbial mat community: sulfate-reducing bacteria localized to the highly oxic chemocline in contrast to a eukaryotic preference for anoxia.”, *Appl. Environ. Microbiol.*, **65**:4659–65.

Mitra A and Bhaumik A (2007), “Nanoscale silver cluster embedded in artificial heterogeneous matrix consisting of protein and sodium polyacrylate”, *Mat. Lett.*, **61**(3):659-662.

Mizukoshi Y, Takagi E, Okuno H, Oshimo R, Maeda Y and Nagata Y (2001), "Preparation of platinum nanoparticles by sonochemical reduction of the Pt(IV) ions: role of surfactants", *Ultrason. Sonochem.*, **8**:1-6.

Mogenson GL, Kjeldson KU and Ingvorsen K (2005), "Desulfovibrio *aerotolerans* sp. nov., an oxygen tolerant sulphate-reducing bacterium isolated from activated sludge", *Anaerobe*, **11**:339-349.

Möller C and van Heerden E (2006), "Isolation of a soluble and membrane-associated Fe(III) reductase from the thermophile, *Thermus scotoductus* (SA-01)", *FEMS Microbiol Lett.*, **265**:237-243.

Mukherjee P, Ahmad A, Mandal D, Senapati S, Sainkar SR, Khan MI, Ramani R, Parischa R, Ajayakumar PV, Alam M, Sastry M & Kumar R (2003), "Bioreduction of AuCl<sub>4</sub><sup>-</sup> Ions by the Fungus, *Verticillium* sp. and Surface Trapping of the Gold Nanoparticles Formed", *Angew. Chem. Int. Edit.*, **40**(19):3585-3588.

Mukherjee P, Senapati S, Mandal D, Ahmad A, Islam Khan M, Kumar R & Sastry M (2002), "Extracellular synthesis of gold nanoparticles by the fungus *Fusarium oxysporum*", *ChemBioChem*, **5**:461-463.

Nadgeri JM, Telkar MM, Rode CV (2008), "Hydrogenation activity and selectivity behavior of supported palladium nanoparticles", *Catal. Commun.*, **9**(3):441-446.

Nakayama T, Nomura N and Matsumura M (2006), "The effect of copper concentration on the virulence of pathogenic *Vibrio harveyi*", *J. Appl. Microbiol.*, **102**(5):1300-1306.

Narayanan R and El-Sayed MA (2005), "Catalysis with Transition Metal Nanoparticles in Colloidal Solution: Nanoparticle Shape Dependence and Stability", *J. Phys. Chem. B*, **109**(26):12663-12676.

Narayanan R and El-Sayed MA (2008), "Some aspects of colloidal nanoparticle stability, catalytic activity and recycling potential", *Top. Catal.*, **47**:15-21.

Nies DH (1999), "Microbial heavy-metal resistance", *Appl. Microbiol. Biotechnol.*, **51**:730-750.

Nies DH and Silver S (1995), "Ion efflux systems involved in bacterial metal resistances", *J. Indust. Microbiol.*, **14**:186-199.

Oberdörster G, Finkelstein JN, Johnston C, Gelein R, Cox C, Baggs R and Elder AC (2000), "Acute Pulmonary Effects of Ultrafine Particles in Rats and Mice", *Res. Rep. Health Eff. Inst.*, **96**:5-74.

Odom JM and Peck HD Jr. (1981), "Hydrogen cycling as a general mechanism for energy coupling in the sulfate-reducing bacteria *Desulfovibrio* sp.", *FEMS Microbiol. Lett.* **12**:47-50.

Opperman DJ and van Heerden E (2007), "Aerobic Cr(VI) reduction by *Thermus scotoductus* strain SA-01", *J. Appl. Microbiol.*, **103**:1907-1913.

Oyekola O and Pletschke B (2006), "ATP-Sulphurylase: An enzymatic marker for biological sulphate reduction?", *Soil Biol. Biochem.*, **38**:3511-3515.

Panyam J & Labhasetwar V (2003), "Biodegradable nanoparticles for drug and gene delivery to cells and tissue", *Adv. Drug Deliver. Rev.*, **55**(3):329-347.

Payne RB, Gentry DM, Rapp-Giles BJ, Casalot L, Wall JD (2002), "Uranium reduction by *Desulfovibrio desulfuricans* strain G20 and a cytochrome c3 mutant", *Appl. Environ. Microbiol.*, **68**:3129-3132.

Pearson RG (1963), "Hard and Soft Acids and Bases", *J. Am. Chem. Soc.*, **85** (22): 3533-3539.

Pearson RG (1968), "Hard and soft acids and bases, HSAB", *J. Chem. Educ.*, **45**: 581643

Peck Jr HD & Lissolo T (1988) "Assimilatory and dissimilatory sulphate reduction: Enzymology and Bionenergetics", *Soc. Gen. Microbiol.*, **42**:99-132.

Penn SG, He L & Natan MJ (2003), "Nanoparticles for bioanalysis", *Curr. Opin. Chem. Biol.*, **7**(5):609-615.

Pfennig N and Widdel F and Postgate JR (1982), "The bacteria of the sulphur cycle", *Phil. Trans. R. Soc. Lond. B*, **298**:433-441.

Pohorelic BKJ, Voordouw JK, Lojou E, Dolla A, Harder JA and Voordouw G (2002), "Effects of deletion of genes encoding Fe-only hydrogenase of *Desulfovibrio vulgaris* Hildenborough on hydrogen and lactate metabolism", *J. Bacteriol.*, **184**:679-686.

Postgate JR (1965), "Recent advances in the study of the Sulphate-reducing bacteria", *Bacteriol. Rev.*, **29**(4):425-441.

Postgate JR (1984), "The Sulphate Reducing Bacteria", (2<sup>nd</sup> Edition), Cambridge University Press, Cambridge.

Postgate JR and Abdollahi H (1982), "Economic Importance of Sulphur Bacteria [and Discussion]", *Phil. Trans. R. Soc. Lond. B*, **298**(1093):583-600.

Raloff J (1985), "The bugs of rust", *Science News*, **128**(3):42-44.

Rashamuse KJ (2003), "The bioaccumulation of platinum(IV) from aqueous solution using sulphate-reducing bacteria – Role of a hydrogenase enzyme", Masters Thesis, Rhodes University, South Africa.

Rashamuse KJ, Mutambanengwe CCZ and Whiteley CG (2008), "Enzymatic recovery of platinum (IV) from industrial wastewater using a biosulphidogenic hydrogenase", *Afr. J. Biotechnol.*, **7**(8):1087-1095.

Rashamuse KJ and Whiteley CG (2007), “ Bioreduction of Pt(IV) from aqueous solution using sulphate reducing bacteria”, *Appl. Microbiol. Biotechnol.* **75**:1429-1435.

Ravnic DJ, Zhang Y, Turhan A, Tsuda A, Pratt JP, Huss HT and Mentzer SJ (2007), “Biological and Optical properties of fluorescent nanoparticles developed for intravascular imaging”, *Microsc. Res. Techniq.*, **70**(9):776-781,

Ren Y, Xing XH, Zhang C and Gou ZX (2005), “A simplified method for assay of hydrogenase activities of H<sub>2</sub> evolution and uptake in *Enterobacter aerogenes*”, *Biotechnol. Lett.*, **27**:1029-1033.

Riddin TL (2005), “Intra- and extracellular production of geometric platinum nanoparticles by *Fusarium oxysporum* f. sp. *Lycopersici*”, Rhodes University, Honours treatise.

Riddin TL, Gericke M & Whiteley CG (2006), “Analysis of the inter- and extracellular formation of platinum nanoparticles by *Fusarium oxysporum* f. sp. *lycopersici* using response surface methodology”, *Nanotechnology*, **17**:3482-3489.

Riklis E and Ritenberg D (1961), “Some observations on the Enzyme Hydrogenase”, *J. Biol. Chem.*, **236**(9):2526-2529.

Rudoy VM, Sukhov NL, Dement'eva OV, Abkhalimov EV, Vereshchagina OF, Kartseva ME and Ershov BG (2005), “Metal Nanoparticles on Polymer Surfaces: 5. Catalytic Activity of Colloidal Platinum Films Incorporated in Polystyrene Surface Layer”, *Colloid Journal*, **67**(3): 357–362.

Salata O (2004), "Applications of nanoparticles in biology and medicine", *Journal of Nanobiotechnology*, **2**(1):3.

Sastry M, Ahmad A, Islam Khan M & Kumar R (2003), "Biosynthesis of metal nanoparticles using fungi and actinomycete", *Curr. Sci.*, **85**:162-163.

Seeman NC and Belcher AM (2002), "Emulating Biology: Building Nanostructures from the Bottom Up", *P. Nat. Acad. Sci-Biol.*, **99**(9:2):6451-6455.

Sepulveda-Guzman A, Elizondo-Villarreal, Ferrer D, Torres-Castro A, Gao X, Zhou JP and Jose-Yacaman M (2007), "In situ formation of bismuth nanoparticles through electron-beam irradiation in a transmission electron microscope", *Nanotechnology*, **18**:335604.

Shankar SS, Rai A, Ahmad A and Sastry M (2001), "Rapid synthesis of Au, Ag and bimetallic Au-core-Ag shell nanoparticles using Neem (*Azadirachta indica*) leaf broth", *J. Colloid Interf. Sci.*, **275**:496-502

Singhal A, Skandan A, Wang A, Glumac N, Kear BH and Hunt RD (1999), "On nanoparticle aggregation during vapour phase synthesis", *NanoStruct. Mater.*, **11**(4): 545–552.

Snyder K (2007), "Giving Platinum Catalysts a Golden Boost for Fuel Cells", Brookhaven National Laboratory News, BNL Media and Communications Office, USA.

**Website:** [http://www.bnl.gov/bnlweb/pubaf/pr/PR\\_display.asp?prID=07-32](http://www.bnl.gov/bnlweb/pubaf/pr/PR_display.asp?prID=07-32)

**Accessed:** 04/08/08

Spear JR, Figueroa LA and Honeyman BD (2000) "Modelling reduction of Uranium U(VI) under variable sulphate concentrations by sulphate-reducing bacteria", *Appl. Environ. Microbiol.*, **66**(9):3711-3721.

Spieker WA, Liu J, Kropf AJ and Regalbuto JR (2002), "An EXAFS study of the coordination chemistry of hydrogen hexachloroplatinate (IV). 1. Speciation in solution", *Appl. Catal.*, **232**:219-235.

Sriamornsak P and Thirawong N (2003), "Use of back-scattered electron imaging as a tool for examining matrix structure of calcium pectinatese of back-scattered electron

imaging as a tool for examining matrix structure of calcium pectinate”, *Int. J. Pharm.*, **267**(1-2):151-156.

Sun CQ, Chen TP, Tai BK, Huang SLH, Zhanga YB, Pan LK, Lau SP and Sun XW (2001), “An extended ‘quantum confinement’ theory: surface-coordination imperfection modifies the entire band structure of a nanosolid”, *J. Phys. D: Appl. Phys.*, **34**:3470–3479.

Sun Y and Xia Y (2002), “Shape-Controlled Synthesis of Gold and Silver Nanoparticles”, *Science, New Series*, **298**(5601):2176-2179.

Tanaka M, Takeguchi M and Furuya K (2002), Behaviour of metal nanoparticles in the electron beam”, *Micron.*, **33**:441-446.

Teske A, Wawer C, Muyzer G and Ramsing NB (1996), “Distribution of sulfate-reducing bacteria in a stratified fjord (Mariager Fjord, Denmark) as evaluated by most-probable-number counts and denaturing gradient gel electrophoresis of PCR-amplified ribosomal DNA fragments”, *Appl. Environ. Microbiol.*, **62**: 1405–1415.

Thaxton CS, Georanopoulou DG, Mirkin CA (2005), “Gold nanoparticle probes for the detection of nucleic acid targets”, *Clin. Chim. Acta*, **363**(1-2):120-126.

Thompson DT (2005), "Catalysis by Gold/Platinum Group Metals. Mixed Metal Systems Displaying Increased Activity", *ChemInform*, **36**(21).

Tripp SL, Pusztay SV, Ribbe AE and Wei A (2002), “Self-Assembly of Cobalt Nanoparticle Rings”, *J. Am. Chem. Soc.*, **124**:7914-7915.

Trüper HG, Kelleher JJ and Jannasch HW (1969), “Isolation and characterisation of sulphate-reducing bacteria from various marine environments”, *Arch. Mikrobiol.*, **65**:208-211.

Tuttle JH, Dugan PR, MacMillan CB & Randles CI (1989), "Microbial dissimilatory sulphur cycle in acid mine water. *J. Bact.*, **97**: 594-602.

Ueki K, Ueki A and Sinogoh Y (1988), " Terminal steps in the anaerobic digestion of municipal sewage sludge: effects of inhibitors of methanogenesis and sulphate reduction" *J. Gen. Appl. Microbiol.*, **34**:425-434.

U.S. Department of Health and Human Services (1978), "Occupational Health Guidelines for Soluble Platinum Salts", USA.

Valix M & Loon LO (2003), "Adaptive tolerance behaviour of fungi in heavy metals", *Miner. Eng.*, **16**(3):193-198.

Vinogradov SV, Bronich TK & Kabanov AV (2002), "Nanosized cationic hydrogels for drug delivery: preparation, properties and interactions with cells", *Adv. Drug Deliver. Rev.*, **54**(1):135-147.

Voordouw G (2002), "Carbon Monoxide Cycling by *Desulfovibrio vulgaris* Hildenborough", *J. Bacteriol.*, **184**(2): 5903–5911.

Wazszczuk P, Wieckowski A, Zelenzy P, Gottesfeld S, Coutanceau C, Léger JM and Lamy C (2001), "Adsorption of CO poison on fuel cell nanoparticle electrodes from methanol solutions: a radioactive labeling study", *J. Electroanal. Chem.*, **511**(1-2):55-64.

White C, Sharman AK and Gadd GM (1998), "An integrated microbial process for the bioremediation of soil contaminated with toxic metals", *Nat Biotechnol.*, **16**:572-575.

Whiteley CG and Lee DJ (2006), "Enzyme technology and biological remediation", *Enzyme Microb. Tech.*, **38**: 291–316.



Wilson K and Walker K (2000), "Principles and Techniques of Practical Biochemistry", 5<sup>th</sup> Edition, Chapter 12: Electrophoretic Techniques, pp 590-591, Cambridge University Press, United Kingdom.

World Health Organisation Regional Office for Europe (2000), "Air Quality Guidelines for Europe" (2<sup>nd</sup> Edition), Chapter 6:11, pp 166-170, published by World Health Organisation Regional Office Europe.

Wu Y, Yang W, Wang C, Hu J & Fu S (2005), "Chitosan nanoparticles as a novel delivery system for ammonium glycyrrhizinate", *Int. J. Pharm.*, **295**(1-2):235-245.

Yong P, Rowson NA, Farr JP, Harris IR and Macaskie LE (2002), "Bioreduction and biocrystallization of palladium by *Desulfovibrio desulfuricans* NCIMB 8307", *Biotechnol. Bioeng.*, **80**(4):369-379.

Zadvorny OA, Zorin NA and Gogotov IN (2005), "Transformation of metals and metal ions by hydrogenases from phototrophic bacteria", *Arch Microbiol*, **184**:279–285.

Zadvorny OA, Zorin NA and Gogotov IN, Gorlenko VM (2004), " Properties of stable hydrogenase from the purple sulfur bacteria *Lamprobacter modestohalophilus*", *Biochemistry-Moscow+*, **69**(2):164-169.

Zhang L, Swift J, Butts CA, Yerubandi V and Dmochowski IJ (2007), "Structure and activity of apoferritin-stabilised gold nanoparticles", *J. Inorg. Chem-USSR*, **101**:1719-1729.

Zhu H, Zhang C and Yin Y (2004), "Rapid synthesis of copper nanoparticles by sodium hypophosphite reduction in ethylene glycol under microwave irradiation", *J. Cryst. Growth*, **270**:722–728.

Zwietering MH, Jongenburger I, Rombouts FM and van 'T Riet K (1990), "Modelling of the bacterial growth curve", *Appl. Environ. Microbiol.*, **56**(6):1875-1881.

---

---

## APPENDICES

---

---

### APPENDIX A - Modified Postgate Medium - C

(Rashamuse & Whiteley, 2007)

For 10 L of media:

<b>Solution A</b>	
Na <sub>2</sub> SO <sub>4</sub> (Merck)	29.6 g
NH <sub>4</sub> Cl (Sigma)	10 g
Yeast Extract (Sigma)	10 g
KH <sub>2</sub> PO <sub>4</sub> (Saarchem),	5 g
Sodium Citrate.2H <sub>2</sub> O (Sigma)	1 g
CaCl <sub>2</sub> .2H <sub>2</sub> O (Sigma)	0.4 g
MgSO <sub>4</sub> .7H <sub>2</sub> O (Sigma),	0.6 g
60% Sodium Lactate (Sigma)	25.2 ml
Dissolve all components up to 9900 ml ddH <sub>2</sub> O.	

<b>Solution B:</b>	
Ascorbic Acid (Sigma),	1.0 g
Sodium Thioglycolate (Sigma)	1.0 g
Dissolve components in 100 ml ddH <sub>2</sub> O	

- Adjust pH of 'Solution A' to pH 7.6 with 5 M NaOH.
- Autoclave 'Solution A' and 'Solution B' separately at 121 °C, 15 psi for 15 min.
- For 10 L media, add 100 ml Solution B to 9900 ml Solution A.

## **APPENDIX B – Buffer Recipes**

### **Tris-HCl buffer**

1) Tris-HCl buffer (20 mM, pH 7.6)

- 2.42 g Tris in 800 ml ddH<sub>2</sub>O
- Adjust pH with 1 M HCl to pH 7.6.
- Add ddH<sub>2</sub>O up to 1 L

2) Tris-HCl buffer (200 mM, pH 7.6)

- 24.23 g Tris in 800ml ddH<sub>2</sub>O
- Adjust pH with 1 M HCl to pH 7.6.
- Add ddH<sub>2</sub>O up to 1 L

### **Sodium-bicarbonate buffer (200 mM, pH 9.0)**

Dissolved 15.96 g NaHCO<sub>3</sub> + 1.06 g Na<sub>2</sub>CO<sub>3</sub> in 1 L ddH<sub>2</sub>O.

## APPENDIX C - Bradford standard curves (Sigma)

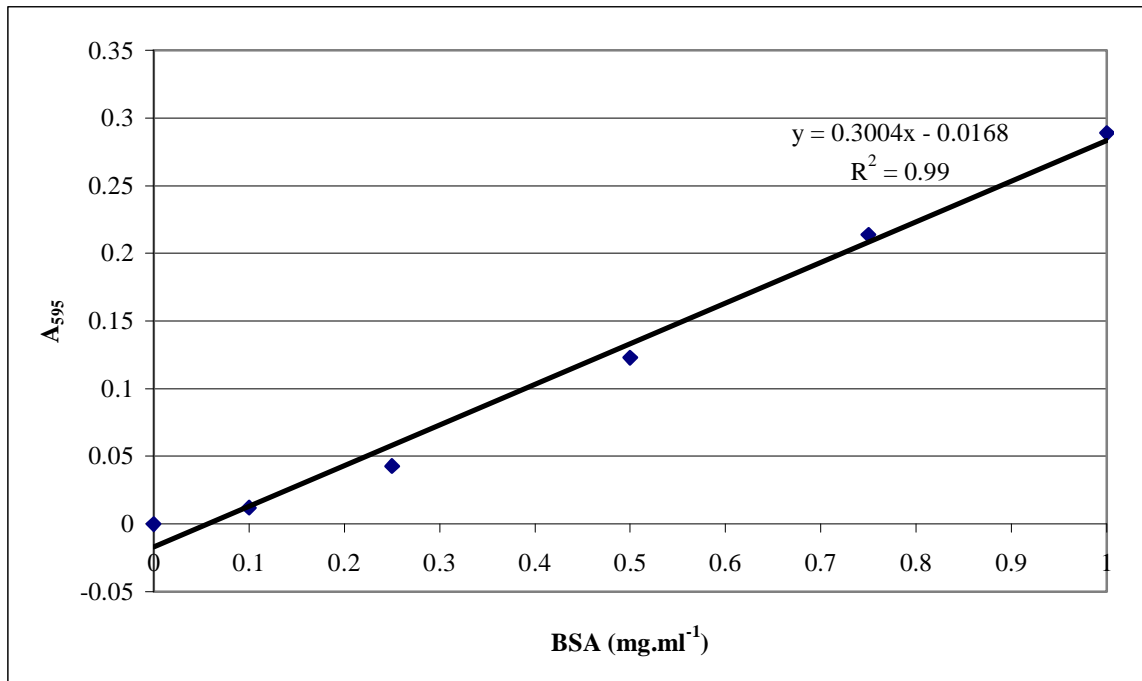
### Bradford standard curve - A

A 10 mg.ml<sup>-1</sup> stock solution (10 ml) of Bovine Serum Albumin (BSA) was made up in Tris-HCl buffer (200 mM, pH 7.6). A series of standards (1 ml) were constructed as follows. The 0 mg.ml<sup>-1</sup> standard was used as the blank:

	BSA Standards (mg. ml <sup>-1</sup> )					
	0	0.1	0.25	0.5	0.75	1.0
BSA Stock (µl)	0	10	25	50	75	100
Tris-HCl buffer (µl)	1000	990	975	950	925	900
A <sub>595</sub> *	0	0.012	0.043	0.123	0.214	0.289

96-well Micro-titer plate assay:

5 µl Standard + 250 µl Bradford Reagent



\* Values shown are averages. Standard deviation < 10 %.

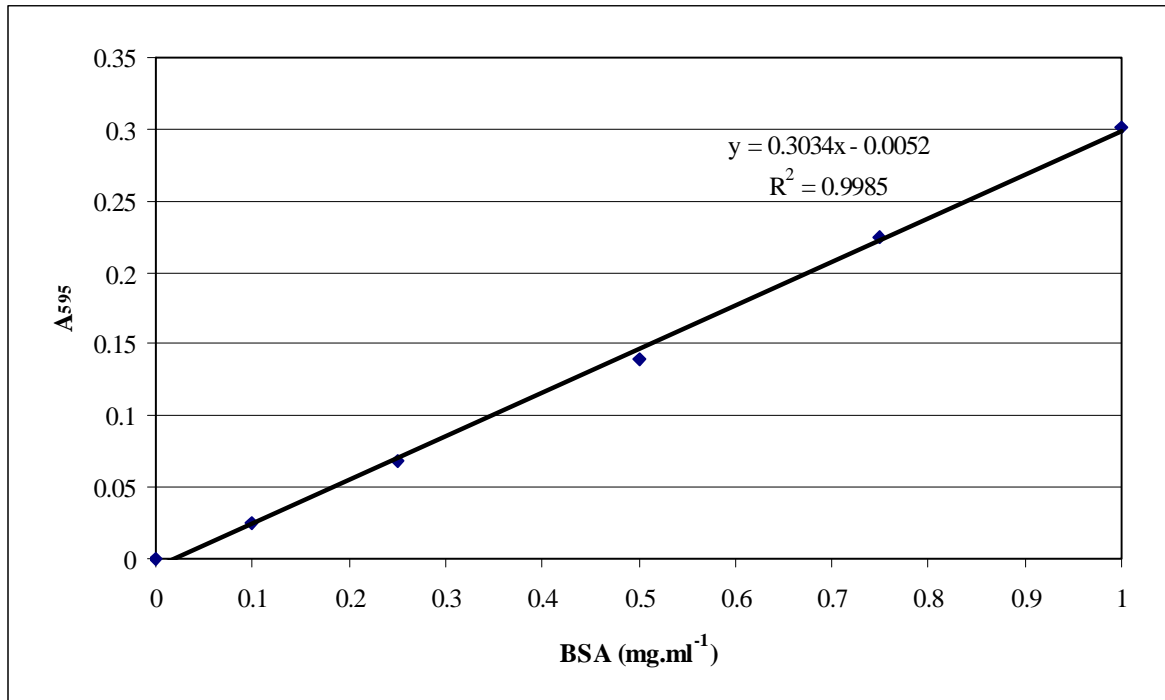
### Bradford standard curve - B (Sigma)

A 1 mg.ml<sup>-1</sup> protein standard solution of Bovine Serum Albumin (BSA) was used in the preparation of the following standards in ddH<sub>2</sub>O. The 0 mg.ml<sup>-1</sup> standard was used as the blank:

	BSA Standards (mg.ml <sup>-1</sup> )					
	0	0.1	0.25	0.5	0.75	1.0
Protein std (μl)	0	25	62.5	125	187.5	250
ddH <sub>2</sub> O (μl)	250	225	187.5	125	62.5	0
A <sub>595</sub> *	0	0.025	0.068	0.139	0.225	0.301

96-well Micro-titer plate assay:

5 μl Standard + 250 μl Bradford Reagent



\* Values shown are averages. Standard deviation < 10 %.

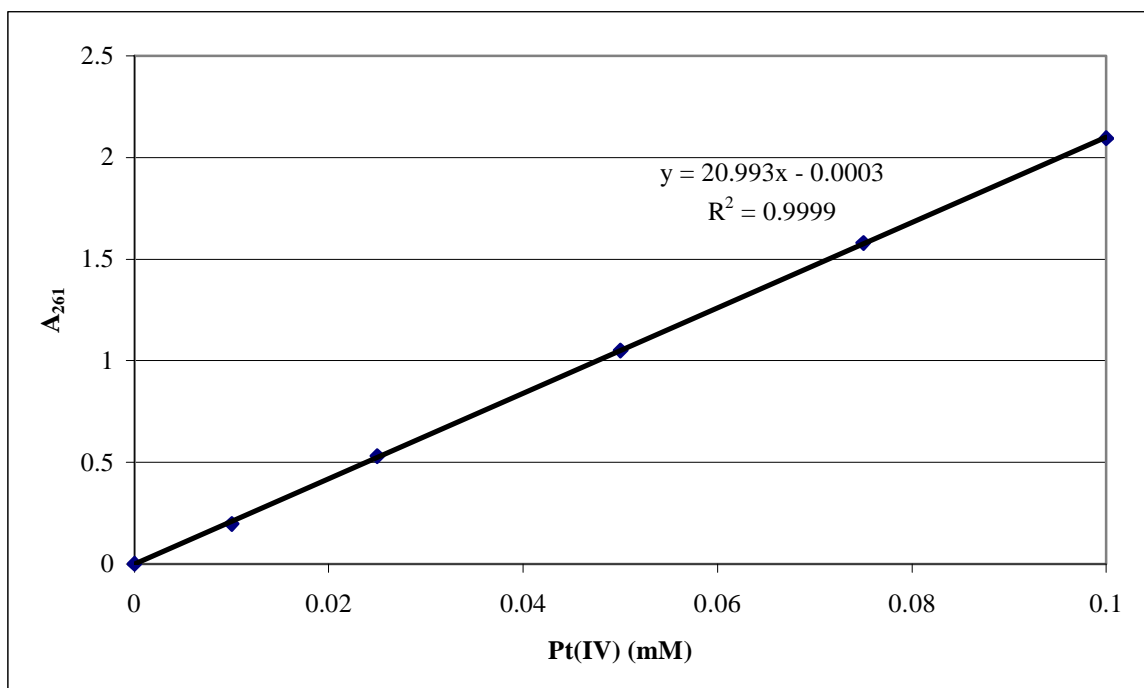
## APPENDIX D - Platinum salt standard curves

### H<sub>2</sub>PtCl<sub>6</sub> [Pt(IV)] standard curve - A

Using a stock solution of 1 mM H<sub>2</sub>PtCl<sub>6</sub> in Tris-HCl buffer (200 mM, pH 7.6), a set of standards were constructed as follows. The 0 mM standard was used as a blank.

Experimental samples were diluted appropriately to within the range of the standard curve and the concentration calculated to take the dilution into account:

	H <sub>2</sub> PtCl <sub>6</sub> Standards (mM)					
	0	0.01	0.025	0.05	0.075	0.10
H <sub>2</sub> PtCl <sub>6</sub> Stock (μl)	0	150	375	750	1125	1500
Tris-HCl buffer (μl)	1500	1350	1125	750	375	0
A <sub>261</sub> *	0	0.198	0.532	1.05	1.58	2.09

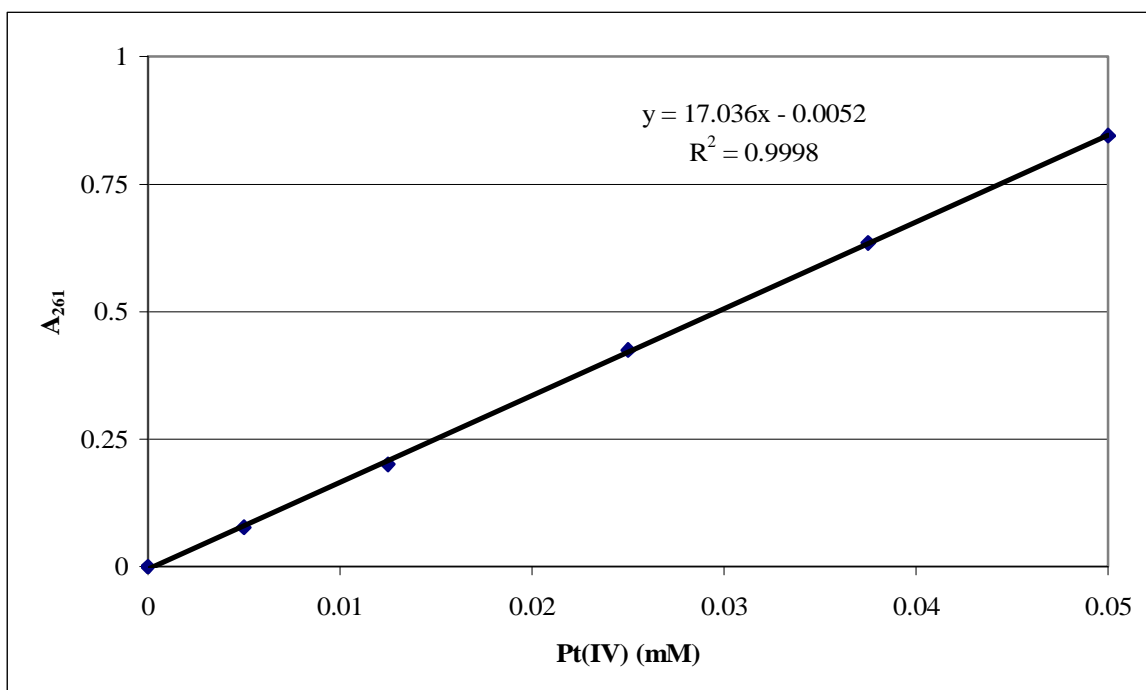


\* Values shown are averages. Standard deviation < 10 %.

### H<sub>2</sub>PtCl<sub>6</sub> [Pt(IV)] standard curve - B

Using a stock solution of 10 mM H<sub>2</sub>PtCl<sub>4</sub> in ddH<sub>2</sub>O, a set of standards were constructed as follows. The 0 mM standard was used as a blank. Experimental samples were diluted appropriately to within the range of the standard curve and the concentration calculated to take the dilution into account:

	H <sub>2</sub> PtCl <sub>6</sub> Standards (mM)					
	0	0.005	0.0125	0.025	0.0375	0.05
H <sub>2</sub> PtCl <sub>6</sub> Stock (μl)	0	10	25	50	75	100
ddH <sub>2</sub> O (μl)	1000	990	975	950	925	900
A <sub>261</sub> *	0	0.077	0.2	0.425	0.635	0.845



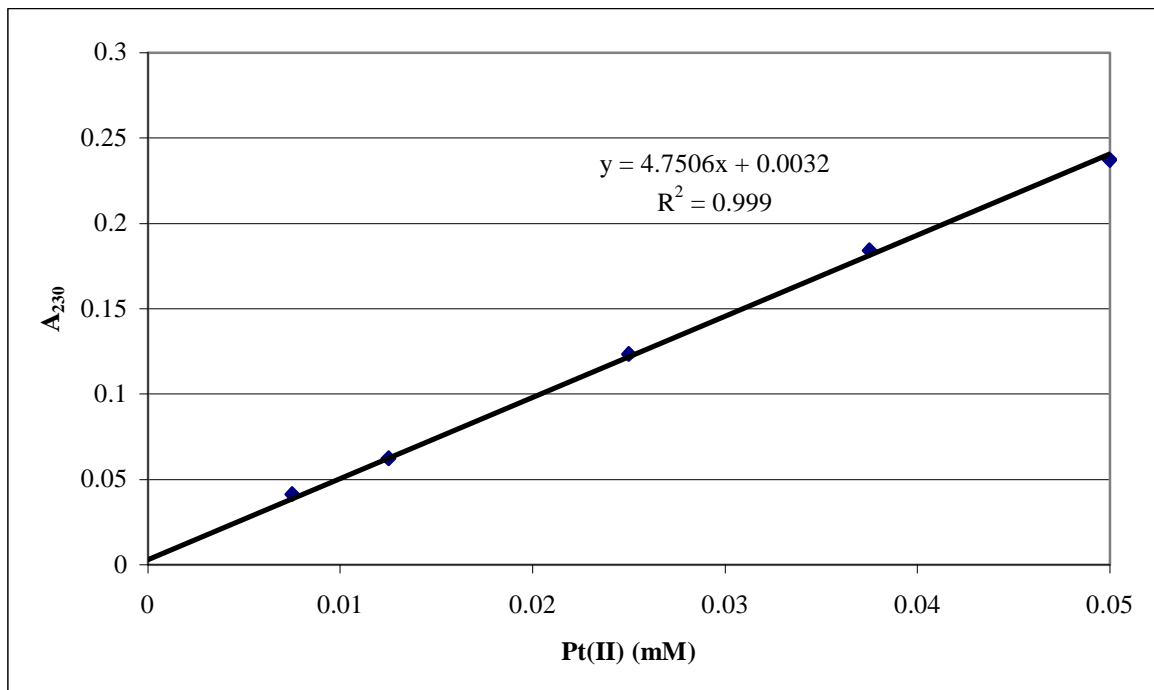
\* Values shown are averages. Standard deviation < 10 %.

### Na<sub>2</sub>PtCl<sub>4</sub> [Pt(II)] standard curve - A

Using a stock solution of 10 mM Na<sub>2</sub>PtCl<sub>4</sub> in Tris- HCl buffer (200 mM, pH 7.6), a set of standards were constructed as follows. The 0 mM standard was used as a blank.

Experimental samples were diluted appropriately to within the range of the standard curve and the concentration calculated to take the dilution into account:

	Na <sub>2</sub> PtCl <sub>4</sub> Standards (mM)					
	0	0.0075	0.0125	0.025	0.0375	0.05
Na <sub>2</sub> PtCl <sub>4</sub> stock (μl)	0	15	25	50	75	100
Tris- HCl buffer (μl)	1000	985	975	950	925	900
A <sub>230</sub> *	0	0.041	0.062	0.124	0.184	0.237



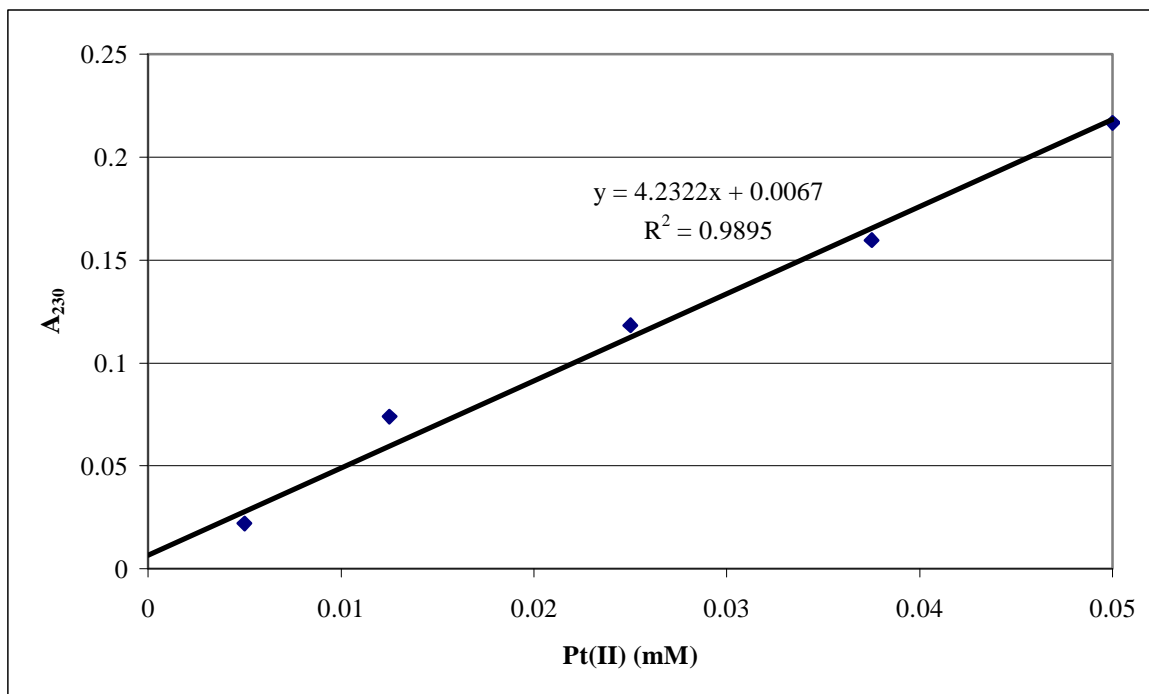
\* Values shown are averages. Standard deviation < 10 %.



### Na<sub>2</sub>PtCl<sub>4</sub> [Pt(II)] standard curve – B

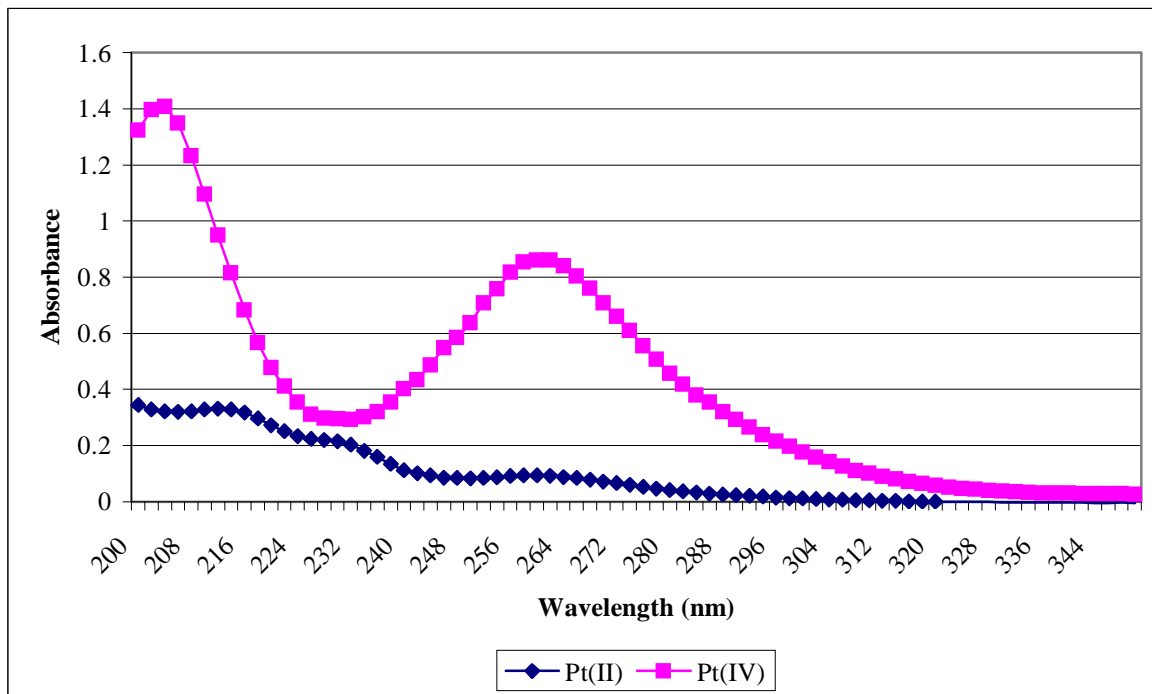
Using a stock solution of 10 mM Na<sub>2</sub>PtCl<sub>4</sub> in ddH<sub>2</sub>O, a set of standards were constructed as follows. The 0 mM standard was used as a blank. Experimental samples were diluted appropriately to within the range of the standard curve and the concentration calculated to take the dilution into account:

	Na <sub>2</sub> PtCl <sub>4</sub> Standards (mM)					
	0	0.0075	0.0125	0.025	0.0375	0.05
Na <sub>2</sub> PtCl <sub>4</sub> stock (μl)	0	15	25	50	75	100
ddH <sub>2</sub> O (μl)	1000	985	975	950	925	900
A <sub>230</sub> *	0	0.022	.0074	0.118	0.16	0.217



\* Values shown are averages. Standard deviation < 10 %.

## APPENDIX E - Spectrum scan of platinum salts



For the Pt(II) salt,  $\text{Na}_2\text{PtCl}_4$ , the spectrum scan exhibited three peaks, a major peak at 220 nm, a shoulder peak at 230 nm and a minor peak at 260-261 nm.

For the Pt(IV) salt,  $\text{H}_2\text{PtCl}_6$ , two major peaks are evident, one at ~206 nm and another at 260-261 nm, with a trough at 230 nm.

It was decided that the shoulder peak of Pt(II) at 230 nm would be used to identify this ion in solution, while the peak at 260-261 nm was chosen for Pt(IV) determinations. It is important to notice here that the Pt(IV) ion also has an absorbance at 230 nm, therefore in all calculations pertaining to Pt(II) determinations, this fact was taken into account and the absorbance values adjusted accordingly.

## **APPENDIX F - Native-PAGE Recipes for the Bio-Rad Mini-Protean II apparatus**

(Bollag *et al.*, 1996)

### **Solution A (100 ml)**

- 30 g Acrylamide + 0.8 % bis-acrylamide
- 100 ml ddH<sub>2</sub>O

### **Solution B (100 ml) [Tris-HCl (1.5 M, pH 8.8)]**

- 18.2 g Tris in 40 ml ddH<sub>2</sub>O
- Add HCl to pH 8.8
- Add H<sub>2</sub>O to 100 ml

### **10 % Ammonium Persulphate (APS) (5 ml)**

- 0.5 g Ammonium Persulphate
- 5 ml ddH<sub>2</sub>O

### **Electrophoresis Buffer (1 L)**

- 3 g Tris
- 14.4 g Glycine
- Add H<sub>2</sub>O to 1 L, pH should be 8.8.

### **5X Sample Buffer (10 ml)**

- 3.1 ml Tris-HCl (1 M, pH 6.8)
- 5ml Glycerol
- 0.5 ml 1 % Bromophenol Blue
- 1.4 ml ddH<sub>2</sub>O

**7.5 % Continuous Native-PAGE gel recipe (2 X 0.75 mm gels)**

Solution A	2.5 ml
Solution B	2.5 ml
ddH <sub>2</sub> O	5 ml
10 % APS	50 ul
TEMED	15 µl

**Coomassie Gel Staining and Destaining (Bollag *et al.*, 1996)**

**Coomassie Stain (1 L)**

- 1.0 g Coomassie Blue R-250
- 450 ml Methanol
- 450 ml ddH<sub>2</sub>O
- 100 ml Glacial acetic acid

**Coomassie Gel Destain (1 L)**

- 100 Methanol
- 100 ml Glacial acetic acid
- 800 ml ddH<sub>2</sub>O